**NASA Contractor Report** 172303-VOL-1

# INVESTIGATION OF THE RELATIONS BETWEEN NEAT RESIN AND ADVANCED COMPOSITE MECHANICAL PROPERTIES

## VOLUME I - RESULTS

Richard S. Zimmerman
Donald F. Adams
David E. Walrath

UNIVERSITY OF WYOMING
Laramie, Wyoming





Grant NAGI-277
November 1984



NASA
National Aeronautics and Space Administration
**Langley Research Center**
Hampton, Virginia 23665

# DISCLAIMER NOTICE


**THIS DOCUMENT IS BEST QUALITY AVAILABLE. THE COPY FURNISHED TO DTIC CONTAINED A SIGNIFICANT NUMBER OF PAGES WHICH DO NOT REPRODUCE LEGIBLY.**

NASA REPORT NO.
NASA CR-172303-VOL-1

WYOMING REPORT NO.
UWME-DR-301-101-1-VOL-1

# INVESTIGATION OF THE RELATIONS BETWEEN NEAT RESIN AND ADVANCED COMPOSITE MECHANICAL PROPERTIES

## VOLUME I - RESULTS

RICHARD S. ZIMMERMAN
DONALD F. ADAMS
DAVID E. WALRATH

NOVEMBER 1984

TECHNICAL REPORT
NASA-LANGLEY RESEARCH CENTER
HAMPTON, VIRGINIA 23665

RESEARCH GRANT NO. NAG-1-277

COMPOSITE MATERIALS RESEARCH GROUP
MECHANICAL ENGINEERING DEPARTMENT
UNIVERSITY OF WYOMING
LARAMIE, WYOMING 82071

# PREFACE

This technical report presents the results of a one-year neat resin characterization and micromechanical prediction program sponsored by NASA-Langley Research Center, under Research Grant NAG-1-277.

All work was performed by the Composite Materials Research Group (CMRG) within the Department of Mechanical Engineering at the University of Wyoming. Co-Principal Investigators were Mr. Richard S. Zimmerman, Staff Engineer and Dr. Donald F. Adams, Professor. The analytical micromechanics studies were under the direction of Mr. David E. Walrath, Staff Engineer. Making major contributions to the program were Larry G. Adams, Beth E. Rogers, and Edward D. Schaffer, graduate students in Mechanical Engineering, and Eric Q. Lewis, Craig H. Johnson, Jeffrey A. Kessler, Thomas A. Ohnstad, Mark Vanderbleek, and Donald B. Hardy, undergraduate students in Mechanical Engineering, and all members of the Composite Materials Research Group. Substantial help in casting neat resin specimens was provided by Mr. Edwin M. Odom, Staff Engineer.

Use of commercial products or names of manufacturers in this report does not constitute official endorsement of such products or manufacturers, either expressed or implied, by the National Aeronautics and Space Administration.

TABLE OF CONTENTS

VOLUME I

TABLE OF CONTENTS
(Continued)

TABLE OF CONTENTS
(Continued)

VOLUME II
(Under Separate Cover)

## SECTION 1

## SUMMARY

One untoughened (baseline) MY720-base epoxy system and three toughened epoxy matrix systems were chosen for this neat resin characterization study. The baseline epoxy was Hercules 3502; the toughened epoxies were Hercules 2220-1 and 2220-3, and Ciba-Geigy Fibredux 914. All resin systems were supplied by NASA-Langley in uncured bulk form, and cast into test specimens by the Composite Materials Research Group (CMRG) at the University of Wyoming. A detailed procedure describing the casting techniques is given in Appendix A. An extensive mechanical characterization study was completed on the four matrix systems at three temperatures, viz, 23°C, 54°C, and 82°C, and two moisture contents, viz, dry and moisture-saturated at 74°C. Tensile, torsional shear, coefficient of thermal expansion, and coefficient of moisture expansion measurements were completed for all environmental conditions. Summary plots in bargraph form are presented in Figures 1 through 3 for tensile and shear moduli, ultimate strengths, and ultimate strains, respectively, for both the dry and moisture-saturated conditions.

Young's modulus, E, decreased for all systems after exposure to temperature or moisture. As expected, the modulus of the 3502 was either the highest or second highest of the four at all environmental conditions. The 2220-1 and 2220-3 materials had the lowest stiffness properties but the values after environmental exposure dropped at about the same rate as 3502 and Fibredux 914. Young's moduli for all systems were very consistent within test groupings.

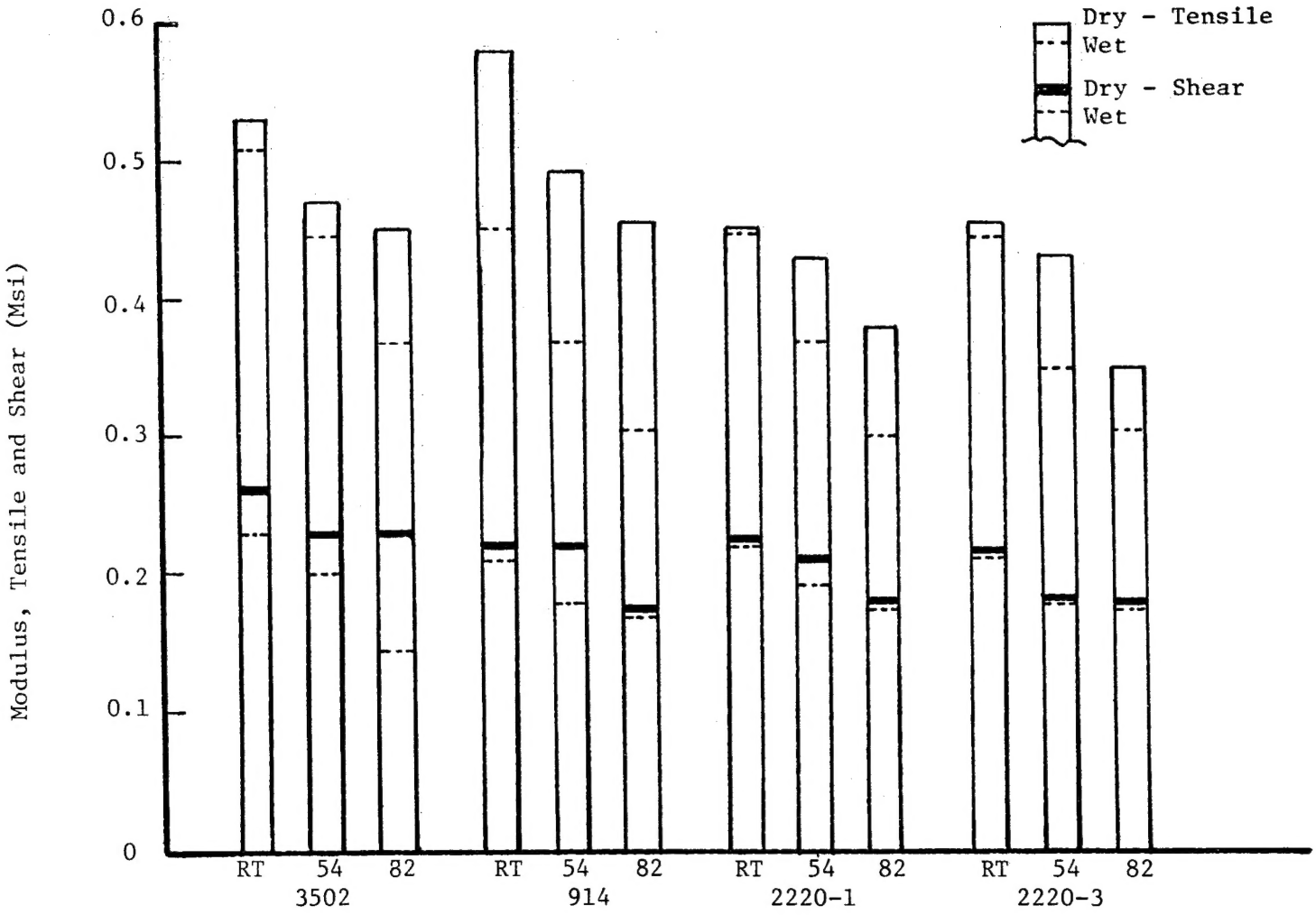


Figure 1. Tensile and Shear Moduli of Neat Resins as a Function of Temperature (°C) and Moisture Preconditioning (Dry or Saturated).

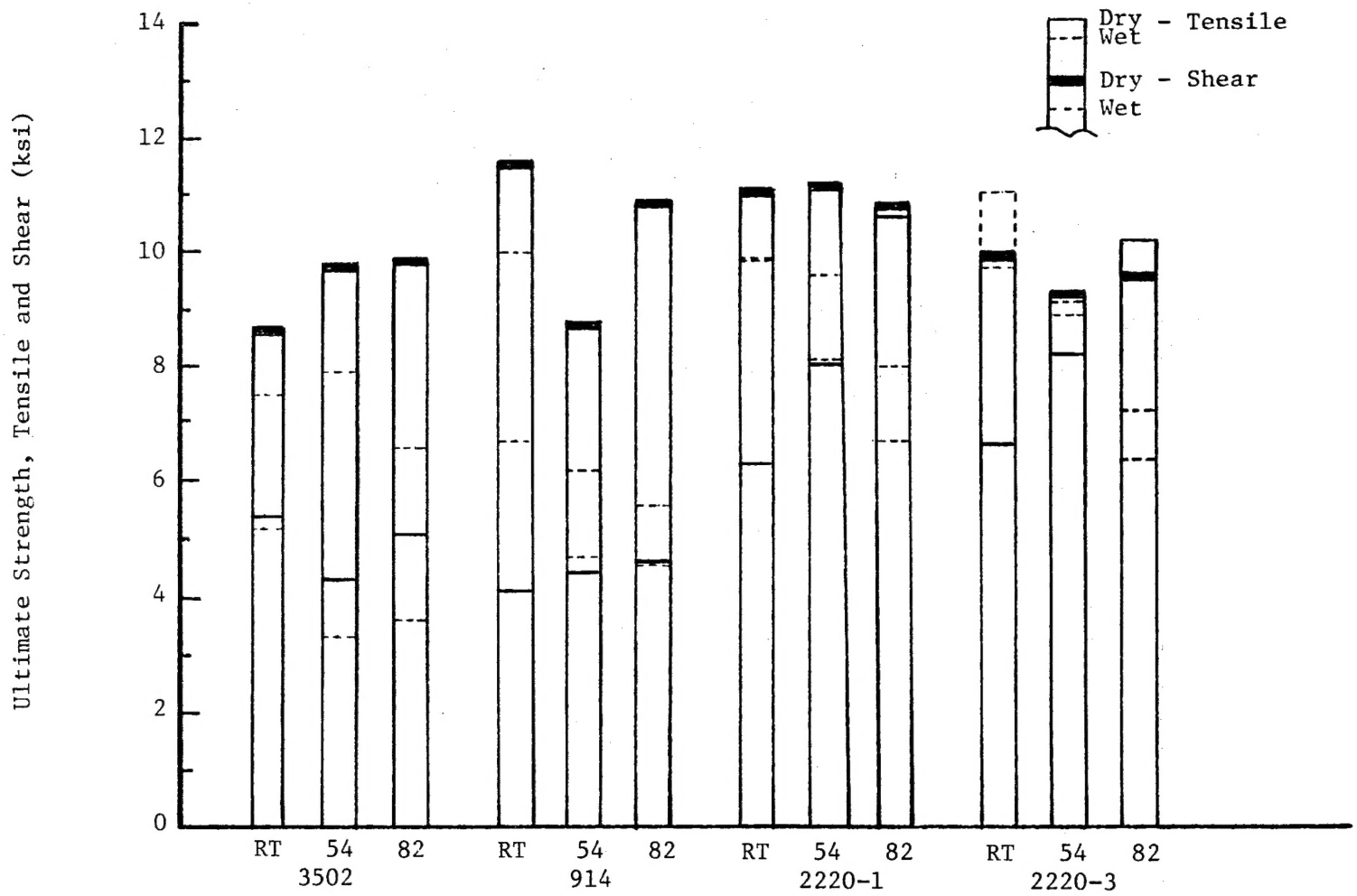


Figure 2. Tensile and Shear Ultimate Strengths of Neat Resins as a Function of Temperature (°C) and Moisture Preconditioning (Dry or Saturated).

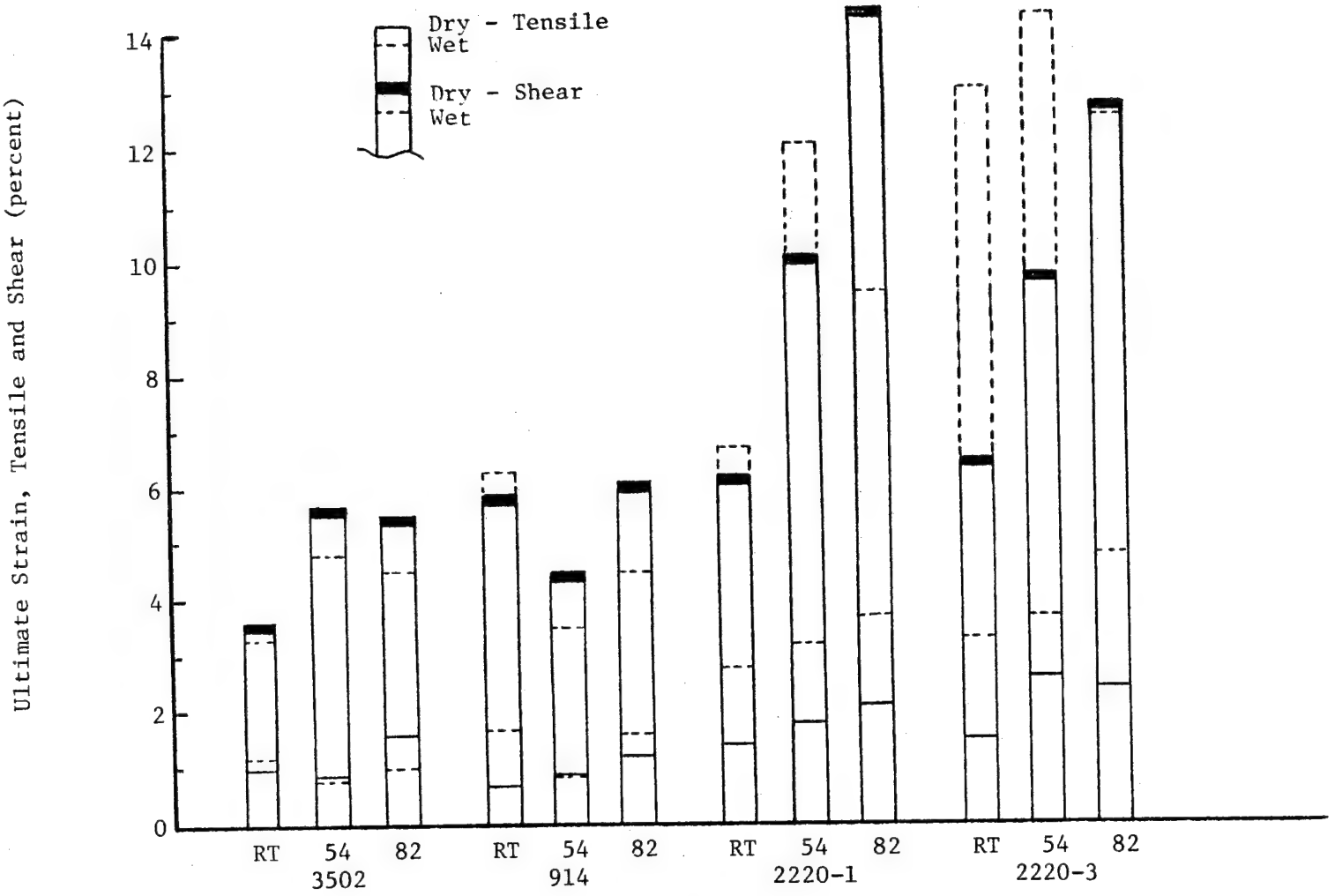


Figure 3. Tensile and Shear Ultimate Strains of Neat Resins as a Function of Temperature (°C) and Moisture Preconditioning (Dry or Saturated).

Tensile strengths were not very consistent within groupings because of the brittle nature of the resins although they reflected the effects of environmental preconditioning. The 3502 epoxy exhibited the lowest or second lowest strength for all test conditions. The 2220-1 and 2220-3 systems performed almost equally under all conditions and had the highest strengths among the four matrix materials tested.

Ultimate strain values for the four resins ranged from 0.7 percent for the dry 914 system at room temperature to 14.5 percent for the 2220-1 system at 82°C, dry. All materials showed a trend to higher strain-to-failure at elevated temperature under a moisture-saturated condition. At any one of the environmental conditions 914 had the lowest strain-to-failure, 3502 was next and 2220-3 the highest.

Poisson's ratio, $\nu$, was reasonably consistent for all resin systems at all test conditions, although the values for the toughened materials were slightly higher than those of most untoughened epoxies. It was also found that Poisson's ratio increased with moisture absorption to a number greater than 0.4. Increasing temperature affected the Poisson's ratio of only the moisture-saturated materials.

Shear modulus, G, was highest in the 3502 epoxy for all conditions except moisture saturation, indicating the sensitivity of the material to a hot, wet environment. The shear moduli of the 2220-1 and 2220-3 epoxies were lowest at all exposures except moisture saturation. Under hot, wet environments, G values were highest for 2220-3 and 2220-1, showing that these two materials had, comparatively, the best moisture resistance. Notably, E, G and $\nu$ values were not consistent with the isotropic materials relation given in Equation (1).

$$G = \frac{E}{2(1 + \nu)} \tag{1}$$

This implies that these epoxy matrix systems are not true isotropic materials.

The 3502 system had the lowest or second lowest shear strength, $\tau_{ult}$, at all environmental conditions except one. No trend for $\tau_{ult}$ at the dry condition could be identified, probably because the somewhat brittle nature of the resins caused high scatter in the data. A definite downward trend in shear strength was observed at moisture saturation compared with values measured under dry conditions. The 2220-1 and 2220-3 resins had the highest strengths observed. The Fibredux 914 exhibited the largest drop in shear strength of all four systems, for all temperature and moisture conditions.

Ultimate shear strain, $\gamma_{ult}$, values were five to six times larger than ultimate tensile strain, $\varepsilon_{ult}$, values. Values for $\gamma_{ult}$ of over 10 percent were common for the 2220-1 and 2220-3 resin, while less than 7 percent shear strain was exhibited by both the 3502 and 914 materials.

Coefficients of thermal expansion, $\alpha$, were measured at both dry and moisture-saturated conditions from 23°C to 93°C. The values were fairly linear over this temperature range, but tended to be higher for moisture-saturated specimens than for dry specimens.

Coefficients of moisture expansion, $\beta$, were measured for all four epoxies, from dry to saturated conditions at 65°C, at three relative humidity levels, viz, 50, 75, and 98 percent. Values of $\beta$ were scattered, but the averages were close to previously measured values for other epoxy systems [4]. The equilibrium moisture content was different for all four resins, ranging from 3.8 percent in 2220-1 to 7.0 percent in 914. The equilibrium moisture level for 3502 was 5.0 percent.

The fracture surfaces of the four matrix systems were studied by

scanning electron microscopy (SEM). Fracture initiation sites and surrounding areas were photographed and compared to determine differences in fracture modes between systems. In many cases, the initiation site is believed to be either a small void area or an insoluble impurity introduced during resin manufacture.

Material properties generated in this program for the four epoxy systems along with Hercules AS4 fiber data taken from the literature were used to perform micromechanics predictions of composite properties. Unidirectional composite stiffnesses in the axial, transverse, and longitudinal shear directions were predicted for each graphite/epoxy material. Experimental composites data will be provided at a later date and correlated with the analytical predictions.

# SECTION 2

# INTRODUCTION

Detailed studies of the mechanical behavior of unreinforced polymer matrix systems have been underway within the Composite Materials Research Group (CMRG) at the University of Wyoming for over six years. The initial work was performed using Hercules 3501-6 epoxy which is a common matrix used in many applications in the aerospace industry. These characterization studies were begun to provide materials property data for use in the micromechanical analyses concurrently being developed by the Composite Materials Research Group [1-4].

Polymer matrix properties are not easily measured. Based on past experience within CMRG, neat resin specimens can be readily cast in the necessary shapes and quantities to fully characterize many different neat resin systems, e.g., Hercules 3501-6, 4001, Fiberite 930 and 934, Hexcel F178, and Shell Epon 9101.

Four systems were chosen for this first-year effort, e.g., Hercules 3502, 2220-1, and 2220-3, and Ciba Geigy Fibredux 914. These were selected because they are being used as matrix materials in composites under evaluation in the Aircraft Energy Efficiency (ACEE) Program and a comprehensive study was needed to fully evaluate them. During this study tension and torsional shear testing was completed, as well as measurements of the coefficients of thermal expansion and moisture expansion. An in-depth examination of the fracture surfaces was performed using a scanning electron microscope (SEM) to catalog and explain the failure morphology. These properties were used in CMRG's micromechanics computer program to predict composite properties as a function of temperature and moisture.

# SECTION 3

# EXPERIMENTAL RESULTS

## 3.1 Introduction

A comprehensive test matrix was completed for each of the four neat epoxy resin systems. Table 1 indicates the particular tests performed, and the test conditions utilized. Sufficient specimens were fabricated to complete the 67 specimen test matrix for each resin system.

The dry test specimens were stored in desiccators to ensure they remained dry after fabrication. The specimens to be moisture-saturated were suspended above distilled water in closed glass containers placed in a Tenney Benchmaster environmental chamber at 74°C. This allowed the test specimens to reach saturation as quickly as possible. Witness specimens were weighed periodically to determine moisture saturation. An average of three months was required for the shear rods to reach saturation, and somewhat less for the flat dog bones which were thinner.

A detailed discussion of test methods is included in Appendix B of Volume II. Static mechanical tests were performed on either an Instron Model 1125 electromechanical test machine or an MTS Model 810 servohydraulic test machine. A BEMCO environmental chamber was utilized for the elevated temperature tests.

## 3.2 Tension Tests

Measurements of E, $\sigma_{ult}$, and $\varepsilon_{ult}$ were made on the four neat epoxy resins for the six environmental conditions noted in Table 1. Complete stress-strain curves to failure are included in Appendix C of Volume II.

The three toughened epoxy matrix systems were compared to the baseline Hercules 3502 epoxy. Figure 4 shows the average tensile strengths for the four systems as a function of test temperature in the

Table 1

Neat Epoxy Resin Test Matrix

| Test Method | Moisture Condition | Test Temperature (°C) 23° | 54° | 82° |
|---|---|---|---|---|
| Tension (flat dogbone) | Dry | 5 | 5 | 5 |
| | Moisture-Saturated | 5 | 5 | 5 |
| | | | | 30 total |
| Torsion (round dogbone) | Dry | 5 | 5 | 5 |
| | Moisture-Saturated | 5 | 5 | 5 |
| | | | | 30 total |
| Coefficient of Thermal Expansion (CTE) (flat bars) | Dry | 2 | 23° to 93°C | |
| | Moisture-Saturated | 2 | 23° to 93°C | |
| | | | | 4 total |
| Coefficient of Moisture Expansion (CME) (flat squares) | 50% RH | 65°C, Dry to Saturation | | |
| | 75% RH | 65°C, Dry to Saturation | | |
| | 98% RH | 65°C, Dry to Saturation | | |
| | | | | 3 total |
| | | | | 67 total each resin system |
| | | | | Program Total - 268* Specimens |

*An additional 60 specimens were fabricated from each resin for notched bend fracture toughness tests. Because of difficulties with the test procedure, the data were omitted from this report.

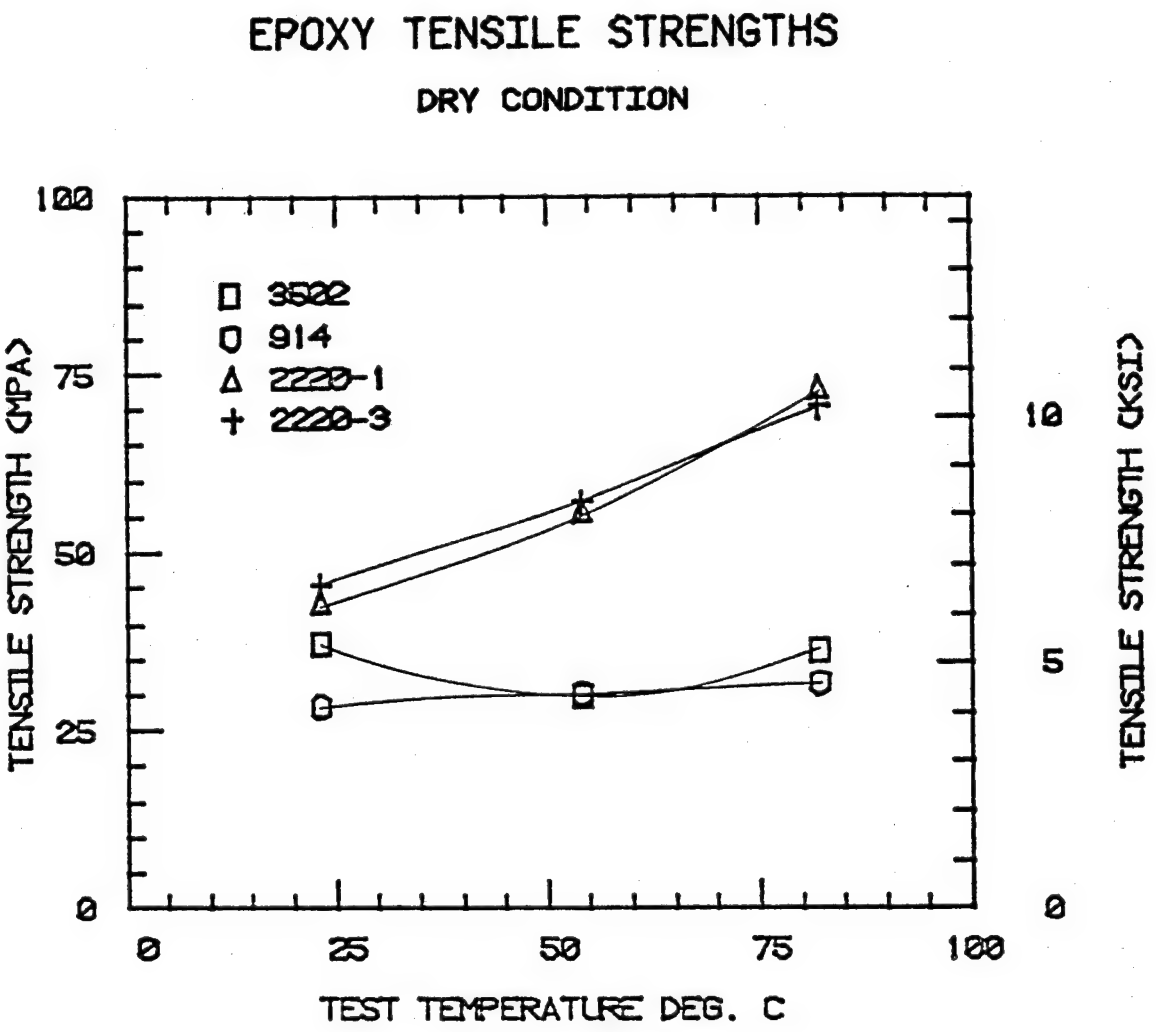


Figure 4. Tensile Strengths as a Function of Temperature, Dry Conditions.

dry, as-cast condition. The 3502 epoxy exhibited a relatively constant low strength at all test temperatures. This particular resin is an MY720 base epoxy and is very brittle. This brittle nature lends itself to a highly linear elastic behavior to failure and a high notch sensitivity which is manifested in increased scatter in ultimate strengths. (See tables in Appendix C of Volume II.) Figures 5 and 6 are photographs of the gage sections and show typical tensile failures for the 3502 epoxy. All of the dry tensile dogbone failures exhibited a missing triangular chip at the failure plane. It is thought that the failure initiated in the fracture plane away from this area, and propagated toward this area, where the crack split into two major cracks and continued to propagate to the edge, resulting in the triangular chip being shattering and ejected in the process. Many failed specimens which had been tested in the moisture-saturated condition exhibited the single fracture surface shown in Figure 6.

The Fibredux 914 tensile strengths are very similar to those of 3502. Figure 7 is a photograph of the gage section of a failed specimen and shows a typical 914 dry tensile failure. A portion of the triangular chip which was recovered has been placed back with the specimen to illustrate the failure more graphically. Many small cracks can be seen extending through the chip and near the fracture area.

The Hercules 2220-1 and 2220-3 toughened epoxies had the highest tensile strengths of the four systems tested. Both showed an increase as the test temperature was increased, a response not exhibited by either 3502 or 914. Figure 8 is a photograph of a typical failure surface for 2220-3. The characteristic triangular chip is missing and many small cracks were evident around the fracture surface. Resin 2220-3 behaved in

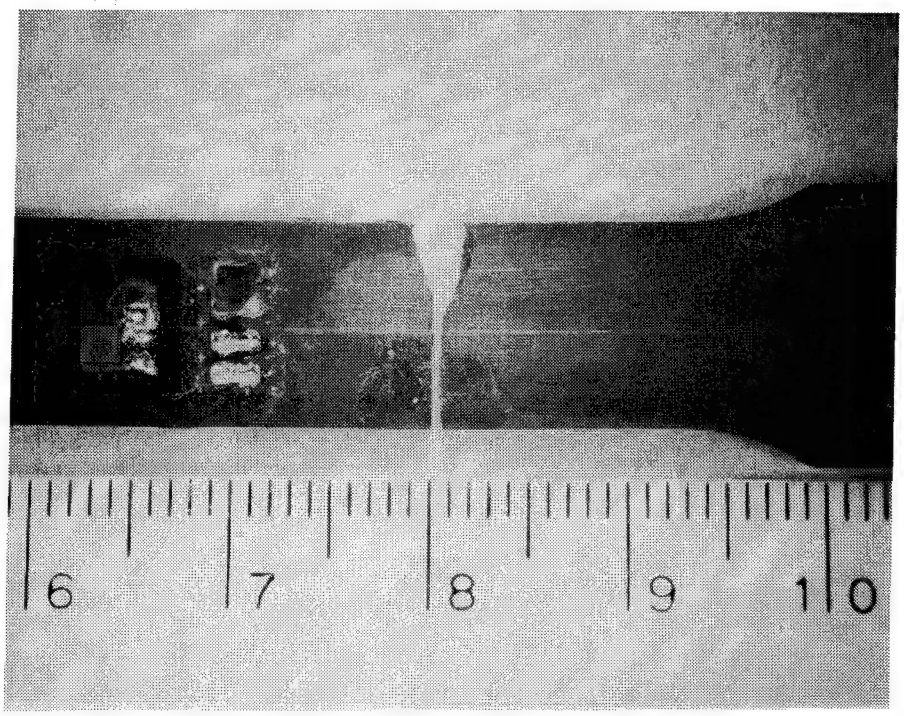


Figure 5. Typical Failed Hercules 3502 Tensile Specimen, 54°C, Dry.

This photograph shows the failure as a single plane at the site of fracture initiation, and the missing triangular chip caused by the splitting and propagation of the fracture to the opposite side of the specimen. All of the dry specimens, and many of the moisture-saturated specimens, displayed this appearance.

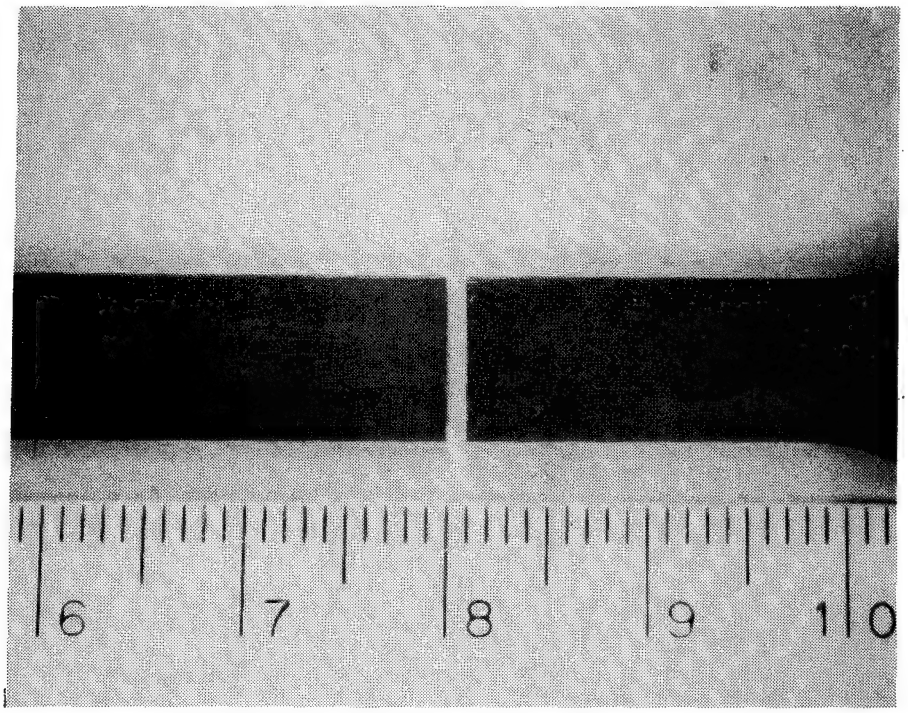


Figure 6. Typical Failed Hercules 3502 Tensile Specimen, 54°C, Moisture-Saturated.

This photograph shows the single fracture plane exhibited by many moisture-saturated specimens.

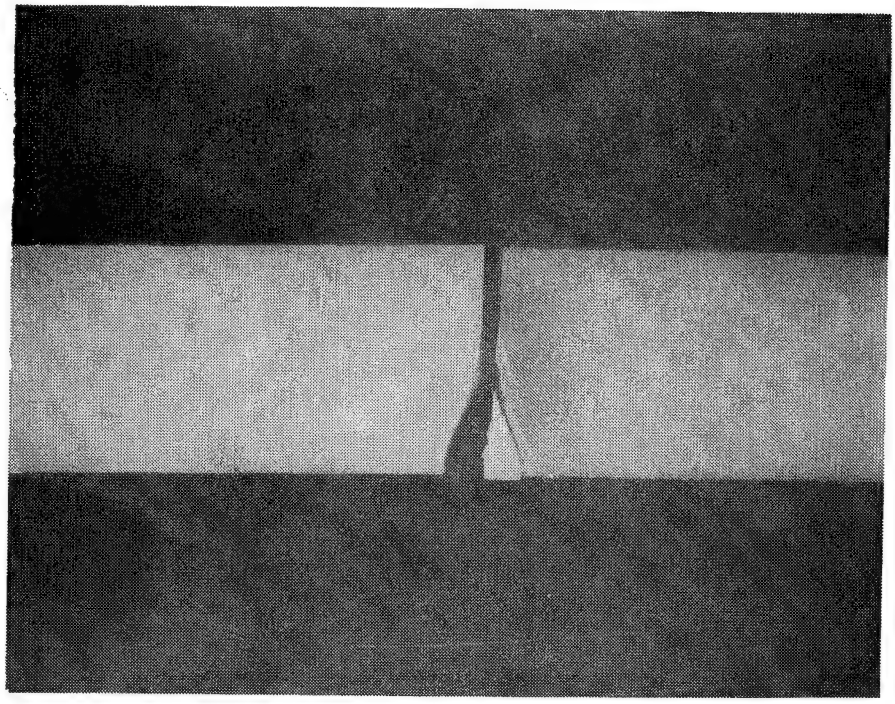

Figure 7. Typical Failed Fibredux 914 Tension Specimen, 23°C, Dry.

This photograph graphically shows the triangular chip created by crack propagation across a tensile specimen. Many small cracks can be seen around the fracture surface.

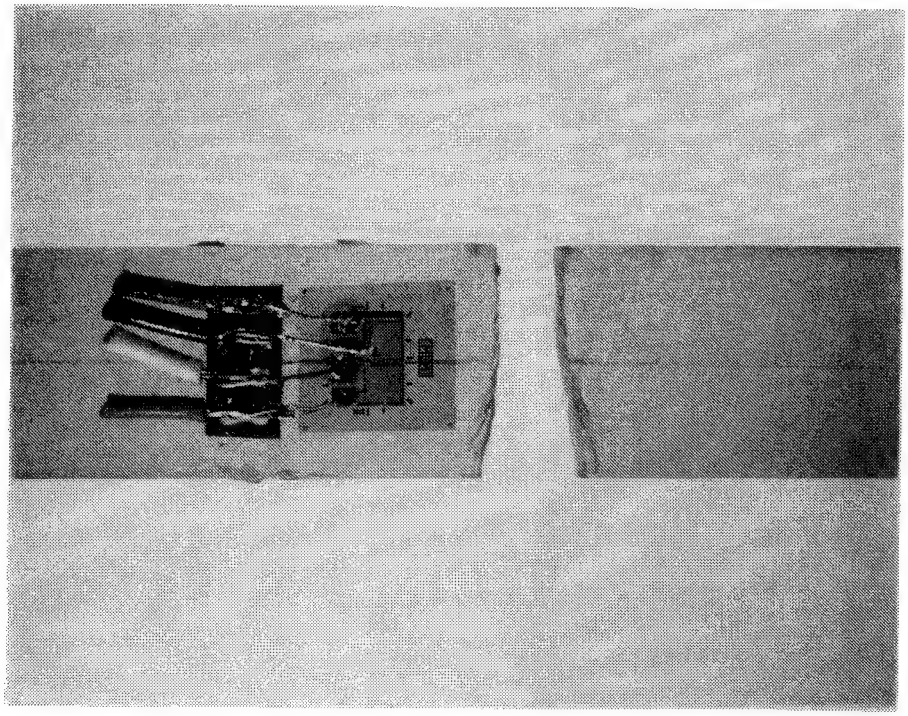

Figure 8. Typical Failed Hercules 2220-3 Tension Specimen, 23°C, Dry.

Many small cracks can be seen at the fracture surface of this specimen. The primary crack presumably initiated in the upper portion of the fracture plane, propagated downward, then split into two or more primary cracks which propagated to the lower edge of the specimen.

a similar fashion.

Figure 9 is a plot of the average tensile strengths as a function of temperature for the four resins after moisture saturation. The 3502 epoxy exhibited the lowest tensile strength at all three temperatures; further, strengths decreased as the test temperature increased. The values for Fibredux 914 were somewhat higher than for the 3502 epoxy, but also decreased at elevated temperatures.

Tensile strengths of the moisture-saturated 2220-1 and 2220-3 epoxies were identical and almost double that of the baseline 3502 system at all test temperatures. The values for these two materials seemed to decrease more rapidly as the test temperature increased, but still remained at more than twice the 3502 strength at 82°C. Also, the effect of moisture saturation in decreasing hot/wet strengths was most notable with the two 2220 resins.

Tensile moduli for the four resin systems under dry conditions as a function temperature are shown in Figure 10. Little temperature effect was observed. The 914 resin had the highest modulus, but the differences were not great. For example, at room temperature, 914 exhibited a modulus of 4.02 GPa (0.58 Msi) and 2220-1 a modulus of 2.96 GPa (0.43 Msi).

Figure 11 is a plot of tensile moduli for moisture-saturated conditions as a function of temperature. All four epoxies displayed a linear decrease in tensile modulus as the temperature was increased. The baseline 3502 had the highest values while the 914, 2220-1, and 2220-3 resins had somewhat lower but almost identical Young's moduli over the entire temperature range.

Ultimate strains for the four resin systems, varied considerably.

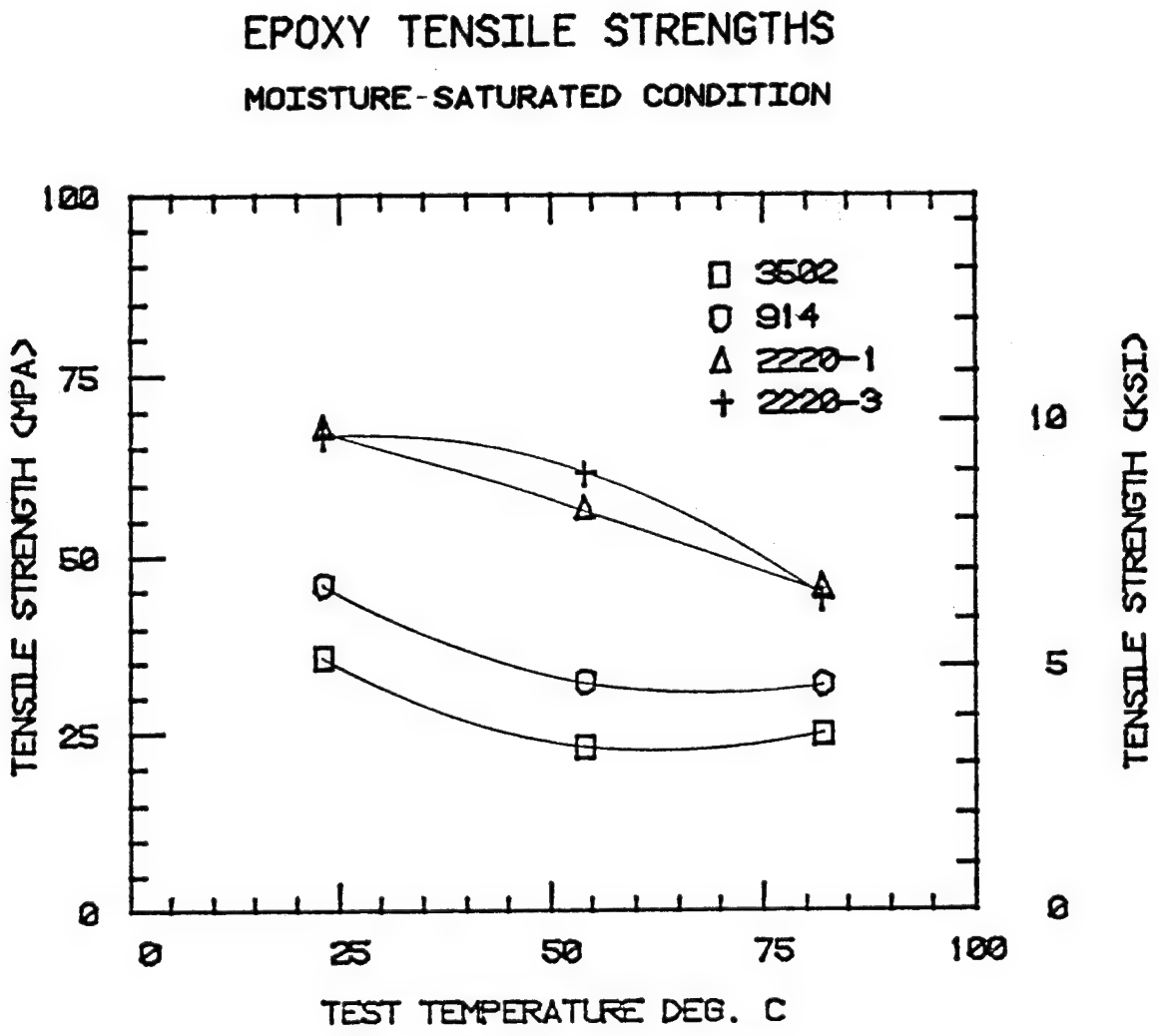


Figure 9. Tensile Strengths as a Function of Temperature, Moisture-Saturated Conditions.

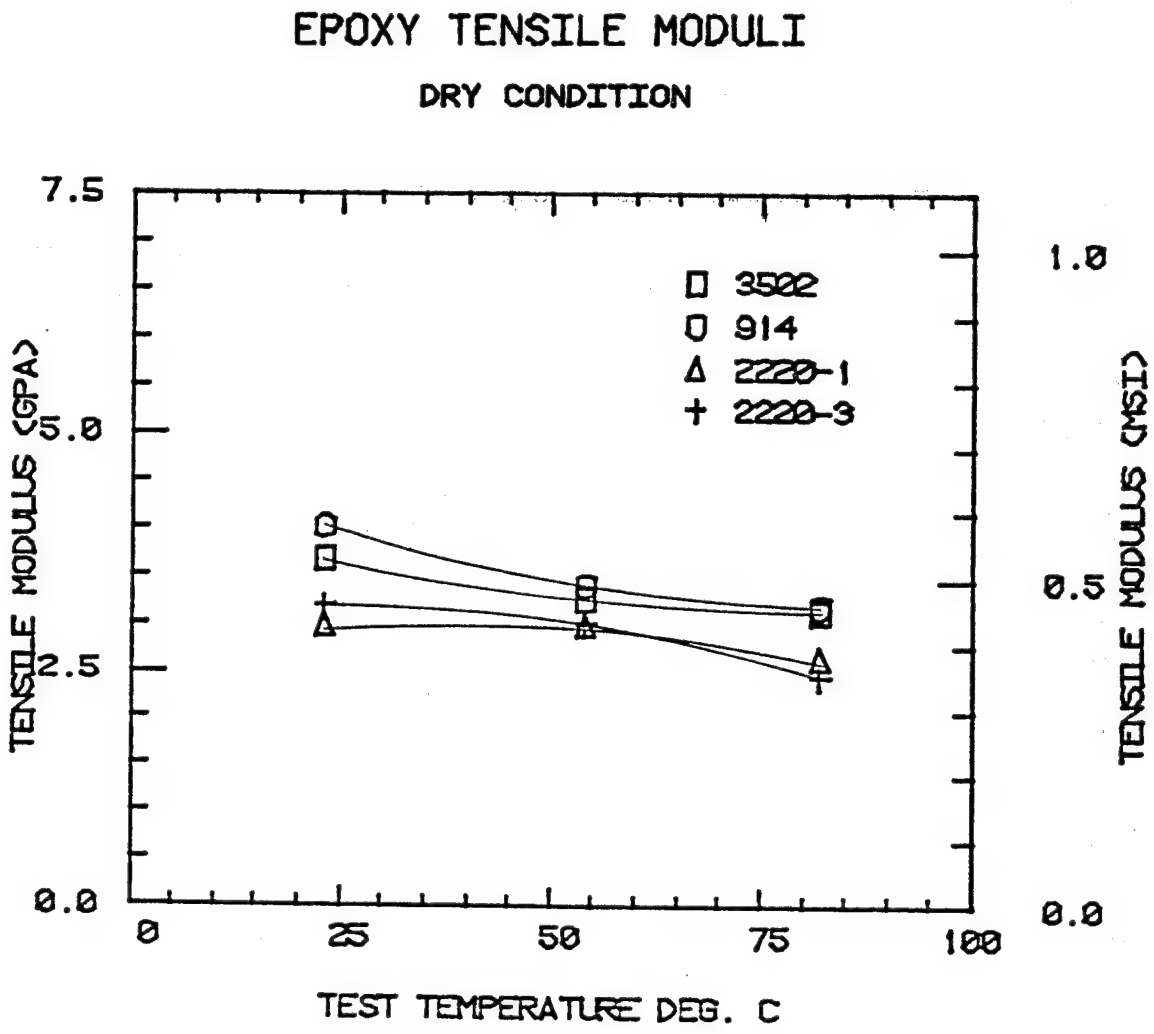


Figure 10. Tensile Moduli as a Function of Temperature, Dry Conditions.

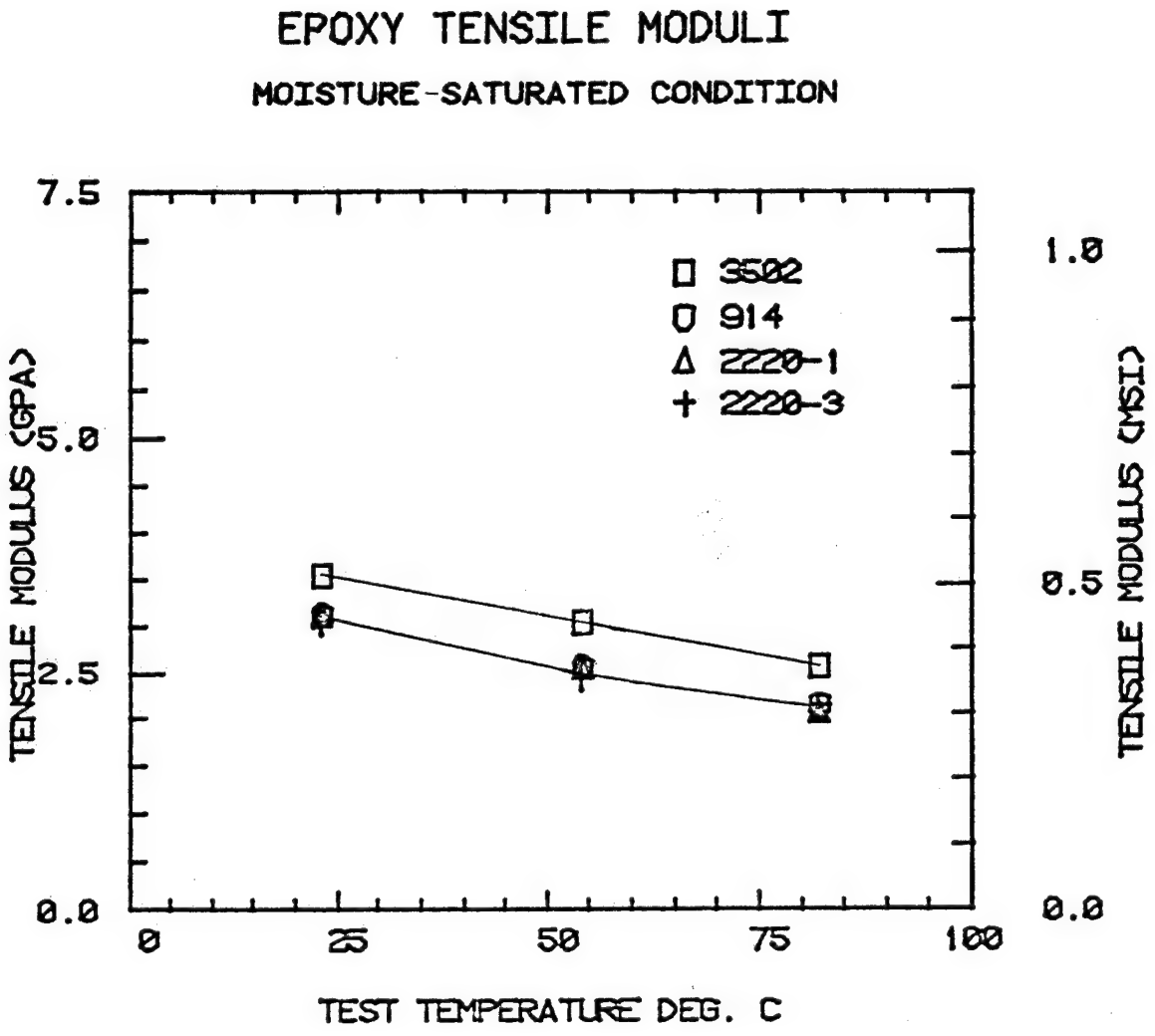


Figure 11. Tensile Moduli as a Function of Temperature, Moisture-Saturated Conditions.

Figure 12 is a plot of ultimate strain in the dry specimens versus test temperature. The baseline 3502 had a sharp increase in strain at 82°C, but remained below 2 percent. The 914 system had the lowest average strain-to-failure (ca. 1 percent). The 2220-1 showed a linear increase in average tensile strain from 1.4 percent to just slightly more than 2 percent while the 2220-3 showed a much more rapid increase with temperature.

Ultimate strains for the moisture-saturated specimens also increased as a function of temperature, as shown in Figure 13, and were similar to those obtained in the dry specimens. Again, the 3502 baseline resin exhibited the smallest strain, Fibredux 914 was slightly higher, and the 2220-1 and 2220-3 were much higher at all temperatures.

Poisson's ratio, $\nu$, was also measured for all four resin systems, for all test conditions. Results are plotted in Figures 14 and 15. The Poisson's ratio of the dry specimens appeared to be insensitive to temperature but increased perceptively in moisture-saturated specimens. All the resins exhibited a slightly higher value of $\nu$ overall than previously encountered in untoughened epoxies [3]. Values greater than 0.4 were common for the moisture-saturated specimens, whereas values of 0.32 to 0.36 would be more common for an untoughened epoxy [3]. This increase might be attributed to the more thermoplastic nature of these toughened epoxy systems. It is not known why the 3502 untoughened epoxy exhibited the high $\nu$ at elevated temperature when moisture saturated.

### 3.3 Torsional Shear Tests

All torsional shear testing was done in an Instron Model 1125 universal testing machine. A rotometer developed at the University of Wyoming was used to measure shear strains. A complete description of the

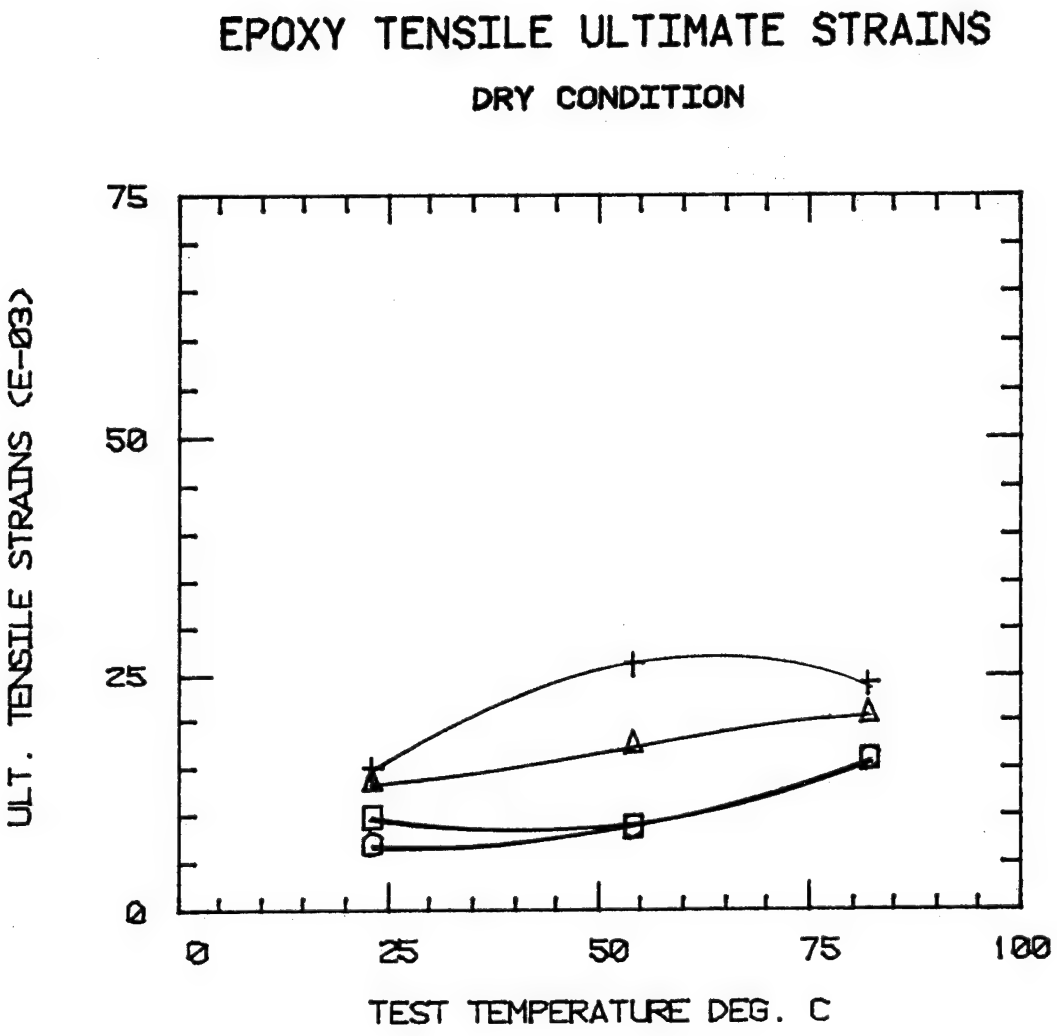


Figure 12. Ultimate Tensile Strains as a Function of Temperature, Dry Conditions.

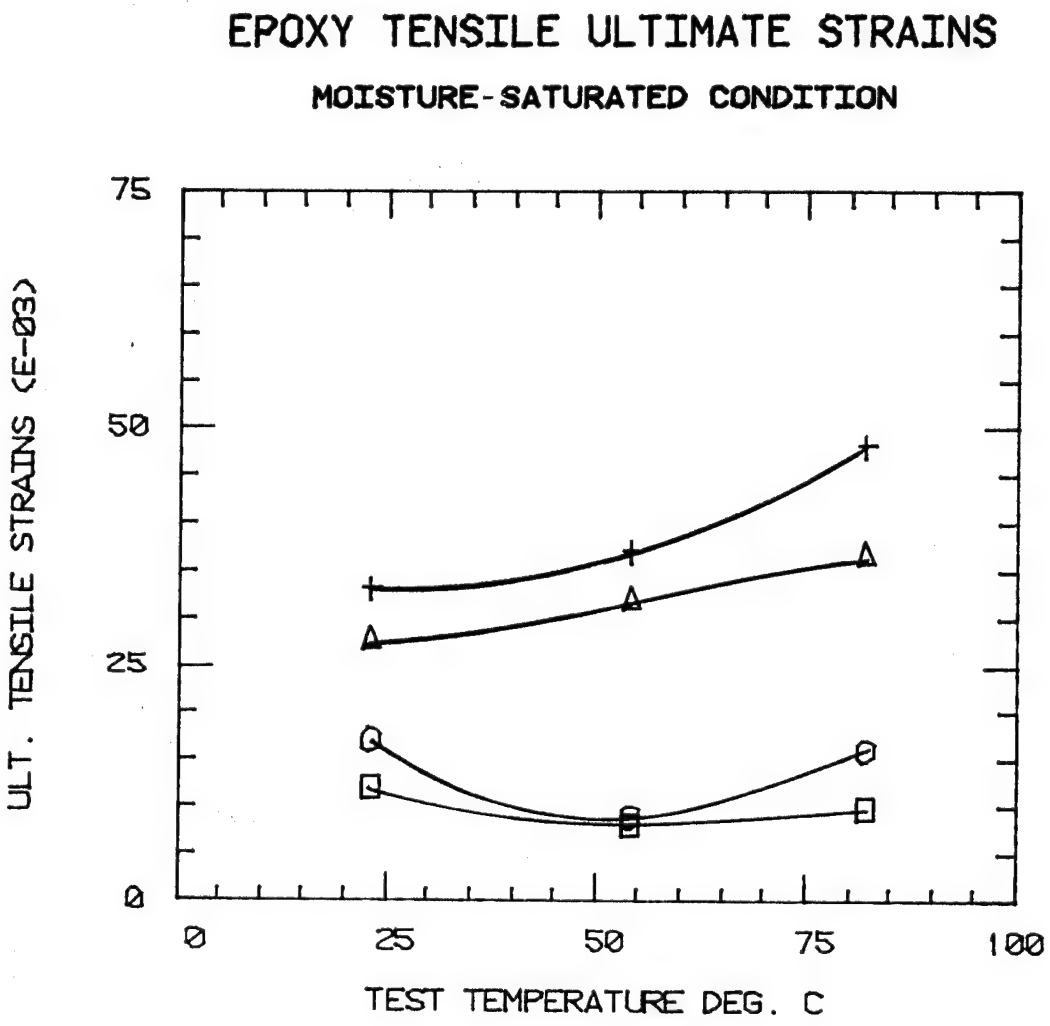


Figure 13. Ultimate Tensile Strains as a Function of Temperature, Moisture-Saturated Conditions.

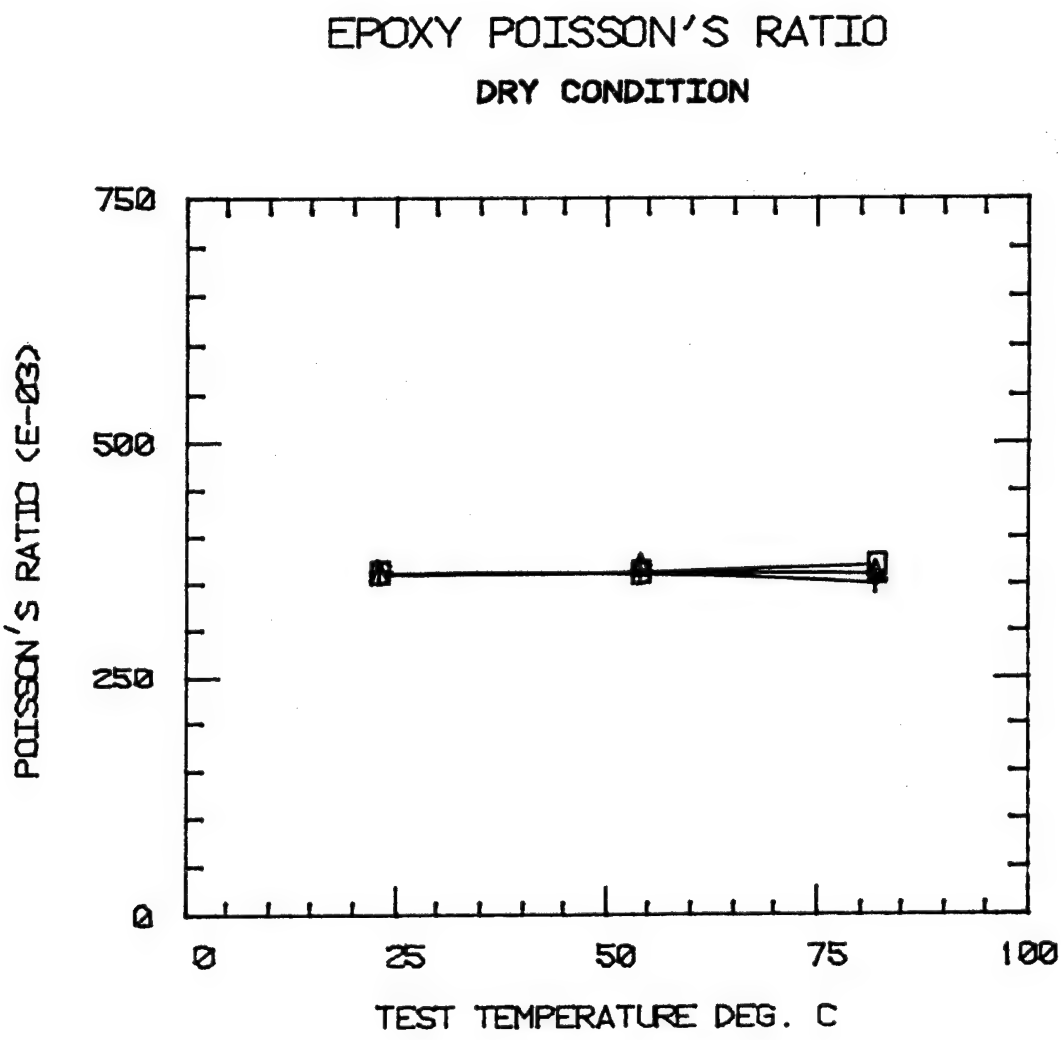


Figure 14. Poisson's Ratio as a Function of Temperature, Dry Conditions.

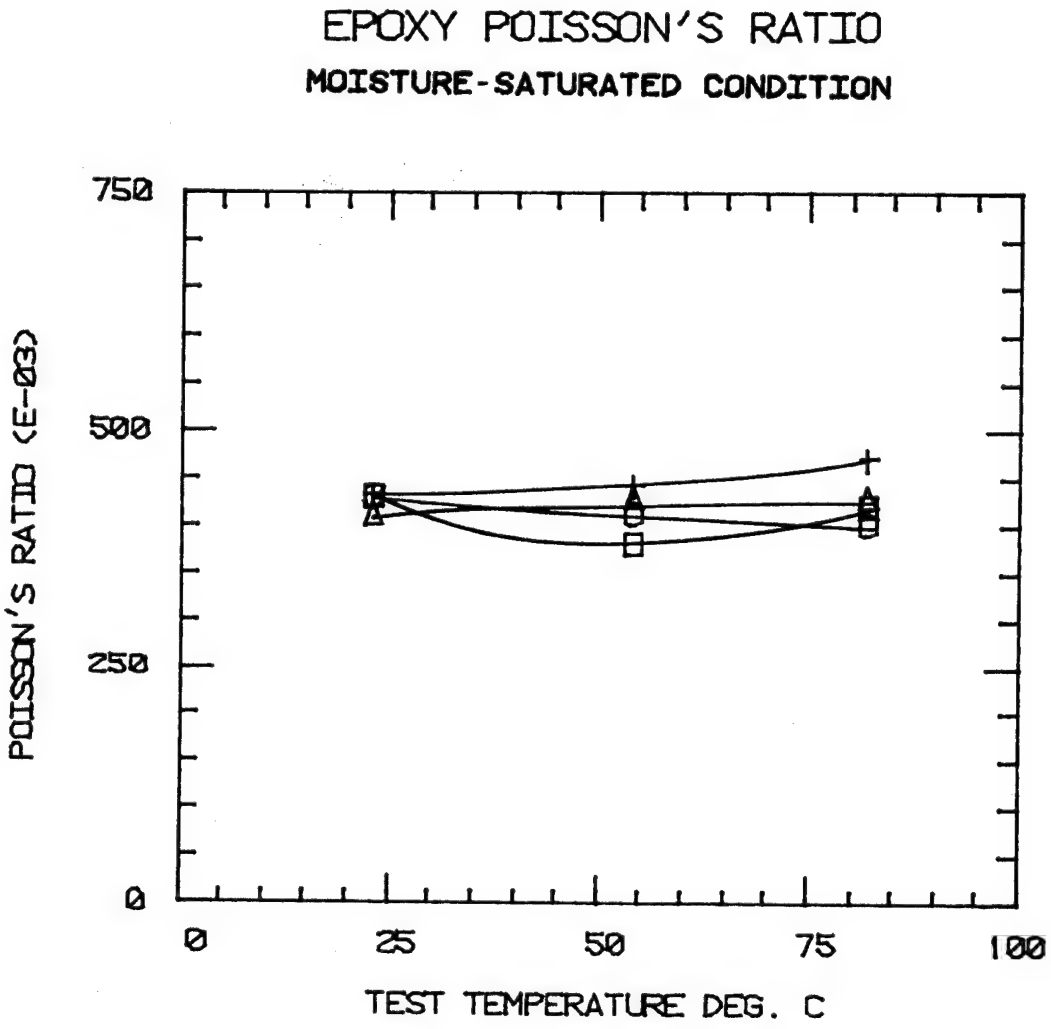


Figure 15. Poisson's Ratio as a Function of Temperature, Moisture-Saturated Conditions.

rotometer and the shear test method is given in Appendix B of Volume II.

Shear strength, shear modulus, and shear strain-to-failure were measured on all specimens. Stress-strain curves to failure are included in Appendix C of Volume II.

Average shear strengths for the four dry epoxy resins are plotted in Figure 16. The untoughened baseline 3502 epoxy had the lowest shear strength at room temperature and its strength was relatively unaffected as test temperature was increased. The shear strength of the 914 was the highest of the four resins at room temperature, decreased at 54°C, and then recovered almost to its room temperature value at 82°C. Strengths of the 2220-1 and 2220-3 were relatively unaffected by temperature.

Figure 17 is a photograph of a shear failure typical of all four resins. The center section of the specimen is missing because the shear failures shatter the gage section of the specimen. The remaining ends have been placed close to their original spacing in an intact specimen. A 1 to 3 cm length of material was fragmented at failure, being reduced to very small chips and dust by the release of energy.

Figure 18 is a plot of moisture-saturated average shear strength versus temperature. As with tensile strengths, the shear strengths also decreased significantly under hot/wet conditions. The Hercules 3502 baseline system exhibited the lowest shear strength at room temperature and the strength seemed relatively unaffected by temperature. Contrawise, the shear strength of 914 decreased rapidly at 54°C and 82°C to values below all other systems. The 2220-1 and 2220-3 shear strengths were higher than those of the other two resins at all temperatures, although the values for 2220-1 were less affected by temperature.

Figures 19 and 20 are photographs of typical failed

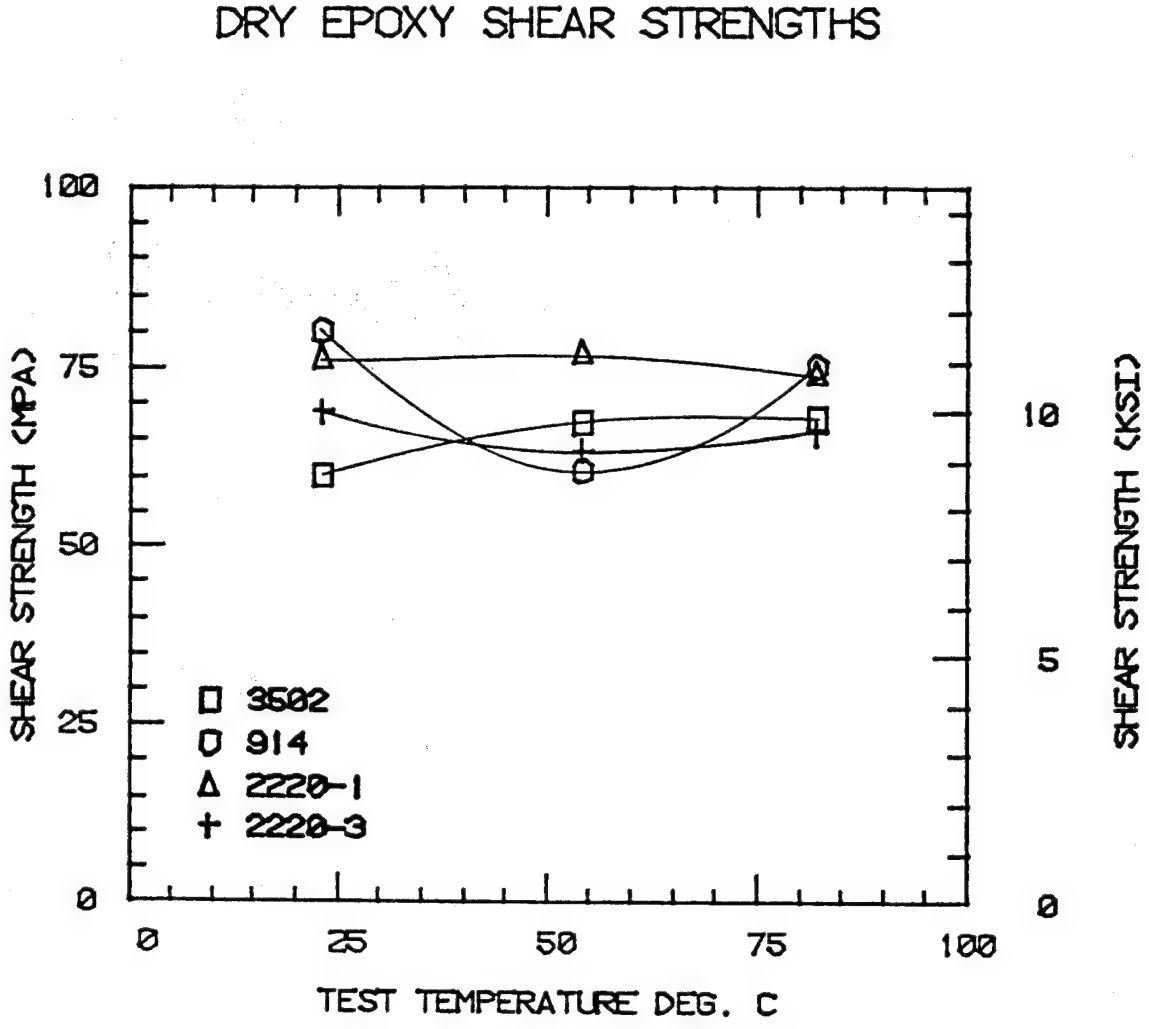


Figure 16. Shear Strengths as a Function of Temperature, Dry Conditions.

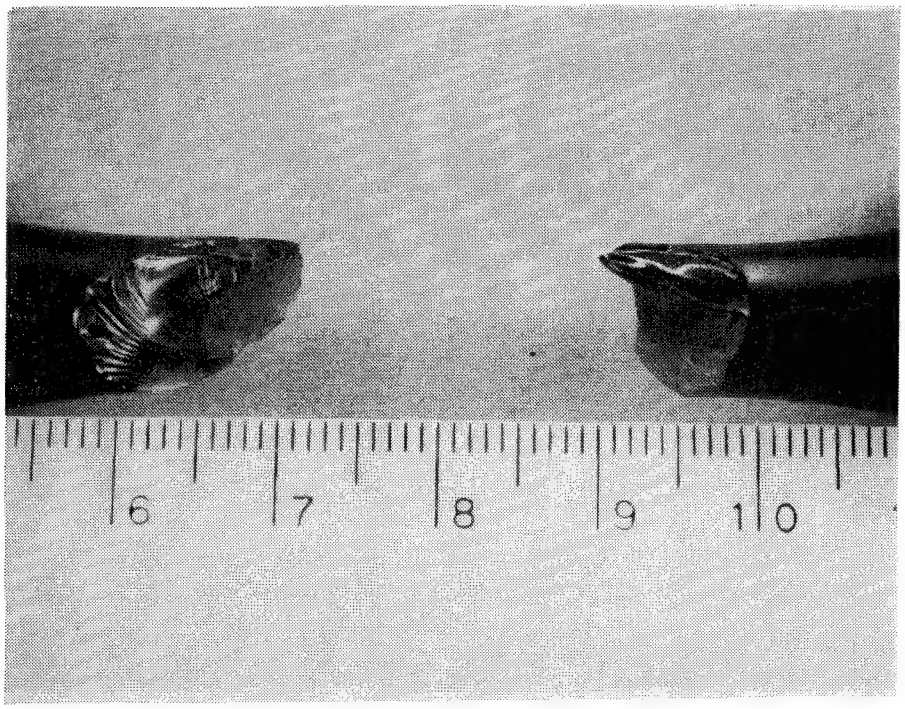


Figure 17. Typical Failed Hercules 3502 Torsional Shear Specimen, 54°C, Dry.

This photograph is a typical torsional shear failure for all shear tests. All four resins exhibited this transitional fracture appearance from smooth to rippled surface regardless of temperature. The ends of this failed specimen have been placed at the approximate positions they had in the untested specimen. More than two centimeters of the gage section length were totally shattered and unrecoverable after the failure, as indicated here.

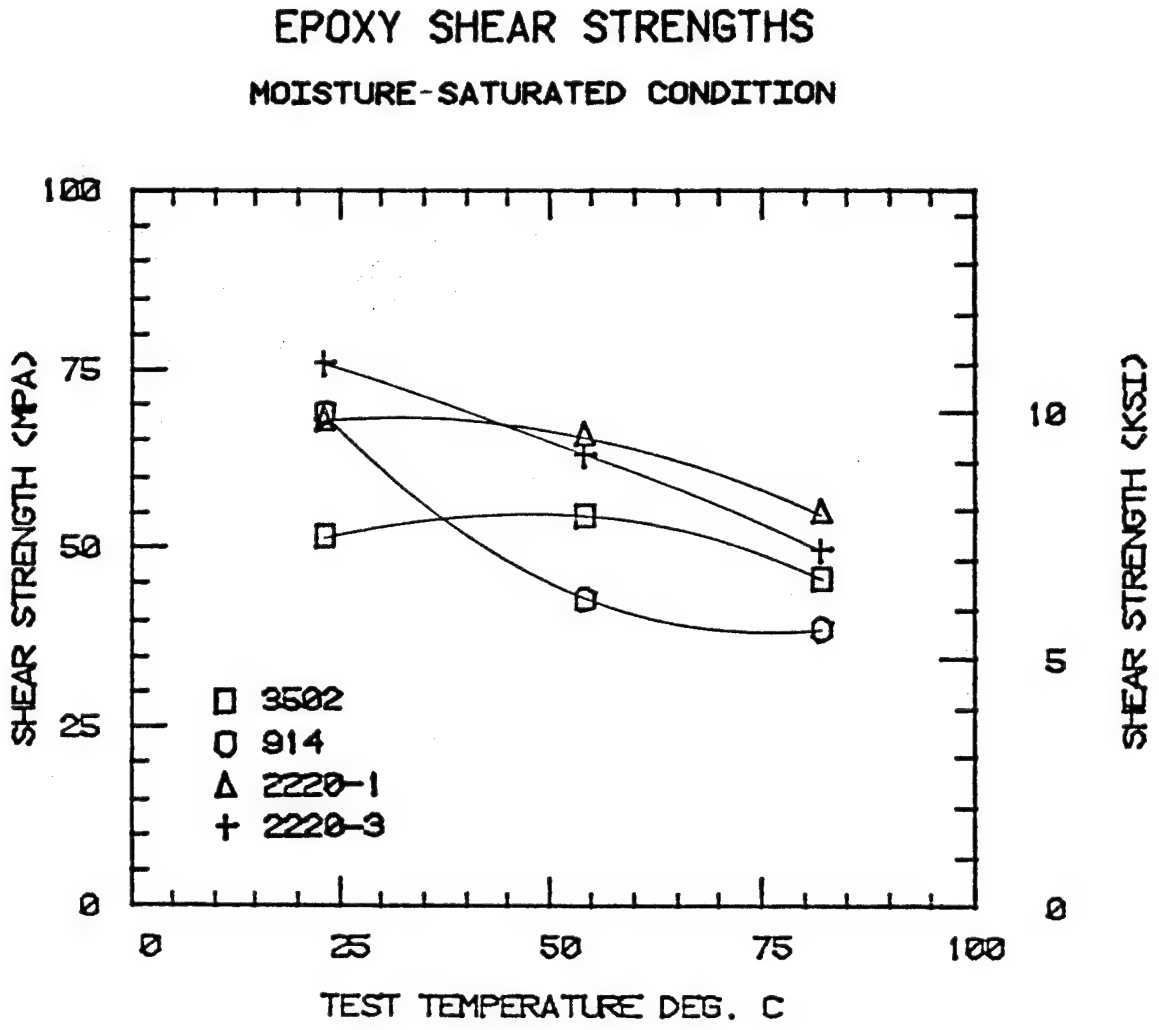


Figure 18. Shear Strengths as a Function of Temperature, Moisture-Saturated Conditions.

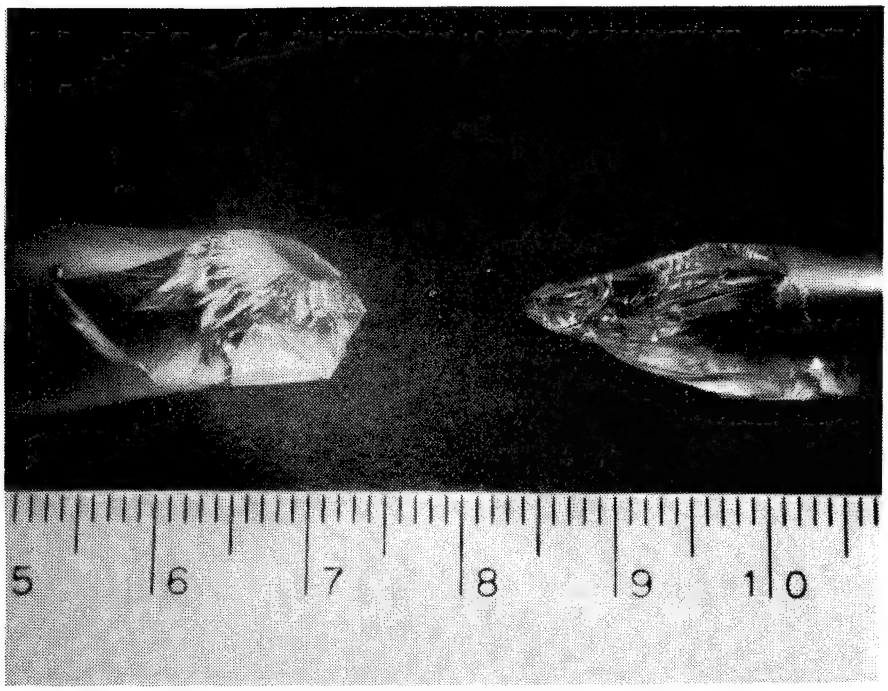


Figure 19. Typical Failed Hercules 2220-1 Torsional Shear Specimen, 82°C, Moisture-Saturated Conditions.

The glassy appearance in some areas and the probable failure initiation site at the top of the lefthand piece will be noted. This initiation site is within the smooth area, which transitions into a coarser surface as the failure progresses.

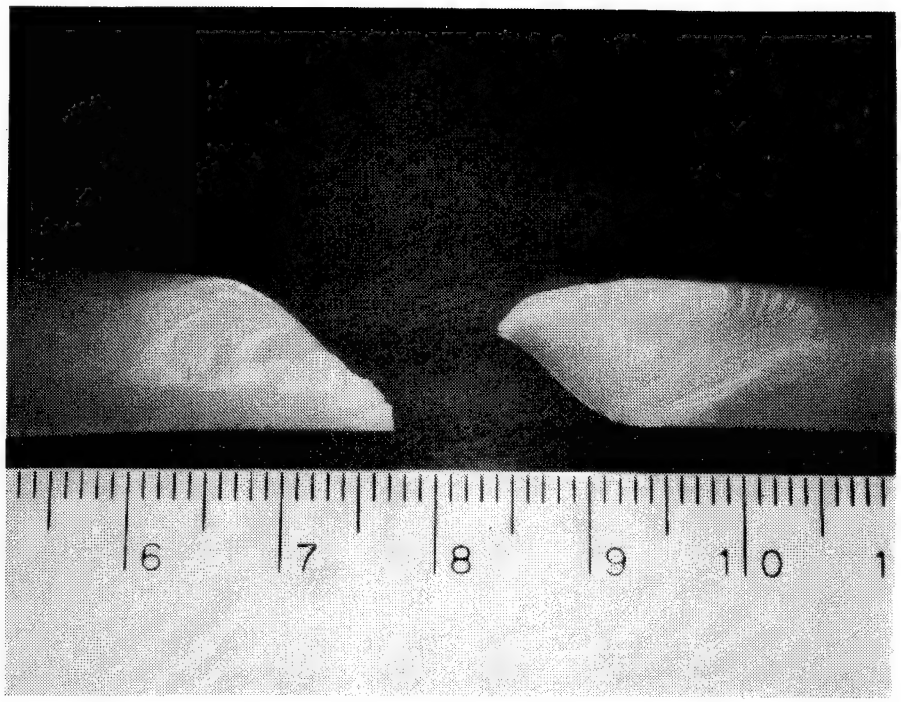


Figure 20. Typical Failed Fibredux 914 Torsional Shear Specimen, 82°C, Moisture-Saturated.

This photograph shows the smooth failure initiation site at the bottom of the righthand piece. The transition into the lined area is not as localized in this specimen as it is for the specimen shown in Figure 17.

moisture-saturated torsion specimens of the 2220-1 and 914 epoxies tested at 82°C. The 2220-1 specimen displayed a glassy appearance whereas the 914 showed the curved lines and smooth areas seen in many failed moisture-saturated specimens.

The 2220-3 toughened epoxy failures appeared to be very similar to those of the 2220-1 epoxy in all cases except one. A one-of-a-kind failure was observed when the 2220-3 was tested at 54°C in the moisture saturated state. This failure illustrates a possible process by which neat epoxy systems propagate fracture lines which result in complete shattering of the gage section of the specimen. A photograph of this specimen, Figure 21, shows an internal spiral helix which, had it progressed further, would probably have resulted in the complete disintegration of the gage section, as was observed in all other shear specimen failures. The strength of this specimen was below average, and the shear strain-to-failure was quite low. A premature failure in the center presumably helped preserve the remainder of the specimen.

The shear strengths for all four epoxies averaged higher than the tensile strengths at all but one environmental condition. It is not understood why this would be the case since the shear failures were typically along the 45° (tensile) plane of the shear test specimens. Several explanations are possible. Some geometry effect between the round and flat specimens may be present. Also, inhomogeneous defects in the cured material may cause some of the disagreement. It is possible that the most highly stressed outer surface of the round torsion specimens contains fewer defects than the bulk material of the uniformly stressed flat tensile specimens. A program to study the defect-volume effect in neat resins is being undertaken by the Composite Materials

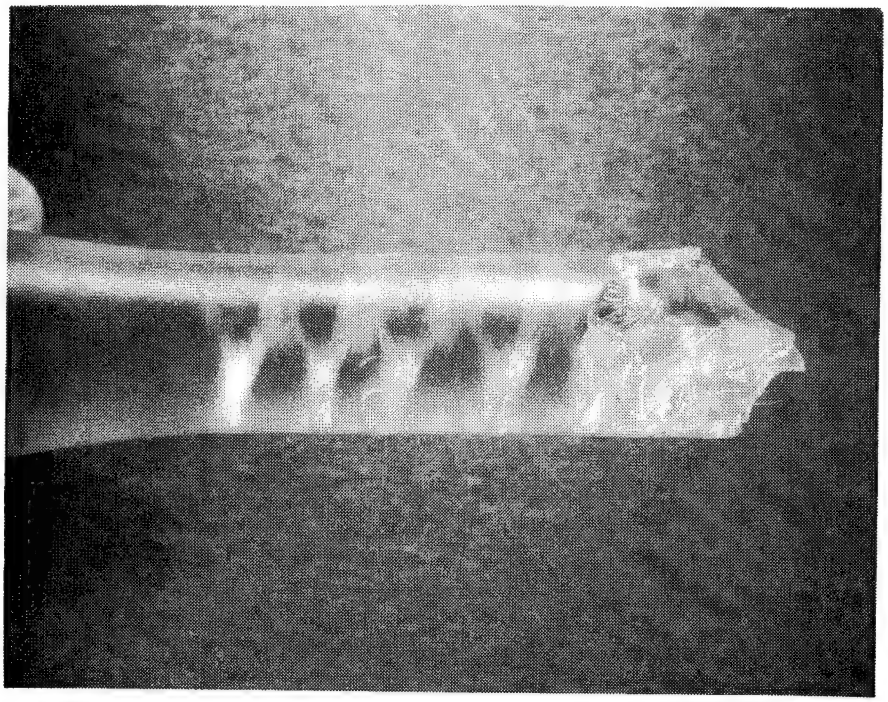

Figure 21. Failed Hercules 2220-3 Torsional Shear-Specimen, 54°C, Moisture-Saturated.

This photograph shows an internal helix failure surface. The failure cracks were blunted and preserved by the combination of moisture and temperature. While all other specimens disintegrated at failure, this one displayed graphically the failure process along its length as a tensile crack on the 45° plane.

Research Group to help resolve some of these questions.

Figure 22 is a plot of shear moduli versus temperature for the dry condition. The baseline 3502 epoxy displayed the highest shear modulus, which decreased only slightly as the test temperature was increased. This result was expected since 3502 also had one of the highest Young's moduli. The 2220-3 exhibited the lowest shear moduli at all temperatures. The 914 and 2220-1 values were intermediate and almost identical over the full test temperature range.

Shear moduli for the moisture-saturated systems are plotted in Figure 23. Data for 914, 2220-1 and 2220-3 were almost identical over the entire temperature range. The shear modulus of 3502 decreased more rapidly than those of the other three systems, which were relatively insensitive to temperature.

Ultimate shear strains for the dry neat epoxies were measured using the rotometer, and plots of strains versus temperature are given in Figure 24. The increase in strain with temperature was fairly small in the 3502 and 914 epoxies, but much larger (a three-fold increase) with both 2220 materials. This dramatic increase in shear strain is one of the most vivid changes in material behavior measured in this study.

Shear strains for moisture-saturated epoxies are plotted in Figure 25. The values for 3502 and 914 epoxies were similar to their average dry values. This indicates that moisture has little affect on the shear strain for these two systems. A comparison of Figures 24 and 25 indicates that the same is not true for the 2220-1 and 2220-3 neat epoxies. Shear strains at room temperature for dry and moisture-saturated 2220-1 specimens were quite similar. However, the strains of wet specimens drop somewhat at 82°C while those of dry

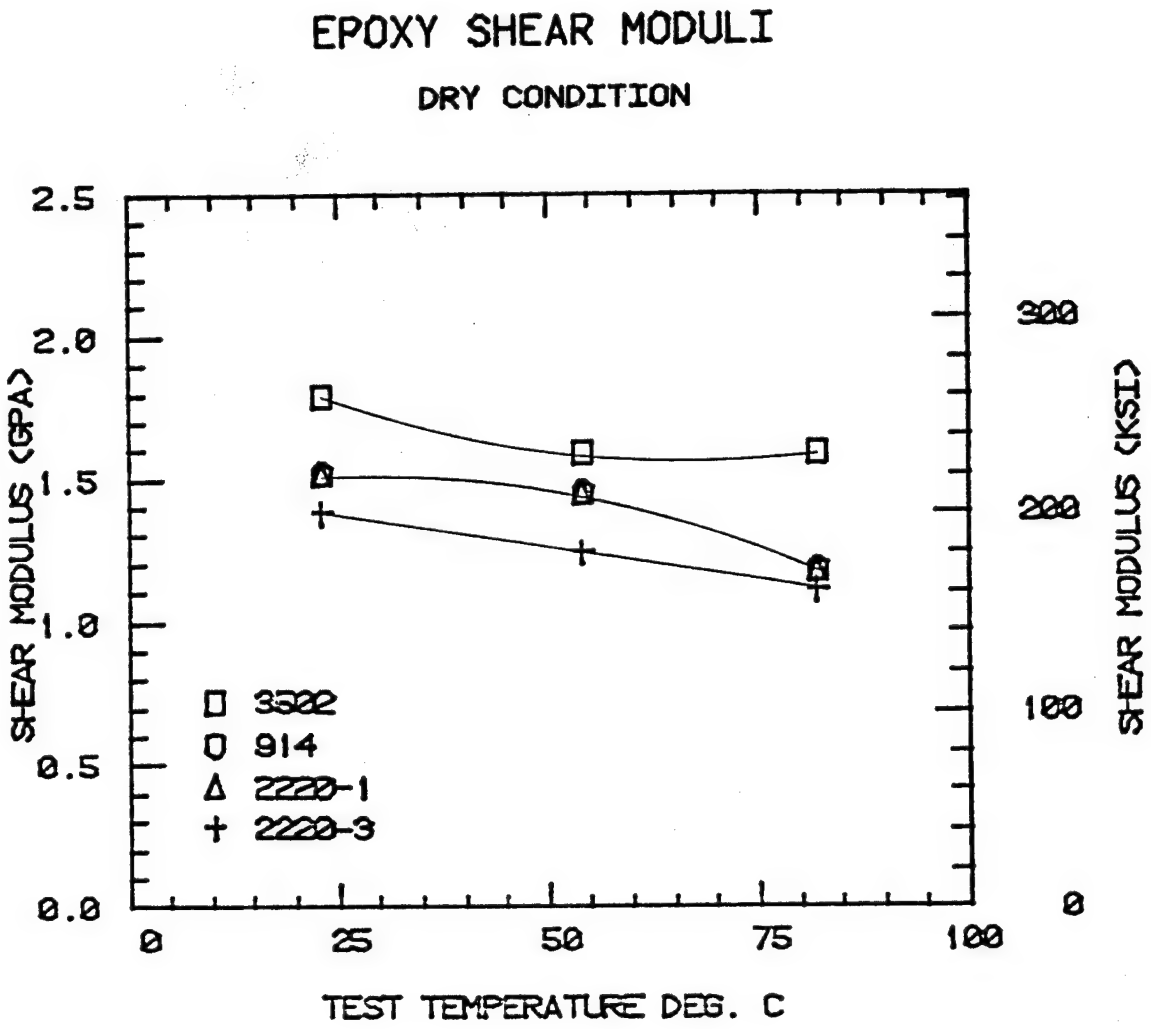


Figure 22. Shear Moduli as a Function of Temperature, Dry Conditions.

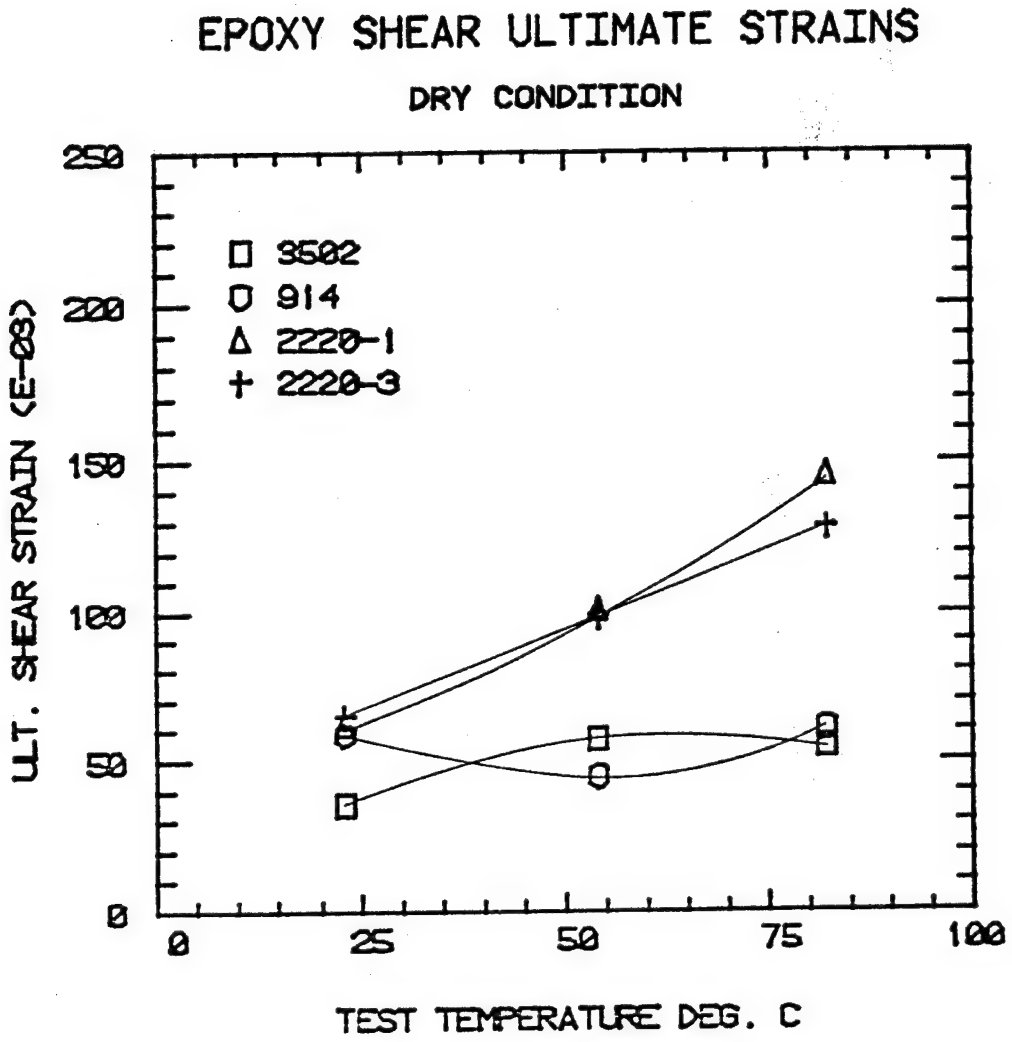


Figure 24. Ultimate Shear Strains as a Function of Temperature, Dry Conditions.

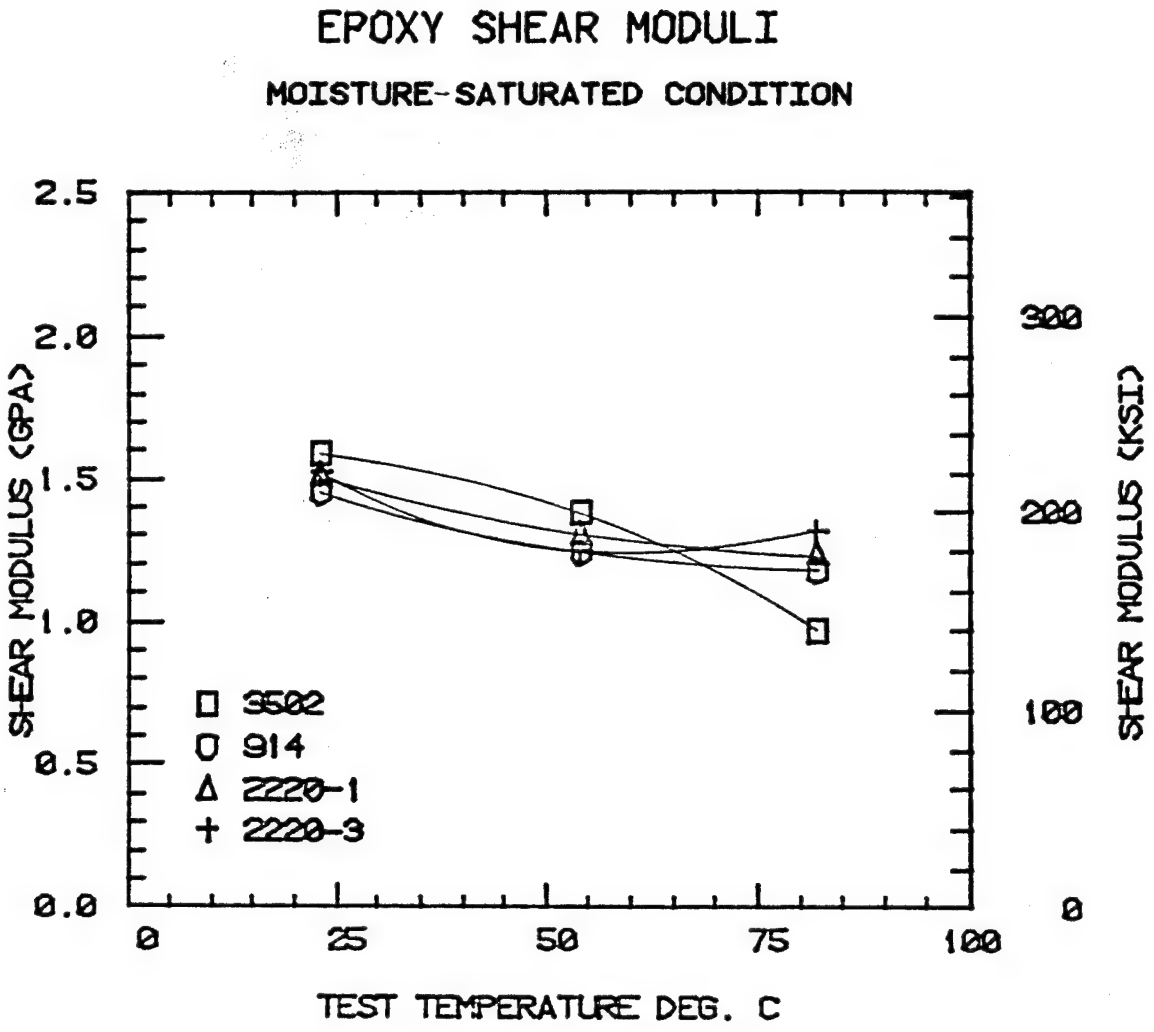


Figure 23. Shear Moduli as a Function of Temperature, Moisture-Saturated Conditions.

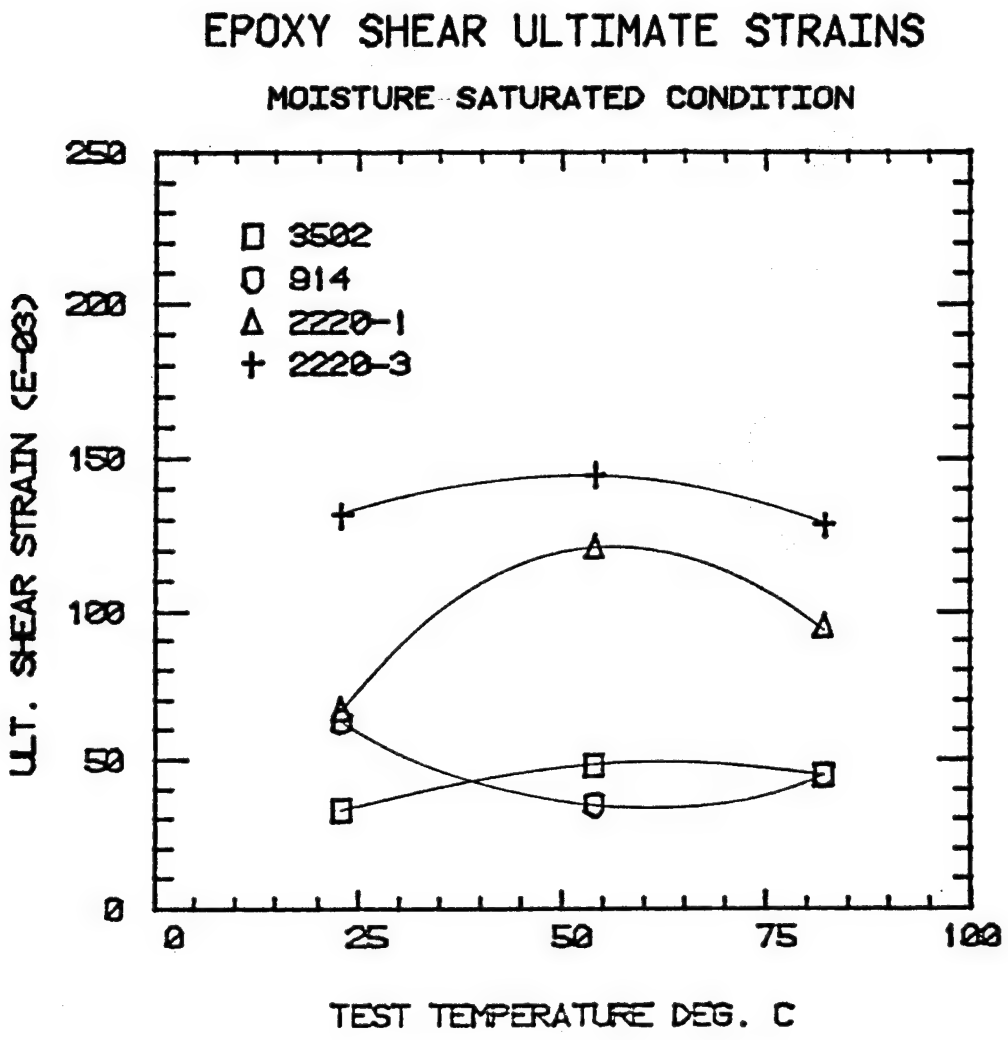


Figure 25. Ultimate Shear Strains as a Function of Temperature, Moisture-Saturated.

specimens increase dramatically. Interestingly the 2220-3 yields to a greater extent than the other resins when moisture-saturated. Its shear strain at the 23°C temperature doubles from dry to wet conditions, and remains high at the other two test temperatures. Its $\gamma_{ult}$ at 82°C is the same for both the dry and wet conditions.

The large differences between ultimate tensile strain and ultimate shear strain will be noted. Ultimate shear strain (5-15 percent) is significantly higher than ultimate tensile strain (1-5 percent). This is apparently associated with the highly nonlinear behavior in shear typically exhibited by most neat resin systems (see, for example, Reference [3]). No satisfactory rationale for this disparity has been theorized as yet.

It should also be noted that the measured stiffness properties of these neat epoxy resins do not obey the isotropic material relation between E, $\nu$ and G, i.e.,

$$G = \frac{E}{2(1 + \nu)} \tag{2}$$

Results are summarized in Table 2. As can be seen, the values of shear modulus G calculated from Eq. (2) using values of E and $\nu$ measured in the uniaxial tensile tests are consistently lower than the measured values of G. This is true for all four matrix materials, at all three test temperatures, for both dry and moisture-saturated conditions. No strong trends from material to material, or between test conditions, are apparent. The 2220 systems tested at the highest temperature in the moisture-saturated condition did indicate the greatest discrepancy, however.

Table 2

Measured and Calculated Elastic Material Constants for Four Neat Resin Systems

| Resin System | Measured Young's Modulus (GPa) | (Msi) | Measured Poisson's Ratio | Measured Shear Modulus (GPa) | (Msi) | Calculated Shear Modulus (GPa) | (Msi) | $\frac{G_{meas}-G_{calc}}{G_{meas}}$ (percent) |
|---|---|---|---|---|---|---|---|---|
| 23°C, Dry Condition | | | | | | | | |
| 3502 | 3.65 | 0.55 | 0.36 | 1.79 | 0.26 | 1.39 | 0.20 | 22 |
| 914 | 4.02 | 0.58 | 0.36 | 1.52 | 0.22 | 1.47 | 0.21 | 3 |
| 2220-1 | 2.96 | 0.43 | 0.36 | 1.52 | 0.22 | 1.09 | 0.16 | 28 |
| 2220-3 | 3.17 | 0.44 | 0.36 | 1.38 | 0.20 | 1.11 | 0.16 | 20 |
| 54°C, Dry Condition | | | | | | | | |
| 3502 | 3.24 | 0.47 | 0.36 | 1.59 | 0.23 | 1.19 | 0.17 | 25 |
| 914 | 3.37 | 0.49 | 0.36 | 1.52 | 0.22 | 1.24 | 0.18 | 18 |
| 2220-1 | 2.96 | 0.43 | 0.37 | 1.38 | 0.21 | 1.08 | 0.16 | 22 |
| 2220-3 | 2.96 | 0.43 | 0.36 | 1.24 | 0.18 | 1.09 | 0.16 | 12 |
| 82°C, Dry Condition | | | | | | | | |
| 3502 | 3.10 | 0.45 | 0.37 | 1.59 | 0.23 | 1.13 | 0.16 | 29 |
| 914 | 3.17 | 0.46 | 0.37 | 1.38 | 0.20 | 1.16 | 0.17 | 16 |
| 2220-1 | 2.62 | 0.38 | 0.36 | 1.17 | 0.17 | 0.96 | 0.14 | 18 |
| 2220-3 | 2.41 | 0.36 | 0.35 | 1.10 | 0.16 | 0.92 | 0.13 | 16 |
| 23°C, Wet Condition | | | | | | | | |
| 3502 | 3.52 | 0.51 | 0.43 | 1.58 | 0.23 | 1.23 | 0.18 | 22 |
| 914 | 3.10 | 0.45 | 0.43 | 1.45 | 0.21 | 1.08 | 0.16 | 26 |
| 2220-1 | 3.11 | 0.45 | 0.41 | 1.52 | 0.22 | 1.10 | 0.16 | 28 |
| 2220-3 | 3.03 | 0.44 | 0.43 | 1.52 | 0.22 | 1.06 | 0.15 | 30 |
| 54°C, Wet Condition | | | | | | | | |
| 3502 | 3.03 | 0.44 | 0.38 | 1.38 | 0.20 | 1.10 | 0.16 | 20 |
| 914 | 2.55 | 0.37 | 0.41 | 1.24 | 0.18 | 0.90 | 0.13 | 27 |
| 2220-1 | 2.56 | 0.37 | 0.43 | 1.31 | 0.19 | 0.90 | 0.13 | 31 |
| 2220-3 | 2.41 | 0.35 | 0.44 | 1.24 | 0.18 | 0.84 | 0.12 | 32 |
| 82°C, Wet Condition | | | | | | | | |
| 3502 | 2.58 | 0.37 | 0.42 | 0.97 | 0.14 | 0.90 | 0.13 | 7 |
| 914 | 2.14 | 0.31 | 0.40 | 1.17 | 0.17 | 0.76 | 0.11 | 35 |
| 2220-1 | 2.07 | 0.30 | 0.43 | 1.24 | 0.18 | 0.72 | 0.10 | 40 |
| 2220-3 | 2.14 | 0.31 | 0.47 | 1.31 | 0.19 | 0.73 | 0.11 | 44 |

It should be emphasized that both the tensile test and the torsional shear test are well established straightforward techniques, and five replicates were used to establish the averages given in Table 2. Thus, these data are considered very reliable. It should also be noted that a similar discrepancy between the isotropic relation (Eq. 2) and experimental data was reported for Hercules 3501-6 epoxy in Reference [3]. That is, the data presented here do not represent an isolated finding. It is planned to investigate this unexpected polymer material response in more detail in a future study.

### 3.4 Fracture Toughness Tests

Fracture toughness testing was performed using the notched bend fracture toughness method described in ASTM E319 [5]. A complete description of the test method used is given in Appendix B of Volume II and in Reference [5]. A larger number of samples than for tension and torsion testing was used for this testing due to the expected scatter for neat resin materials. However, the $G_{IC}$ values measured appeared to be about an order of magnitude too high. Thus, no results are presented here. In retrospect it appears that the precrack was not introduced properly.

### 3.5 Coefficient of Thermal Expansion Tests

Coefficients of thermal expansion, CTE, were measured with a glass-tube dilatometer apparatus utilizing an LVDT and X-Y plotter for recording the change in length versus temperature. A detailed description of the apparatus and test method is included in Appendix B of Volume II. Only two specimens from each of the four resin systems were tested in the dry and moisture-saturated conditions. The data for CTE displayed a high degree of scatter and are not considered reliable.

Additional testing will be performed during the follow-on study to provide a much better basis for the CTE values. Improvement to the apparatus will also be made to alleviate the high variance encountered during the present testing. A linear regression curve-fit computer routine was used to calculate the best-fit equation for the data points. These equations are listed in Table 3. Coefficient of thermal expansion (CTE) values as a function of temperature are shown in Figures 26 and 27, for dry and moisture-saturated conditions, respectively. The Hercules 3502 baseline resin exhibited the lowest CTE of the four resin systems; the value is similar to those previously measured on Hercules 3501-6 epoxy, which is also an MY720 base epoxy system [4]. All CTE values were fairly linear with temperature except those for 914, which increased 50 percent from room temperature to 82°C, probably because of the presence of a thermoplastic additive. CTE values for moisture-saturated specimens remained fairly constant over the temperature range studied.

### 3.6 Coefficient of Moisture Expansion Tests

Coefficients of moisture expansion, CME, of the four neat epoxy resins were measured by using exposure conditions from dry to moisture saturation. A glass tube dilatometer apparatus with an LVDT was used to measure the expansion in a moisture chamber, while an electronic balance was used to simultaneously measure the moisture weight gain of a second specimen of equal size and thickness in the same chamber. A complete description of the apparatus and test method is given in Appendix B of Volume II. A linear regression curve-fit computer program was used to fit the data and to calculate CME's. These values are given in Table 4. The CME, or $\beta$, values compare favorably with those of other epoxy

Table 3

Coefficients of Thermal Expansion
(curve-fit equations, where T is in °C)

Hercules 3502 Epoxy

| | |
|---|---|
| Dry | $\alpha$ = 3.691E-05+3.581E-08*T*2.0+3.075E-10*T**2*3.0 |
| Moisture-Saturated | $\alpha$ = 4.319E-05+3.065E-07*T*2.0-1.718E-09*T**2*3.0 |

Fibredux 914 Epoxy

| | |
|---|---|
| Dry | $\alpha$ = 1.868E-06-8.231E-08*T*2.0-9.766E-11*T**2*3.0 |
| Moisture-Saturated | $\alpha$ = 5.881E-05-2.533E-08*T*2.0+2.010E-10*T**2*3.0 |

Hercules 2220-1 Epoxy

| | |
|---|---|
| Dry | $\alpha$ = 1.334E-05-1.237E-07*T*2.0-2.651E-10*T**2*3.0 |
| Moisture-Saturated | $\alpha$ = 1.612E-04-2.286E-06*T*2.0+1.584E-08*T**2*3.0 |

Hercules 2220-3 Epoxy

| | |
|---|---|
| Dry | $\alpha$ = 2.354E-05+4.365E-08*T*2.0-7.772E-11*T**2*3.0 |
| Moisture-Saturated | $\alpha$ = 4.984E-05+3.039E-07*T*2.0-1.647E-09*T**2*3.0 |

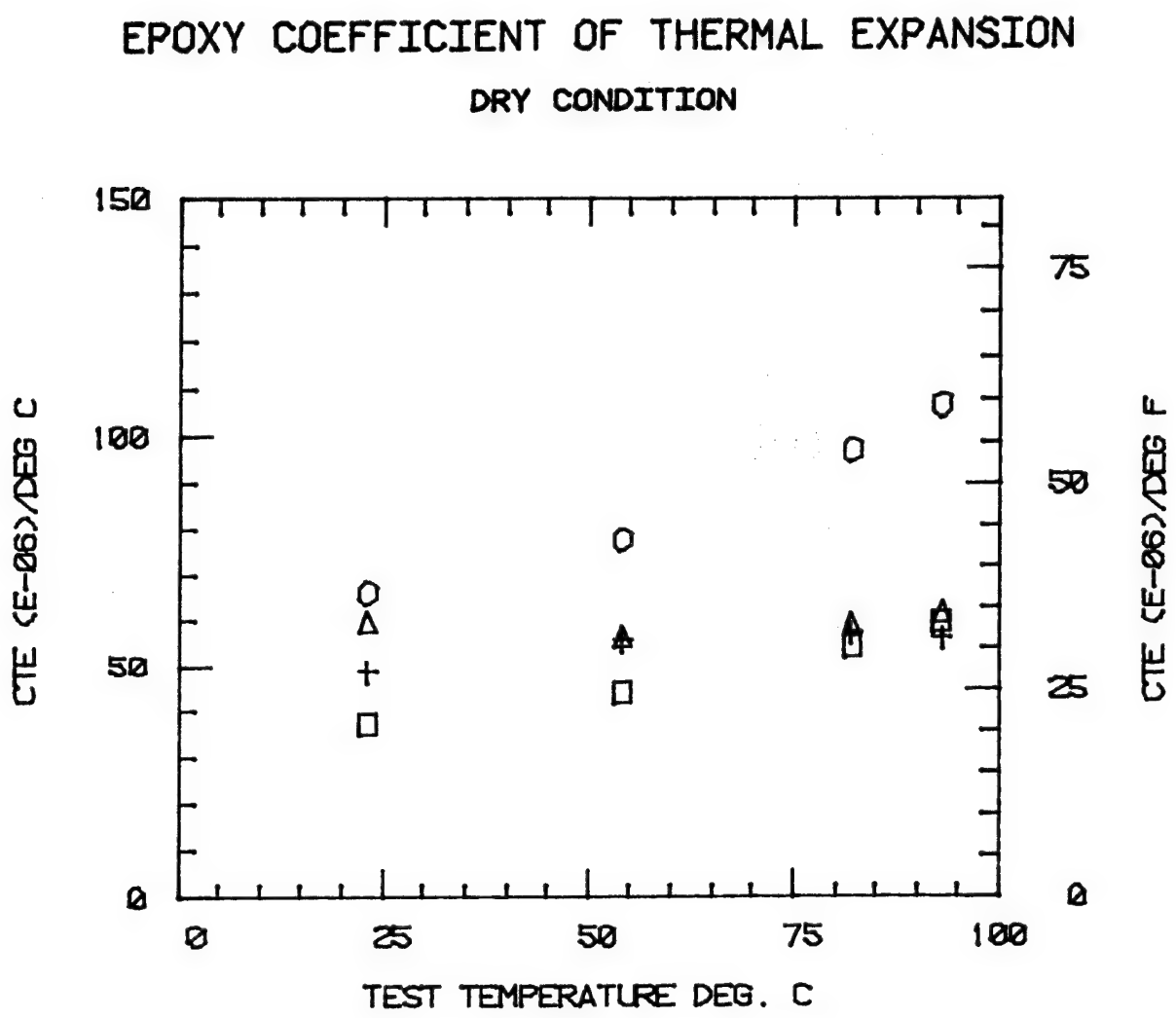


Figure 26. Coefficient of Thermal Expansion as a Function of Temperature, Dry Condition.

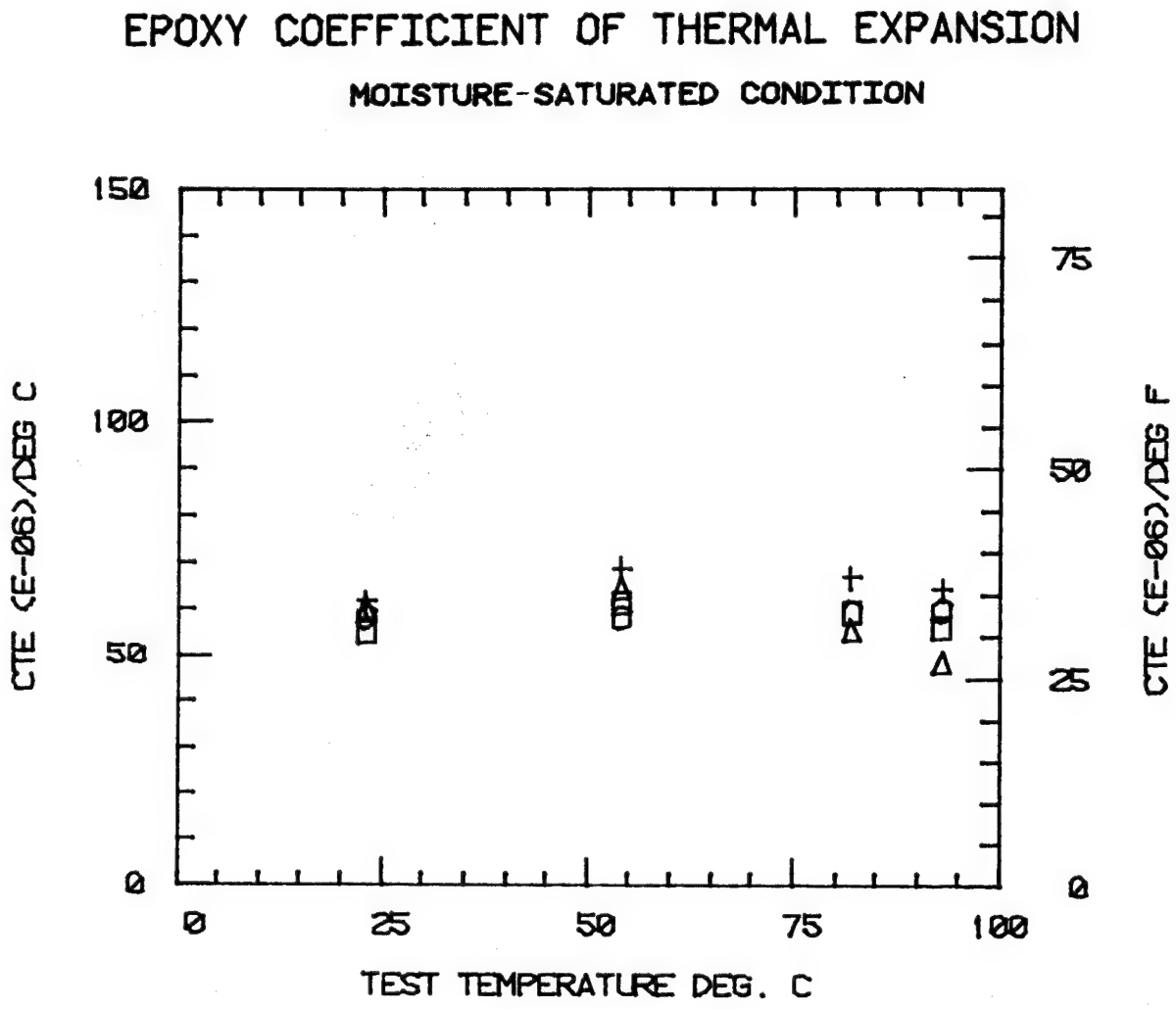


Figure 27. Coefficient of Thermal Expansion as a Function of Temperature, Moisture-Saturated.

systems [4], except the data tend to have higher scatter than previously observed.

Table 4

Coefficients of Moisture Expansion
(Dry to Saturation at 98% RH, 74°C)

3502 Neat Epoxy

$\beta$ = 1.925E-03/%M

Fibredux 914 Neat Epoxy

$\beta$ = 2.132E-03/%M

2220-1 Neat Epoxy

$\beta$ = 1.547E-03/%M

2220-3 Neat Epoxy

$\beta$ = 2.499E-03/%M

# SECTION 4

# SCANNING ELECTRON MICROSCOPE RESULTS

## 4.1 Introduction

A JEOL JSM-35C scanning electron microscope was used for all of the work of the present study. This relatively new instrument has a magnification range from 10X to 180,000X, a depth of field of 30μ at 1000X, and a resolution of 60Å.

## 4.2 Specimen Preparation

A total of 55 specimens were mounted for examination, representing all of the environmental conditions for the tension and shear testing of the four neat epoxy resins. One-inch diameter SEM specimen mounts were used.

A Buehler No. 4150 silicon carbide cutoff blade was used to cut the SEM specimens from the failed test articles. A silver conducting paint was used to bond the SEM specimens to the brass mounts, after which the specimens were ultrasonically cleaned to remove loose surface debris. All specimens were subsequently vapor-coated with gold to make them electrically conductive.

## 4.3 Explanation of SEM Photographs

Specimens representing all test temperatures, moisture conditions, and test types were studied. On the following pages, SEM photographs are shown along with, to the extent possible, a description/interpretation of the fracture surface features.

The photographic system of the SEM records information directly across the bottom of each SEM photograph. Referring, for example, to Figure 28, the caption reads:

25 KV X20 5039 1000.0U UW83

The interpretation is as follows:

25 KV electron beam accelerating voltage, in kilovolts

X20 magnification

5039 photograph number

1000.0U length of the scale bar, in microns

UW83 the SEM unit identification number, i.e., University of Wyoming and the current year, 1983

The specimen numbering system is summarized here for convenience. A typical specimen identification is divided into three sets of characters. For example, the specimen number in Figure 28 is LTWA33. This is interpreted as follows:

L identifies the program, for NASA-Langley, related to the neat resin testing program

TWA identifies the type of specimen, environmental condition, and test temperature

33 identifies the resin system and specimen number

The complete set of codes, for all specimens tested, is as follows:

Type of Mechanical Test

T - Tension

S - Shear

Specimen Conditioning

D - Dry

W - Moisture-Saturated

Test Temperature

A - Room temperature

B - 54°C

C - 82°C

Individual Neat Resin Specimen Numbers

| | |
|---|---|
| 00-10 | Hercules 2220-1 epoxy |
| 11-20 | Hercules 2220-3 epoxy |
| 21-30 | Fibredux 914 epoxy |
| 31-40 | Hercules 3502 epoxy |

Usually, only five specimens at any condition were tested so only the first five numbers from any one group were used.

## 4.4 Fracture Surfaces from Neat Resin Tension Tests

Fracture surfaces of both dry and moisture-saturated neat resin tension specimens were studied in the SEM. There are a number of prominent features associated with a tensile-type failure. The primary feature is a smooth surface with radial striations emanating in all directions. Within this smooth region is what is suspected to be a failure initiation site. This site could be a void, a contamination particle, or a location of a statistically weak crosslinking network. Numerous SEM closeups are included to help discern which of these features initiated a particular failure. Bordering the smooth region which surrounds the suspected failure initiation site is a transition region connected to a very coarse appearing region. This transition region is comprised, in most cases, of radial lines thought to be caused by a rapid propagation of the failure and concurrent rapid increase in stress level. The outer, very coarse, region is considered to be formed during the final stages of fracture, and is generated immediately before catastrophic fracture of the specimen. The coarseness is thought to be created when the fracture surface splits into many planes and cracks and propagates across the specimen. For the four resins involved in this program, a relatively large triangular chip was a common artifact of

this fracture mode and was almost never recovered after fracture. Frequently, the region adjacent to the chip area contained fracture cracks. The actual chip, when recovered and viewed as in Figure 7, contained many internal fracture lines.

The following SEM photographs are a sampling of representative views of tensile failure surfaces. One specimen from each test condition was examined.

Some general observations can be made. For most of the specimens, the smooth region surrounding the failure initiation site seemed to become more coarse as temperature and/or humidity increased. The relative size of the smooth area to the overall fracture plane area was a function of tensile strength. The smaller the smooth area surrounding the failure initiation site, the higher the recorded strength. The size of the void or particle at the suspected failure initiation site appeared to have little relation to the tensile strength.

Figures 28 through 31 are photographs of typical Hercules 3502 tensile failures. Being an untoughened brittle epoxy, the rough portion of the failure was relatively small when compared to the three toughened epoxy systems.

Figures 32 through 38 are SEM photographs of the Fibredux 914. This toughened epoxy exhibited somewhat smaller smooth initiation regions than the baseline 3502 untoughened epoxy, perhaps due to the greater degree of fracture surface splintering at failure. A greater sensitivity to moisture-induced stresses was also evident in this resin. Some SEM specimens even cracked during the gold vapor deposition process in vacuum. The specimens obviously dried out rapidly during this process, producing the large crack seen in Figure 34. During moisture

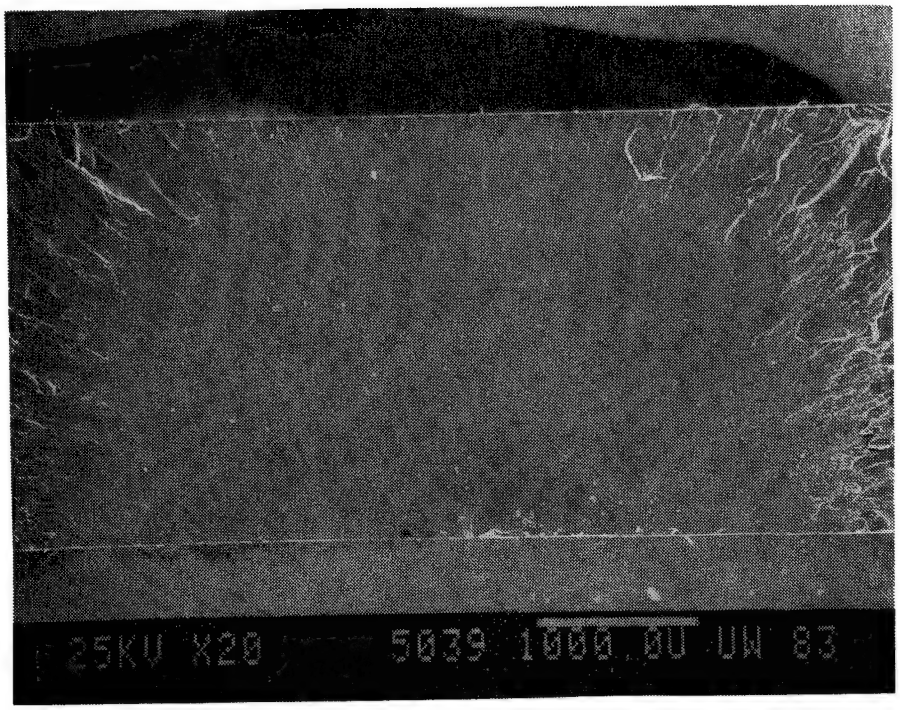


Figure 28. Failed Hercules 3502 Neat Epoxy Tensile Specimen No. LTWA33, 23°C, Moisture-Saturated.

This photograph shows a large smooth region and a comparable rough area similar to those observed in dry specimens failed at room temperature. The failure initiation site is thought to be on the bottom surface in the center of the specimen.

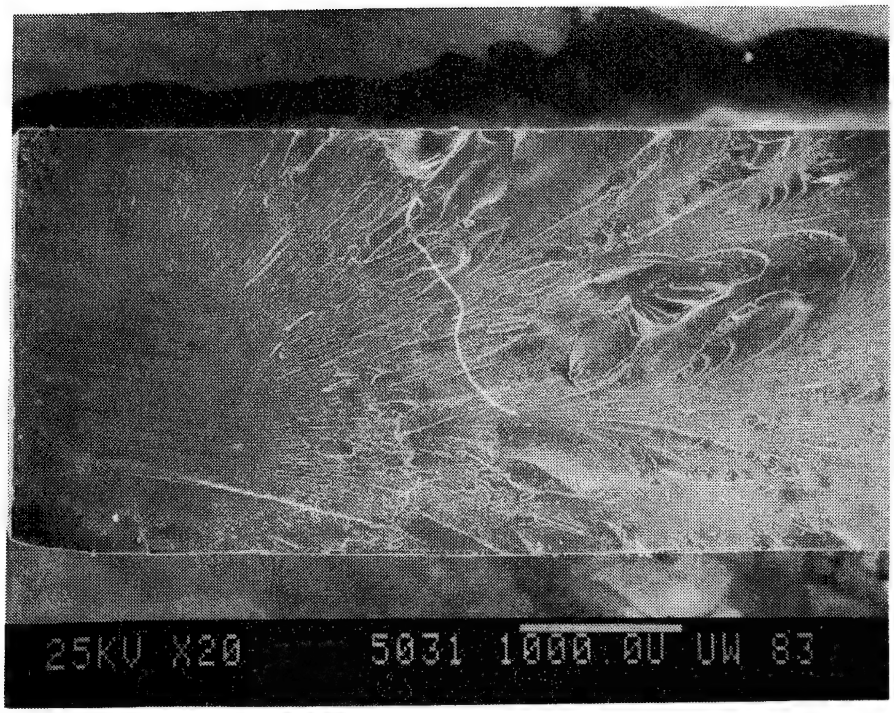


Figure 29. Failed Hercules 3502 Neat Epoxy Tensile Specimen No. LTDC32, 82°C, Dry.

This photograph is typical of tensile failure surfaces; an initiation site is seen in the center of the smooth region with a transition area containing radial lines connected to the rough region.


Figure 30. Failed Hercules 3502 Neat Epoxy Tensile Specimen No. LTDC32, 82°C, Dry.

A close-up of the suspected failure initiation site observed in Figure 29 is shown here. The site appears to be a small void about 100μ in diameter.

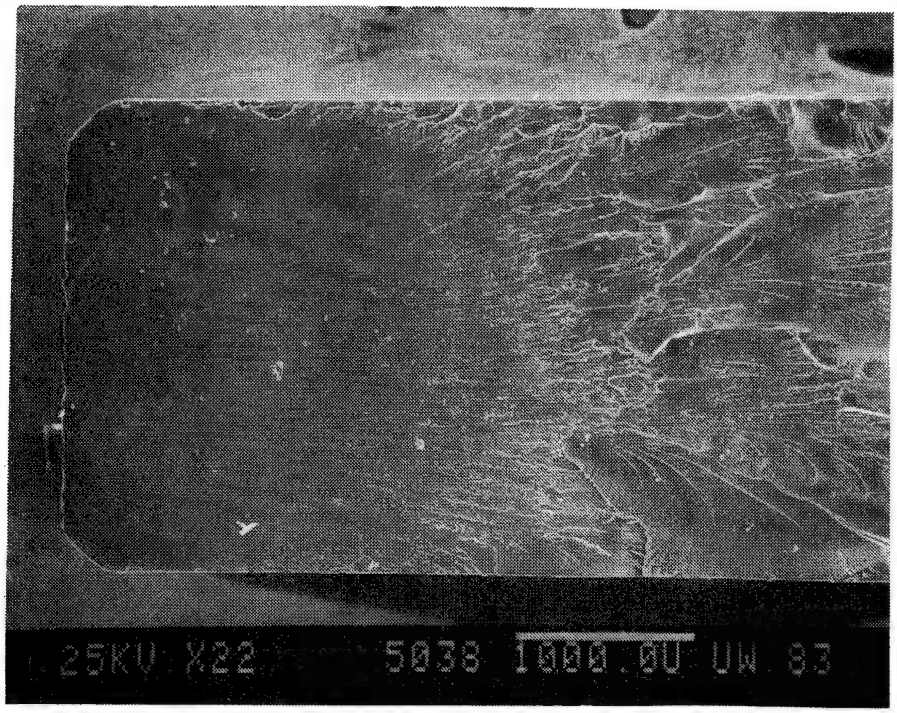


Figure 31. Failed Hercules 3502 Neat Epoxy Tensile Specimen No. LTWC35, 82°C, Moisture-Saturated.

This photograph is nearly identical in appearance to the photograph of the 82°C, dry specimen shown in Figure 29. No initiation site is clearly evident, however.

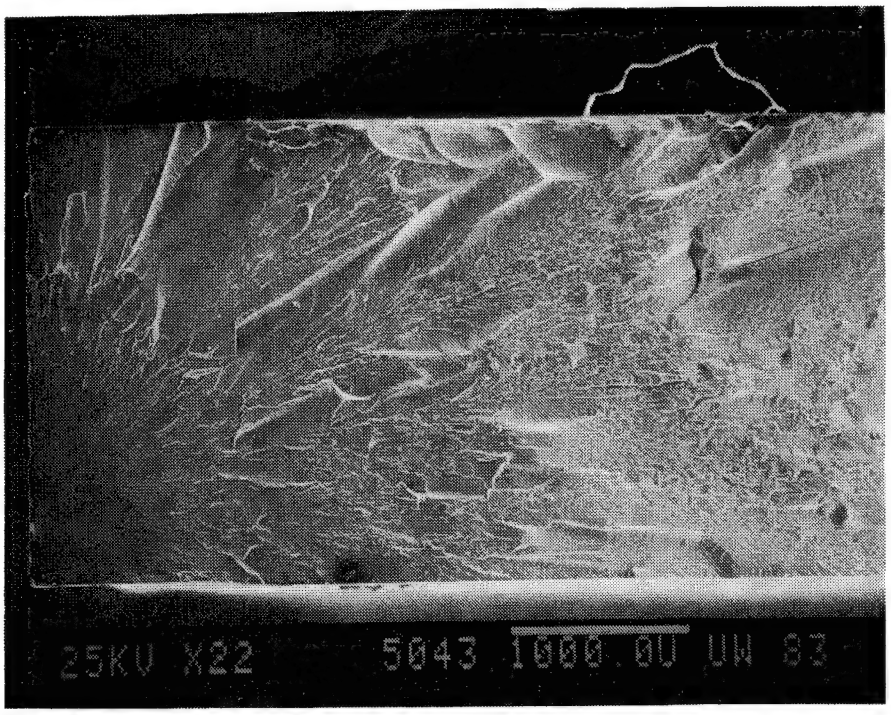


Figure 32. Failed Fibredux 914 Neat Epoxy Tensile Specimen No. LTWA24, 23°C, Moisture-Saturated.

This photograph shows a relatively small smooth area in the lower left surrounding the suspected initiation site. The large rough region mated to a larger triangular chip missing from the specimen.

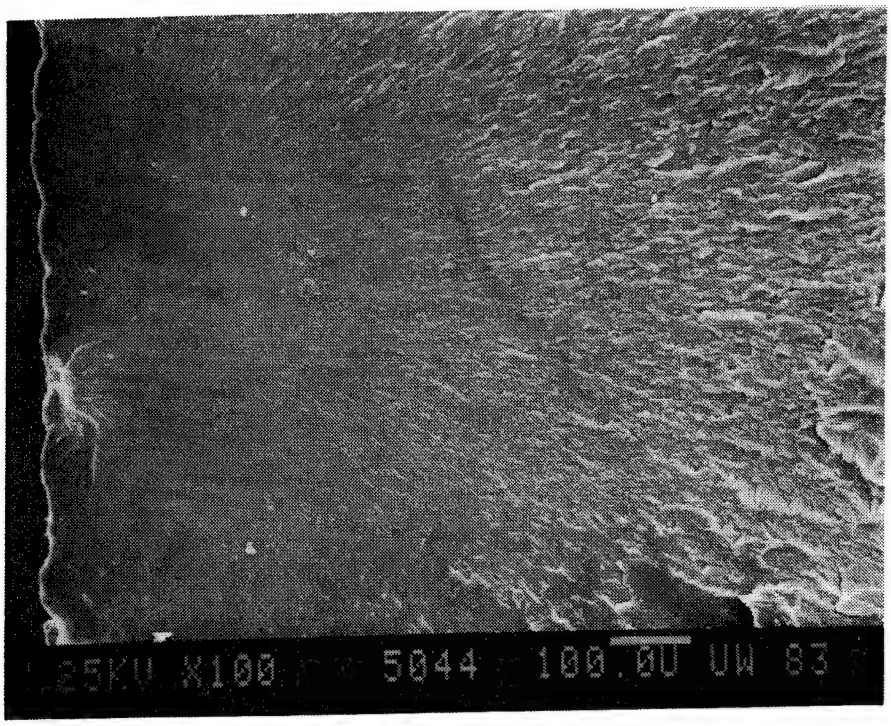


Figure 33. Failed Fibredux 914 Neat Epoxy Tensile Specimen No. LTWA24, 23°C, Moisture-Saturated.

This photograph is a close-up of the smooth area shown in Figure 32. It shows the suspected initiation site to be a void near the surface of the specimen.

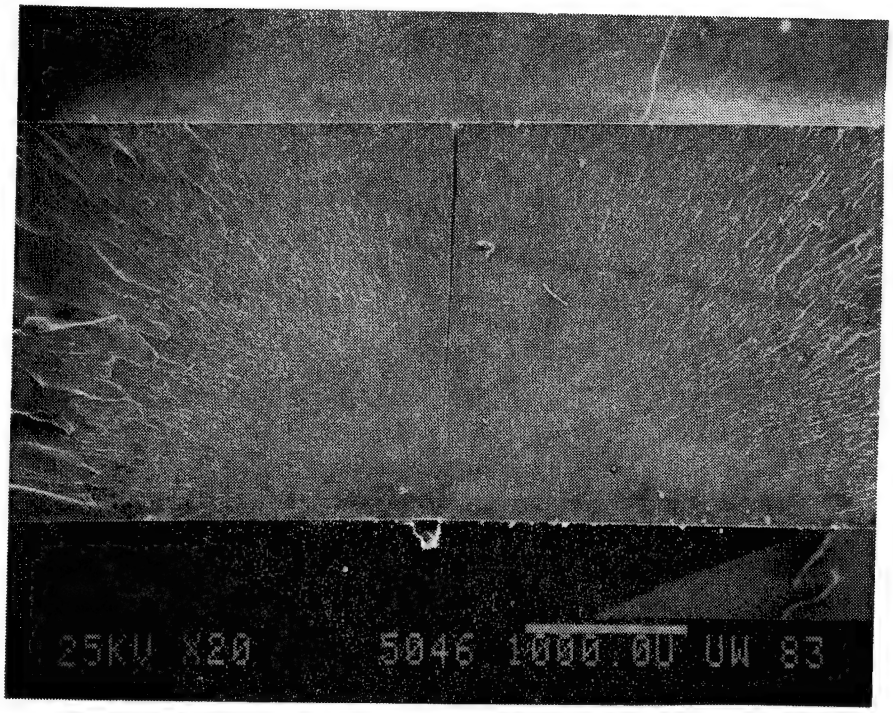


Figure 34. Failed Fibredux 914 Neat Epoxy Tensile Specimen No. LTWB24, 54°C, Moisture-Saturated.

A series of small cracks can be seen extending from the bottom surface of this failed specimen. The large single crack at the top occurred during the gold vapor deposition process and was caused by vacuum-induced rapid drying of the SEM specimen.


Figure 35. Failed Fibredux 914 Neat Epoxy Tensile Specimen No. LTWB24, 54°C, Moisture-Saturated.

This close-up of the specimen shown in Figure 34 shows a series of small cracks extending up from the bottom of the specimen. The large post-failure crack extends almost into this area.

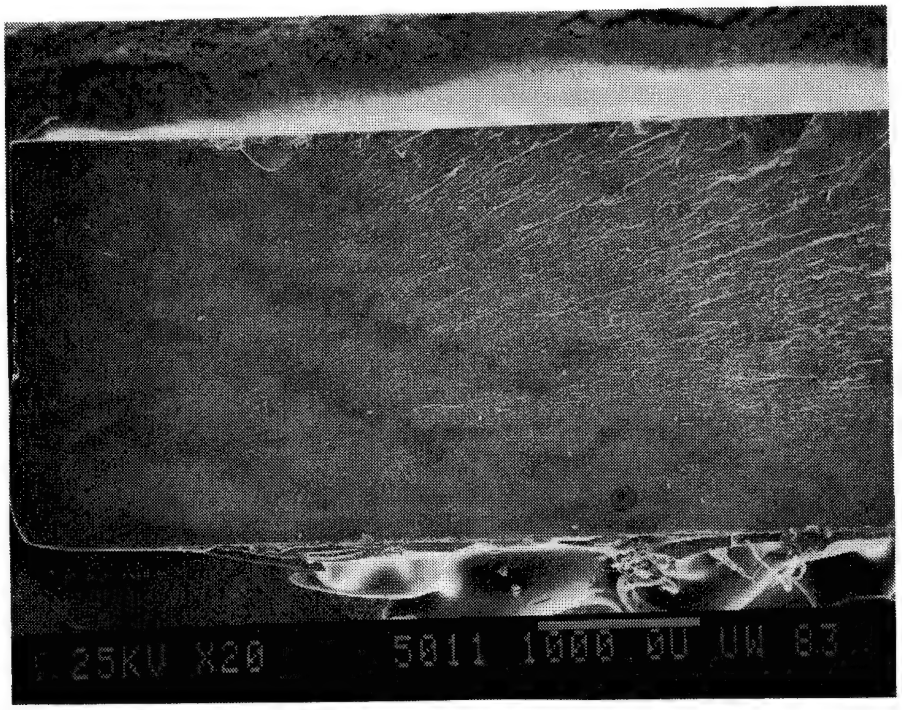


Figure 36. Failed Fibredux 914 Neat Epoxy Tensile Specimen No. LTDC25, 82°C, Dry.

No perceptible failure initiation site is evident in this photograph.

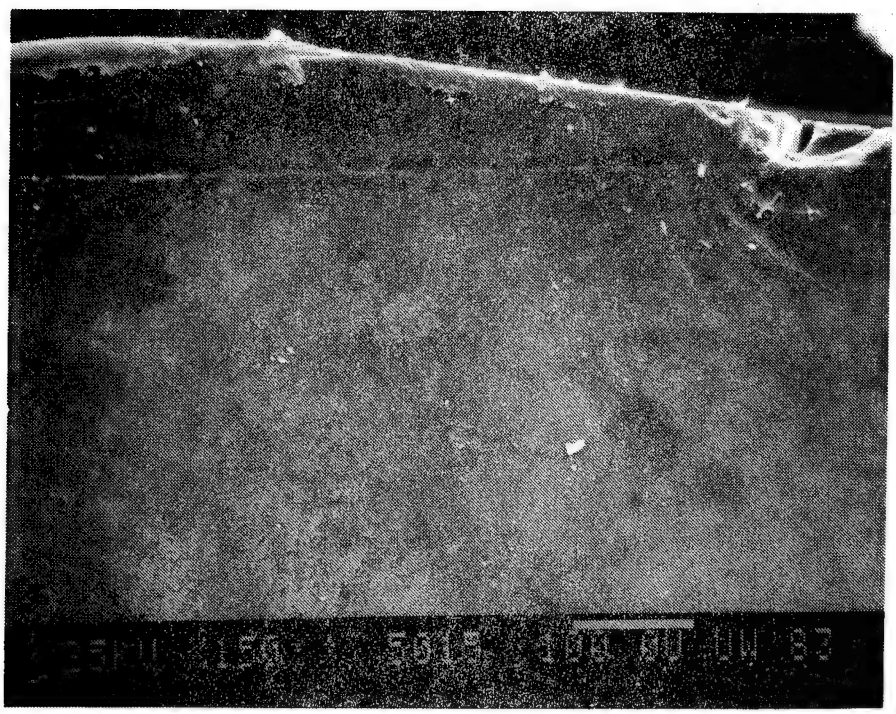

Figure 37. Failed Fibredux 914 Neat Epoxy Tensile Specimen No. LTDC25, 82°C, Dry.

This close-up of the specimen shown in Figure 36 shows that no discernible initiation site can be identified in the smooth area of the fracture.


Figure 38. Failed Fibredux 914 Neat Epoxy Tensile Specimen No. LTWC25, 82°C, Moisture-Saturated.

The fracture surface of this moisture-saturated specimen appears to be somewhat similar to the fracture surface shown in Figure 36. A small region near the left edge appears to be the failure initiation site. The very rough surface on the right-hand side of the photograph remained after the characteristic triangular chip was ejected.

conditioning, a number of Fibredux 914 specimens were lost due to cracking when they were inadvertently allowed to dry out quickly. A high moisture-induced stress gradient in these specimens was blamed for these failures. This problem was not evident in the Hercules 2220-1 or 2220-3 epoxies, but did occur occasionally with the untoughened Hercules 3502 epoxy. The round torsion specimens with the larger cross section were prominently affected.

Figures 39 through 43 are SEM photographs of the Hercules 2220-1 tensile fracture surfaces. All fracture surfaces exhibited the three zones discussed at the beginning of this section.

Figures 44 through 50 are SEM photograhs of the Hercules 2220-3 epoxy tensile fracture surfaces. A slight increase in overall coarseness was seen in the fracture surfaces when compared to those of the other three systems. Although these SEM photographs are very representative of the observed failure surfaces for the four neat epoxy resin systems studied, additional SEM photographs are included in Appendix D of Volume II to allow a more complete catalog of fracture modes.

## 4.5 Fracture Surfaces from Neat Resin Torsional Shear Tests

Torsional shear SEM specimens representing all test conditions were prepared in a manner similar to that for the tension specimens. Typically, a large portion of the test specimen was irrecoverable due to complete fracture into multiple small pieces and dust. Only the ends held in the grips were usable as SEM specimens. Due to the large portions of missing pieces, few SEM photographs contain a relevant history of the fracture surfaces for shear. Therefore, only a small number of shear SEM photographs are included in this section. The remainder of the SEM photographs are contained in Appendix D of Volume

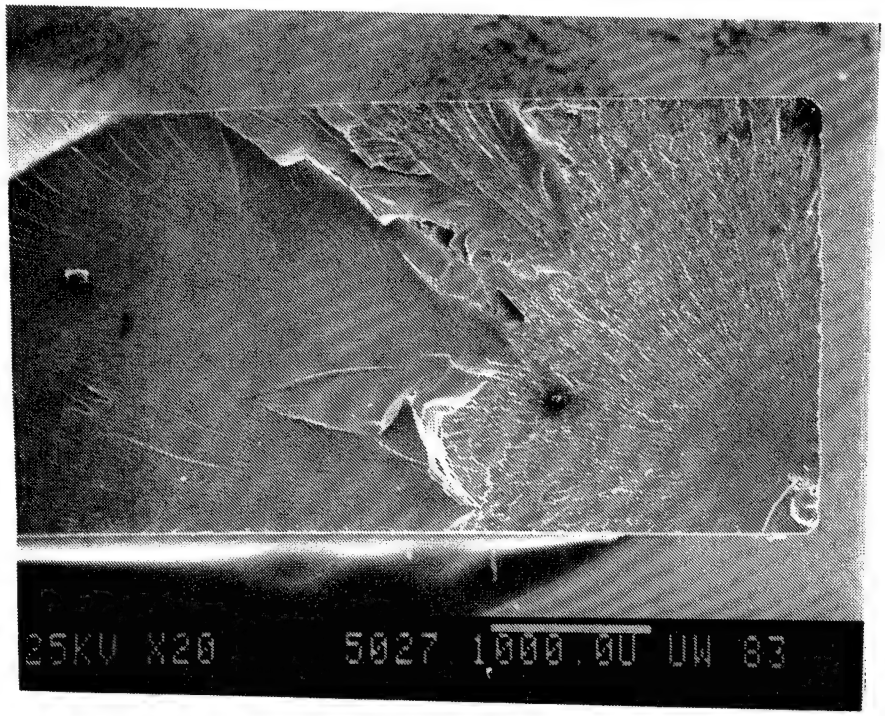


Figure 39. Failed Hercules 2220-1 Neat Epoxy Tensile Specimen No. LTWA03, 23°C, Moisture-Saturated.

A large area of voids is seen within the failure initiation region on the lower right side of the photograph. A very small smooth region surrounds this suspected initiation site, indicating the specimen achieved a fairly high strength. Actual strength was 81.4 MPa (11.8 ksi), the highest individual specimen strength recorded for this environmental condition.

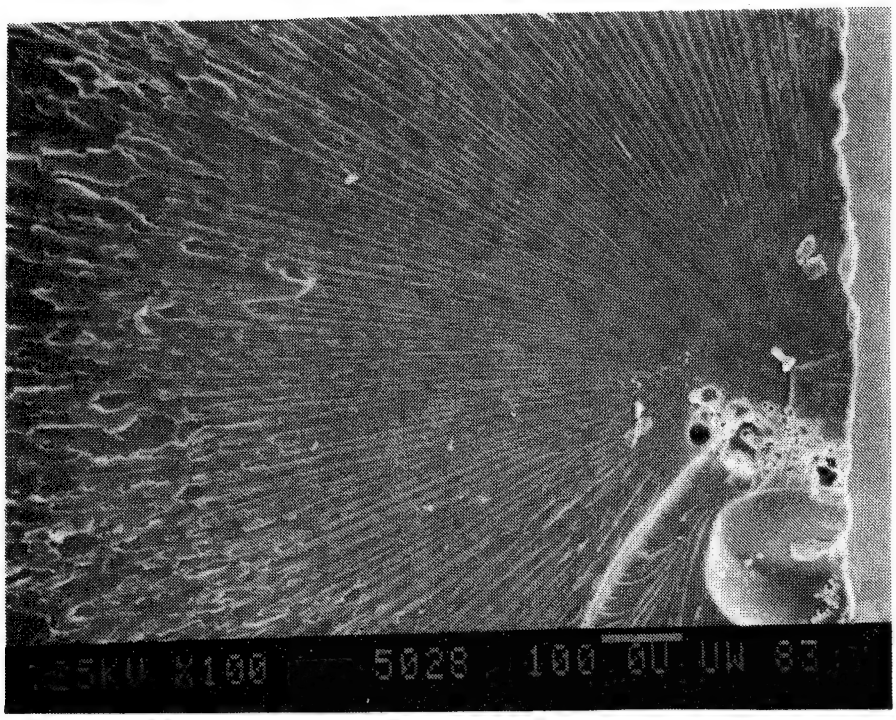

Figure 40. Failed Hercules 2220-1 Neat Epoxy Tensile Specimen No. LTWA03, 23°C, Moisture-Saturated.

This close-up of the specimen shown in Figure 39 shows the void area to be greater than 200μ long, and near the edge of the specimen.

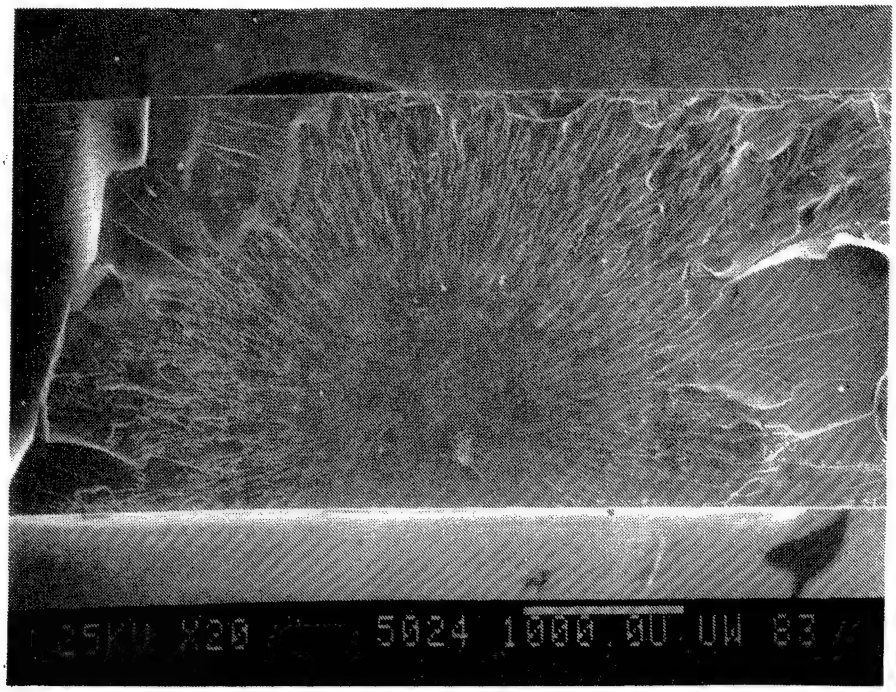


Figure 41. Failed Hercules 2220-1 Neat Epoxy Tensile Specimen No. LTWB03, 54°C, Moisture-Saturated.

An internal void area is quite evident in the center of the smooth area. Failure probably began there.

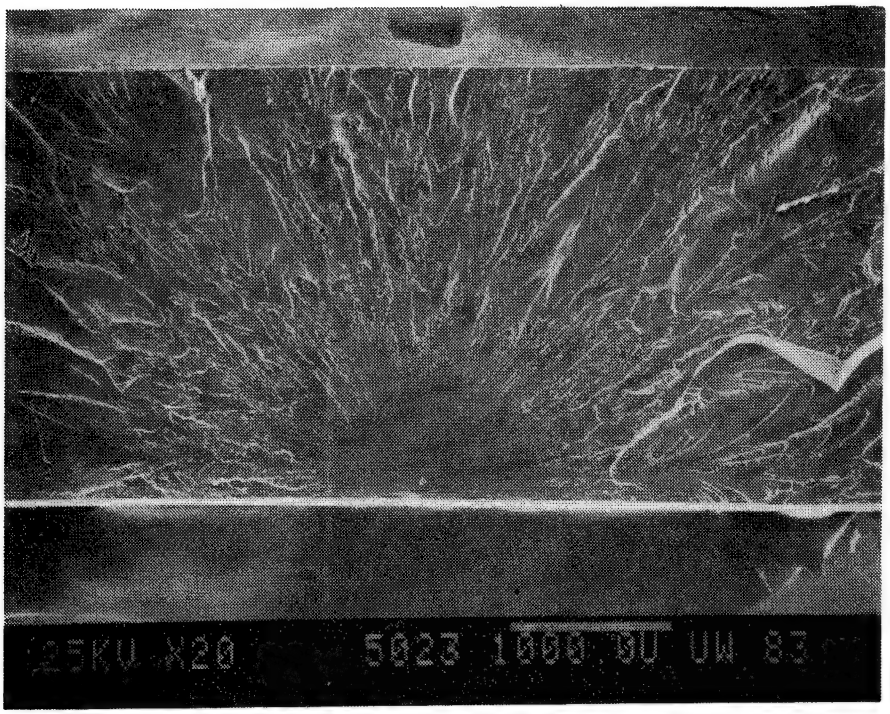


Figure 42. Failed Hercules 2220-1 Neat Epoxy Tensile Specimen No. LTDC01, 82°C, Dry.

A small void is seen in the center of the smooth region at the surface of the specimen. Consistent with our current understanding of fracture morphology, this specimen had a relatively high strength and a relatively small smooth region surrounding the failure site.

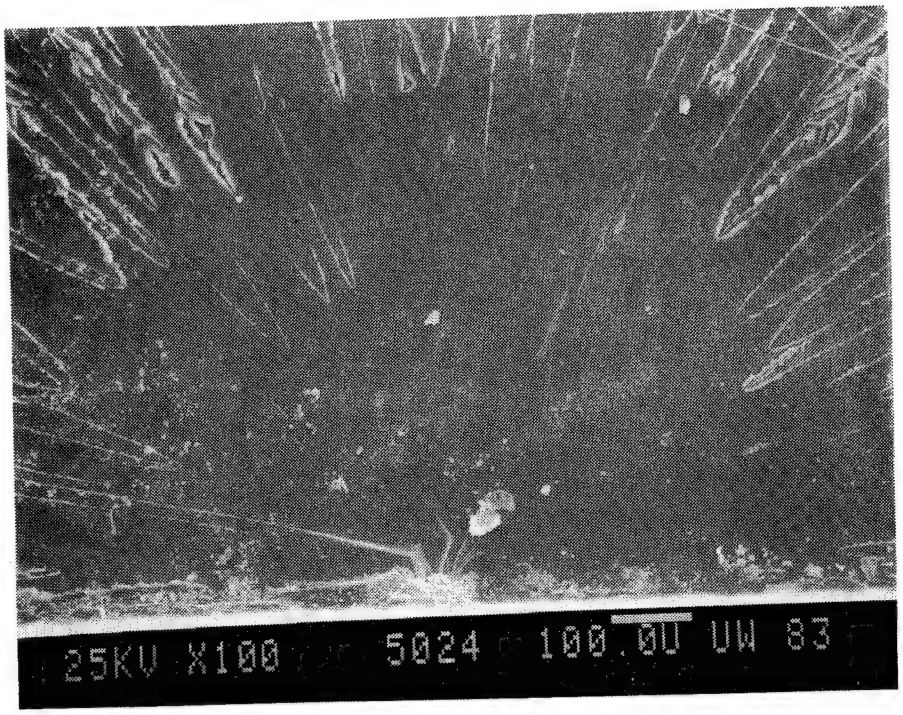


Figure 43. Failed Hercules 2220-1 Neat Epoxy Tensile Specimen No. LTDC01, 82°C, Dry.

A close-up of the specimen shown in Figure 42 shows the small suspected failure site and the smooth area surrounding it.

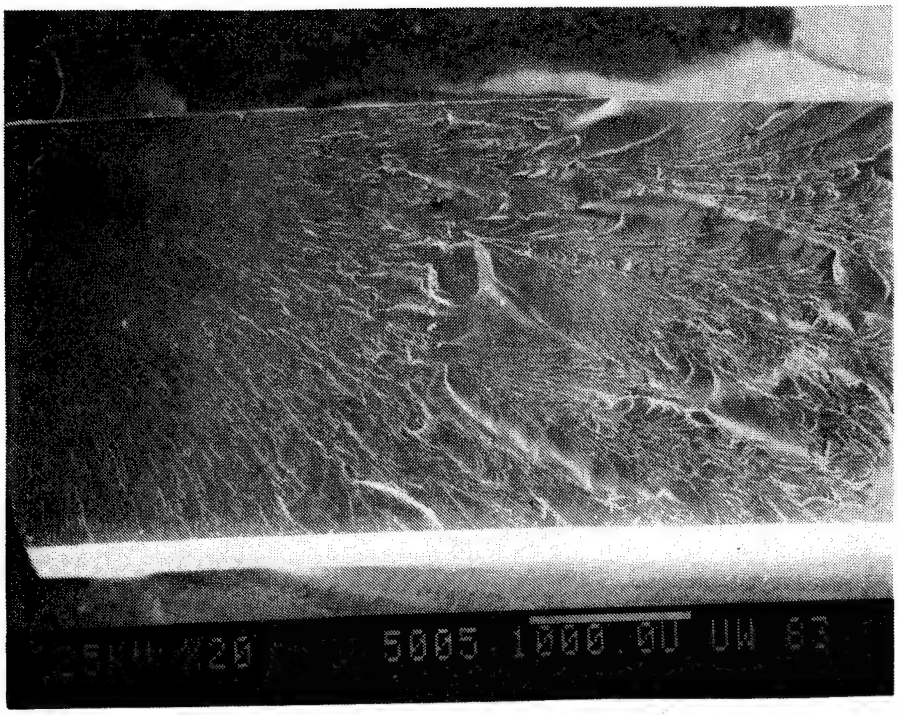


Figure 44. Failed Hercules 2220-3 Neat Epoxy Tensile Specimen No. LTDA14, 23°C, Dry.

This photograph shows the smooth region in the upper left corner and the transition area leading into the coarse region. This coarse region is the fracture surface left when the characteristic chip is ejected at failure.

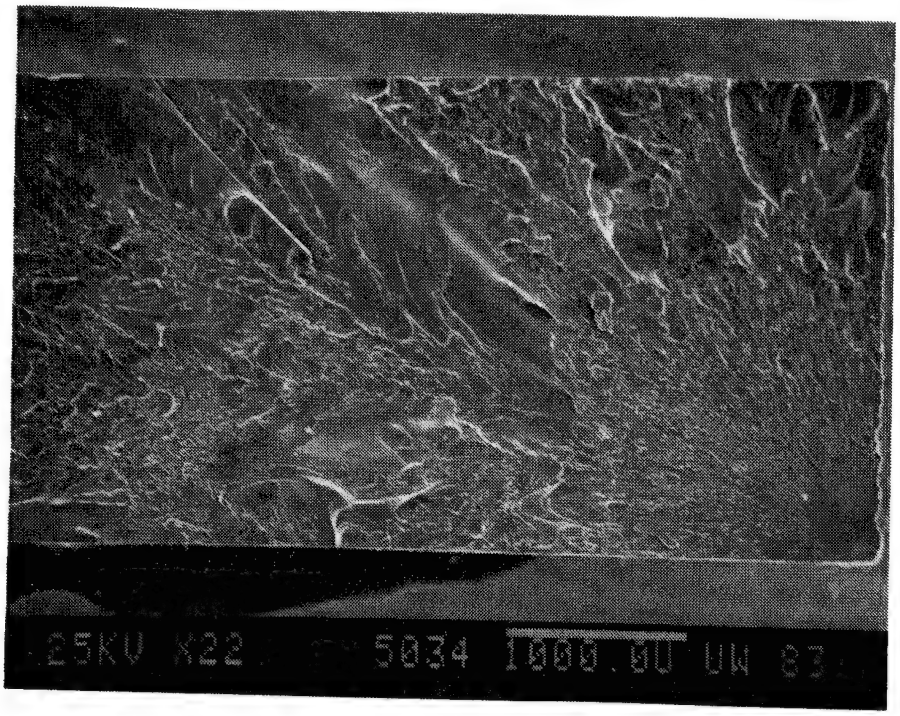


Figure 45. Failed Hercules 2220-3 Neat Epoxy Tensile Specimen No. LTWA11, 23°C, Moisture-Saturated.

The failure surface of this moisture-saturated specimen appears slightly rougher than that of the dry specimen at 23°C. The suspected failure site was a small void slightly beneath the surface at the lower right.

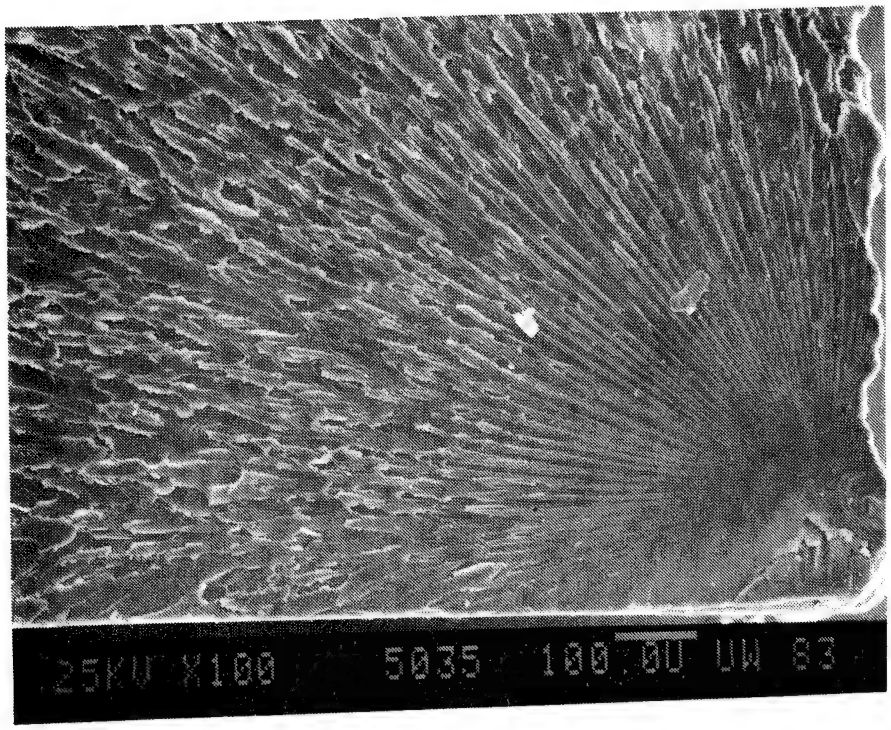


Figure 46. Failed Hercules 2220-3 Neat Epoxy Tensile Specimen No. CTWA11, 23°C, Moisture-Saturated.

This close-up of the specimen shown in Figure 45 shows the small void area beneath the surface, the transition area, which is quite small, and the rough region.

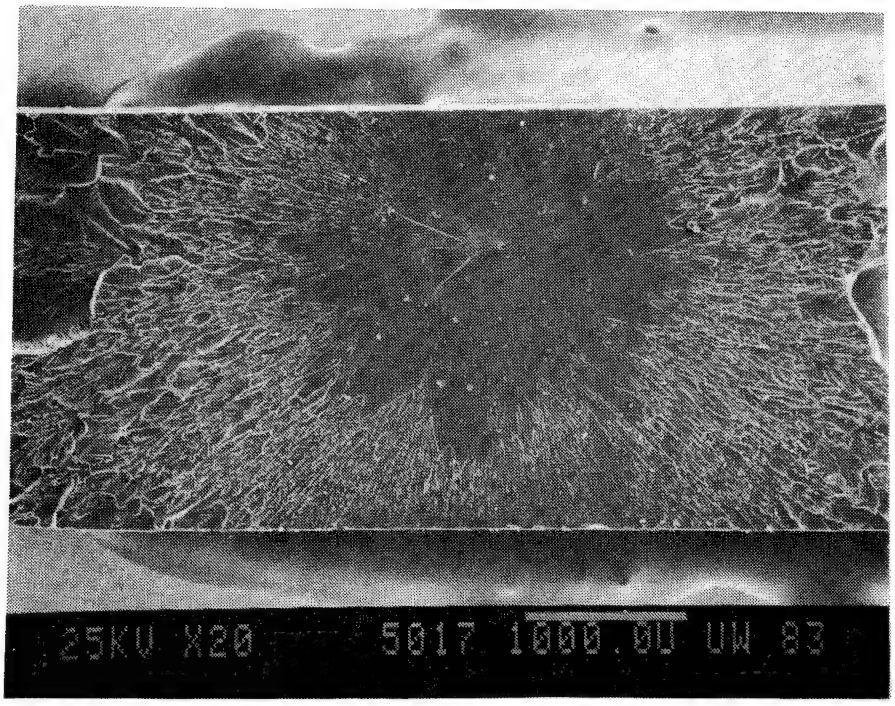


Figure 47. Failed Hercules 2220-3 Neat Epoxy Tensile Specimen No. LTDB13, 54°C, Dry.

This specimen probably failed due to a defect located in the upper center.

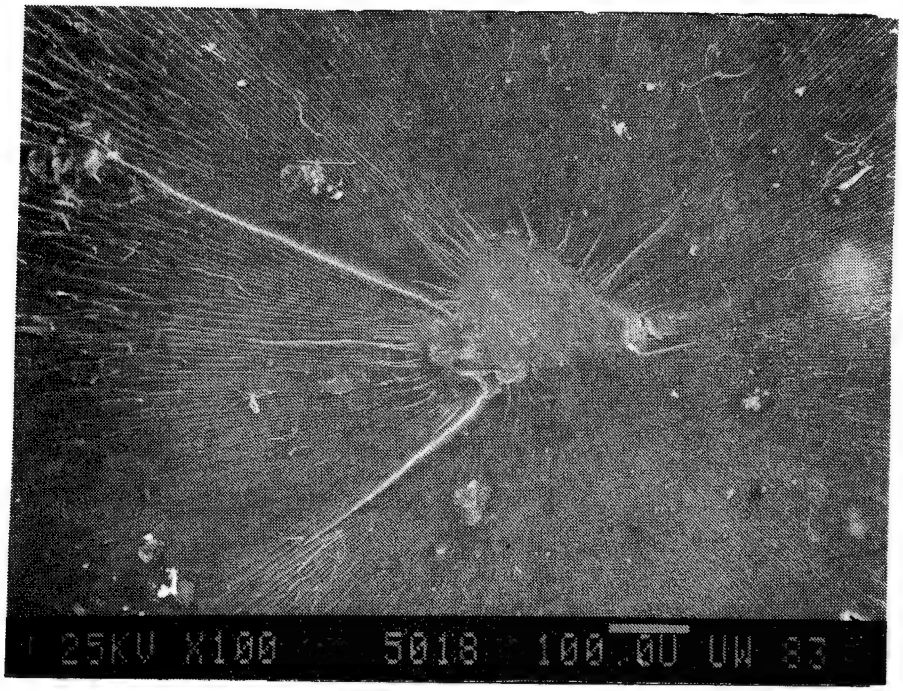


Figure 48. Failed Hercules 2220-3 Neat Epoxy Tensile Specimen No. LTDB13, 54°C, Dry.

This close-up of the specimen shown in Figure 47 shows the suspected failure site as a small void approximately 200μ in diameter.

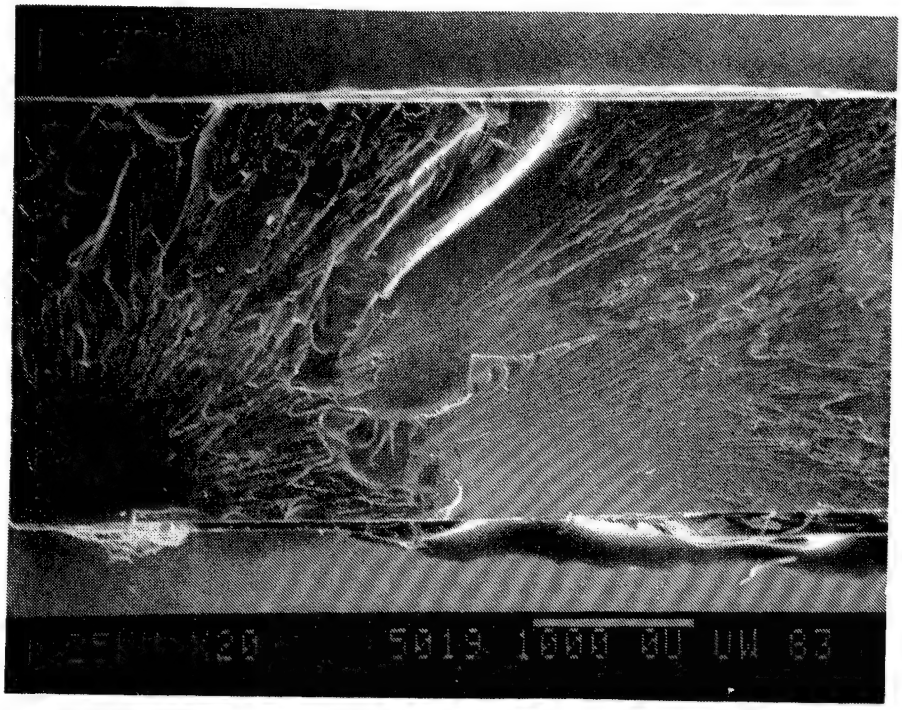

Figure 49. Failed Hercules 2220-3 Neat Epoxy Tensile Specimen No. LTDC1X, 82°C, Dry.

This specimen probably failed initially at a site shown in the lower left corner of the photograph. No observable feature is evident on the fracture surface to distinguish it from the other tensile failures.

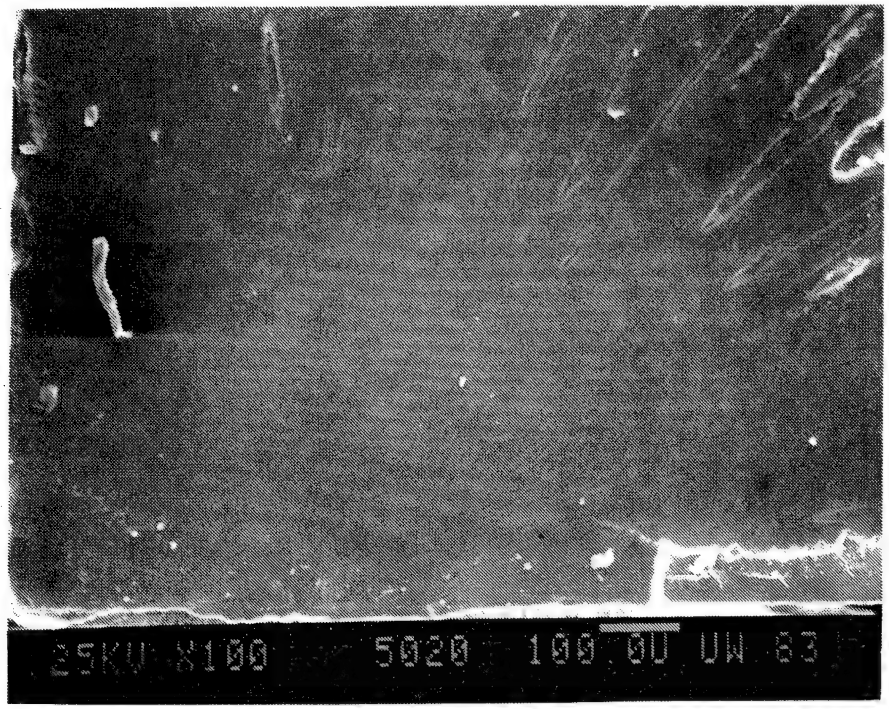


Figure 50. Failed Hercules 2220-3 Neat Epoxy Tensile Specimen No. LTDC1X, 82°C, Dry.

This close-up of the specimen shown in Figure 49 shows no specific initiation site in the smooth area. The long bright spot on the left is debris on the surface of the specimen.

II as a representative collection of fracture surfaces.

The shear failures appeared similar to the tension failures in some ways. There were observable regions of failure initiation, transition, and tertiary failure rough areas. The transition areas that were visible had somewhat curved lines due to the torsional load.

High moisture-induced stresses were developed during the process of preparing specimens for SEM viewing. The wet specimens were stored after failure in a moist environment to try to preserve the fracture surfaces. During SEM specimen preparation, however, the specimens had to be evacuated in a vacuum chamber for vapor depositing the gold onto their surfaces. It is thought that during this process the moisture-saturated specimens were secondarily cracked, as identified in some of the following figures. Specimen numbers are not given on the following figures for the shear specimens because the numbers were not marked on individual failed specimens. Only the material and test conditions are available to identify these failed specimens.

Figures 51 and 52 are SEM photographs of the 3502 epoxy torsional shear failures. Possible failure sites are visible as are regions of very glassy appearance which indicate subsequent bending failures after the initial shear failures.

Figure 53 is representative of the failure surfaces of the Fibredux 914 torsion specimens. Some evidence is visible of a shear failure, but most of the surfaces are very smooth, indicating that secondary bending was present after the initial shear failure. Two cracks are present which were induced by the high stress gradients present when the moisture-saturated specimen dried out after testing.

Figures 54 through 57 show 2220-1 neat epoxy shear failures. The

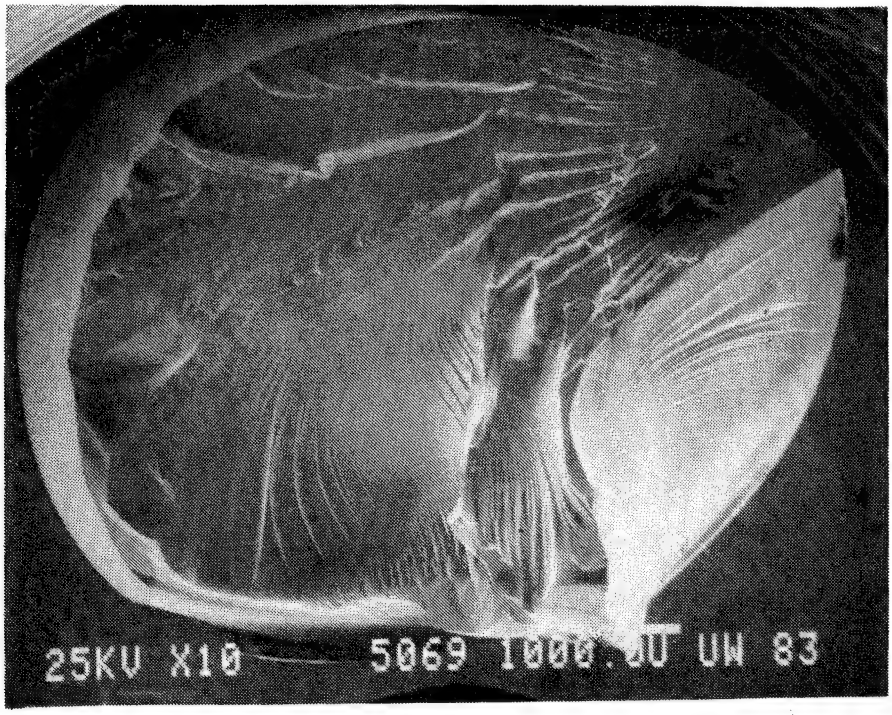


Figure 51. Failed Hercules 3502 Neat Epoxy Torsional Shear Specimen, 23°C, Moisture-Saturated.

This is a representative torsional shear failure for 3502 neat epoxy in either the dry or wet condition. The particles in the upper righthand corner are impurities in the resin. It appears the failure could have initiated in that area, as indicated by the smooth area and the direction of the transition zone striations.

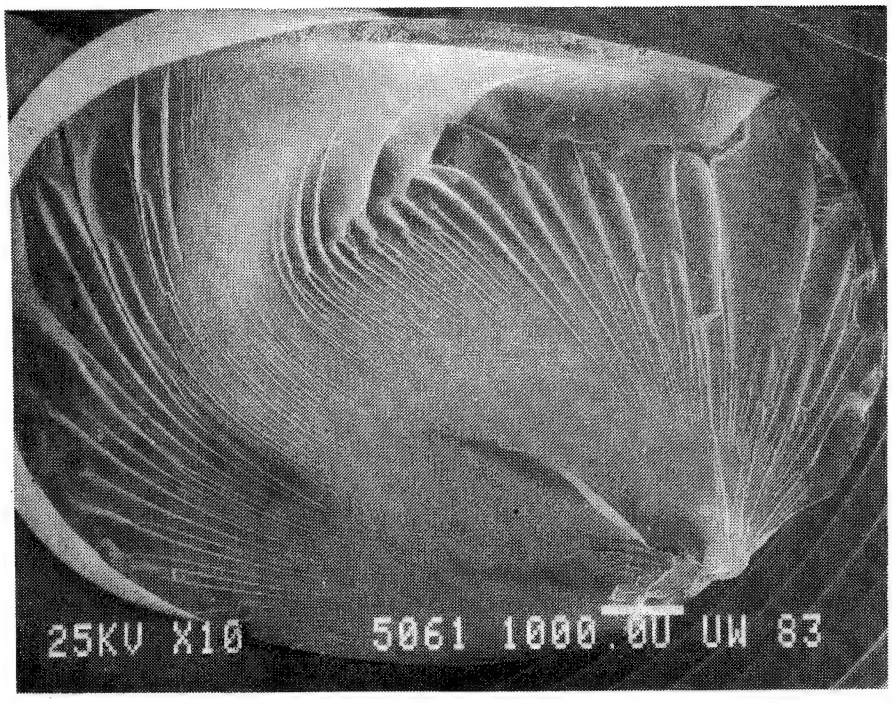


Figure 52. Failed Hercules 3502 Neat Epoxy Torsional Shear Specimen, 54°C, Dry.

This failure probably initiated in the lower righthand corner. The curved transition zone lines are characteristic of all torsion failures.

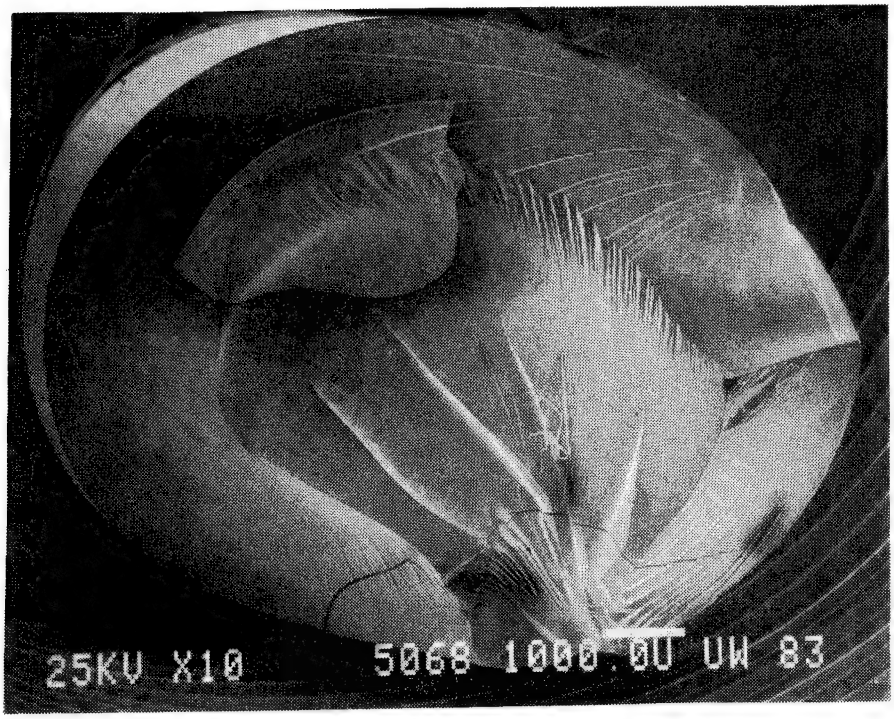


Figure 53. Failed Fibredux 914 Neat Epoxy Torsional Shear Specimen, 23°C, Moisture-Saturated.

The large cracks visible in this photograph occurred after failure due to moisture-induced stresses during the drying out process after testing. Note the smooth sloping surfaces caused by bending subsequent to the initial shear failure.

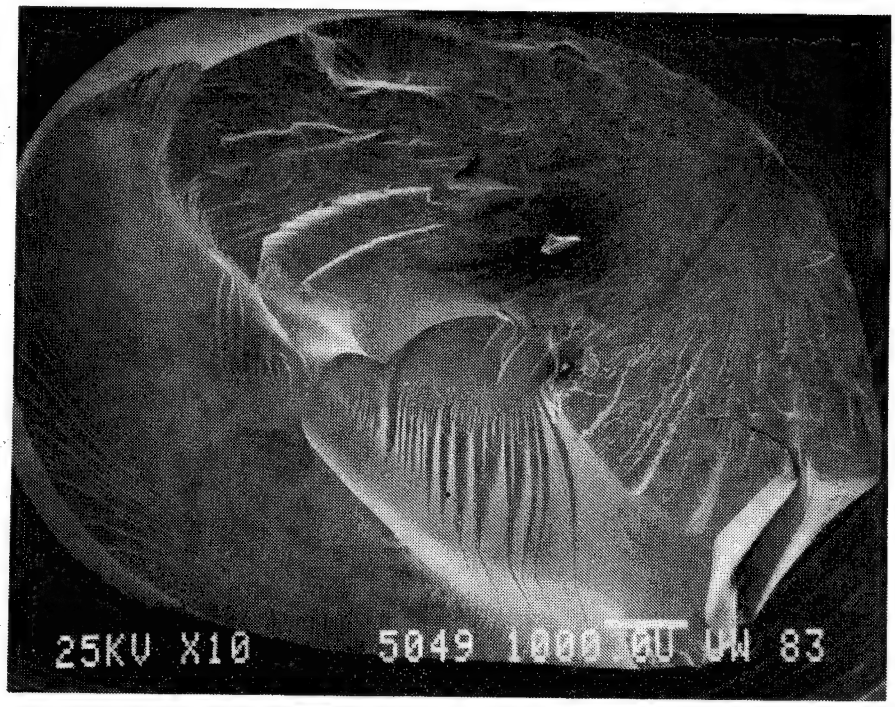


Figure 54. Failed Hercules 2220-1 Neat Epoxy Torsional Shear Specimen, 23°C, Dry.

This is a very representative failure surface. Features are evident which are similar to those observed on tension failure surfaces.


Figure 55. Failed Hercules 2220-1 Neat Epoxy Torsional Shear Specimen, 23°C, Dry.

This close-up of the specimen shown in Figure 54 shows the probable initiation site on the surface of the specimen, surrounded by a smooth region, transition area, and a coarse region.

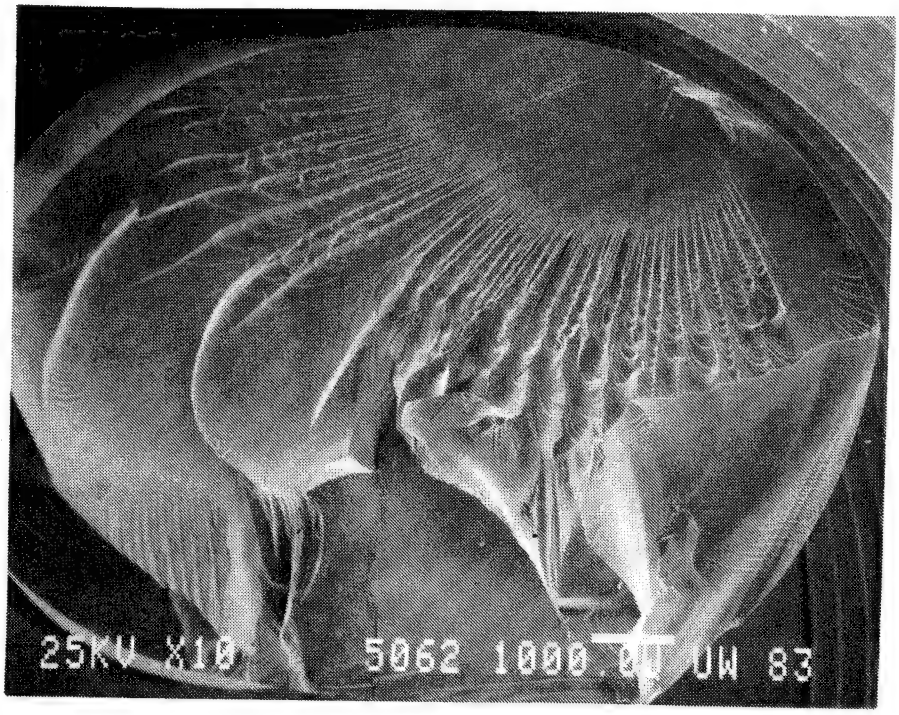


Figure 56. Failed Hercules 2220-1 Neat Epoxy Torsional Shear Specimen, 82°C, Moisture-Saturated.

This photograph is very similar to Figure 54 and shows the possible shear failure morphology and smooth sloping surfaces presumed to have been caused by bending.

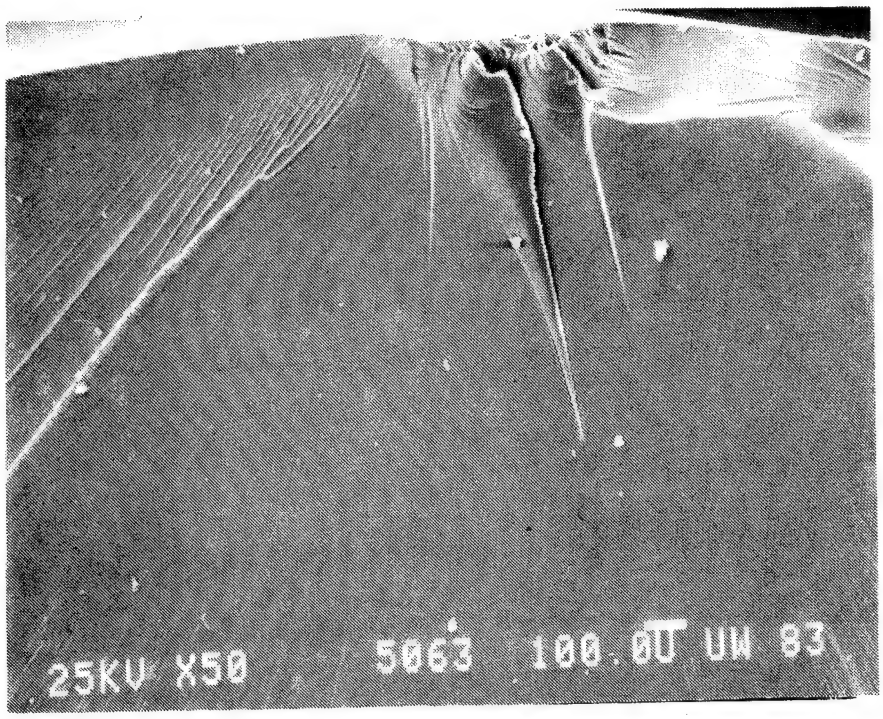


Figure 57. Hercules 2220-1 Neat Epoxy Torsional Shear, 82°C, Moisture-Saturated.

This close-up of the specimen shown in Figure 56 shows the apparent failure initiation site on the surface, and the fairly smooth region surrounding it. The beginning of the transition region is barely visible near the bottom of the photograph. The relatively large smooth region surrounding the initiation site is prominent.

salient features are similar to tension failures. The initial failures probably began at the outer surface in the upper right corner of the specimens. In each case, the probable failure initiation site is surrounded by a smoother region and then transitions into a coarse region similar to tension failures seen earlier. Also shown are the smooth sloping surfaces which are thought to be secondary to the initial shear failure.

Figures 58 through 60 show shear failures of the Hercules 2220-3 epoxy. Figure 59 contains both the shear failure and secondary bending mode surface features. Figure 60 illustrates the similarity of the shear failure surface to tensile failure surfaces.

The fracture surfaces of the four neat epoxies are similar when viewed in the SEM. The Hercules 3502 and Fibredux 914 fractures tended to exhibit more smooth sloping surfaces associated with secondary bending while both Hercules 2220 systems shattered more and had fewer secondary bending features. Additional SEM photographs of torsion specimens are included in Appendix D of Volume II.

## 4.6 Fracture Toughness Tests

Few SEM photographs were taken of the fracture toughness specimen failures, since the emphasis was on the tension and shear failures, and because of their similarity to the tension and shear fracture surfaces. The notched-edge bend specimen is placed into tension at the root of the razor blade notch and the resulting fracture surface typically showed a similar appearance to the tension specimen failures, and sometimes the shiny surface associated with bending failures. Figure 61 is a typical fracture surface of a fracture toughness specimen. Figure 62 is a photograph of another common appearance seen in the fracture toughness

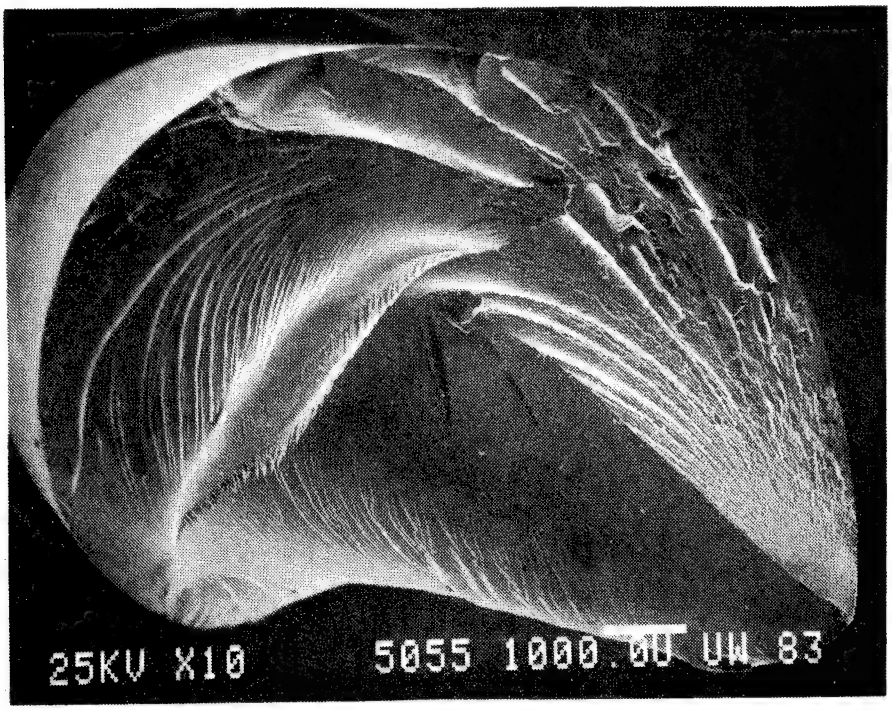


Figure 58. Hercules 2220-3 Neat Epoxy Torsional Shear, 54°C, Dry.

Prominent in this photograph are the curved lines of the transition region and some coarse region in the upper right hand corner. The initiation site is not evident; it was probably lost when the specimen shattered at failure.


Figure 59. Hercules 2220-3 Neat Epoxy Torsional Shear, 82°C, Dry.

The shear failure initiation region is clearly seen in the upper right corner. The smooth region and transition area are quite small. More than half of the fracture surface is the curving smooth surface due to bending.

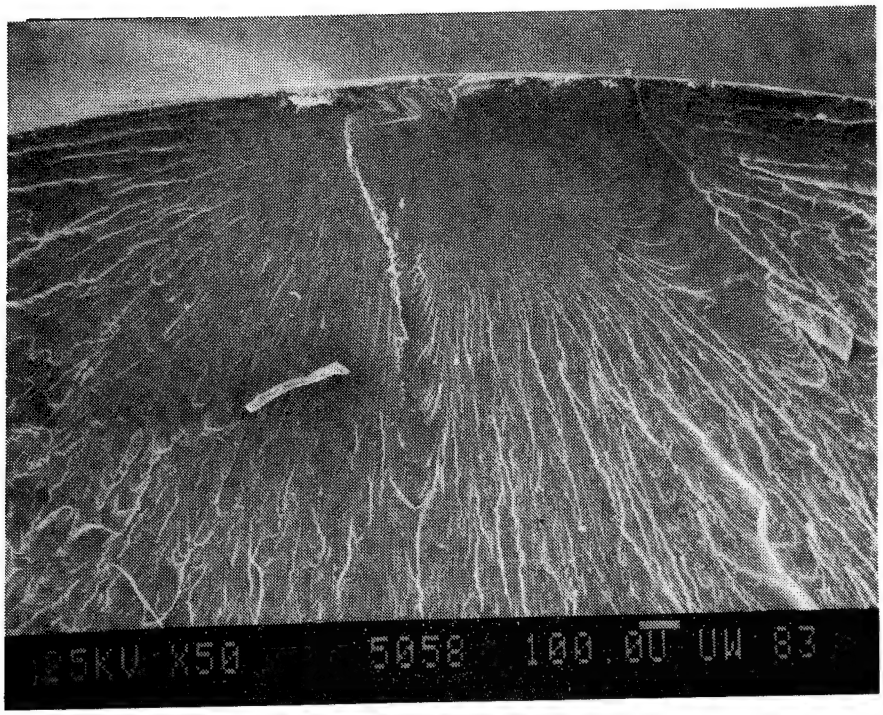


Figure 60. Hercules 2220-3 Neat Epoxy Torsional Shear, 82°C, Dry.

This close-up of the specimen shown in Figure 59 shows the probable initiation site on the surface of the specimen and a relatively small smooth region around it.

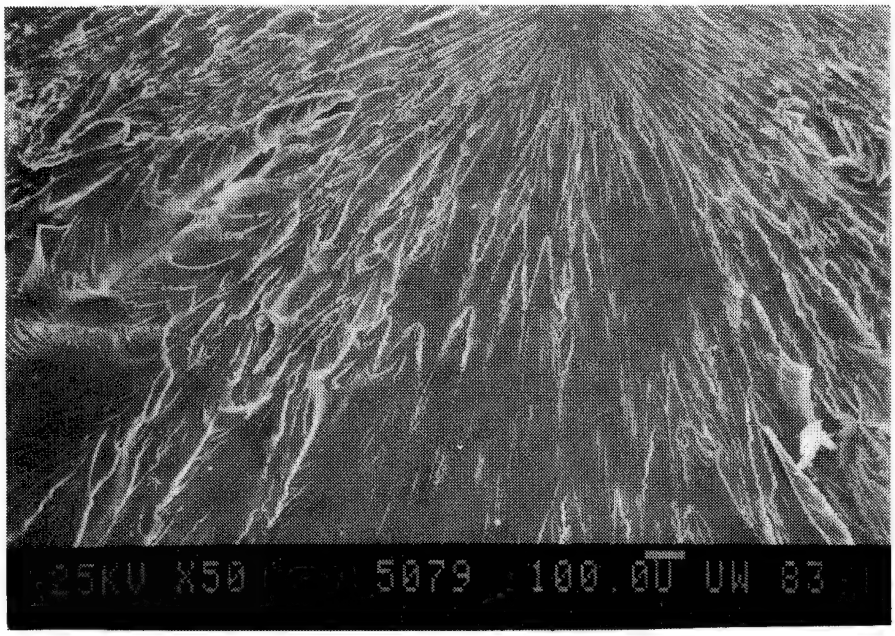


Figure 61. Hercules 2220-3 Neat Epoxy Fracture Toughness, 54°C, Dry.

This failure bears much similarity to a tensile type failure. The razor blade cut is across the top of the photograph, and the fracture initiation site is at that surface. It is surrounded by a very small transition area into the coarse final failure area.

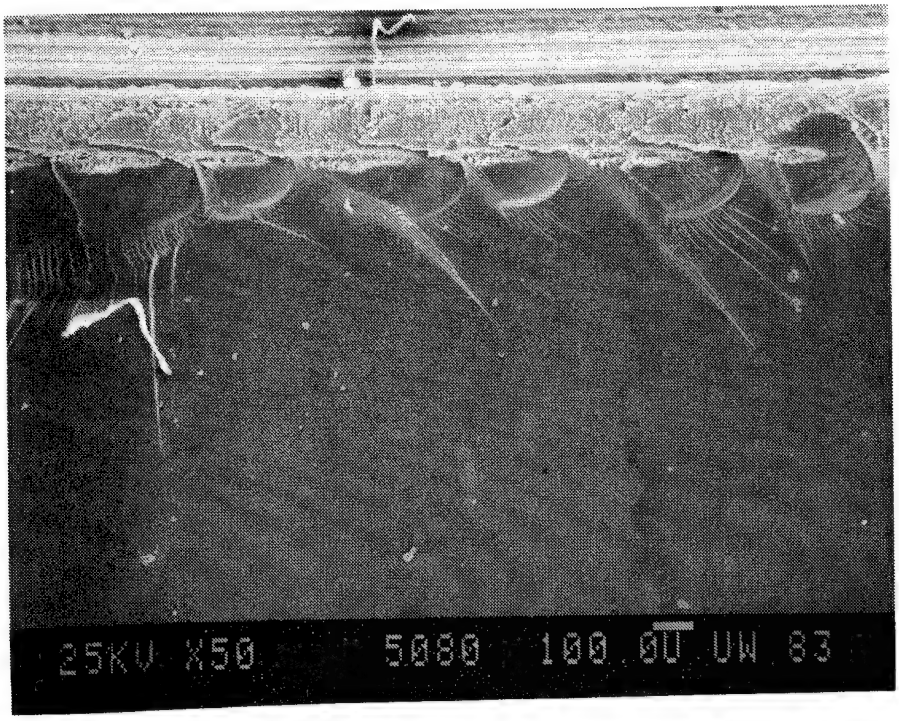


Figure 62. Hercules 2220-3 Neat Epoxy Fracture Toughness, 82°C, Moisture-Saturated.

This fracture toughness failure surface is just as typical as Figure 61. The notched area is across the top of the photograph. Numerous clam shell markings are seen here, with very little extension into the specimen. The majority of the fracture surface is glassy in appearance, indicating a greater dependence on bending as the dominant failure process.

failure surfaces. A smooth glassy surface extends across the majority of the specimen, indicating a high dependence on bending as a failure mode. More SEM photographs of fracture toughness specimens are included in Appendix D of Volume II.

# SECTION 5

# MICROMECHANICS PREDICTIONS OF COMPOSITE RESPONSE

## 5.1. Introduction

One important purpose of testing neat resin systems is to determine the mechanical and physical properties needed as input to a micromechanics analysis. This micromechanics analysis can then be used to predict all of the properties of a unidirectional composite, e.g., axial, transverse and shear moduli, major and minor Poisson's ratios, axial and transverse thermal expansion coefficients, axial and transverse moisture expansion coefficients, axial, transverse and shear strengths, complete (nonlinear) stress-strain curves to failure, fiber-matrix interface stress distributions (both normal and shear stresses), and complete local stress and strain distributions in both the fiber and the surrounding matrix material. All of these properties can be predicted for any combination of test tmperature and prior moisture exposure.

It is often prohibitively expensive to experimentally measure all of these unidirectional ply properties, even though they are required as input to any subsequent laminate analysis and design process. By measuring the properties of the matrix material instead (a much less expensive and time consuming process since the matrix is isotropic and therefore has fewer properties to measure), and having literature values of the fiber properties available, any of the composite ply properties for any environmental and loading conditions can be predicted at any subsequent time. This could even include biaxial loadings (laminate analyses) and triaxial loadings (interlaminar stresses) associated with free edge effects, e.g., adhesive-bonded joints and the surfaces of

attachment holes (bolts and rivets) and access cutouts. There are an infinite number of combinations of geometries and loading conditions of practical interest, and not all can be tested.

The philosophy of the Composite Materials Research Group (CMRG) has been to develop rigorous analysis procedures for predicting composite material response from constituent material properties, and to develop efficient procedures for measuring these constituent material properties. To gain general acceptance of this approach by the composite materials community, it is necessary to demonstrate that the composite properties predicted by the micromechanics analysis, using fiber and matrix constituent properties as input, correlate with experimentally measured unidirectional composite data.

This has been done as part of prior CMRG studies, e.g., for Hercules AS/3501-6 graphite/epoxy and S2/3501-6 glass/epoxy stiffness properties [6], AS/3501-6 graphite/epoxy stiffness and strength properties [7,8], AS/3501-6 graphite/epoxy and S2/3501-6 glass/epoxy shear properties [3,9], and AS/3501-6 graphite/epoxy and S2/3501-6 glass/epoxy thermal expansion and moisture expansion coefficients [4]. In addition, CMRG correlated unidirectional glass/epoxy axial, transverse and shear properties as part of a study for General Motors [11]. Good correlations were achieved, but as will be noted, the same Hercules 3501-6 epoxy matrix was used in all programs except the one recently completed for General Motors [11]. Also, in all of these prior programs, CMRG either generated the composite data or, in the case of the studies of References [7,8], was directly involved in a program with the outside group which did generate the data.

In the present study, four additional neat resin matrix materials

have been characterized, as documented in the prior sections of this report. Thus, the opportunity to further verify the ability of the micromechanics analysis to predict composite material response has been greatly expanded. The present study did not include the testing of any composites, only the neat resin matrix. Thus it was not possible to present meaningful correlations in the present report. However, selected analytical predictions will be presented here to demonstrate the types of information which are available. It is anticipated that more detailed data on unidirectional graphite fiber-reinforced composites utilizing these four polymer matrix materials will become available during the next year. Detailed correlations will then be made and presented in a subsequent report.

## 5.2 Micromechanics Predictions Methodology

The micromechanics predictions methodology presently available at the University of Wyoming is the result of work initiated in the mid-1960's primarily by Adams [12,13] and Foye [14]. Work has continued in the intervening years, to extend these analyses to random fiber arrays [15], inelastic matrix response [16-18], temperature- and moisture-dependent material properties [1,20], crack propagation [21-28], nonlinear viscoelasticity [2,10], and most recently, a full three-dimensional analysis [29]. These analytical tools were fully available to the present study, and have been used as appropriate.

Specifically, the basic two-dimensional micromechanics finite element analysis and associated computer program [1,19,20] with the addition of longitudinal shear loading capability [3,9] was used. The fiber is assumed to be anisotropic (transversely isotropic) and linearly elastic to failure. The matrix is inelastic but isotropic. An octahedral

shear stress yield criterion and a Prandtl-Reuss flow rule were used. The matrix material properties are assumed to be fully temperature- and moisture-dependent.

For the present analytical presentation, since no composites experimental data are available for comparison, a 60 percent fiber volume was assumed in all cases. AS4 graphite fibers were modeled in a square array. If a regular array is assumed, a single fiber and the surrounding matrix can be isolated as a typical repeating unit for analysis purposes. In fact, only one quadrant of this repeating element need be analyzed because of symmetry. This is discussed in detail in the various references previously cited. The finite element grid used to model this first quadrant is shown in Figure 63. It consists of 288 constant strain triangular elements, and 169 node points.

## 5.3 Constituent Material Properties

### 5.3.1 Matrix Materials

The full experimental details of the four matrix materials characterized as part of the present study, viz, Hercules 3502, Hercules 2220-1 and 2220-3, and Fibredux 914, are discussed in Section 3 of this report. For use in the micromechanics analysis, it is necessary to express these data in a form which can be input to the associated computer program. The experimental data could be input point by point, i.e., by expressing each stress-strain curve as a series of point values. This would be tedious. Also, since matrix tests were performed at discrete temperature and moisture conditions and the analysis is capable of predicting composite response at any combination of conditions, it is necessary to interpolate (and sometimes even to extrapolate) the available experimental data to other hygrothermal

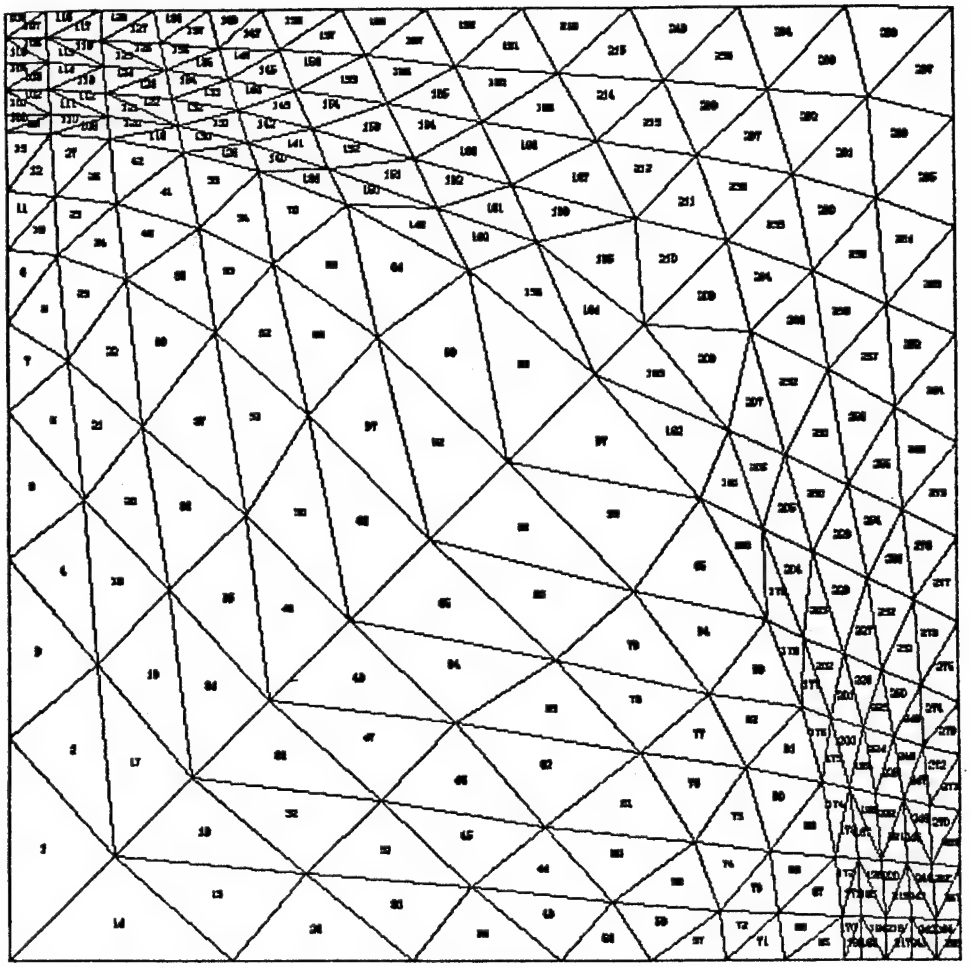


Figure 63. Finite Element Grid Utilized in the Present Study to Model the First Quadrant of a Square Array of Fibers.

conditions. Thus, it is convenient to fit the temperature- and moisture-dependent data to an equation. This permits easy interpolation, and at the same time provides a means, by linear regression, of averaging the typical five individual stress-strain curves at each test condition together. This was done using the same Richard-Blacklock relation [30] utilized in the prior studies. This expression is of the form:

$$\sigma = \frac{E\varepsilon}{\left[1 + \left|\frac{E\varepsilon}{\sigma_o}\right|^n\right]^{1/n}} \tag{3}$$

where $\sigma$ and $\varepsilon$ are the stress and strain quantities being fitted (i.e., normal, shear, or octahedral shear quantities, as appropriate), and E, $\sigma_o$ and n are the fit parameters. The E is the initial slope (modulus) of the stress-strain relation, and $\sigma_o$ is the asymptotic value of stress. The parameter n governs the sharpness of the curvature of the fitted curve (larger values of n giving sharper curvatures). The averaged test data are presented in Section 3 and the individual test specimen results along with the Richard-Blacklock curve-fits in Appendix C of Volume II. These curve-fit data are summarized here in Figures 64 through 67. Both tensile and shear tests were conducted on each of the four matrix systems and are included here. The tensile data are plotted to the same scale for all four materials, as are the shear data. Thus, the stress-strain response of all four materials can be directly compared. The Hercules 3502 data, considered as the baseline matrix system for the present study, are presented in Figures 64a and 64b, the Hercules 2220-1 data in Figures 65a and 65b, the Hercules 2220-3 data in Figures 66a and 66b, and the Fibredux 914 data in Figures 67a and 67b. The solid curves

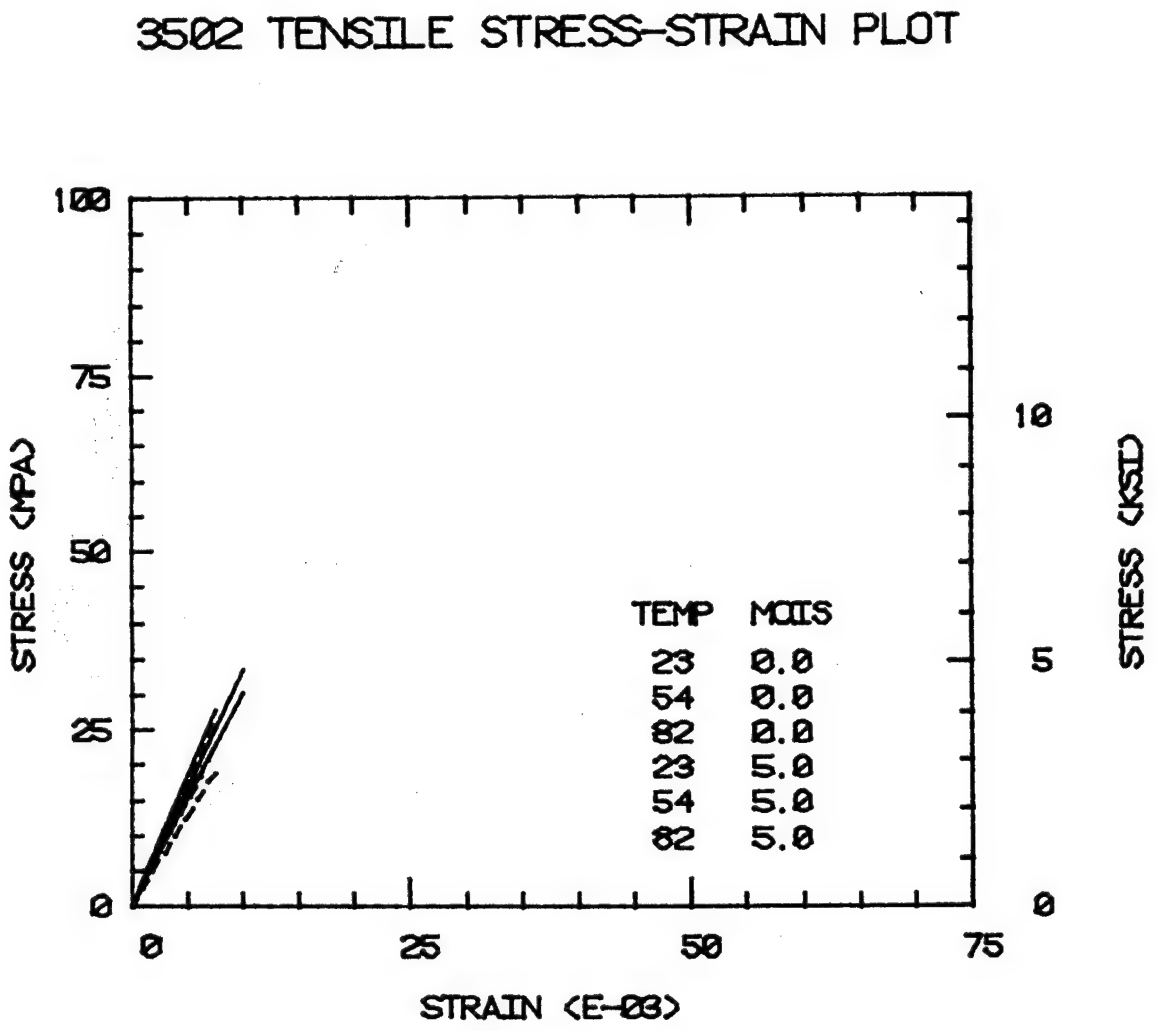


a) tensile data

Figure 64. Hercules 3502 Baseline Epoxy Stress-Strain Curves; Average Response at Each Test Condition (dry-solid lines, wet-dashed lines).

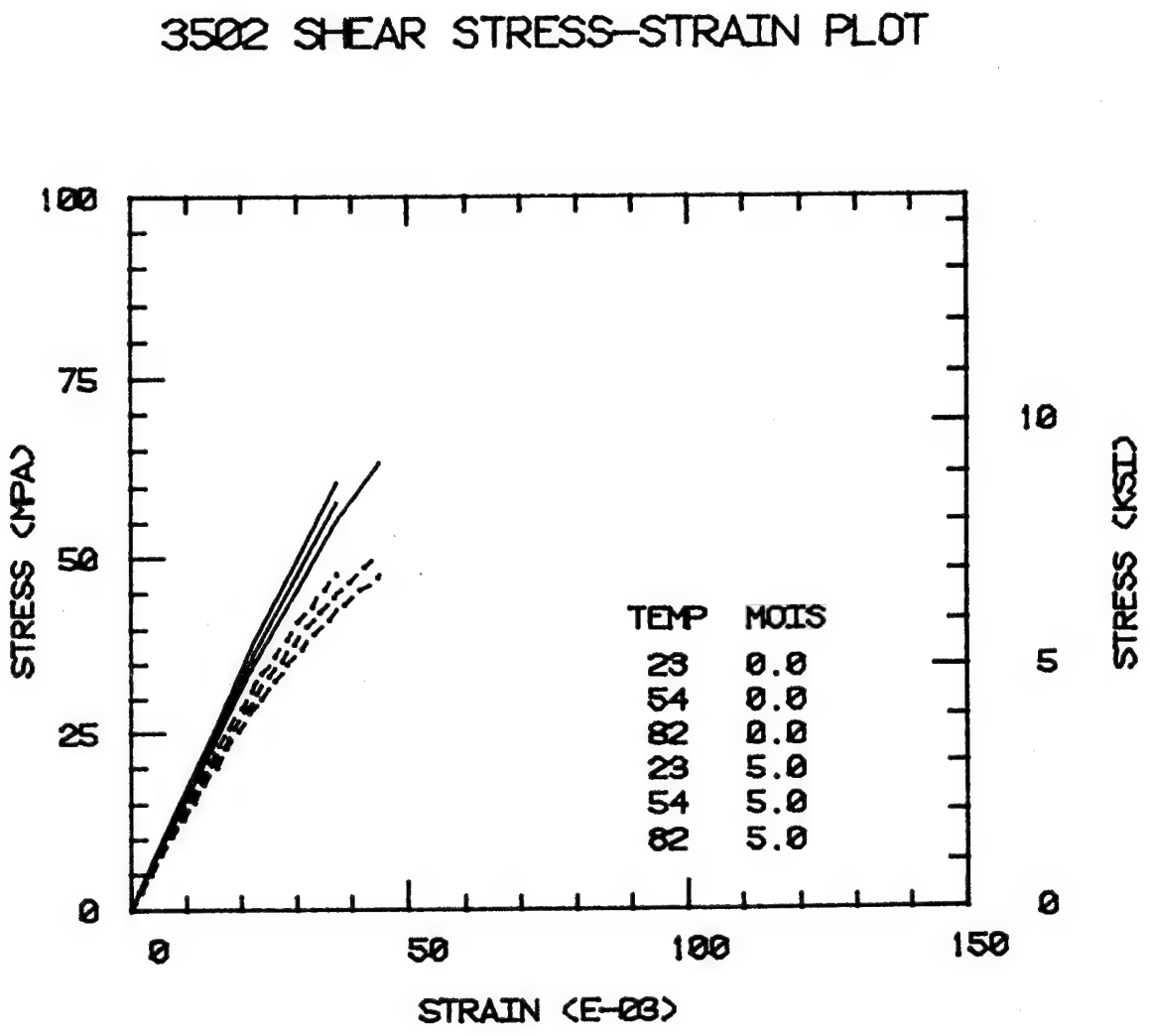


b) shear data

Figure 64 (continued). Hercules 3502 Baseline Epoxy Stress-Strain Curves; Average Response at Each Test Condition (dry-solid lines, wet-dashed lines).

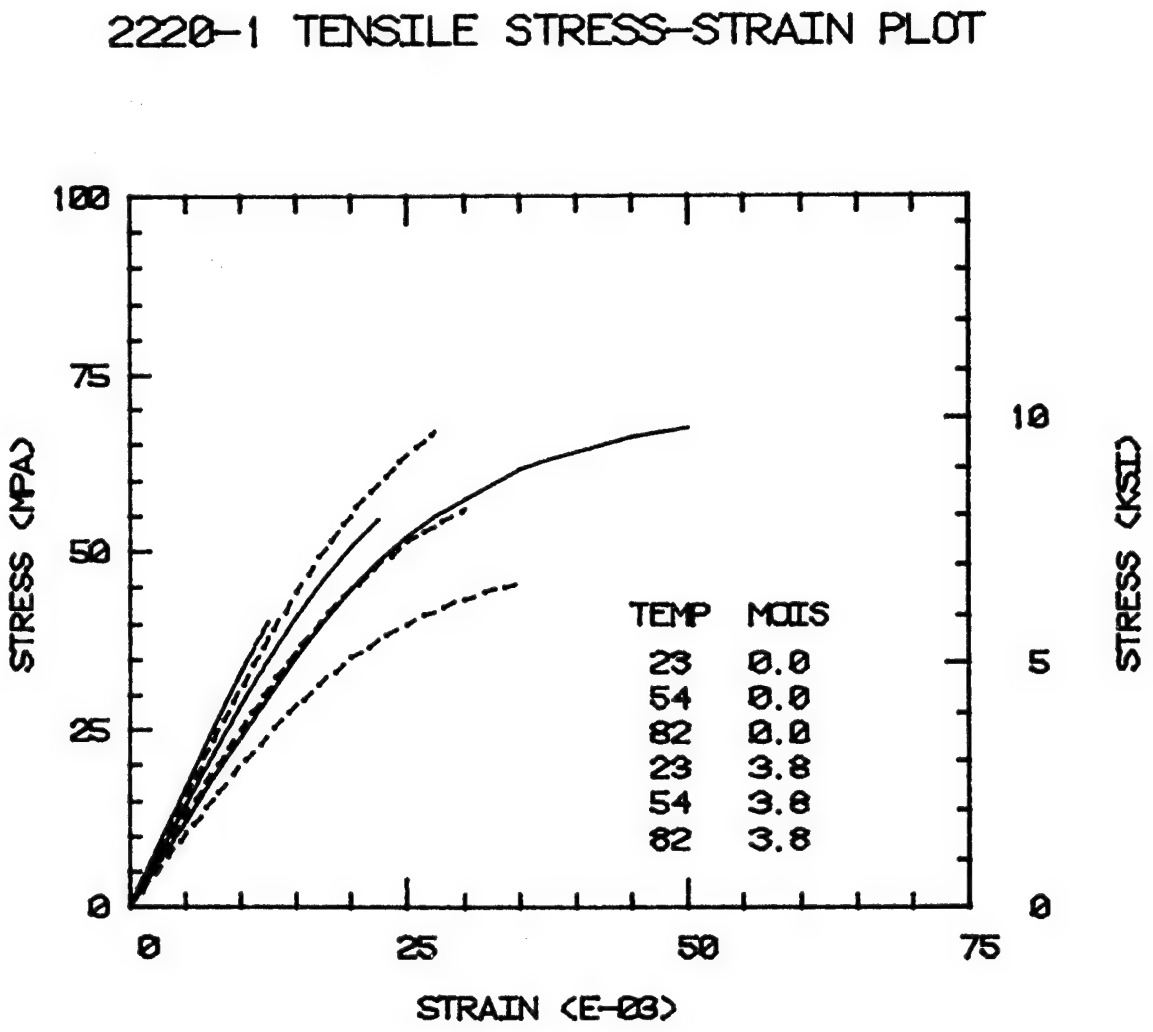


a) tensile data

Figure 65. Hercules 2220-1 Toughened Epoxy Stress-Strain Curves; Average Response at Each Test Condition (dry-solid lines, wet-dashed lines).

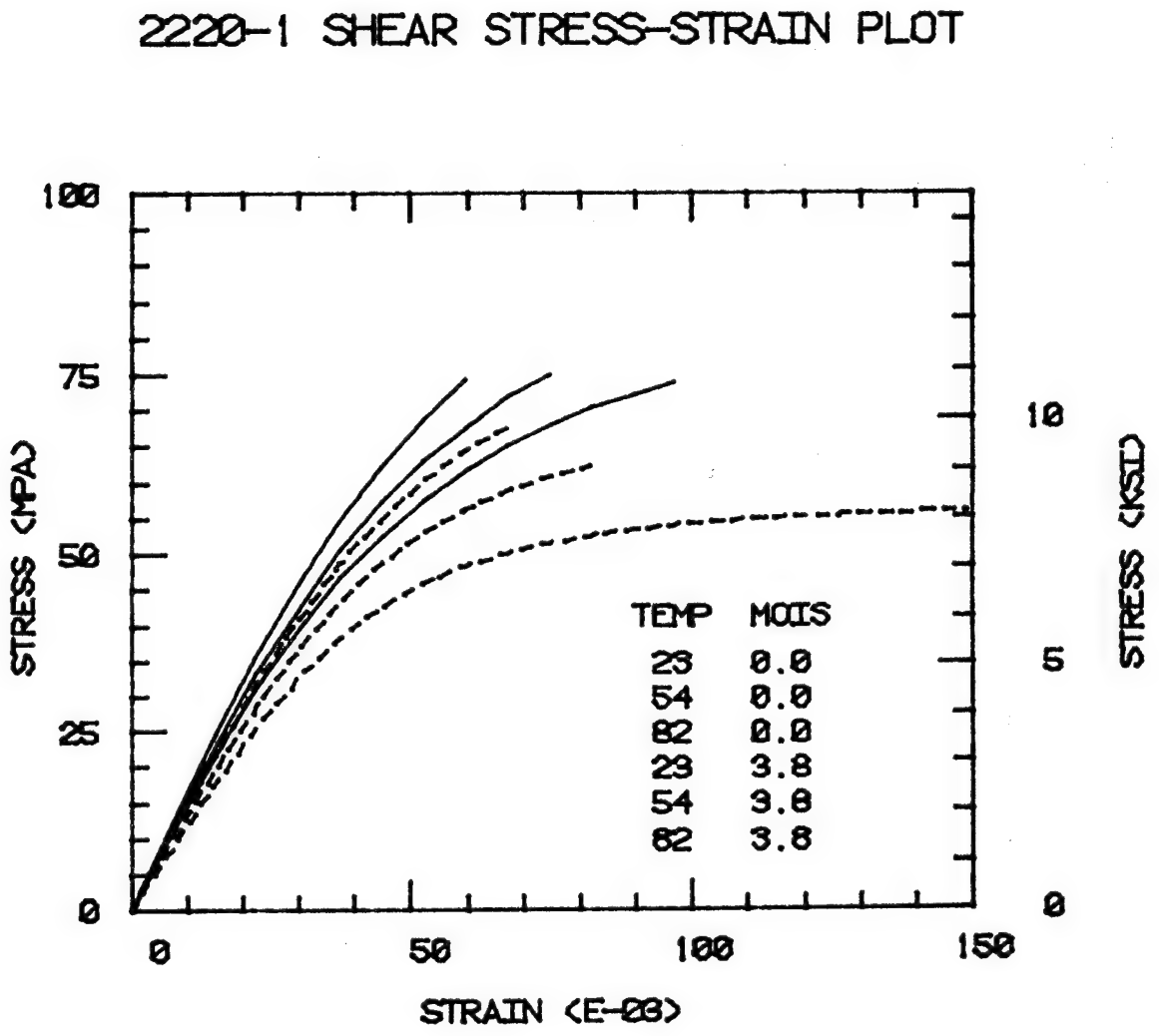


b) shear data

Figure 65 (continued). Hercules 2220-1 Toughened Epoxy Stress-Strain Curves; Average Response at Each Test Condition (dry-solid lines, wet-dashed lines).

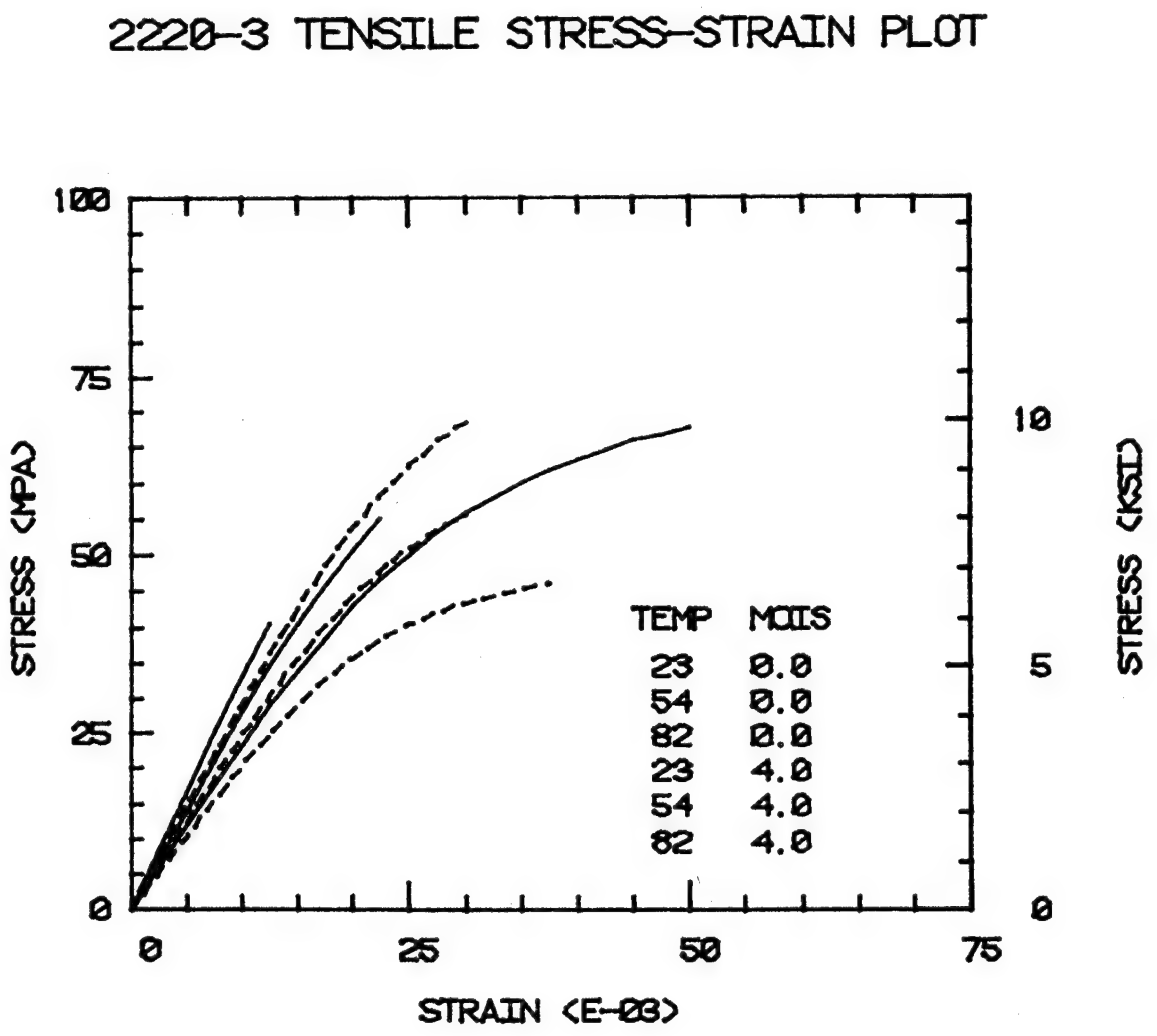


a) tensile data

Figure 66. Hercules 2220-3 Toughened Epoxy Stress-Strain Curves; Average Response at Each Test Condition (dry-solid lines, wet-dashed lines).

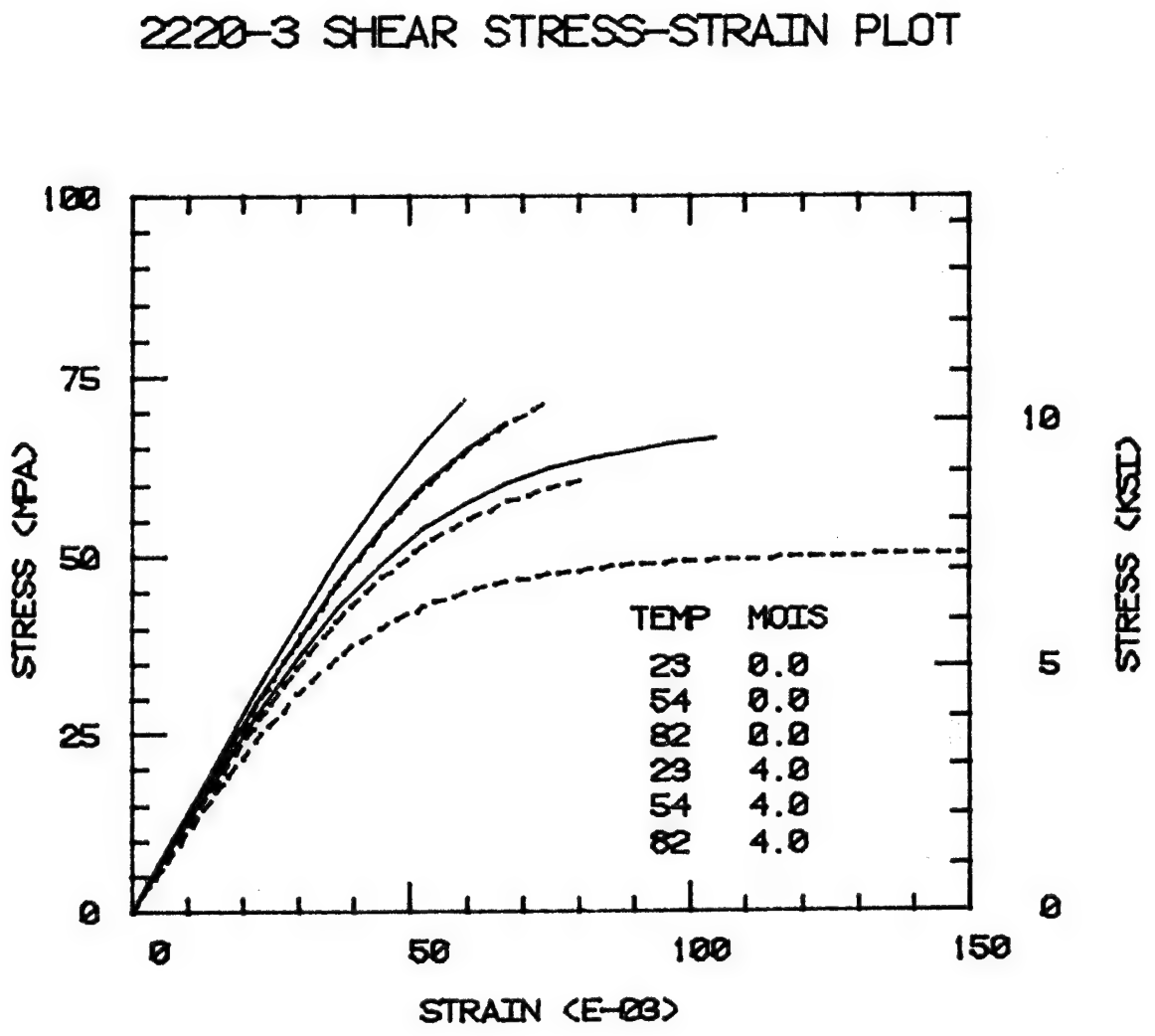


b) shear data

Figure 66 (continued). Hercules 2220-3 Toughened Epoxy Stress-Strain Curves; Average Response at Each Test Condition (dry-solid lines, wet-dashed lines).

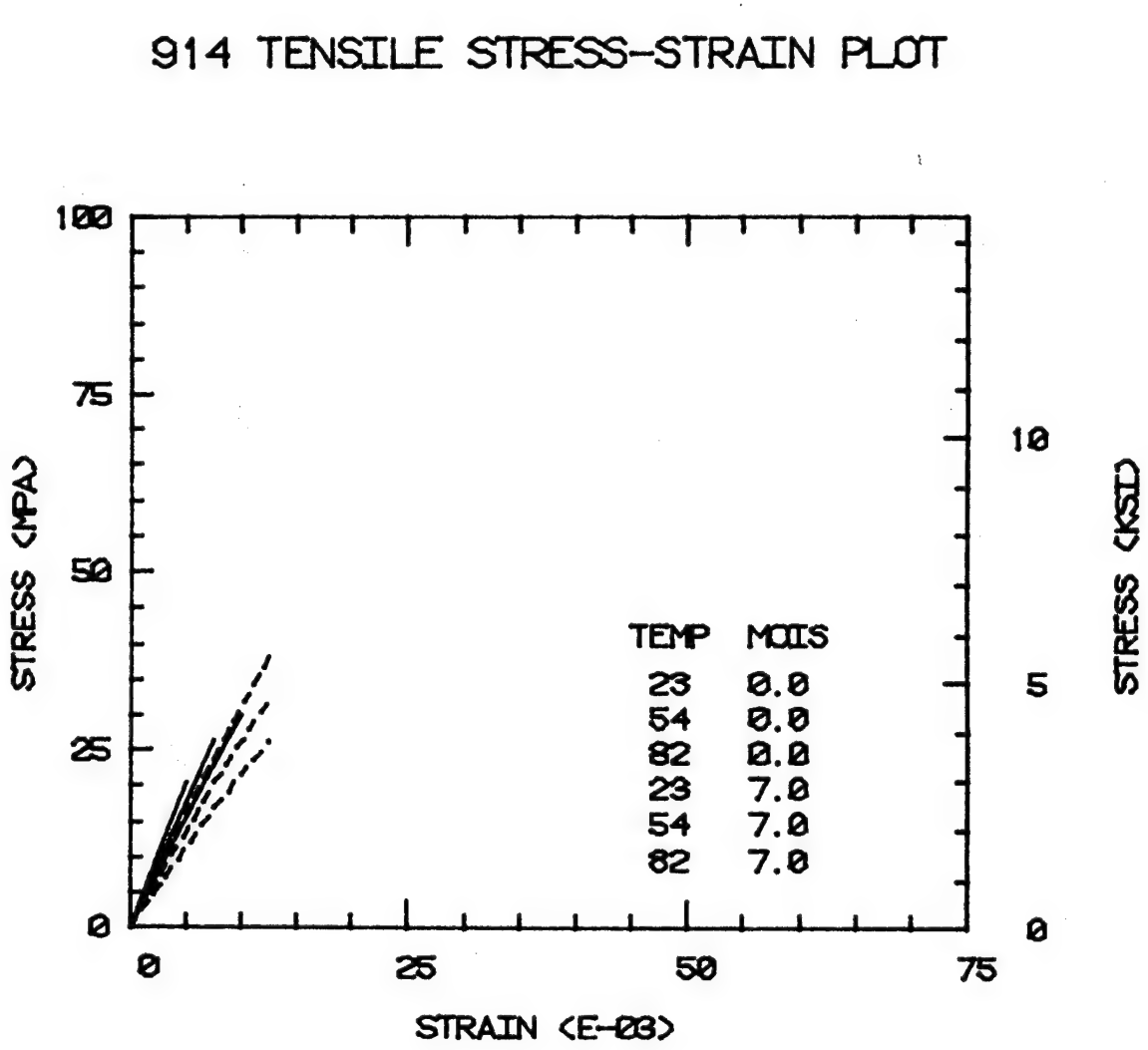


a) tensile data

Figure 67. Fibredux 914 Toughened Epoxy Stress-Strain Curves; Average Response at Each Test Condition (dry-solid lines, wet-dashed lines).

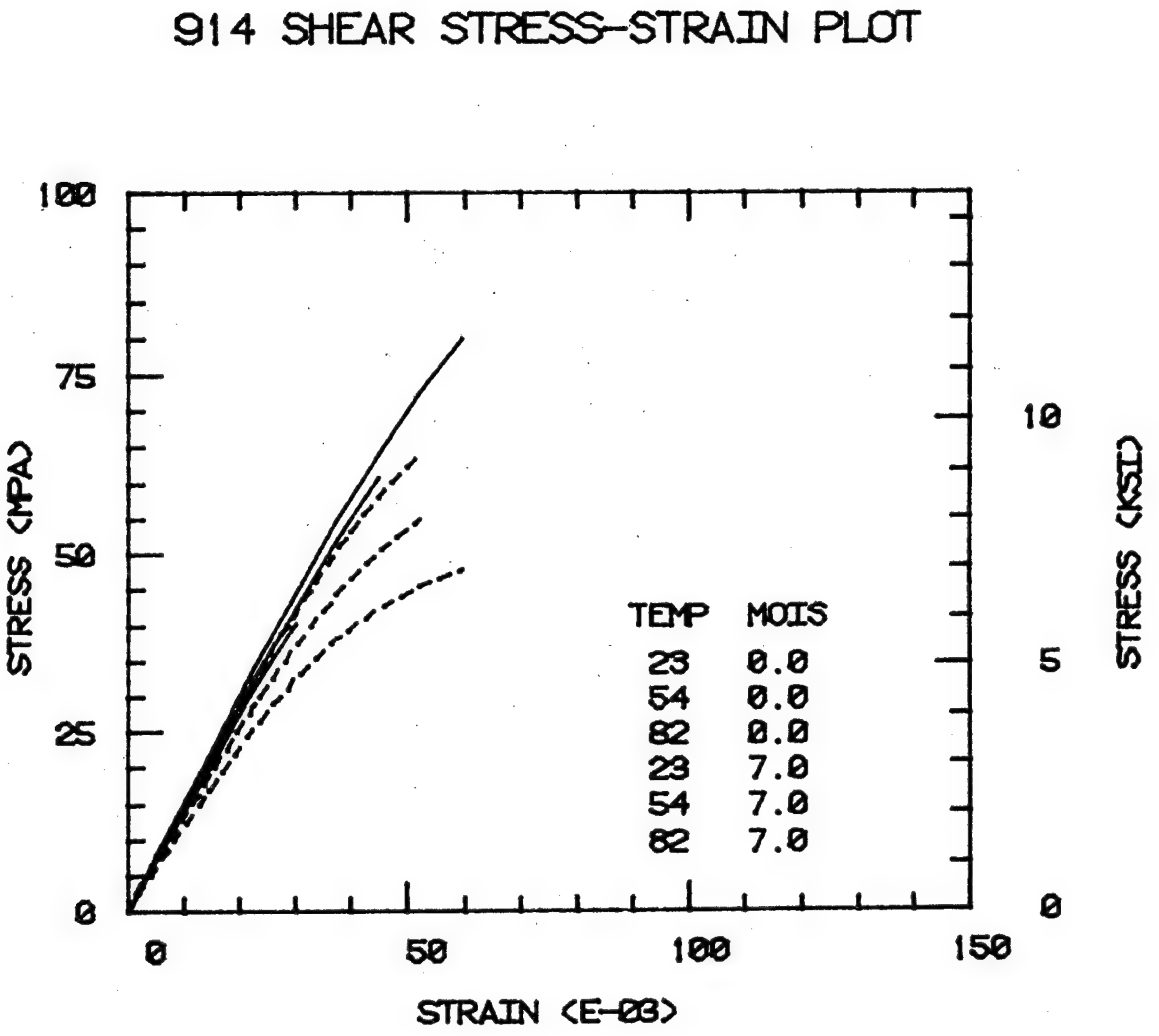


b) shear data

Figure 67 (continued). Fibredux 914 Toughened Epoxy Stress-Strain Curves; Average Response at Each Test Condition (dry-solid lines, wet-dashed lines).

represent the dry specimen tests, the dashed curves the moisture-conditioned specimen tests. As expected, the matrix materials in the dry condition tend to exhibit higher stresses and lower strains to failure. They also exhibit less nonlinear stress-strain response. These plots include all three test temperature curves for each of the two moisture conditions, i.e., the top (solid line) curve represents the 23°C, dry condition and the bottom (dashed line) curve represents the 82°C, wet condition.

The general trends exhibited by the four materials represented in Figures 64 through 67 are discussed in detail in Section 3. Only a brief summary of these trends as they relate to the micromechanics predictions will be given here.

The Hercules 2220-1 and 2220-3 toughened epoxy systems exhibited very similar stress-strain response at all test conditions. The tensile properties were almost identical. The shear stress-shear strain curves of the 2220-1 were slightly higher than the corresponding shear curves of the 2220-3 at all environmental conditions.

The stress-strain response of the two Hercules 2220 systems was much different from that of the untoughened Hercules 3502 epoxy and the toughened Fibredux 914 systems, however. The latter two systems exhibited much lower tensile strengths (approximately one-half as high). Even more significantly, the 3502 and 914 systems exhibited little nonlinearity. Thus, their tensile failure strains were only about one-third those of the 2220 systems. In contrast, the shear strengths of the 3502 and 914 systems were not significantly lower than those of the 2220 systems. The room temperature, dry shear strength of the Fibredux 914 matrix materials was actually the highest of the four materials. The

3502 and 914 systems exhibited little nonlinearity in shear, just as they did in tension, so that the shear strains at failure were about one-half those of the other two materials.

As previously discussed, the stress-strain curves of Figures 64 through 67 were obtained by fitting the actual data to a Richard-Blacklock function. The curve-fit parameters E, $\sigma_o$ and n, as well as the ultimate strength $\sigma_u$, were plotted as functions of temperature for each moisture condition, to permit the easy visualization of their variations. These plots for E for each material are included here as Figures 68 and 69 for the dry and moisture-conditioned tests, respectively. Figures 70 and 71 are corresponding results for G (for the shear data), while Figures 72 and 73 and Figures 74 and 75 represent the ultimate tensile strengths $\sigma_u$ and the ultimate shear strengths $\tau_u$, respectively. The computer-generated best-fit straight line through the three temperature data points in each plot extends out to the cure temperature, 177°C (350°F). It will be noted that this extrapolation to the cure temperature (an extrapolation of 95°C) is greater than the range of the data (23°C to 82°C, i.e., a range of 59°C). In future work, it would be advisable to increase the temperature range over which the properties are measured to provide better input for the micromechanics analysis.

Returning to Figure 68, it can readily be observed that the Young's moduli (E) of the 3502 and 914 resin systems in the dry condition are about 20 percent higher than those of the 2220 systems, the 3502 indicating slightly less temperature sensitivity.

Figure 69, in which the E values for the moisture-conditioned materials are plotted, indicates that all four materials are influenced

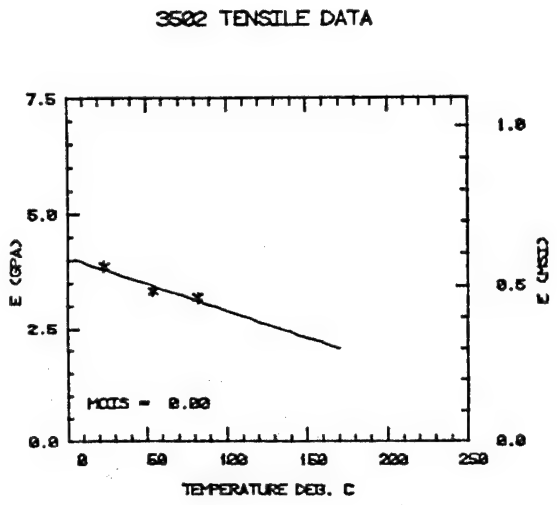


a) Hercules 3502

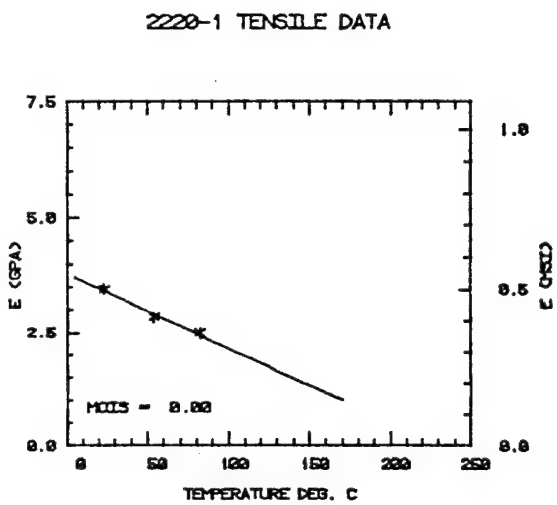


b) Hercules 2220-1

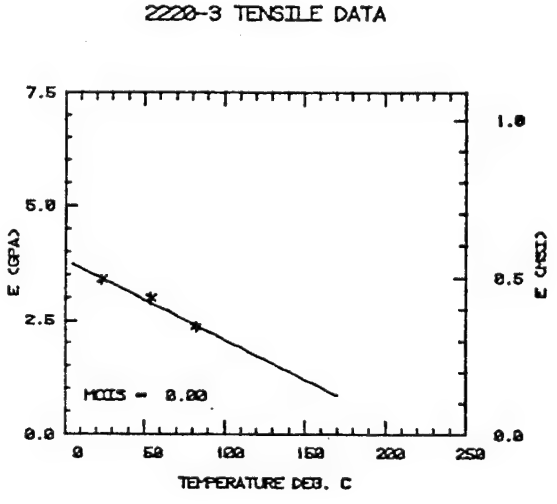


c) Hercules 2220-3

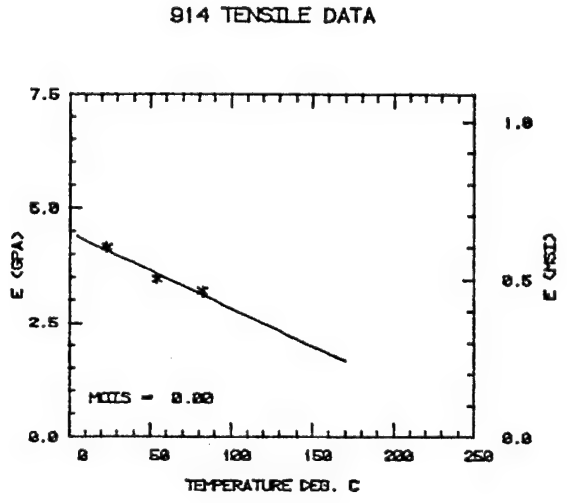


d) Fibredux 914

Figure 68. Tensile Modulus as a Function of Temperature; Dry Condition (Richard-Blacklock Curve-Fits)

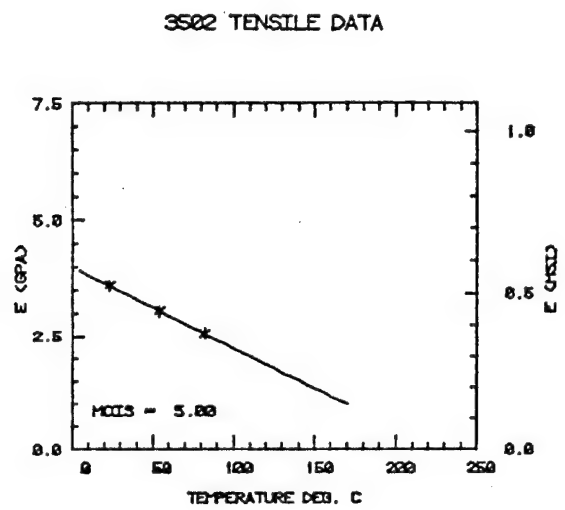


a) Hercules 3502

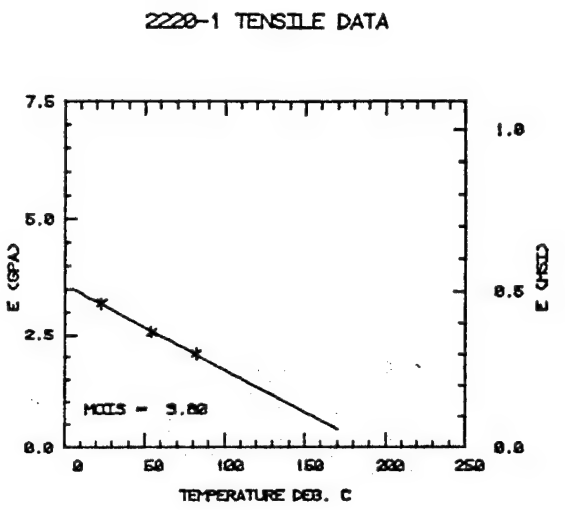


b) Hercules 2220-1

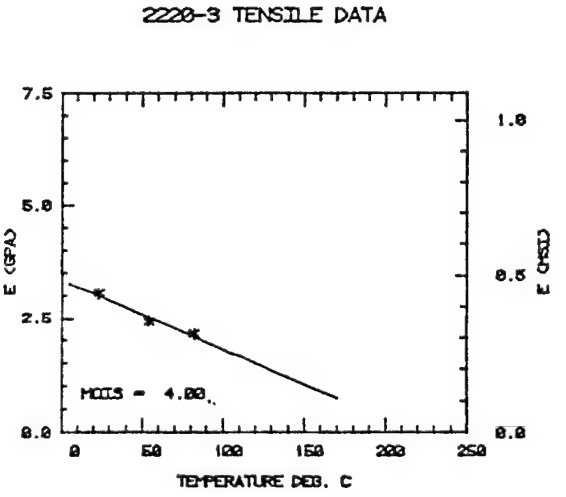


c) Hercules 2220-3

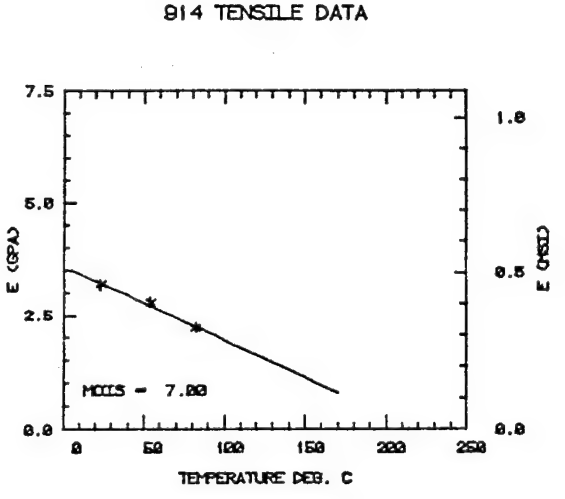


d) Fibredux 914

Figure 69. Tensile Modulus as a Function of Temperature; Moisture-Saturated (Richard-Blacklock Curve-Fits)

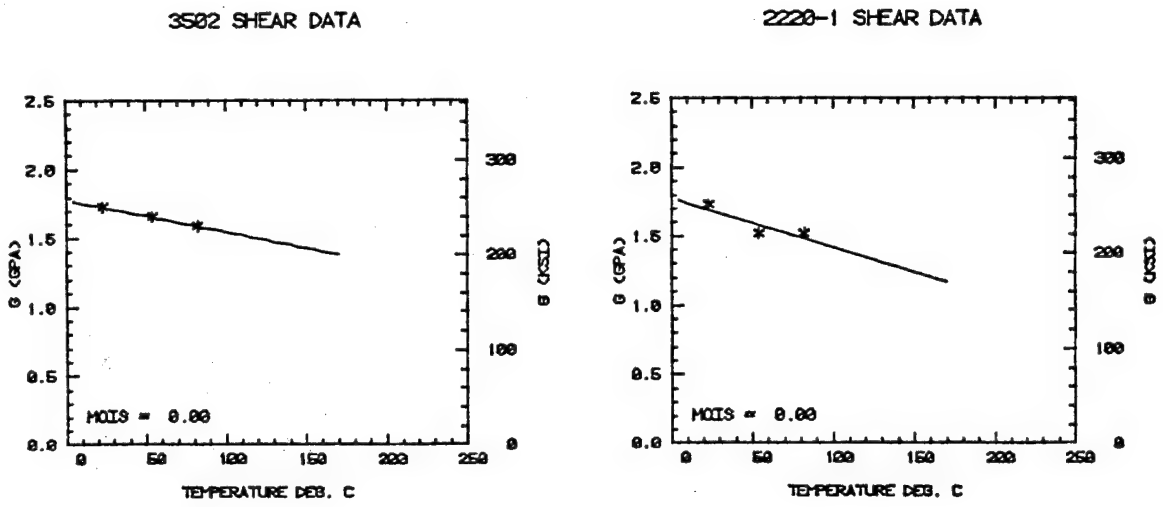


a) Hercules 3502

b) Hercules 2220-1

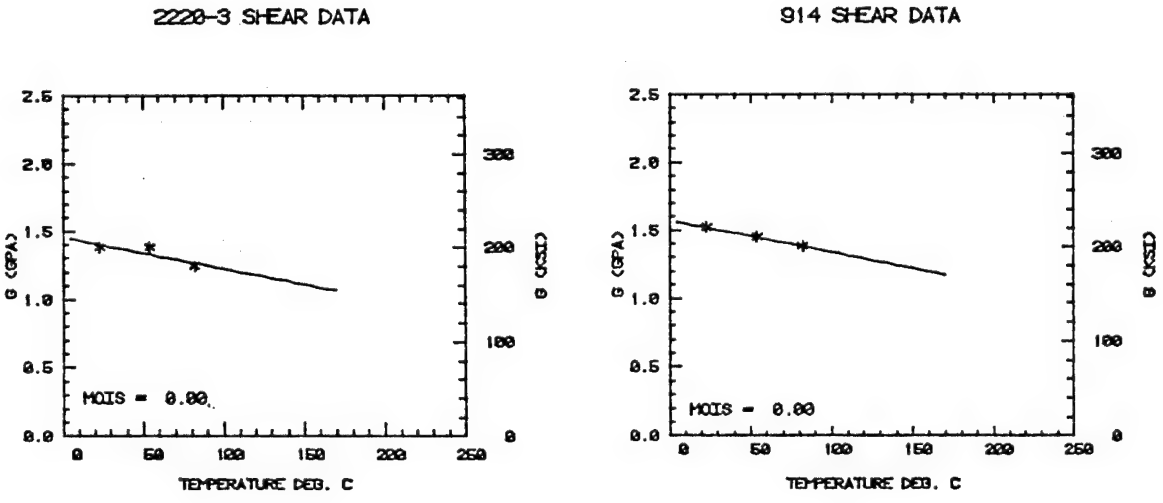


c) Hercules 2220-3

d) Fibredux 914

Figure 70. Shear Modulus as a Function of Temperature; Dry Condition (Richard-Blacklock Curve-Fits)

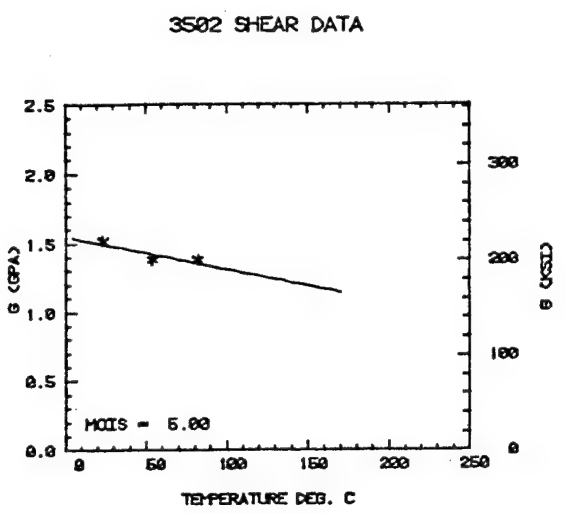


a) Hercules 3502

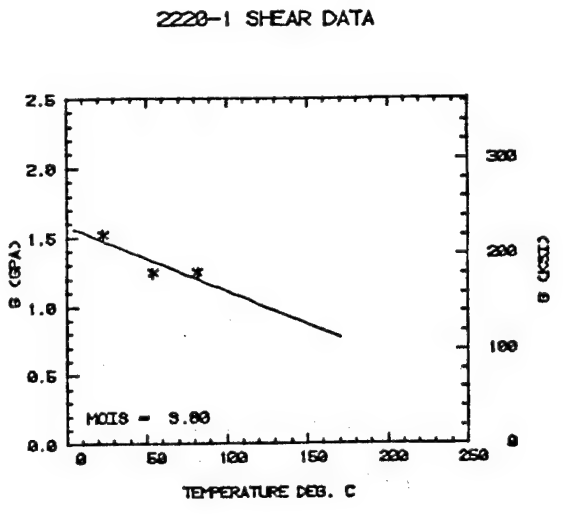


b) Hercules 2220-1

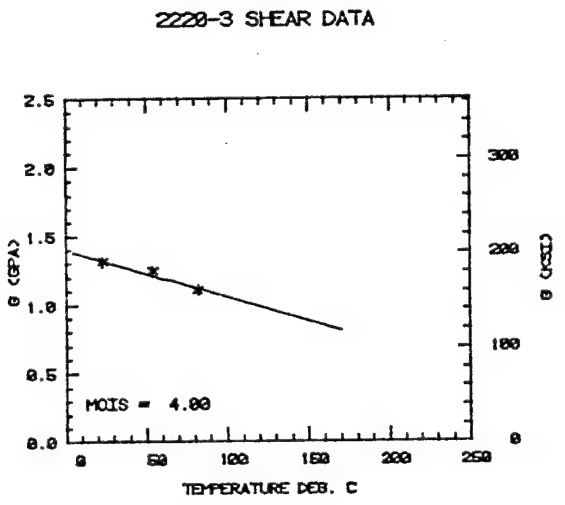


c) Hercules 2220-3

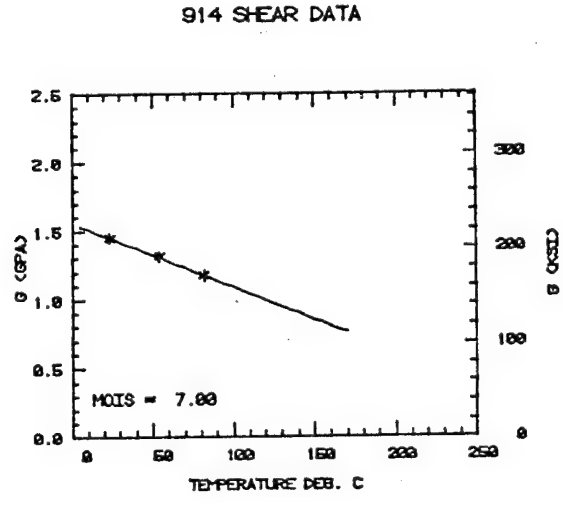


d) Fibredux 914

Figure 71. Shear Modulus as a Function of Temperature; Moisture - Saturated (Richard-Blacklock Curve-Fits)

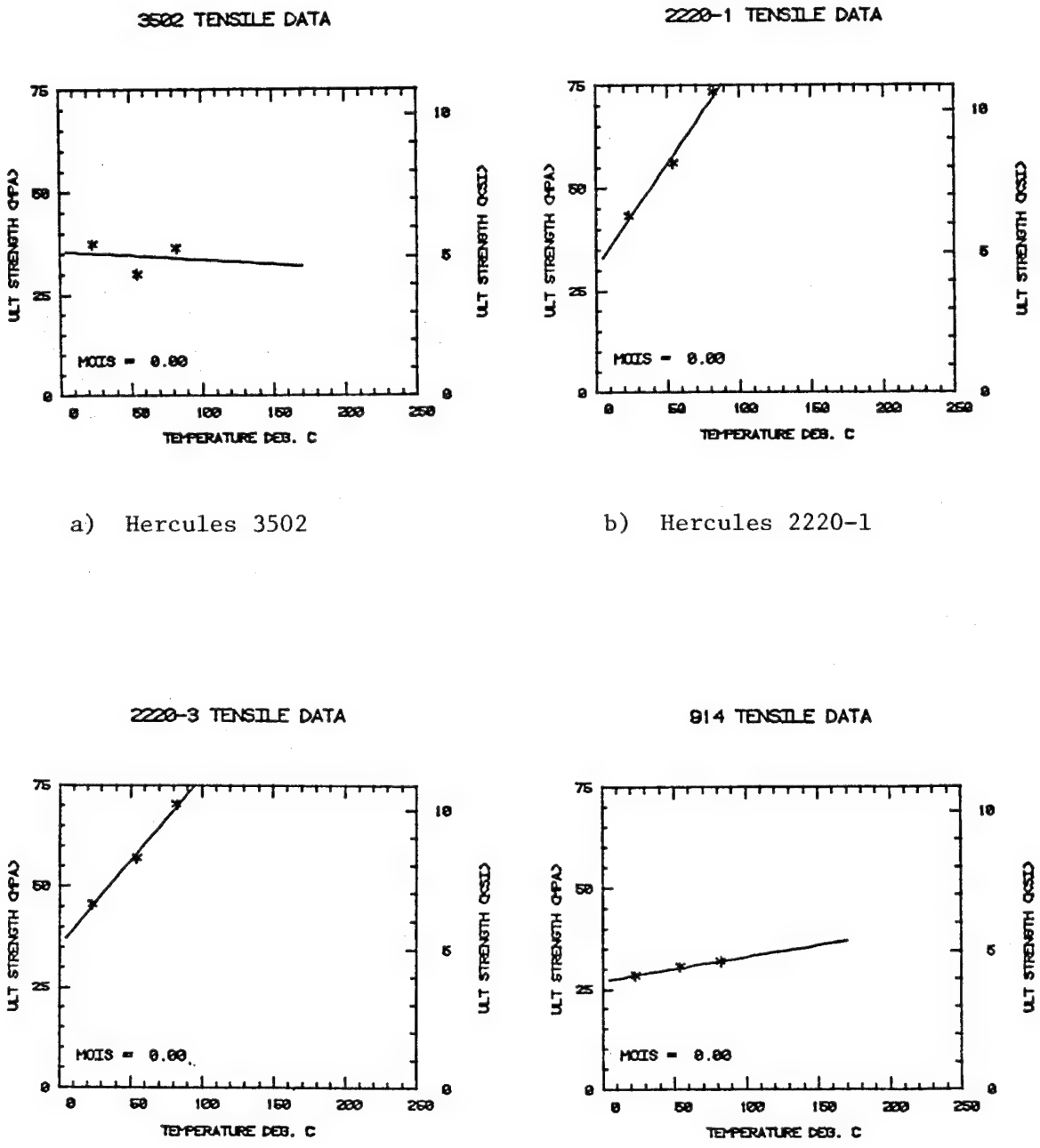


a) Hercules 3502

b) Hercules 2220-1

c) Hercules 2220-3

d) Fibredux 914

Figure 72. Tensile Strength as a Function of Temperature; Dry Condition (Richard-Blacklock Curve-Fits)

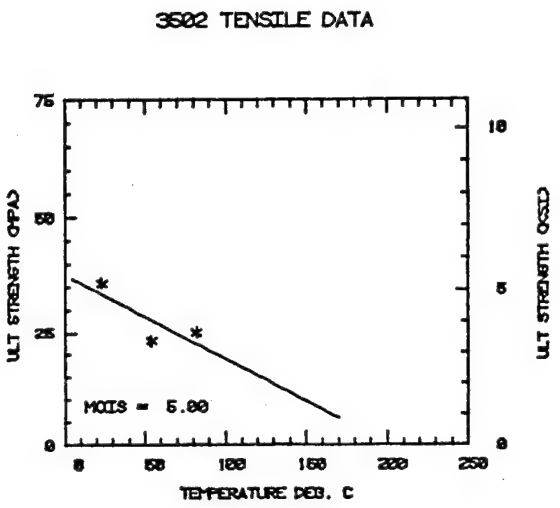


a) Hercules 3502

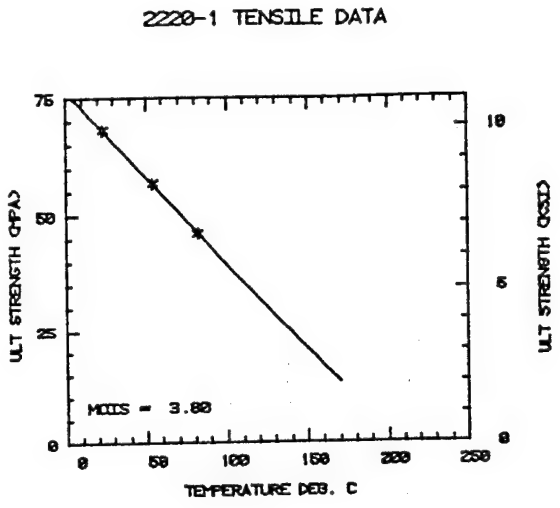


b) Hercules 2220-1

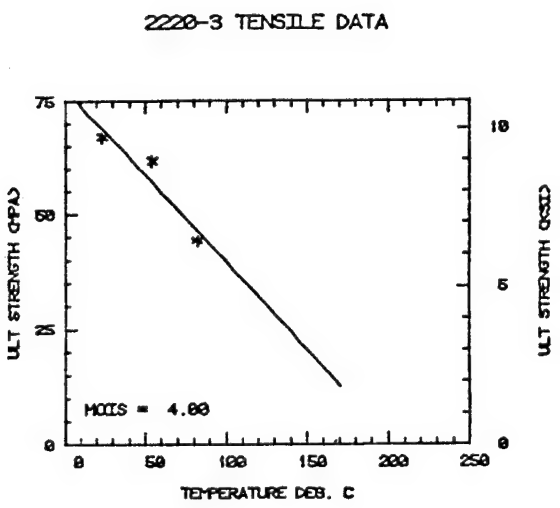


c) Hercules 2220-3

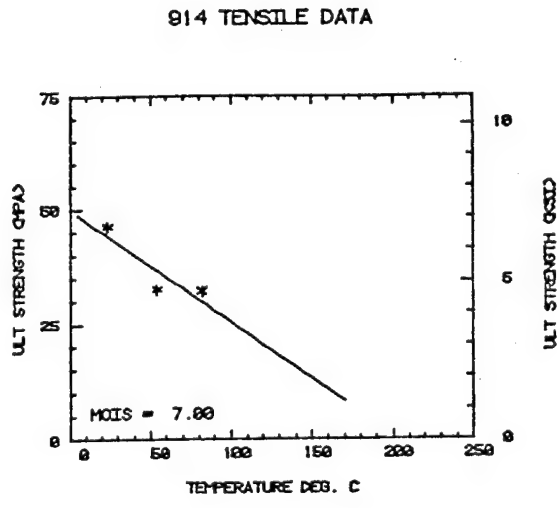


d) Fibredux 914

Figure 73. Tensile Strength as a Function of Temperature; Moisture-Saturated (Richard-Blacklock Curve-Fits)

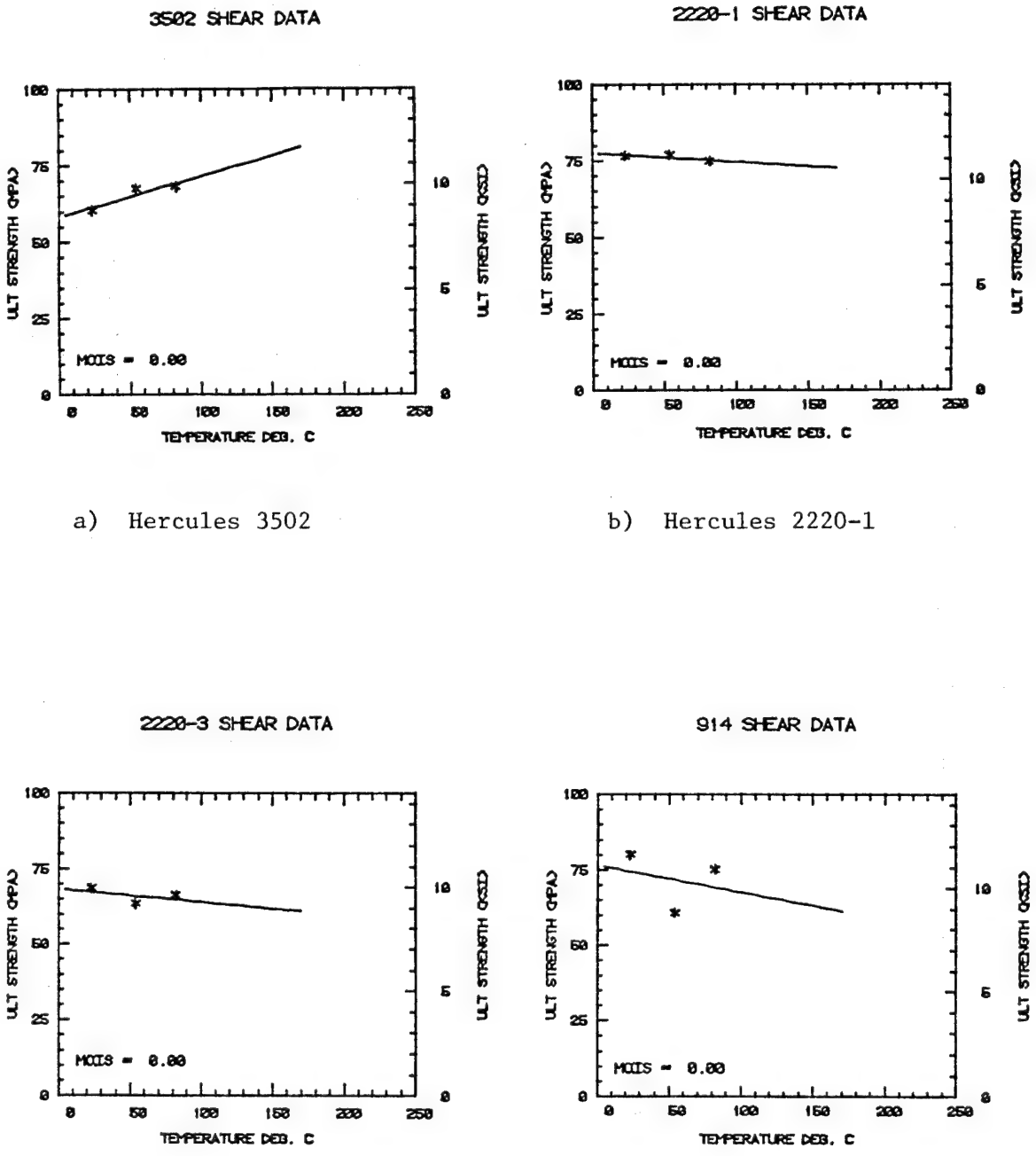


a) Hercules 3502

b) Hercules 2220-1

c) Hercules 2220-3

d) Fibredux 914

Figure 74. Shear Strength as a Function of Temperature; Dry Condition (Richard-Blacklock Curve-Fits)

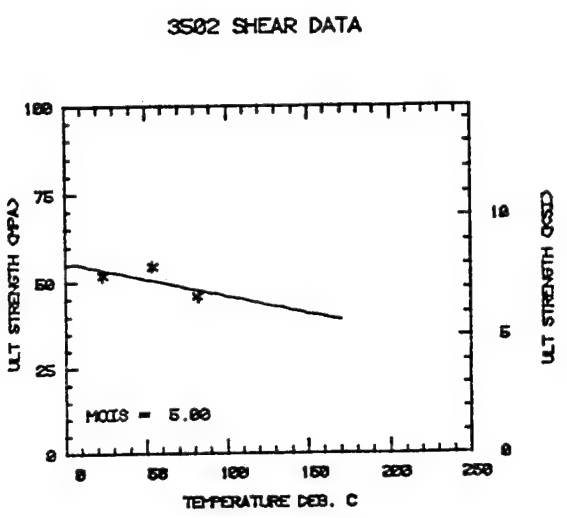


a) Hercules 3502

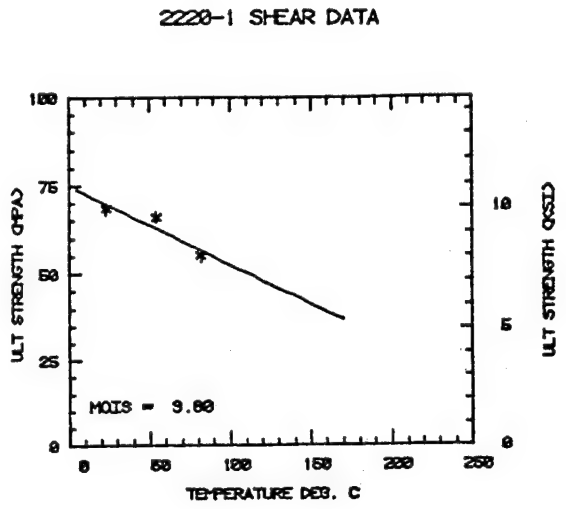


b) Hercules 2220-1

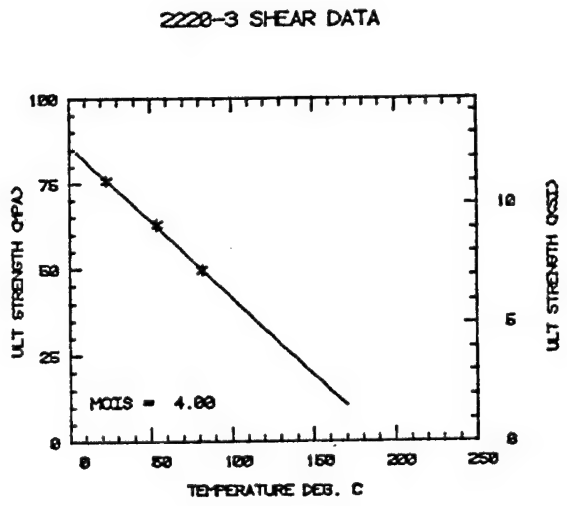


c) Hercules 2220-3

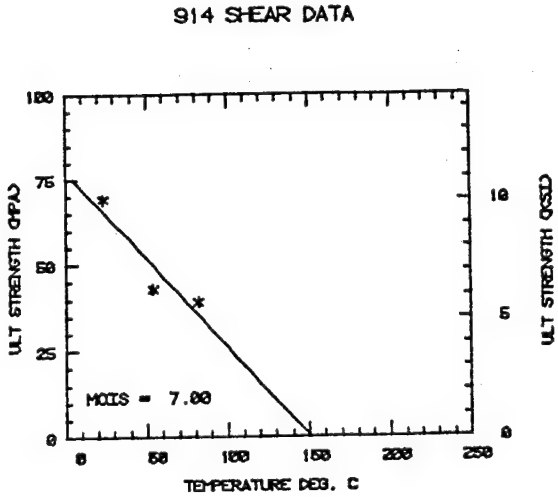


d) Fibredux 914

Figure 75. Shear Strength as a Function of Temperature; Moisture - Saturated (Richard-Blacklock Curve-Fits)

similarly by moisture absorption, even though the 3502 absorbed about 25 percent more moisture than the 2220 systems, and the 914 system about 75 percent more. This was also observed in Section 3, by comparing Figures 10 and 11.

Figure 70 indicates that the room temperature shear modulus (G) of the 2220-3 epoxy is about 25 percent lower than that of the 2220-1 system (even though the E values were comparable). The values of G for the 3502 and 914 systems were comparable, being in the same range as the 2220 systems.

As indicated in Figure 71, the shear modulus of the various systems tended to exhibit a slightly greater temperature sensitivity in the moisture-conditioned state than when tested dry.

Tensile ultimate strength data are presented in Figures 72 and 73, for dry and wet conditions, respectively. Although there is some scatter in these strength data, particularly for the 3502 and 914 systems (which exhibited less ductility), the trends are very distinct. The ultimate tensile strengths of all four materials increased with temperature when the materials were tested dry, and decreased when they were tested wet. It is to be noted that each data point in these plots typically represents the average of five individual tests.

Since it is not expected that the tensile strengths of the dry specimens would have continued to increase with further increases in temperature, the data suggest there is a temperature at which the tensile strength is a relative maximum. Also, since most polymers tend to get stronger at cryogenic temperatures, it is conceivable that the strength would attain a relative minimum at some subambient temperature and then increase with further decreases in temperature. The observed

trend of the dry specimen tensile strength data to increase with increasing temperature may be a defect-related phenomenon. Although the neat resin specimens tested here were of excellent quality and free of any visible defects, microscopic defects exist in any real material. In brittle materials, such as those tested here, even these microscopic flaws act as stress concentrators and can cause failure initiation. The existence of such sites is demonstrated and discussed in Section 4 using scanning electron microscopy of the failed test specimen fracture surfaces. It can be postulated that with increasing test temperature, and hence with increasing strain to failure (as demonstrated in Figures 64 through 67), these pre-existing flaws tend to be blunted by the local plastic flow.

As indicated in Figure 73, at the moisture-saturated condition all four matrix materials exhibited decreasing tensile strength with increasing temperature, an expected trend. Here it can be postulated that the moisture has an effect similar to increasing temperature, i.e., it plasticizes the polymer, increasing its strain capability and blunting stress concentrations created by pre-existing flaws. Thus, these microscopic flaws become relatively ineffective at all test temperatures, and the influence of temperature itself becomes dominant.

The ultimate shear strength data presented in Figures 74 and 75 for the dry and moisture-saturated conditions, respectively, are not as well behaved as the tensile data. While the 3502 system tested dry did increase in shear strength with increasing temperature (Figure 74a), the other three materials did not. Shear specimens tested in the moisture-saturated condition (Figure 75) did indicate a decrease in shear strength with increasing temperature, although the data do

indicate some scatter.

One possible explanation for the difference in ultimate strength response of the dry specimens tested in tension (Figure 72) versus shear (Figure 74) is that in a tensile test the entire cross section of the specimen is subjected to the maximum stress, while in torsional shear the maximum stress occurs only at the outer surface (increasing from zero at the center of the specimen). Thus, the shear specimens might be expected to be less sensitive to pre-existing internal flaws, and hence benefit less from an increase in the stress-concentration blunting effect of increasing test temperature.

Obviously, more data need to be generated and studied before all of the above speculations can be verified or discounted.

Since the data are actually used in the form of octahedral shear stress-octahedral shear strain relations in the micromechanics analysis, it is necessary to convert the data to this form. Sample plots are given in Figure 76. Actually, the data only differ from the uniaxial tensile or shear data by appropriate constant factors. Thus the shapes of the curves shown in Figure 76 are the same as those previously presented in Figures 64 through 67.

In theory, if octahedral shear (distortional energy) is a valid representation of multiaxial stress state effects, then either uniaxial tensile or shear data, when converted to octahedral values, should give the same results. The purpose of Figure 76 is to present the data from both types of test on the same plots, for the two environmental extremes, i.e., room temperature, dry (RTD) and elevated temperature, wet (ETW) conditions.

As can be seen, the tensile tests appear to result in premature

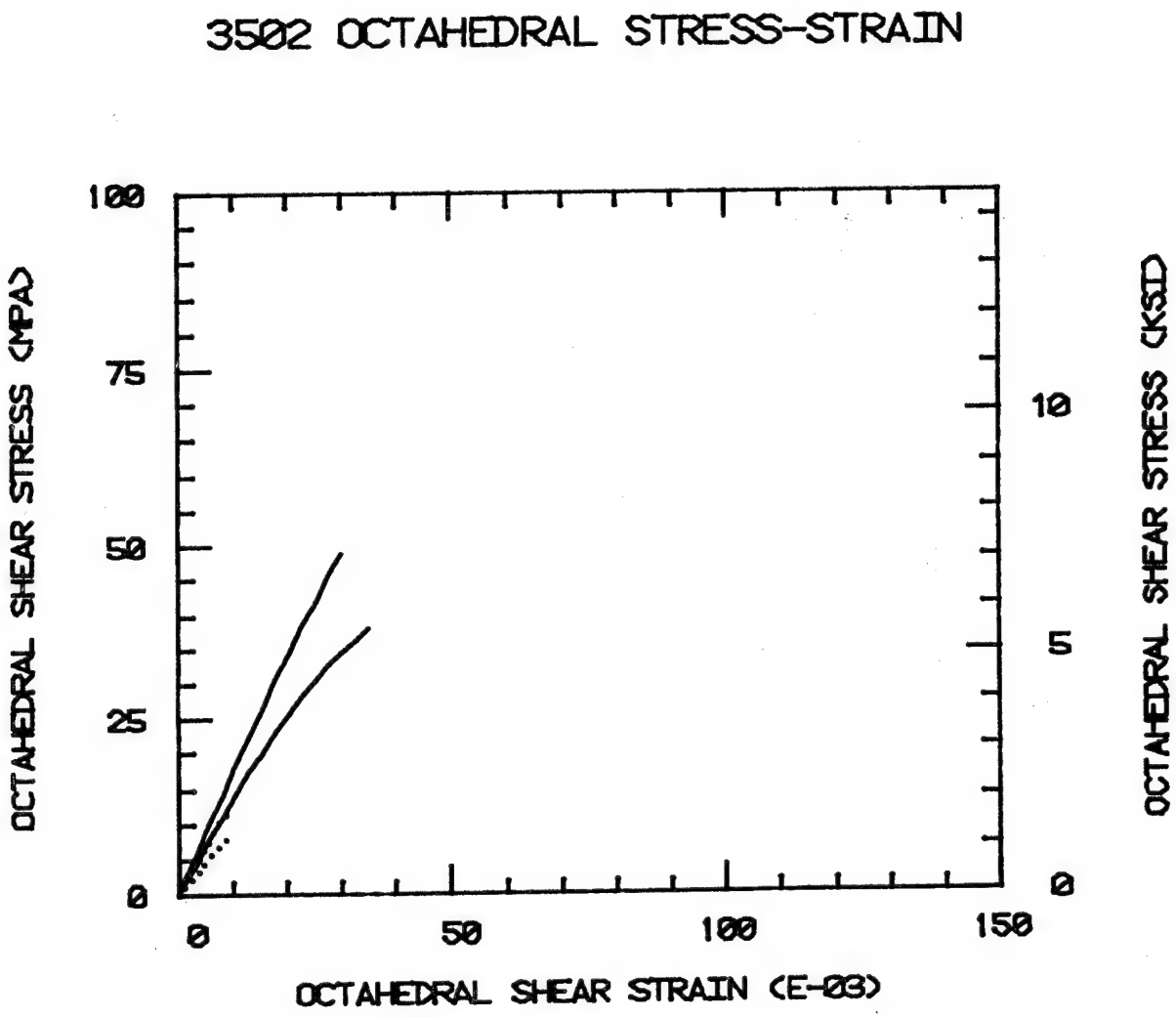


a) Hercules 3502 Baseline Epoxy

Figure 76. Neat Epoxy Octahedral Shear Stress-Shear Strain Curves, from Tensile (dashed lines) and Shear (solid lines) Tests; Only RTD (upper curve) and ETW (lower curve) Data Shown.

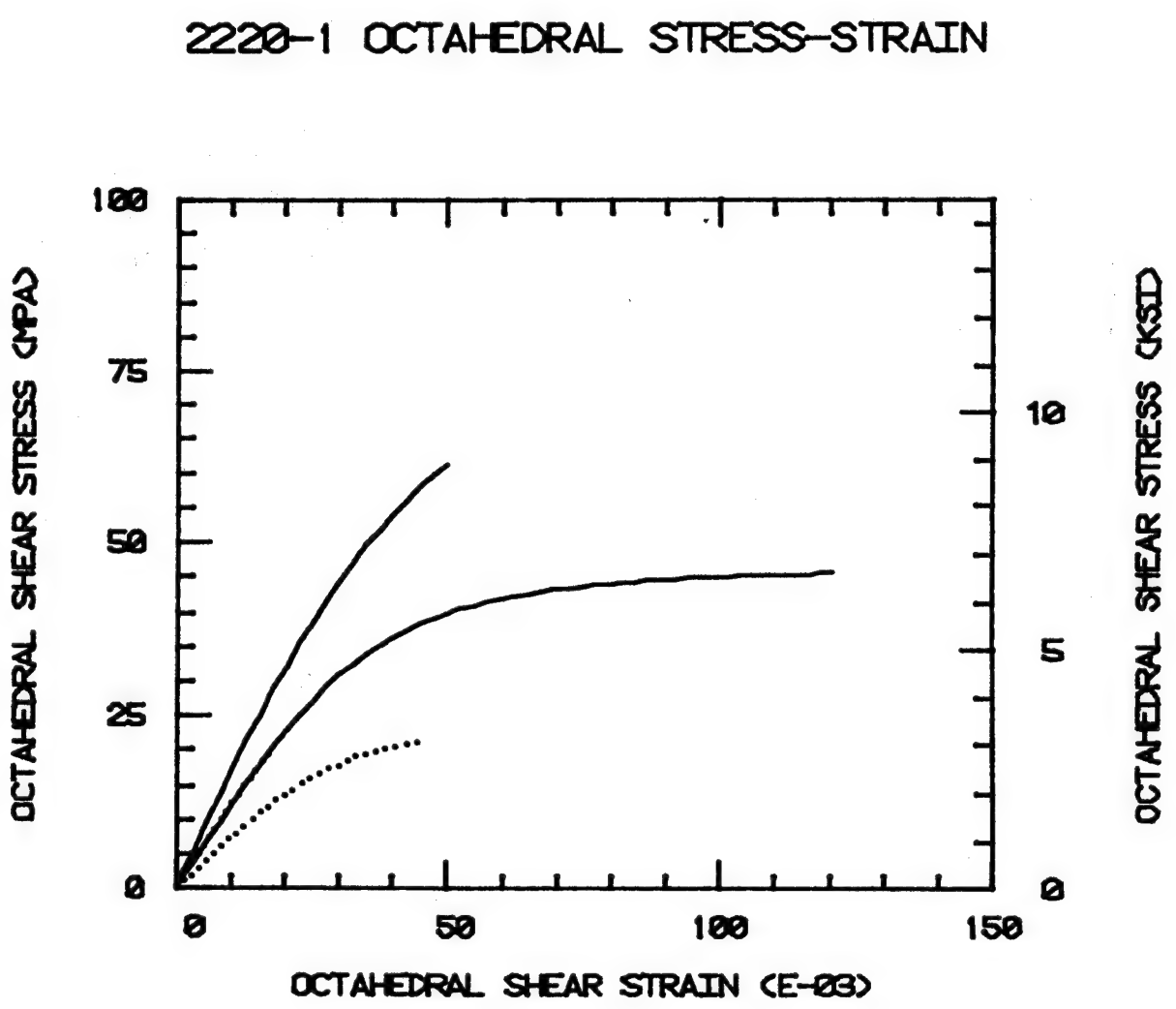


b) Hercules 2220-1 Toughened Epoxy

Figure 76 (continued). Neat Epoxy Octahedral Shear Stress-Shear Strain Curves, from Tensile (dashed lines) and Shear (solid lines) Tests; Only RTD (upper curve) and ETW (lower curve) Data Shown.

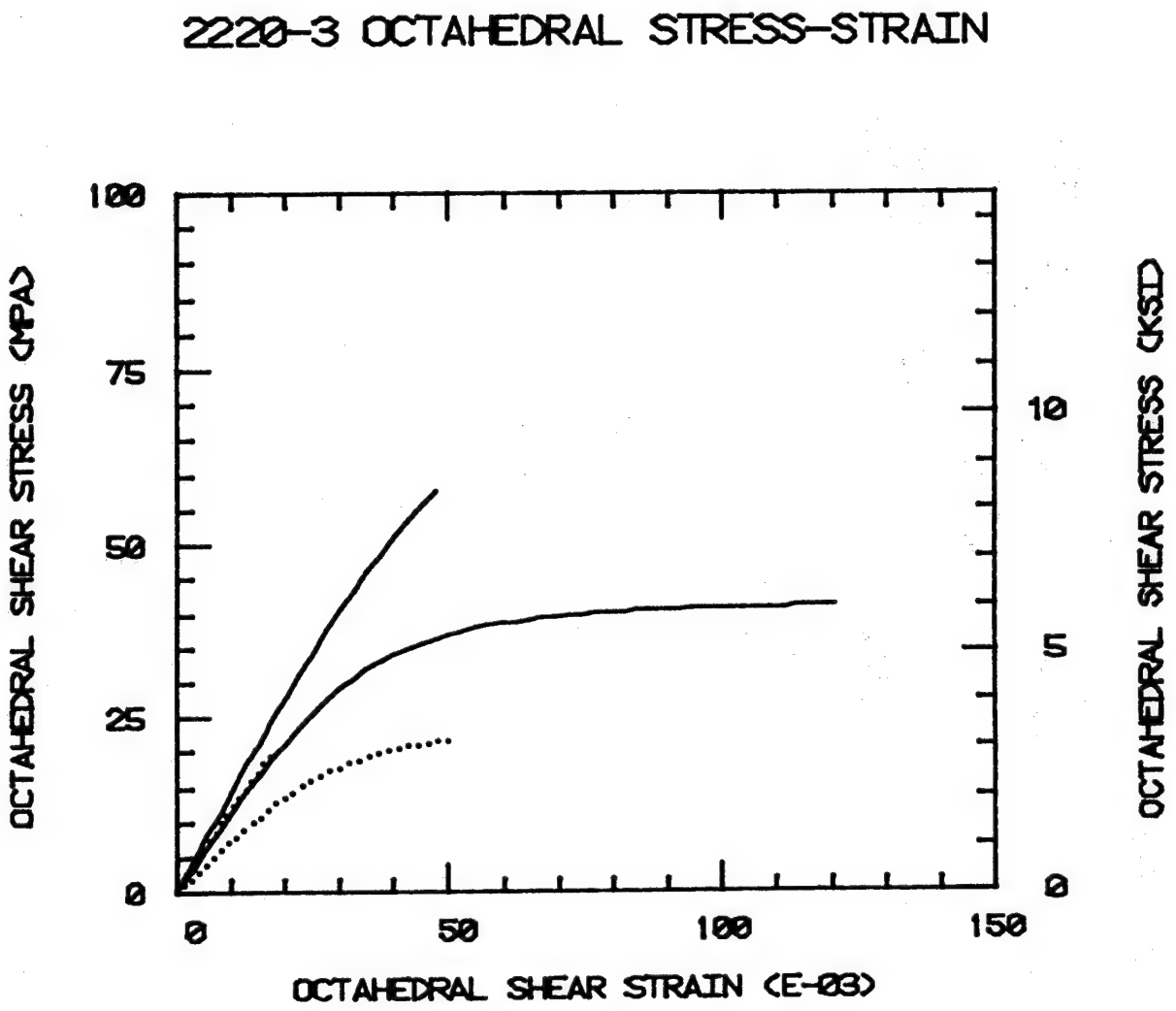


c) Hercules 2220-3 Toughened Epoxy

Figure 76 (continued). Neat Epoxy Octahedral Shear Stress-Shear Strain Curves, from Tensile (dashed lines) and Shear (solid lines) Tests; Only RTD (upper curve) and ETW (lower curve) Data Shown.

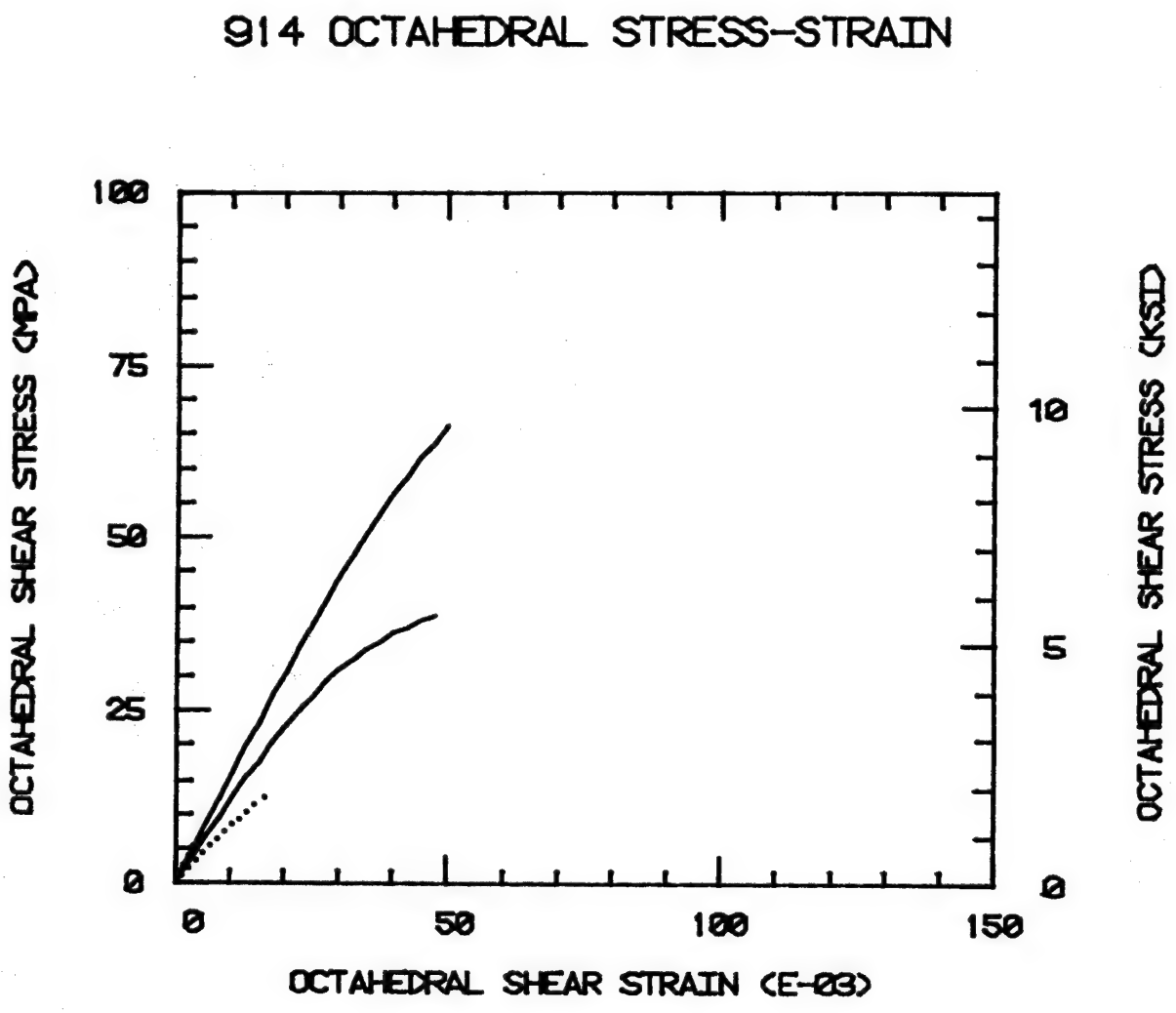


d) Fibredux 914 Toughened Epoxy

Figure 76 (continued). Neat Epoxy Octahedral Shear Stress-Shear Strain Curves, from Tensile (dashed lines) and Shear (solid lines) Tests; Only RTD (upper curve) and ETW (lower curve) Data Shown.

failures, which is most pronounced for the less ductile Hercules 3502 and Fibredux 914 epoxies (Figures 76a and 76d). However, the Hercules 2220 systems (Figures 76b and 76c) both indicate that if premature tensile failures did not occur, the tensile data probably would not have followed the shear data. This difference has been observed previously also, and is as yet unexplained. For the present predictions of composite response, the neat epoxy data generated from the shear tests will be utilized.

In addition to the stiffness and strength properties of the matrix material as a function of temperature and moisture, the coefficients of thermal expansion and moisture expansion are also required as input to the micromechanics analysis.

As discussed in detail in Section 3, thermal expansion was measured over the temperature range from 21°C to 93°C. For use in the analysis, these data were fit to a second-order polynomial function of temperature. These fits are plotted with the corresponding experimental data in Figures 77 and 78, for the dry materials and the moisture-saturated materials, respectively. The normalized length is the change in length divided by the original length, i.e., $\Delta\ell/\ell$, which when divided by the temperature change for a given interval gives the coefficient of thermal expansion $\alpha$. As will be noted, $\alpha$ is essentially constant over the temperature range of interest, in both the dry and wet conditions. Also, $\alpha$ tends to be slightly higher for the moisture-saturated materials relative to the materials in the dry state, the 914 matrix being a minor exception. Also, the 3502 system does have a somewhat lower $\alpha$ than the other three materials.

Moisture expansion plots are presented in Figures 79 through 82 for

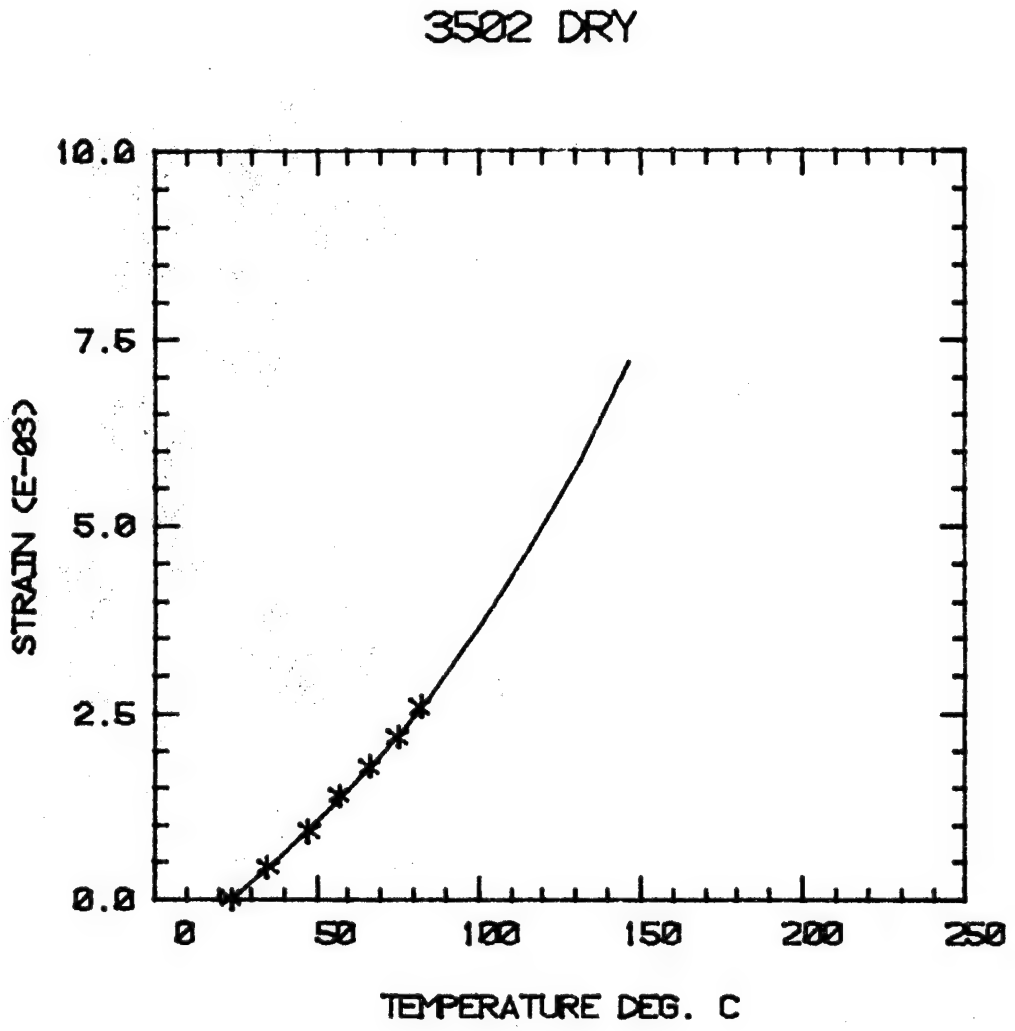


a) Hercules 3502 Baseline Epoxy

Figure 77. Neat Epoxy Thermal Expansion as a Function of Temperature; Dry Condition.

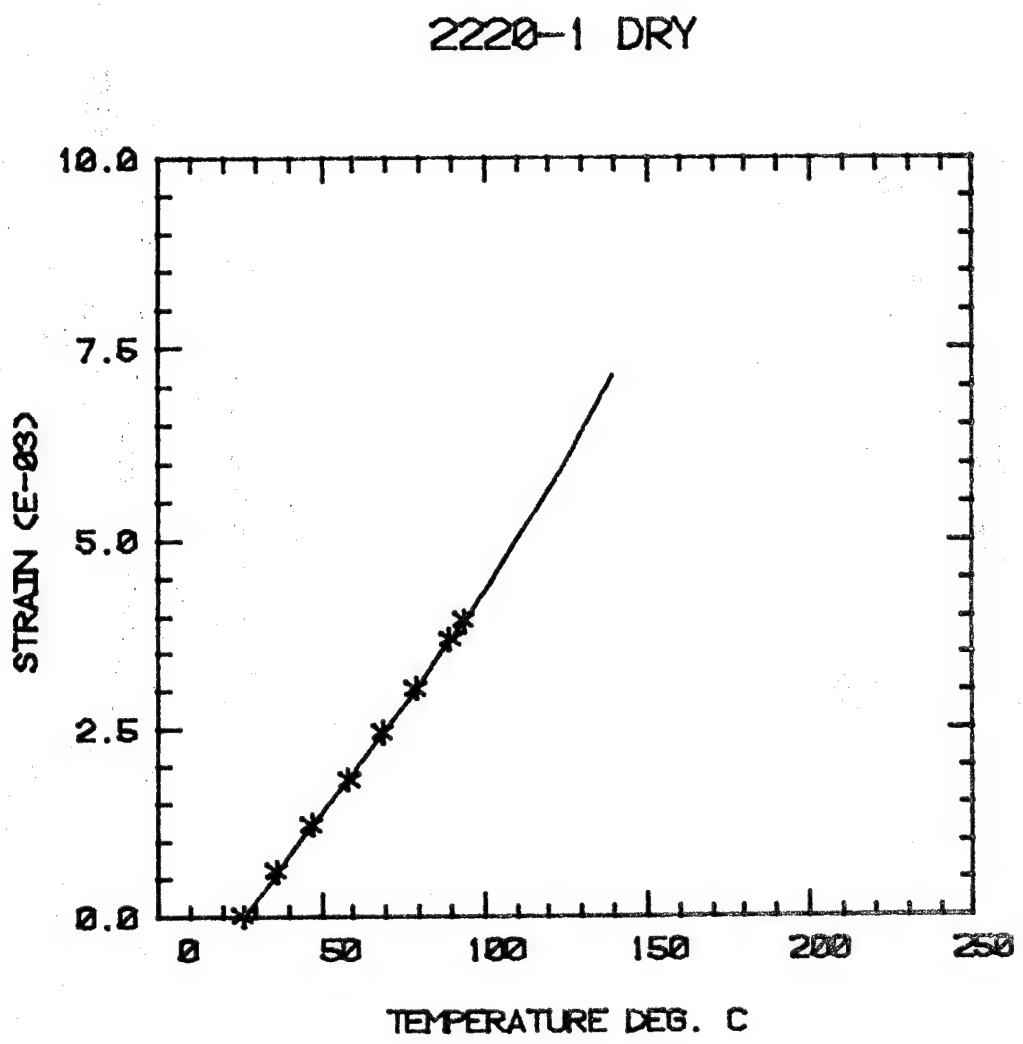


b) Hercules 2220-1 Toughened Epoxy

Figure 77 (continued). Neat Epoxy Thermal Expansion as a Function of Temperature; Dry Condition.

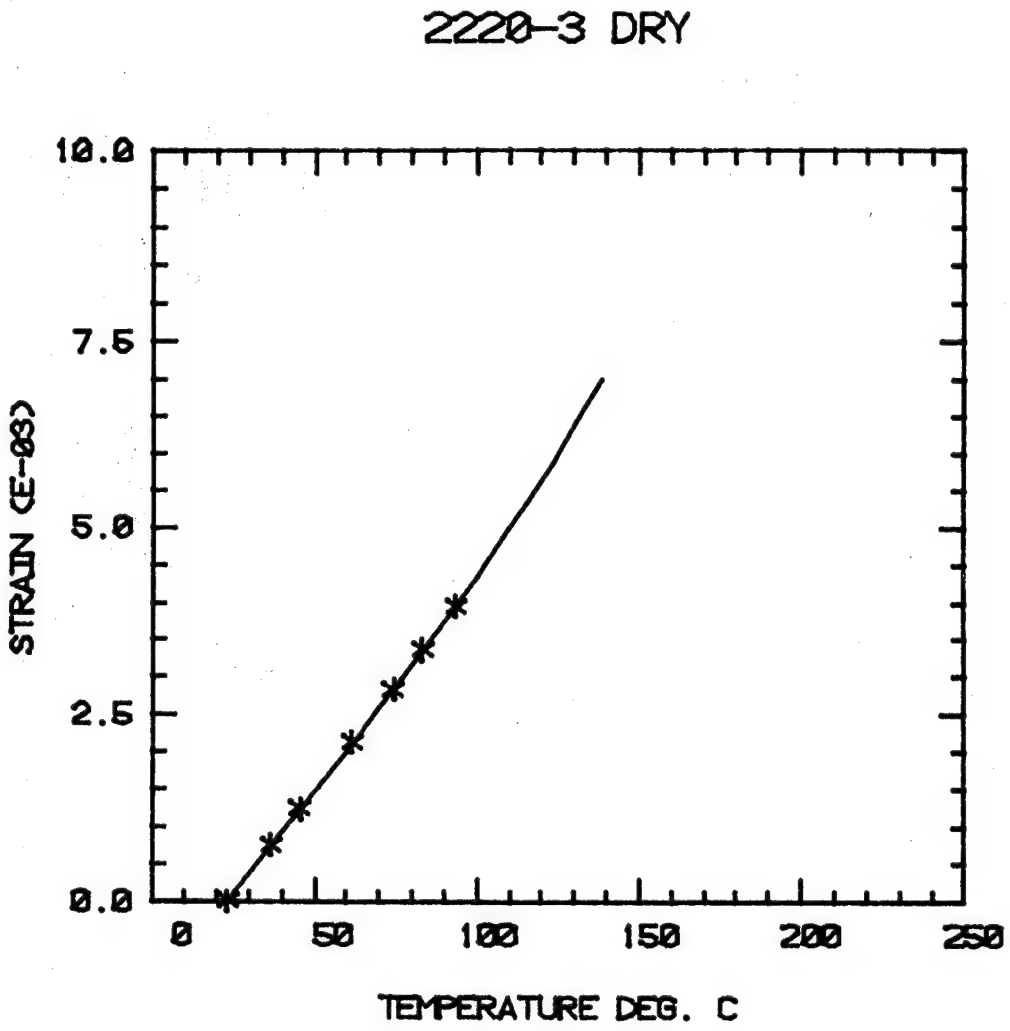


c) Hercules 2220-3 Toughened Epoxy

Figure 77 (continued). Neat Epoxy Thermal Expansion as a Function of Temperature; Dry Condition.

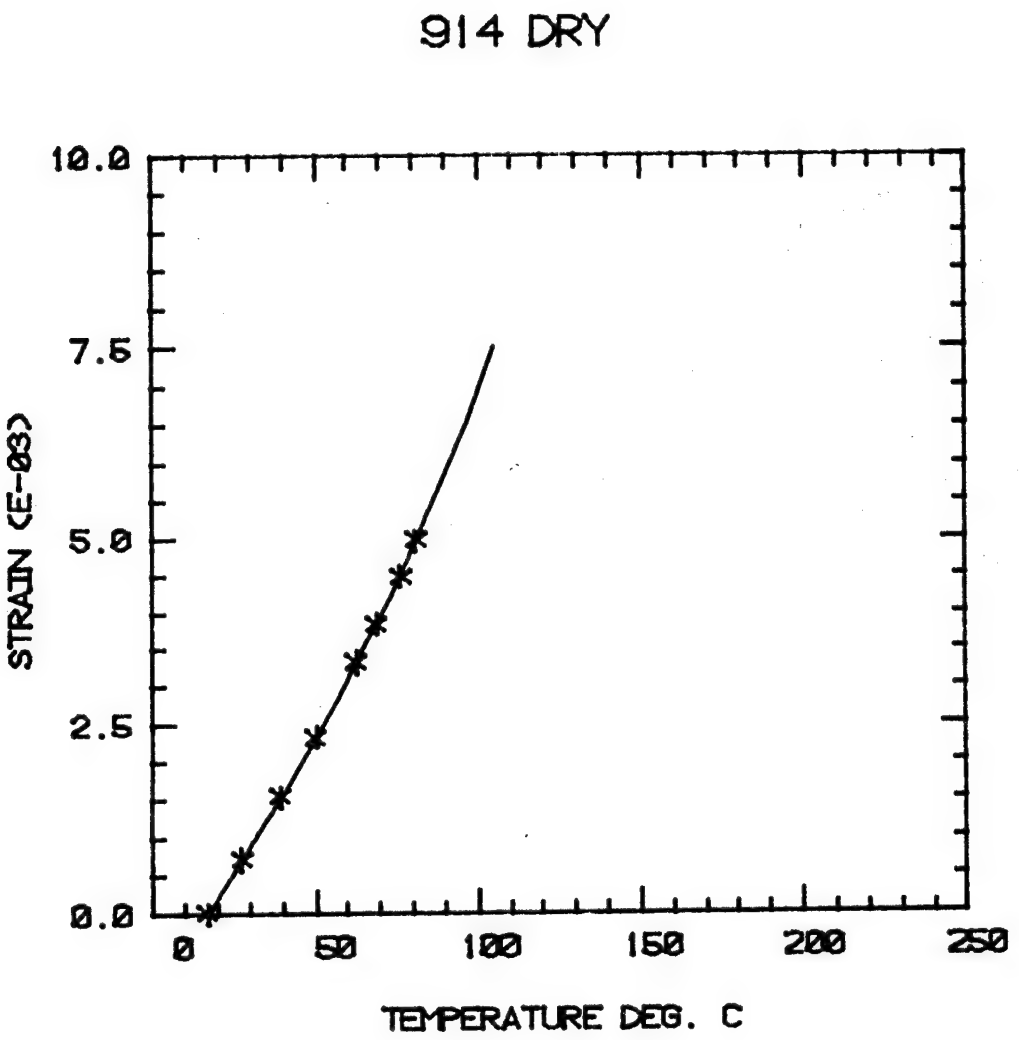


d) Fibredux 914 Toughened Epoxy

Figure 77 (continued). Neat Epoxy Thermal Expansion as a Function of Temperature; Dry Condition.

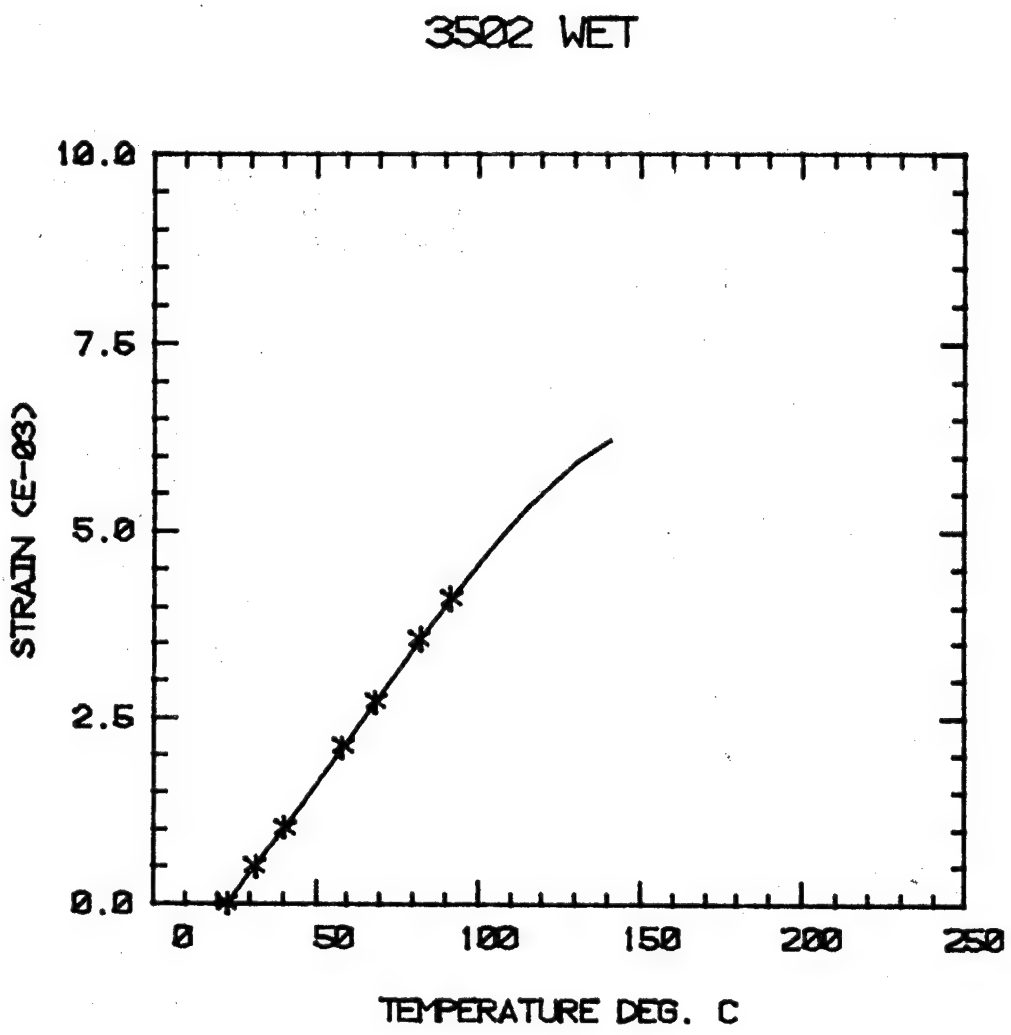


a) Hercules 3502 Baseline Epoxy

Figure 78. Neat Epoxy Thermal Expansion as a Function of Temperature; Moisture-Saturated.

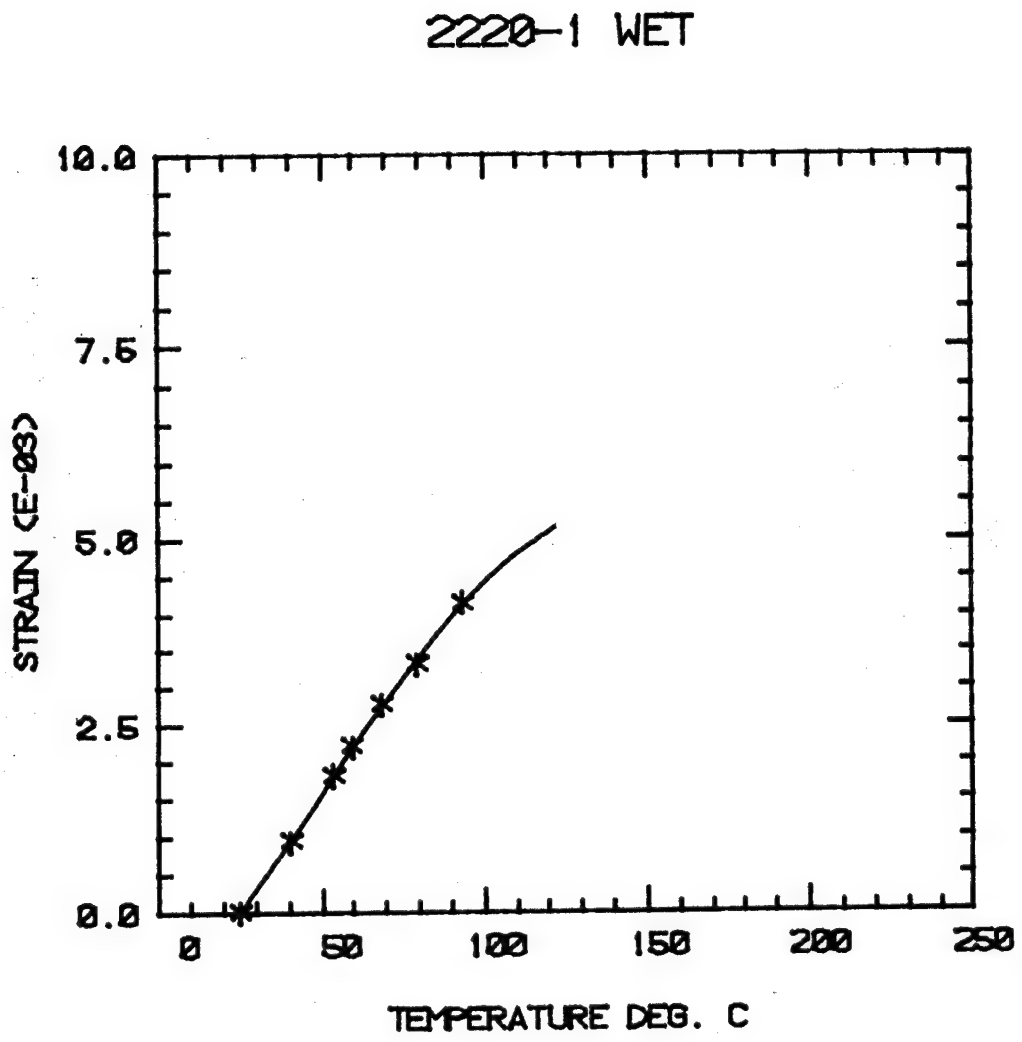


b) Hercules 2220-1 Toughened Epoxy

Figure 78 (continued). Neat Epoxy Thermal Expansion as a Function of Temperature; Moisture - Saturated.

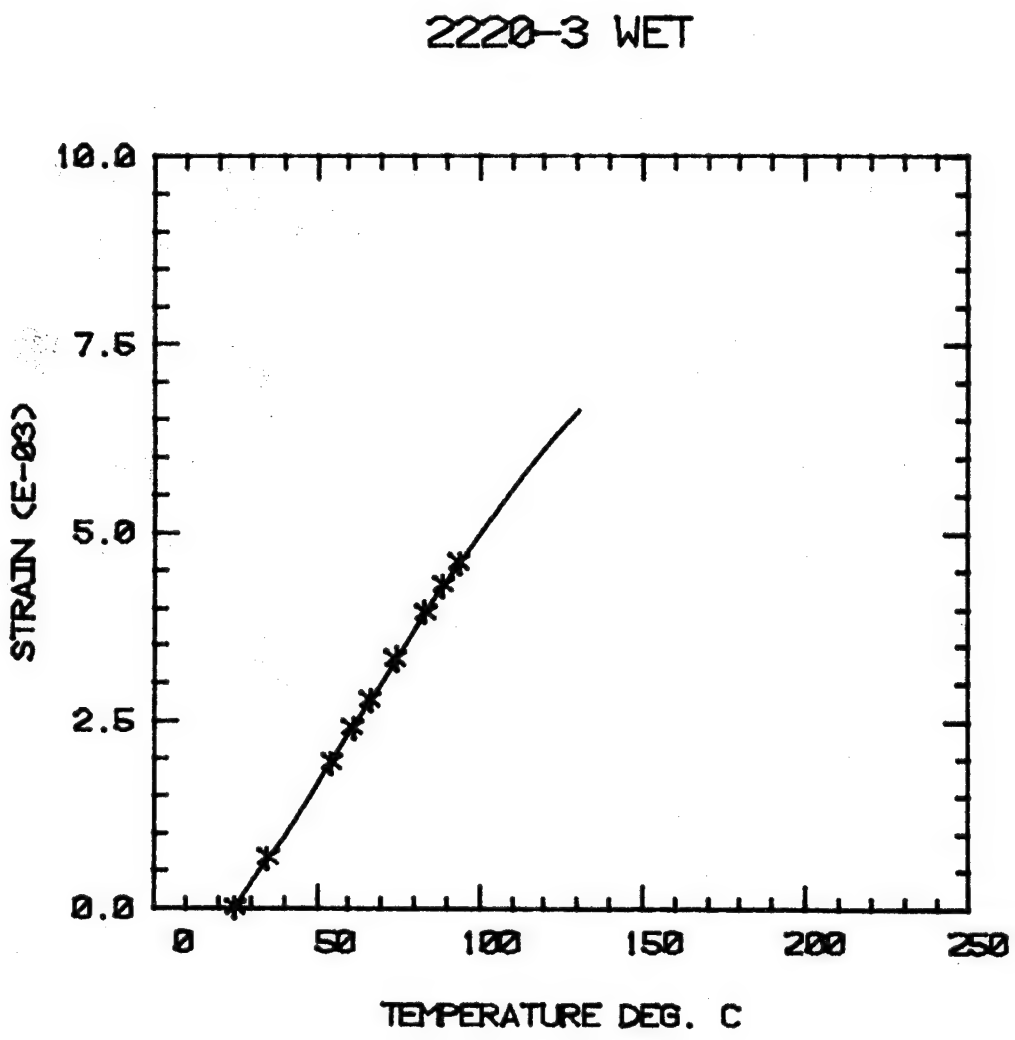


c) Hercules 2220-3 Toughened Epoxy

Figure 78 (continued). Neat Epoxy Thermal Expansion as a Function of Temperature; Moisture-Saturated.

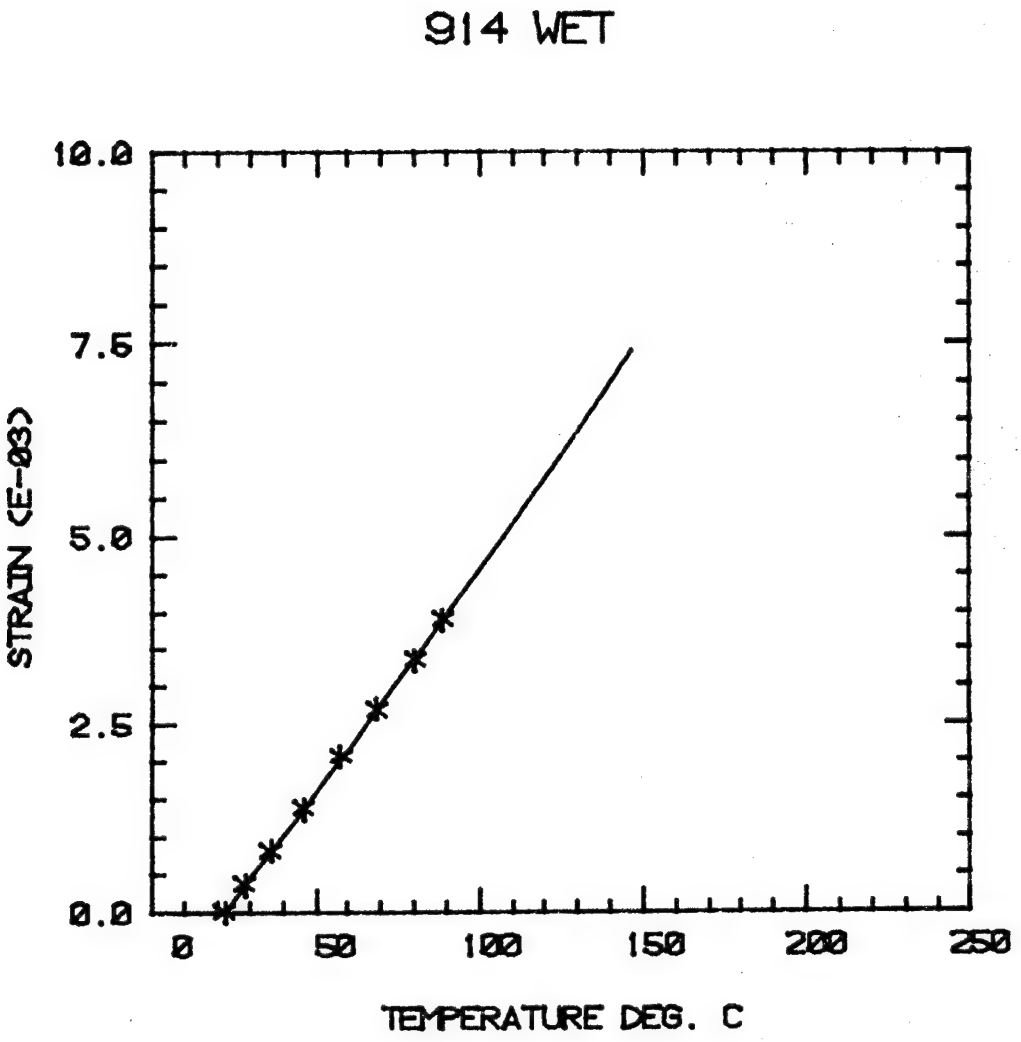


d) Fibredux 914 Toughened Epoxy

Figure 78 (continued). Neat Epoxy Thermal Expansion as a Function of Temperature; Moisture - Saturated.

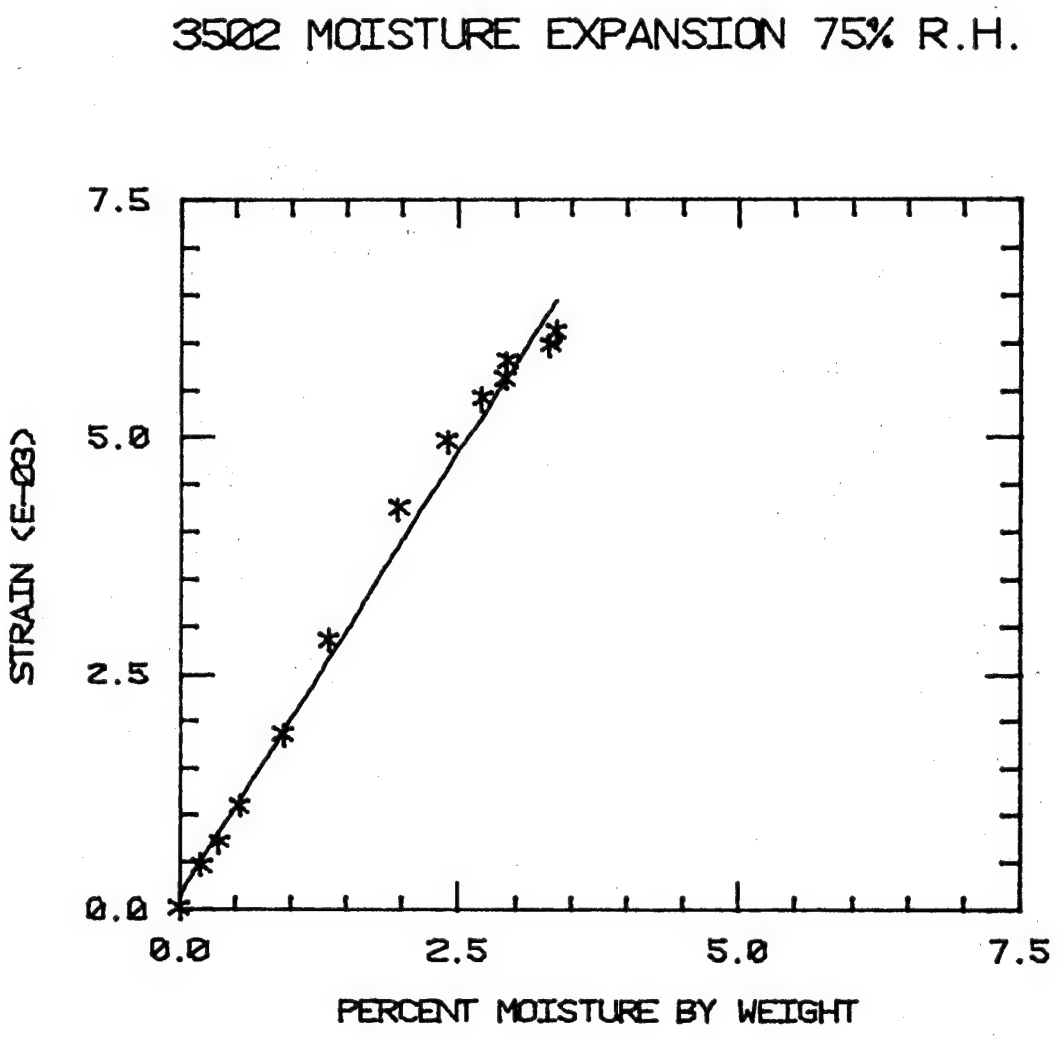


Figure 79. Hercules 3502 Baseline Epoxy Moisture Expansion as a Function of Moisture Content; 75 Percent Relative Humidity Exposure.

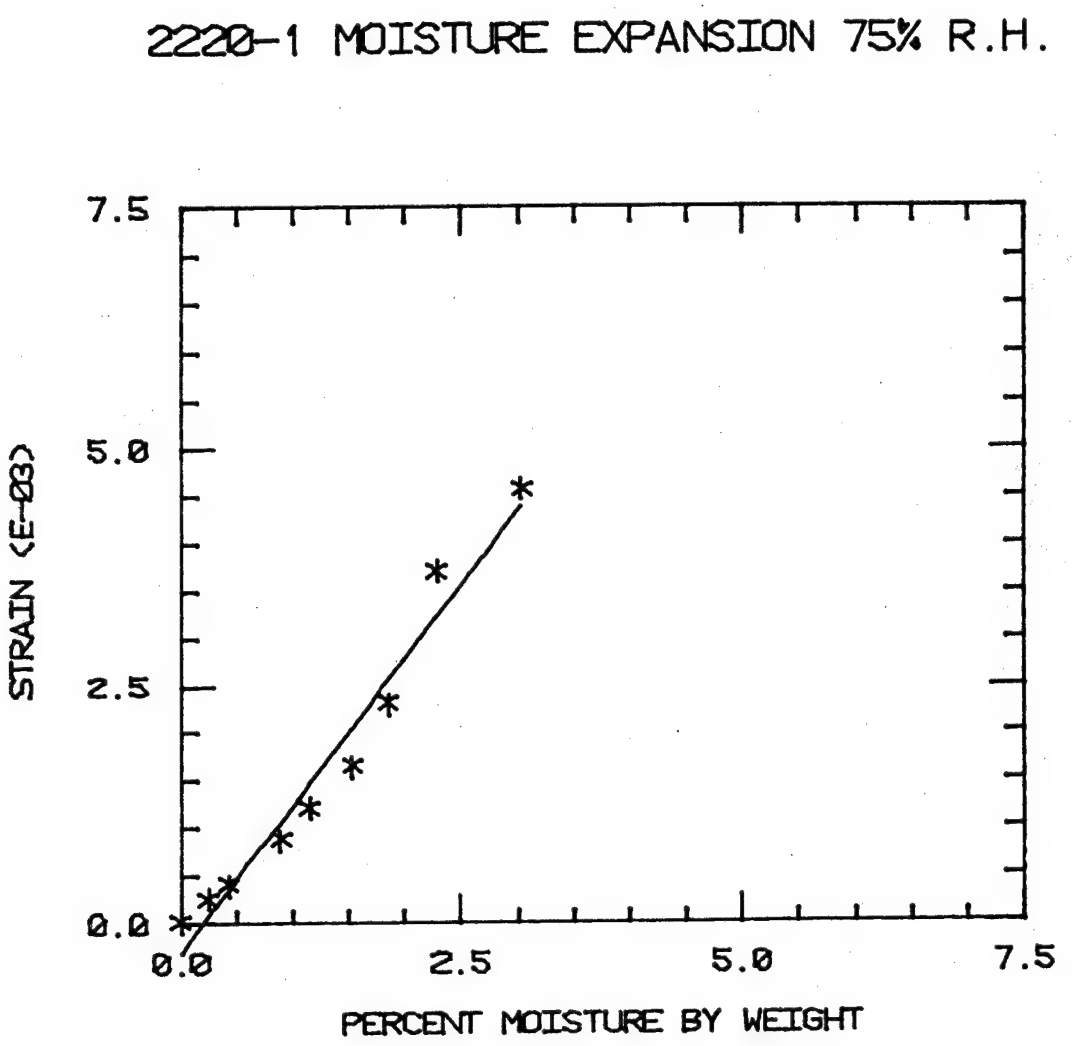


Figure 80. Hercules 2220-1 Toughened Epoxy Moisture Expansion as a Function of Moisture Content; 75 Percent Relative Humidity Exposure.

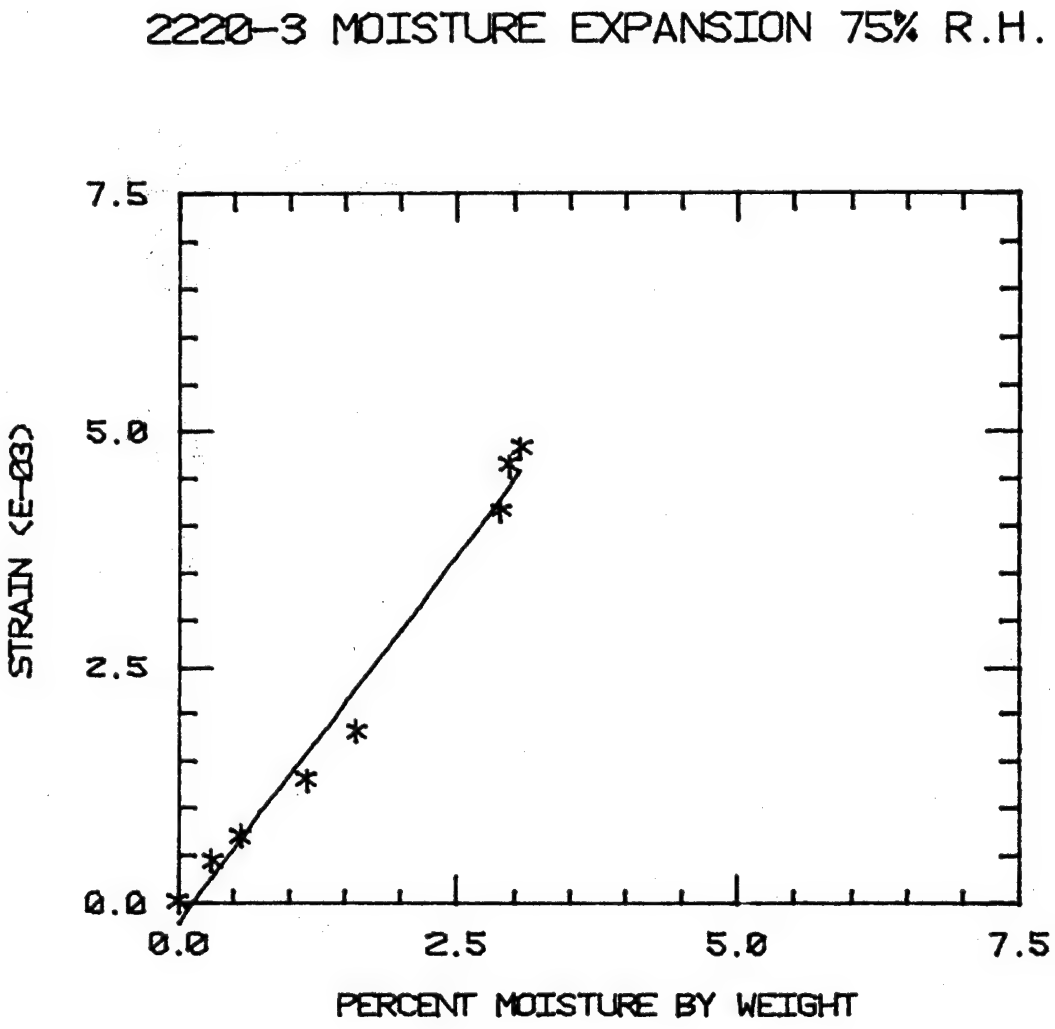


Figure 81. Hercules 2220-3 Toughened Epoxy Moisture Expansion as a Function of Moisture Content; 75 Percent Relative Humidity Exposure.

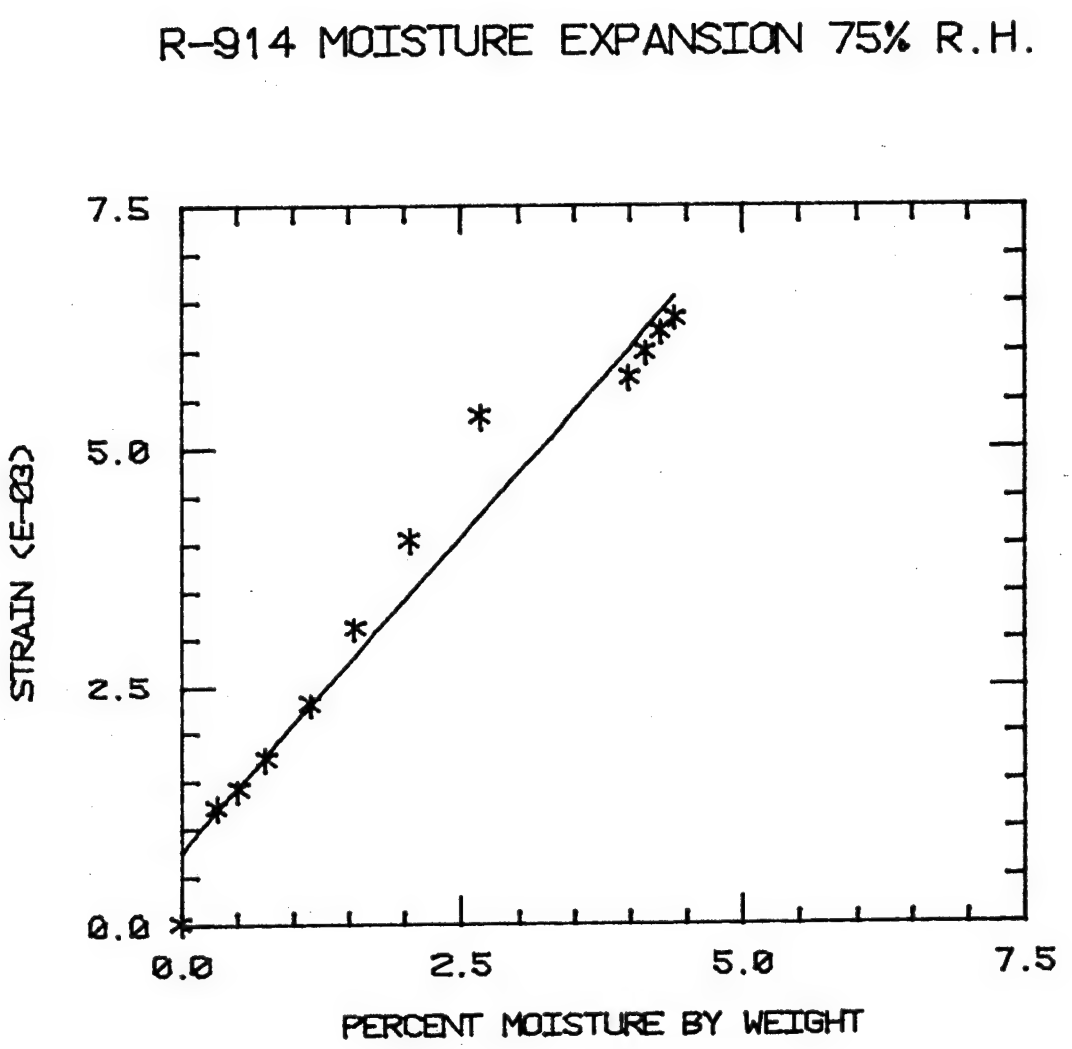


Figure 82. Fibredux 914 Toughened Epoxy Moisture Expansion as a Function of Moisture Content; 75 Percent Relative Humidity Exposure.

all four matrix materials, for the 75 percent relative humidity moisture exposure condition. Data were generated at 50 percent and 100 percent relative humidity also, as discussed in Section 3. The data were fit to a linear function of moisture (i.e., a straight line), as indicated. This represents a best indicator of the trends observed.

### 5.3.2 Fiber Properties

Since no actual composites experimental data were available to be compared to, a specific graphite fiber was arbitrarily assumed for calculation purposes. The assumed properties of this Hercules AS4 graphite fiber are given in Table 5. The transverse normal strength and the axial and in-plane shear strengths were assumed to be arbitrarily high values, to insure that the fiber did not fail in these modes.

## 5.4 Predicted Unidirectional Composite Response

The predicted unidirectional composite response will be presented individually for each of the four matrix material systems, to aid the reader interested in making direct correlations with available experimental data for a specific system. A square fiber packing array of continuous Hercules AS4 graphite fibers of circular cross section in a 60 volume percent unidirectional composite has been assumed as representing a typical composite. The analysis is fully capable of handling other geometric and/or material configurations as well.

The micromechanics analysis methodology was discussed in Section 5.2. For the present application, the key references for additional information on this analysis technique include References [1,3,9,19,20].

In the following subsections, predictions of composite response will be included only for uniaxial loadings, viz, longitudinal tension, transverse tension, and longitudinal shear. No compression loadings or

Table 5

Hercules AS4 Graphite Fiber Properties [31]

| | | |
|---|---|---|
| Longitudinal Modulus, $E_\ell$ | 235 GPa | (34 Msi) |
| Transverse Modulus*, $E_t$ | 14 GPa | (2 Msi) |
| Major Poisson's Ratio*, $\nu_{\ell t}$ | 0.20 | |
| In-Plane Poisson's Ratio*, $\nu_{tt}$ | 0.25 | |
| Longitudinal Shear Modulus*, $G_{\ell t}$ | 28 GPa | (4 Msi) |
| In-Plane Shear Modulus**, $G_{tt}$ | 5.5 GPa | (0.8 Msi) |
| Coefficient of Longitudinal Thermal Expansion, $\alpha_\ell$ | $-0.36 \times 10^{-6}$/°C | |
| Coefficient of Transverse Thermal Expansion*, $\alpha_t$ | $18 \times 10^{-6}$/°C | |
| Longitudinal Tensile Strength, $\sigma_\ell^u$ | 3.59 GPa | (520 ksi) |
| Transverse Tensile Strength*, $\sigma_t^u$ | 0.35 GPa | (50 ksi) |

*Estimated (see References [4, 32]

**Calculated, $G_{tt} = E_t/2(1 + \nu_{tt})$

biaxial loading combinations will be included, although the analysis is capable of applying any type or combination of loadings simultaneously.

It is of interest to study the internal stresses in the matrix material induced by the cooldown from the 177°C cure temperature, before any mechanical loading is applied. These residual stresses are altered by each of the three possible successive changes in the environment prior to mechanical loading. That is, the internal stress state in the matrix of the composite prior to loading at each of the four environmental conditions, viz, room temperature, dry (RTD), elevated temperature (100°C), dry (ETD), room temperature, wet (RTW), and elevated temperature (100°C), wet (ETW) is of interest. The residual stress results will be presented first, followed by the predicted stress-strain responses and internal stress states for each type of mechanical loading.

A detailed discussion of the predicted internal stress states will be presented in the remainder of this section for the Hercules 2220-1 toughened epoxy only. The baseline system, Hercules 3502, and the Fibredux 914 system both exhibited much less toughness and strain to failure than the two Hercules 2220 systems. The latter two systems were very similar in their response. Hence, the 2220-1 system was arbitrarily selected for detailed discussion here. The complete data plots for the other three matrix systems, i.e., Hercules 3502 and 2220-3, and Fibredux 914, are included in Appendix E of Volume II.

Comparisons of all four systems will be presented in Section 5.5, along with a general discussion of the relative merits of these matrix materials for use in composites.

### 5.4.1 AS4/2220-1 Unidirectional Composite

5.4.1.1 Hygrothermal Initial Stress States

The micromechanics computer program is currently set up to print out any combination of eight different quantities of interest for any specified solution increment. These quantities are: octahedral shear stress, octahedral shear strain, maximum principal stress, minimum principal stress, third (intermediate) principal stress, maximum shear stress, interface normal stress, and interface shear stress. Since as many as 30 or 40 increments may be involved in a typical computer run, a considerable amount of data is available for study. However, since actual experimental data are not yet available for correlation, only a representative sample of these available analytical results will be included here.

5.4.1.1.1 Cooldown From Curing Temperature

Figure 83 presents all eight quantities available for study, plotted for the matrix region around an individual AS4 graphite fiber. Since a square array of fibers of circular cross-sectional shape has been assumed here, symmetry exists and only one quadrant of the repeating element consisting of a fiber and square region of surrounding matrix need be shown. The quantities included in Figure 83 are for the state existing in the 2220-1 matrix after the unidirectional composite has been cooled down to room temperature (21°C) from the 177°C cure temperature, corresponding to a temperature change of -156°C. As the printout under the plot indicates, a total of 16 temperature increments were used to achieve this total temperature change. The matrix material properties were adjusted at the beginning of each increment to account for the changing material properties (presented in Figures 65b and 76b). The moisture content is zero, and no applied stresses are present. The contour lines have not been smoothed for presentation and are a direct

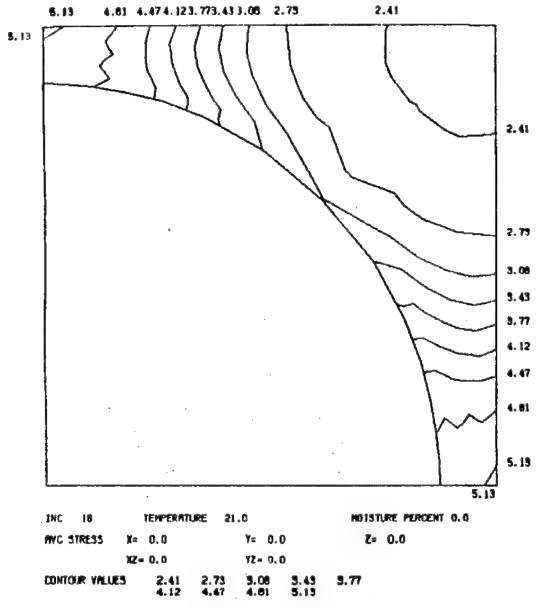


a) Octahedral Shear Stress (ksi)

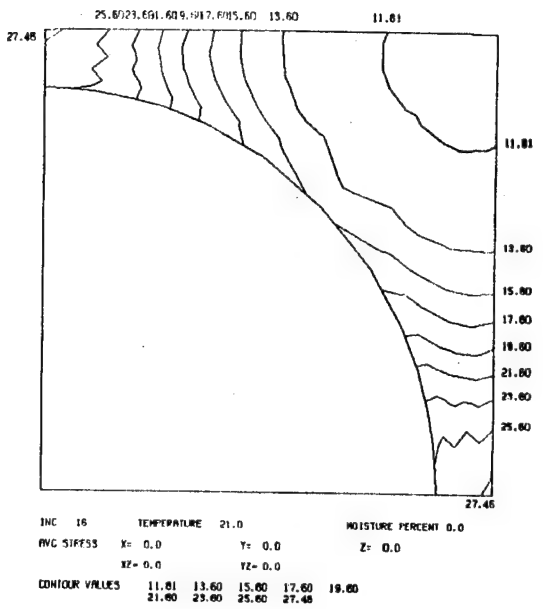


b) Octahedral Shear Strain ($10^{-3}$)

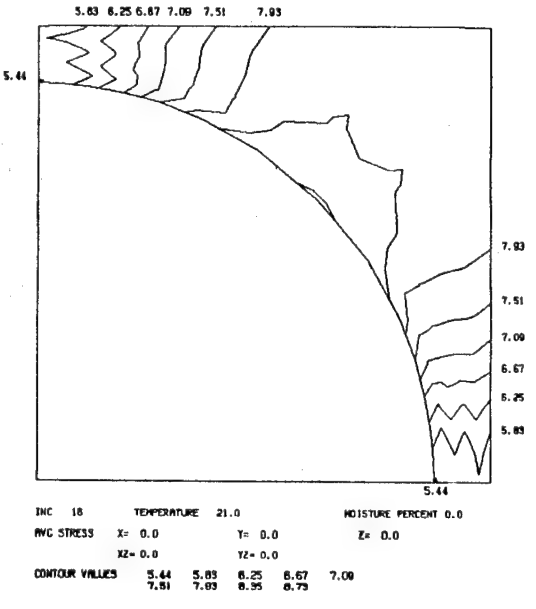


c) Maximum Principal Stress (ksi)

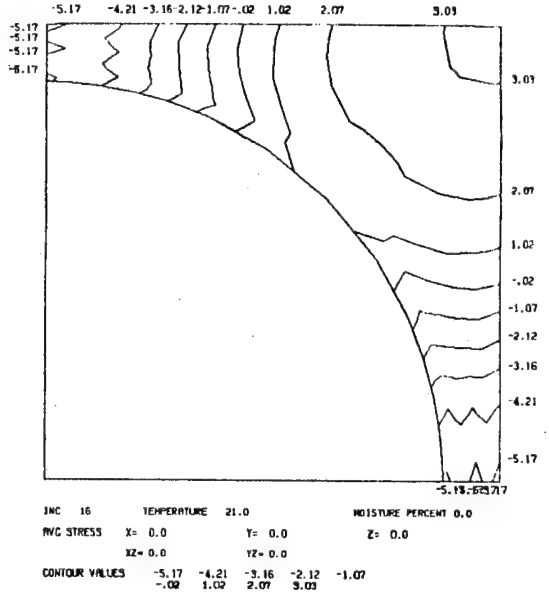


d) Minimum Principal Stress (ksi)

Figure 83. AS4/2220-1 Graphite/Epoxy Unidirectional Composite, Room Temperature, Dry (RTD); No Mechanical Loading.

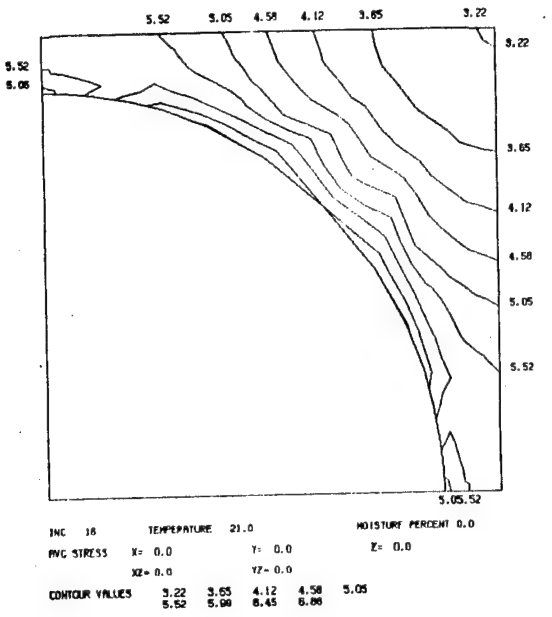


e) Intermediate Principal Stress(ksi)

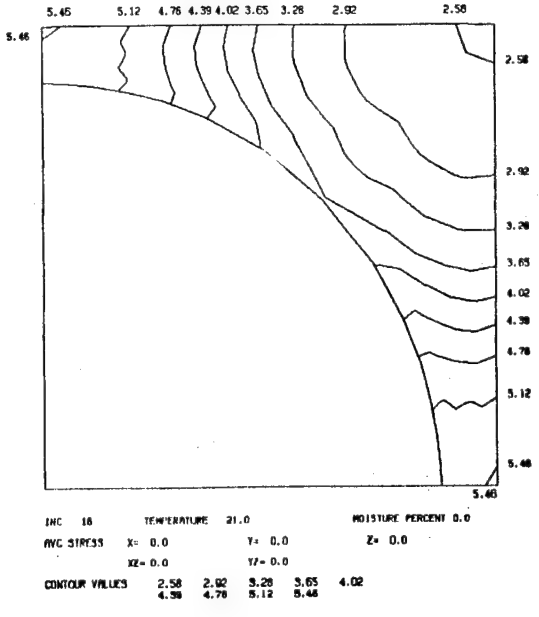


f) Maximum Shear Stress (ksi)

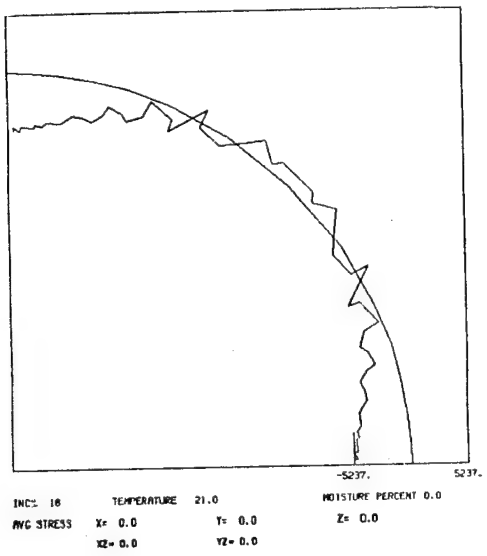


g) Interface Normal Stress (psi)

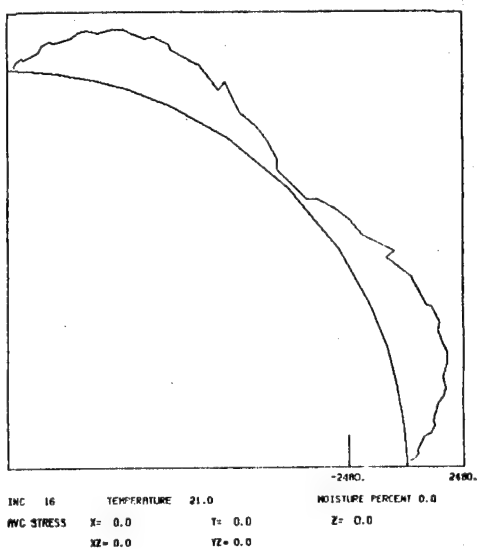


h) Interface Normal Stress (psi)

Figure 83 (continued). AS4/2220-1 Graphite/Epoxy Unidirectional Composite, Room Temperature, Dry (RTD); No Mechanical Loading.

output of the finite element analysis. Smoothing can be used if desired.

Figure 83a is a contour plot of the octahedral shear stress distribution in the matrix. For reference, the yield value of the matrix octahedral shear stress at the room temperature, dry (RTD) condition should be stated. However, since the yield point is not well-defined for this matrix material (see Figure 76b), a yield value of 6.89 MPa (1000 psi) will be arbitrarily chosen (all of the stress contour plots to be included here are in English rather than SI units). As can be seen in Figure 83a, the stress distribution is symmetrical about the 45° diagonal (because of the assumed square packing array of the fibers). Also, the octahedral shear stress is maximum at the mid-distance between the closest fiber spacings, i.e., along the horizontal (x) axis and the vertical (y) axis. Along the 45° diagonal (the direction of farthest fiber spacing), the stress is the lowest. Octahedral shear stress is a quantity of special interest since this is the criterion for yield in the elastoplastic micromechanical analysis formulation. Octahedral shear stress can also be used as one possible criterion of matrix failure (i.e., a distortional energy criterion).

Since the present plotting routine only labels contour values which intersect an external boundary, a list of all contour values plotted is also given in the printout under each plot. This allows unlabeled contours to be identified should they occur. (None occur in Figure 80a.)

No contours have been plotted here for the fiber region since, as previously discussed in Section 5.3.2, the fiber has been given arbitrarily high strength properties. The analysis and plotting routine are fully capable of calculating and plotting fiber stresses, however.

Figure 83b is a contour plot of the octahedral shear strains. Here,

also, the maximum values are in the regions of closest fiber spacing, and the minimum values in the regions of largest fiber spacing.

The maximum (most positive), minimum (most negative), and third (intermediate) principal stresses are plotted in Figures 83c, 83d and 83e, respectively. Since the temperature change by itself does not induce longitudinal shear stresses, in these particular plots the maximum and minimum principal stresses are in the x-y plane (the transverse plane), and the intermediate principal stress is in the z-direction (the fiber axis direction). In general, however, this is not true (if longitudinal shear stresses are present). The full computer printout gives the direction of each principal stress, within every finite element. The highest stresses generally tend to occur in the regions of closest fiber spacings; this is not always true, as Figures 83c and 83e demonstrate.

The maximum shear stresses are plotted in Figure 83f. Again, in the present case of thermal loading only, the longitudinal shear stresses are zero and the maximum shear stress is in the transverse plane.

Frequently it is the normal or shear stress at the fiber-matrix interface which reaches a critical value first, and initiates composite failure. Thus, it is of interest to plot these quantities. Figure 83g is a plot of the thermally induced normal stress distribution around the interface. Contour values outside the interface indicate tensile normal stress, and values inside the interface indicate compression. The interface normal stress is compressive in the regions of closest fiber spacing due to the matrix having a higher thermal expansion coefficient than the fiber and contracting around the fiber during cooldown. The distribution is not uniform, however, because of the square fiber

packing geometery. In fact, the interface normal stress is tensile in the region of the 45° diagonal. As can be seen, the highest (compressive) normal stress is -36.1 MPa (-5237 psi). This is approximately 90 percent of the (tensile) ultimate stress for this matrix material at the room temperature, dry (RTD) condition (see Figure 65a).

The shear stress distribution at the fiber-matrix interface is shown in Figure 83h. The shear stress is zero at the horizontal and vertical axes symmetry, and passes through zero at the 45° diagonal. The sign change (change in direction) is not shown in the plot since, when longitudinal shear stresses are present, the shear stress is generally not in the transverse plane. It is necessary to refer to the full computer printout to establish the direction of the shear stress in this case.

5.4.1.1.2 Heating to 100°C

To simulate the internal stress state in the matrix if the composite is to be tested at a 100°C, dry (ETD) condition, the temperature can be incremented back up to 100°C from the room temperature, dry (RTD) condition of Figure 83. Selected results are presented in Figure 84. For brevity, only the octahedral shear stress, maximum principal stress, interface normal stress and interface shear stress plots are included here, although all eight plots were available for study. As expected, the stresses are roughly half those of Figure 83 since the temperature has been increased approximately half-way back to the stress-free cure temperature of 177°C (and accounting for the slight nonlinear response which occurred during the initial cooldown to room temperature).

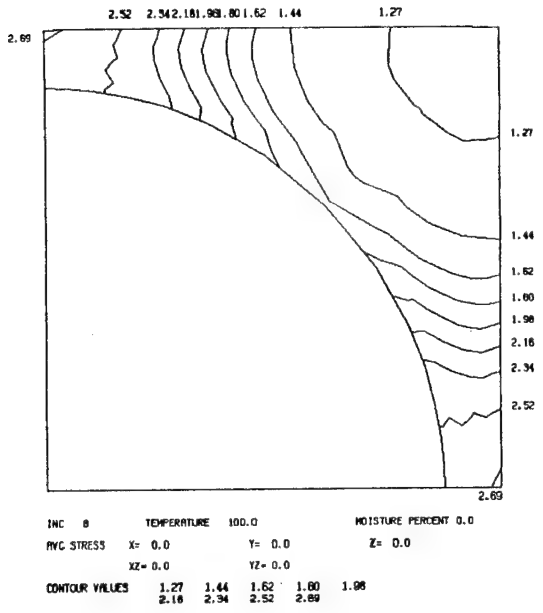


a) Octahedral Shear Stress (ksi)

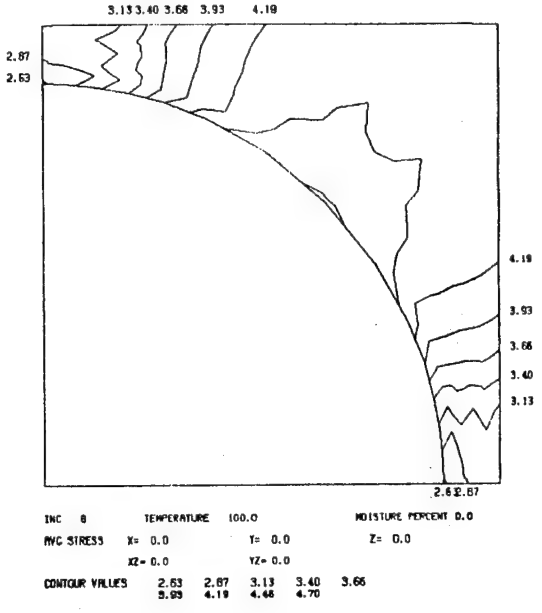


b) Maximum Principal Stress (ksi)

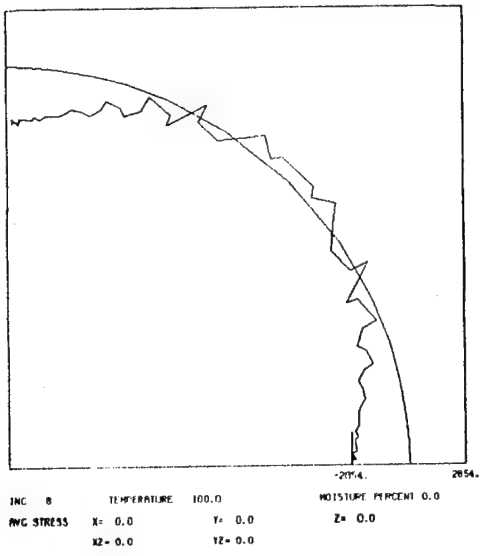


c) Interface Normal Stress (psi)

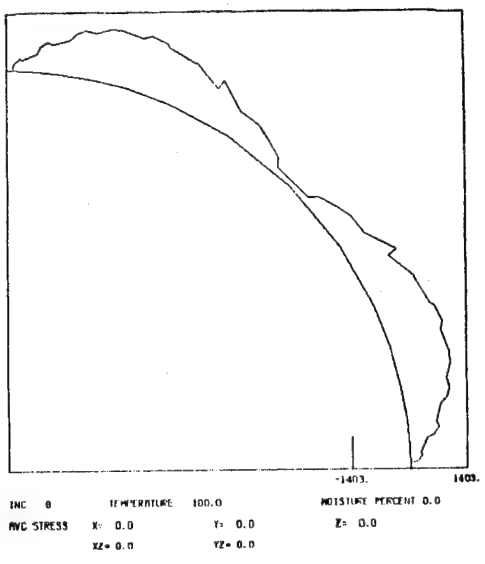


d) Interface Shear Stress (psi)

Figure 84. AS4/2220-1 Graphite/Epoxy Unidirectional Composite, 100°C, Dry (ETD); No Mechanical Loading.

5.4.1.1.3 Moisture Saturation at Room Temperature

This environmental condition represents the initial stress state prior to a room temperature, wet (RTW) mechanical loading. Selected results for octahedral shear stress, maximum principal stress, minimum principal stress, third principal stress, interface normal stress, and interface shear stress are presented in Figure 85. Here and in all subsequent figures, only selected plotted quantities will be presented. This is done for brevity; all eight quantities presented in Figure 83 were available for interpretation of all results.

By comparing the results of Figure 85 with the corresponding plots of Figure 83 it can be seen that the addition of moisture has a major influence on the internal stress state in the composite. For example, the octahedral shear stress, the parameter assumed to govern the onset of matrix yielding (and a possible criterion for defining failure), is decreased approximately 75 percent by the addition of moisture (3.8 percent by weight to saturation). Likewise, the maximum principal stress is also decreased drastically (by about 65 percent; compare Figure 85b with Figure 83c), while the minimum principal stress is decreased by more than 80 percent.

In fact, what has happened is that the matrix swelling associated with the moisture addition has induced stresses of opposite sign and approximately the same magnitude as those thermally induced by the matrix contraction during cooldown from the original cure temperature.

The same reversal can be seen in the interface normal stress (Figure 85e versus Figure 83g). After moisture addition, the interface normal stress is much lower than that of the previously existing thermal residual stress. This fact alone, independent of the different stiffness

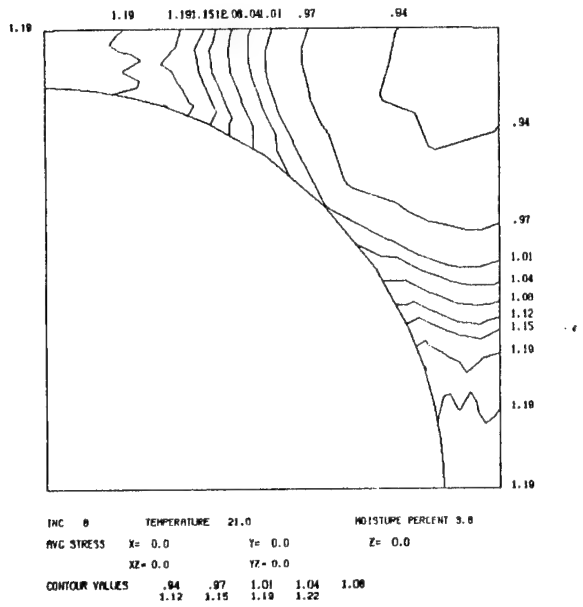


a) Octahedral Shear Stress (ksi)

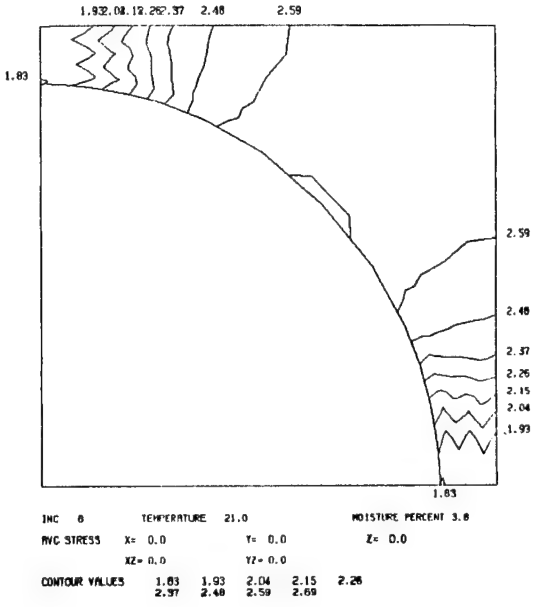


b) Maximum Principal Stress (ksi)

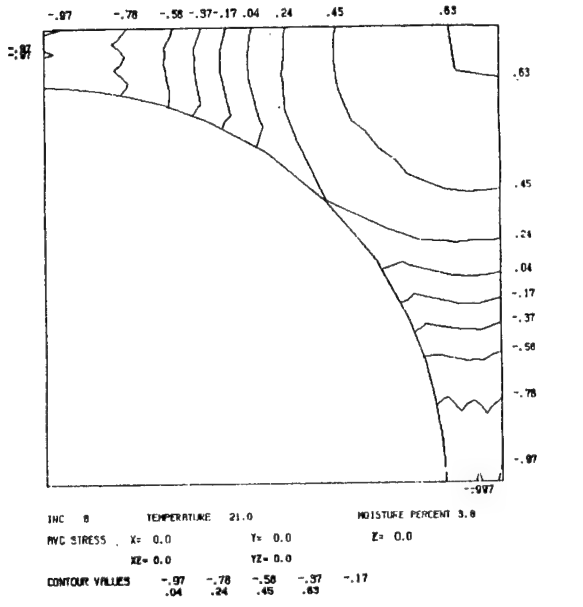


c) Maximum Principal Stress (ksi)

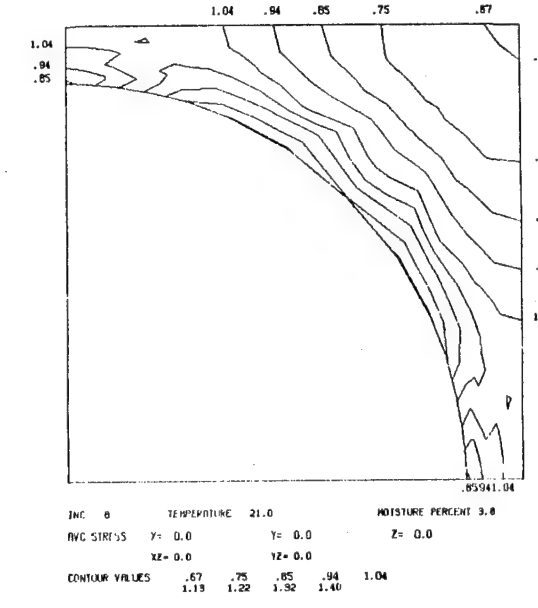


d) Intermediate Principal Stress (ksi)

Figure 85. AS4/2220-1 Graphite/Epoxy Unidirectional Composite, Room Temperature, 3.8 Percent Moisture (RTW); No Mechanical Loading.

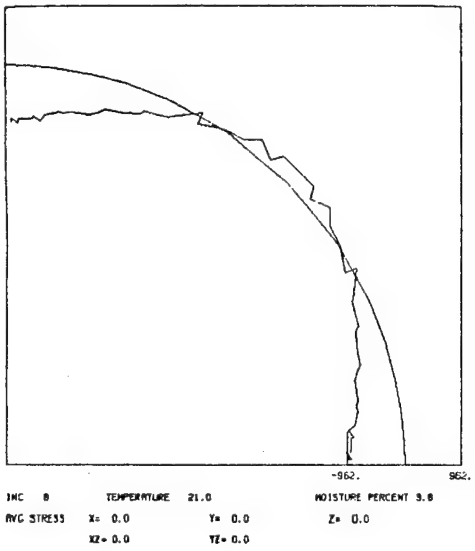


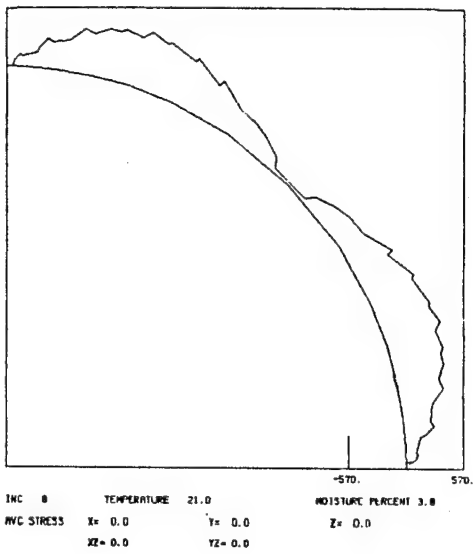


e) Interface Normal Stress (psi) f) Interface Shear Stress (psi)

Figure 85 (continued). AS4/2220-1 Graphite/Epoxy Unidirectional Composite, Room Temperature, 3.8 Percent Moisture (RTW); No Mechanical Loading.

and strength properties of the Hercules 2220-1 matrix at room temperature wet and dry conditions (as previously presented in Figure 65), insure that the composite will respond differently under subsequent mechanical loadings, particularly transverse normal loadings.

5.4.1.1.4 Moisture Saturation at 100°C

This environmental condition represents the pre-existing stress state in the composite for the elevated temperature, wet (ETW) loadings to be subsequently presented. Results are indicated in Figure 86. It will be noted that the stresses are of the same general magnitudes for this condition as for the RTD and the RTW conditions. This is because, as previously noted, the stresses due to the original cooldown from the cure temperature were of opposite sign from the moisture-induced stresses. Thus, as the composite is reheated the thermal curing stresses become less, allowing the moisture-induced stresses to more fully offset them. Hence, the very slightly lower net stresses exhibited in Figure 86.

In general, it is not possible to just look at the magnitudes of the individual stresses. Locations of maximum stresses must also be noted, since the location is different under different environmental conditions. In this regard, it is often possible to observe the interface normal stress as an indicator. For example, in the present case, at the RTD condition, the highest interface normal stress is highly negative (Figure 83g). For the RTW condition, it is still negative, but only slightly (Figure 85e), indicating that the moisture addition has not fully offset the thermally-induced stress. At the ETW condition (Figure 86e), the interface normal stress is positive, indicating that the thermal stress relief due to the reheating to 100°C

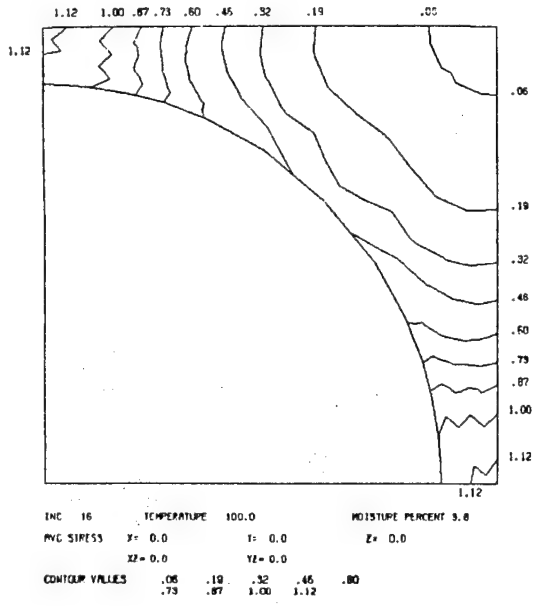

a) Octahedral Shear Stress (ksi)

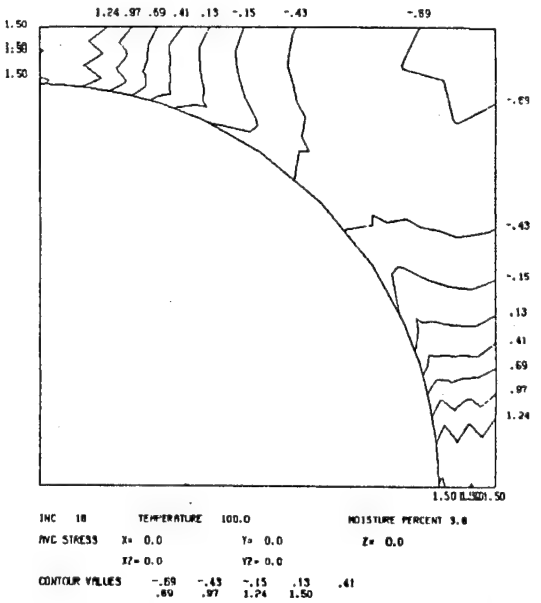

b) Maximum Principal Stress (ksi)

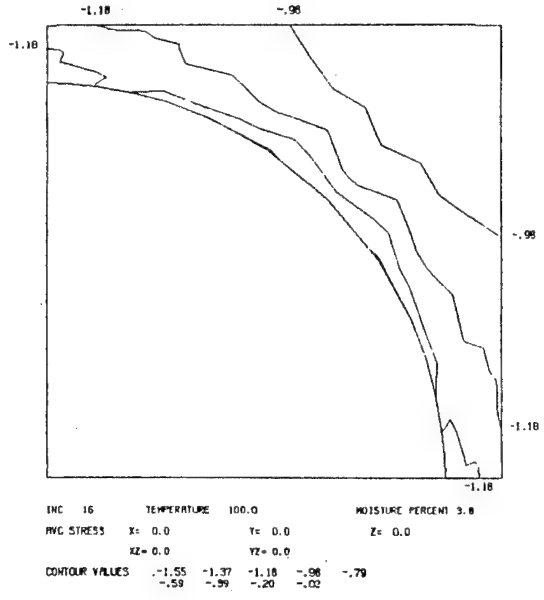

c) Minimum Principal Stress (ksi)

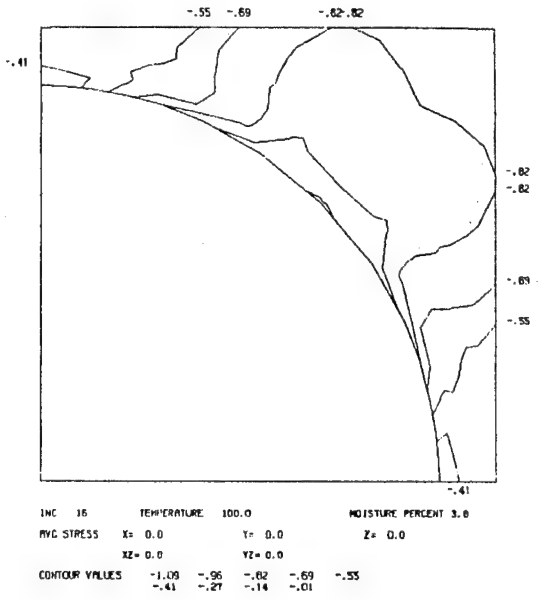

d) Intermediate Principal Stress (ksi)

Figure 86. AS4/2220-1 Graphite/Epoxy Unidirectional Composite, 100°C, 3.8 Percent Moisture (ETW); No Mechanical Loading.

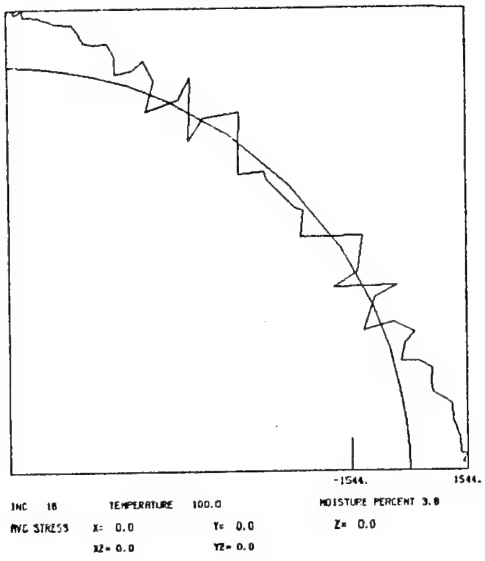


e) Interface Normal Stress (psi)

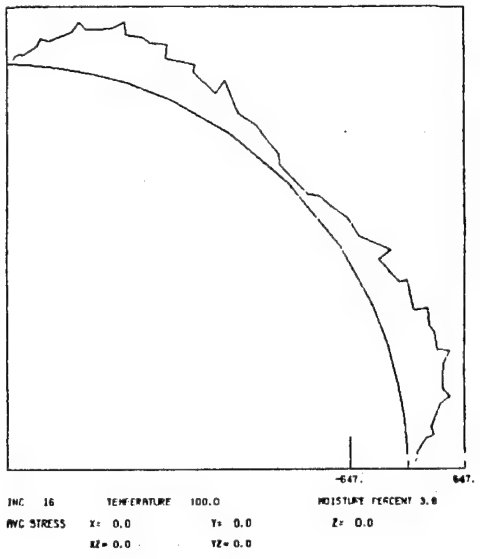


f) Interface Shear Stress (psi)

Figure 86 (continued). AS4/2220-1 Graphite/Epoxy Unidirectional Composite, 100°C, 3.8 Percent Moisture (ETW); No Mechanical Loading.

was sufficient to make the moisture influence the dominant effect.

These interacting influences are nonlinear, since the matrix itself is nonlinear, and because the matrix stiffness properties are a nonlinear function of temperature. The result is a very complex interactive process, which can only be interpreted by a careful study of Figures 83 through 86.

The key conclusion is, however, that these widely different pre-existing stress states due to the different environments can be expected to have a major influence on the subsequent response of the composite to mechanical loadings.

5.4.1.2 Mechanical Loadings

The predictions will be grouped in the following order: longitudinal tension, transverse tension, and longitudinal shear. First, the dry composite predictions will be given, at room temperature (21°C) and one elevated temperature (100°C), followed by the moisture-saturated composite predictions at the same two temperatures. In all cases, the thermal residual stress effects due to cooldown from the 177°C curing temperature to room temperature are included. For those cases where moisture is assumed to be present, the moisture swelling-induced stress effects are also included, as presented in Section 5.4.1.1 previously.

5.4.1.2.1 Longitudinal Tension

Since longitudinal tension stress-strain response of the composite is dominated by the graphite fiber, it is expected that there will be very little influence of either temperature or moisture. This is verified by comparing the four individual plots of Figure 87, which are all plotted to the same scale. The composite response is essentially linear, since the AS4 graphite fiber is assumed to exhibit linear

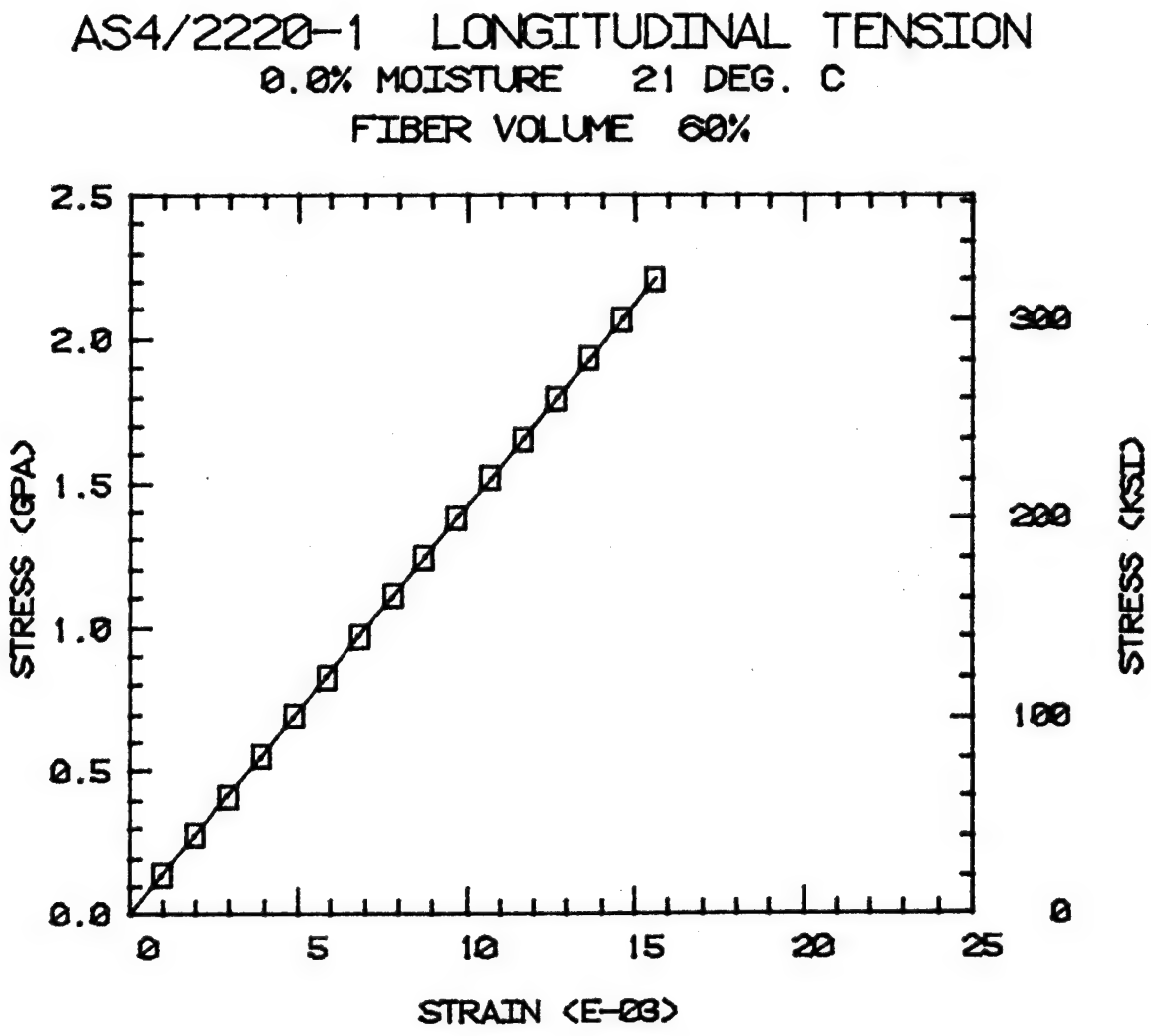


a) Room Temperature, Dry (RTD)

Figure 87. AS4/2220-1 Graphite/Epoxy Unidirecitonal Composite, Longitudinal Tensile Stress-Strain Response.

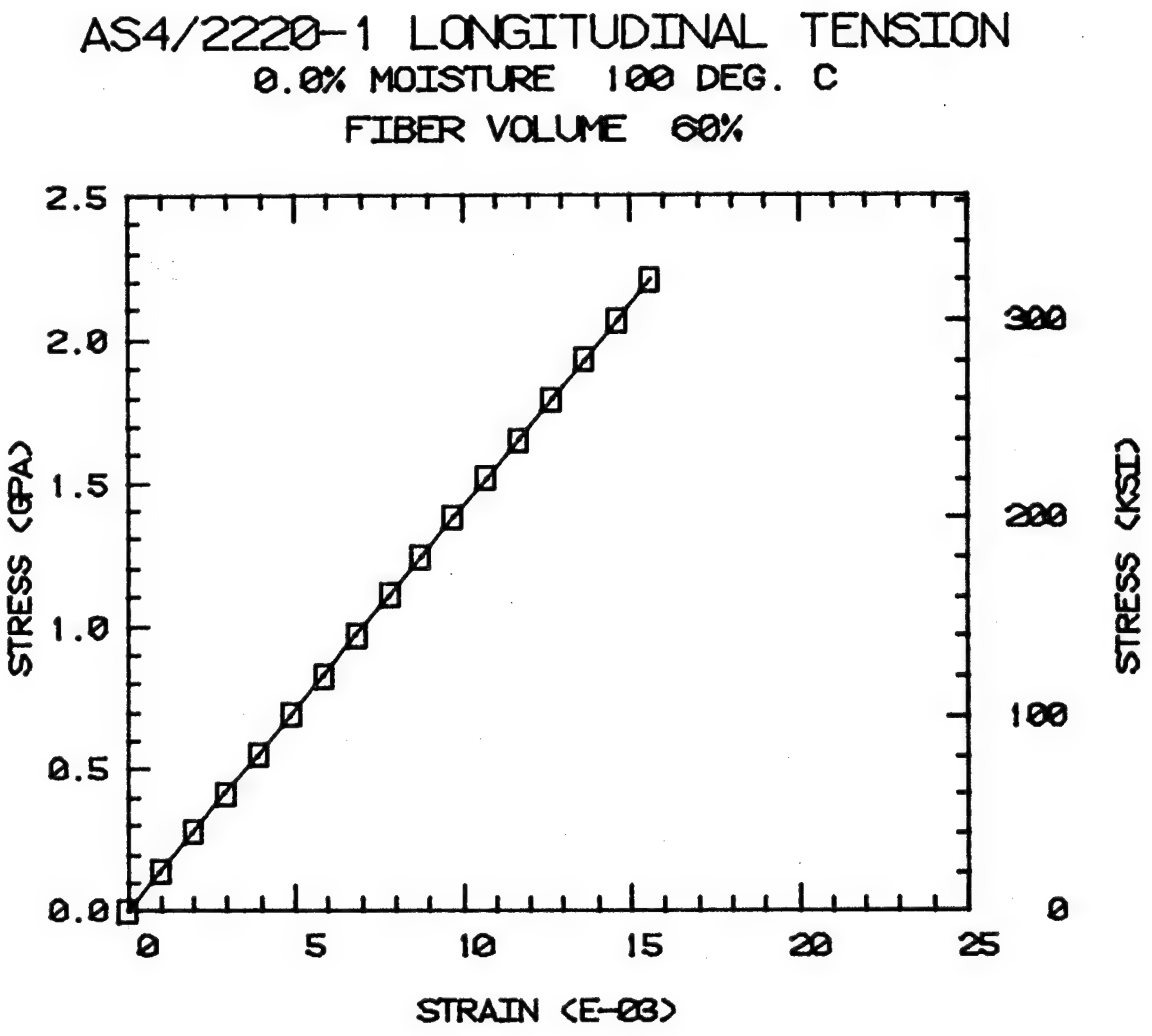


b) Elevated Temperature (100°C), Dry (ETD)

Figure 87 (continued). AS4/2220-1 Graphite/Epoxy Unidirectional Composite, Longitudinal Tensile Stress-Strain Response.

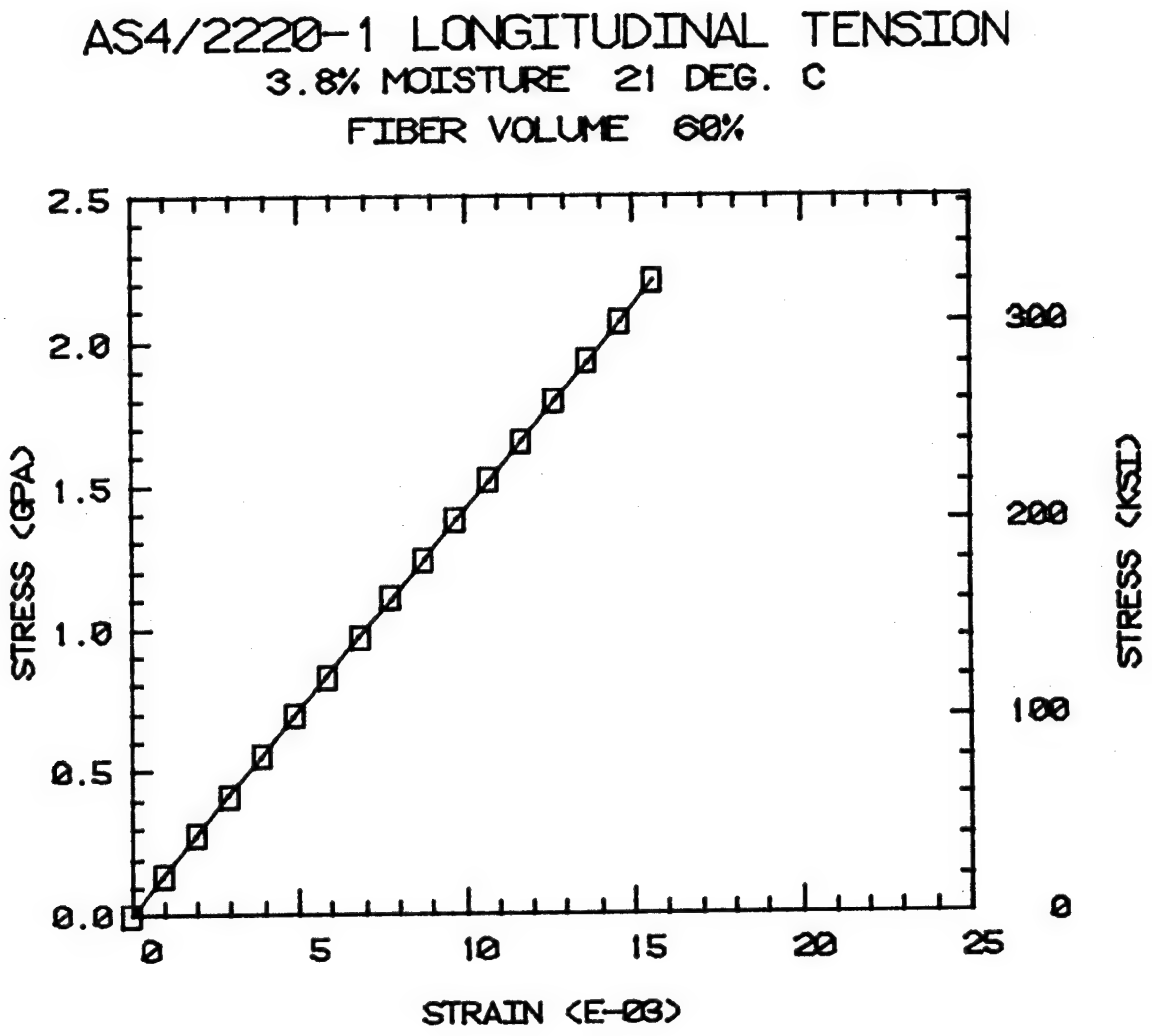


c) Room Temperature, 3.8 Percent Moisture (RTW)

Figure 87 (continued). AS4/2220-1 Graphite/Epoxy Unidirectional Composite, Longitudinal Tensile Stress-Strain Response.

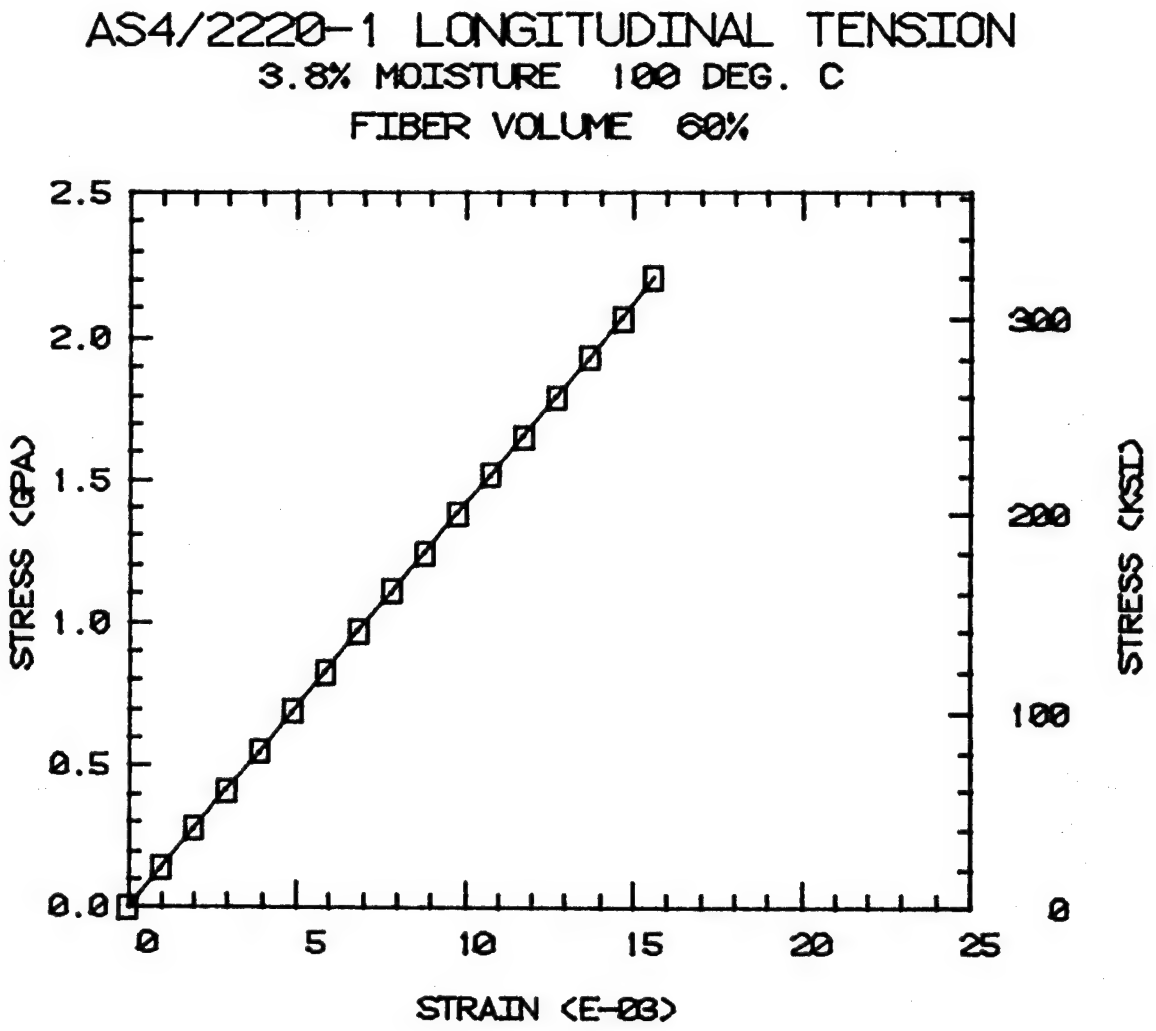


d) Elevated Temperature (100°C), 3.8 Percent Moisture (ETW)

Figure 87 (continued). AS4/2220-1 Graphite/Epoxy Unidirectional Composite, Longitudinal Tensile Stress-Strain Response.

stress-strain response to failure. The predicted composite modulus is approximately 140 GPa (20.4 Msi).

The predicted ultimate strength is essentially that predicted by the rule of mixtures. In order to compare the influence of environmental preconditioning on the local internal stress state in the unidirectional composite subjected to longitudinal tension, results will be given for the same applied stress in all cases, viz, 2.20 GPa (320 ksi). Figure 88 is a plot of the octahedral shear stress, the maximum principal stress, the interface normal stress, and the interface shear stress for the longitudinal loading at the room temperature, dry (RTD) condition. Because of the assumed square fiber packing array, the axial loading produces a symmetric stress distribution about the 45° diagonal, just as for thermal and mechanical loadings.

Figure 89 presents the corresponding set of plots for the elevated temperature, dry (ETD) condition. As expected, the matrix stresses are not as high as for the RTD condition, even though the composite is carrying the same total stress. This is because the matrix stresses were relieved somewhat by the temperature increase to 100°C prior to loading (as can be seen by comparing Figure 84 to Figure 83).

The room temperature, wet (RTW) condition is shown in Figure 90. It will be noted that the matrix stresses are increased when the axial loading is applied, but not drastically. For example, the highest octahedral shear stress is increased from 8.4 MPa (1.22 ksi) to 37.7 MPa (5.47 ksi) and the highest maximum principal stress is increased from 18.6 MPa (2.69 ksi) to 84.5 MPa (12.25 ksi), but the maximum interface normal stress is only increased from -6.6 MPa (-962 psi) to -19.0 MPa (-2755 psi). This increase in the interface normal stress is due to the

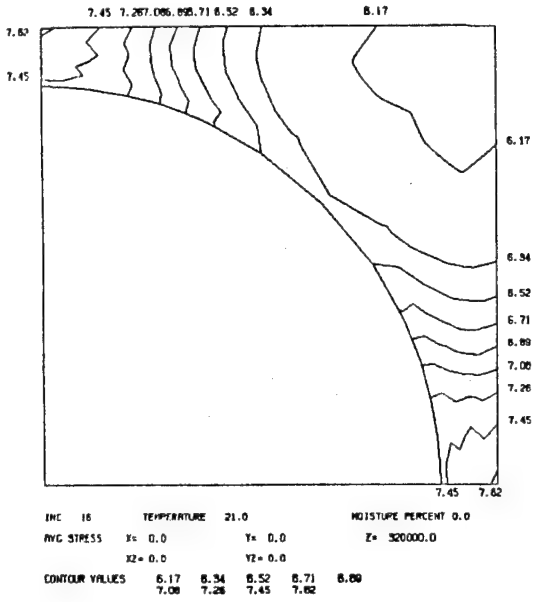


a) Octahedral Shear Stress (ksi)

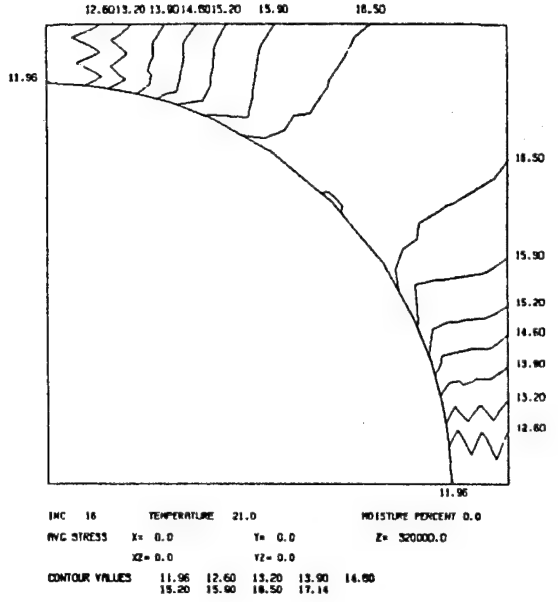


b) Maximum Principal Stress (ksi)

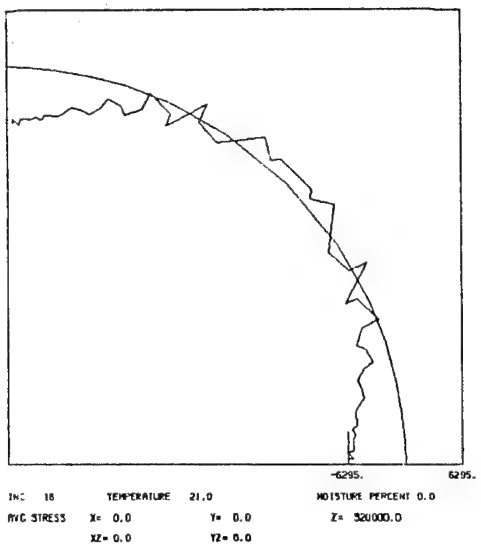


c) Interface Normal Stress (psi)

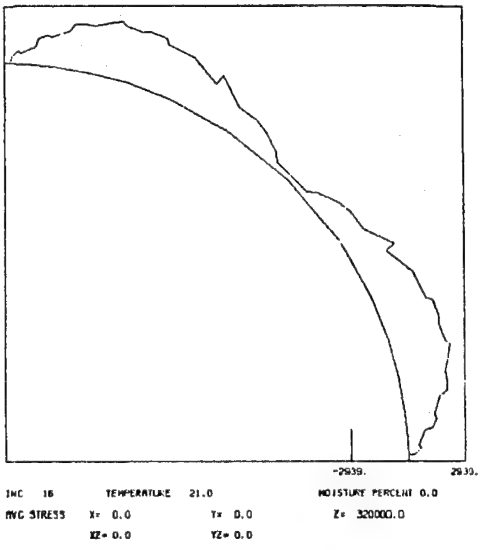


d) Interface Shear Stress (psi)

Figure 88. AS4/2220-1 Graphite/Epoxy Unidirectional Composite, Room Temperature, Dry (RTD); 2.20 GPa (320 ksi) Longitudinal Tensile Applied Stress.

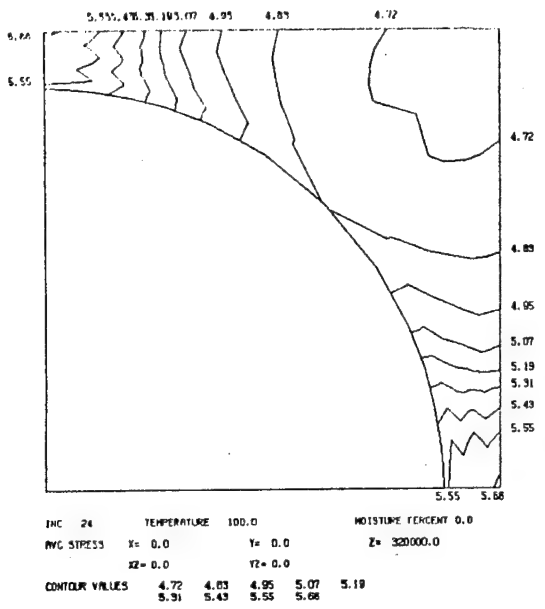


a) Octahedral Shear Stress (ksi)

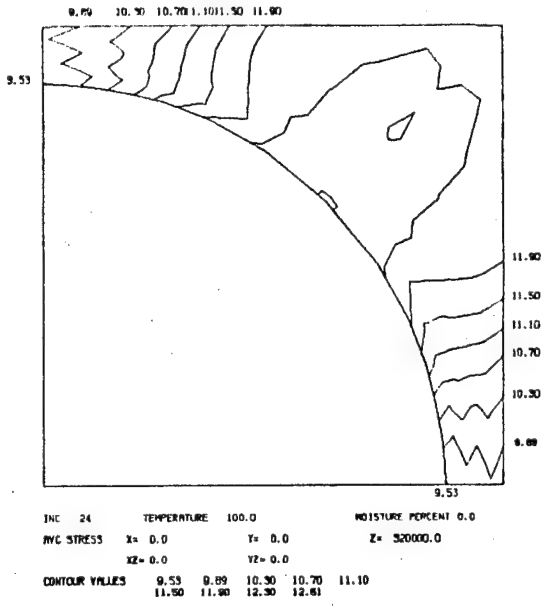


b) Maximum Principal Stress (ksi)

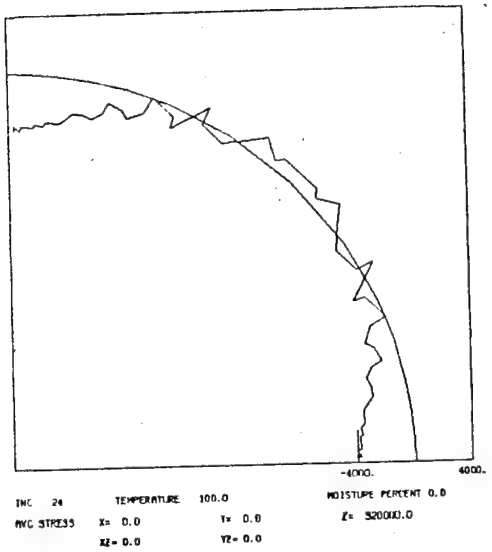


c) Interface Normal Stress (psi)

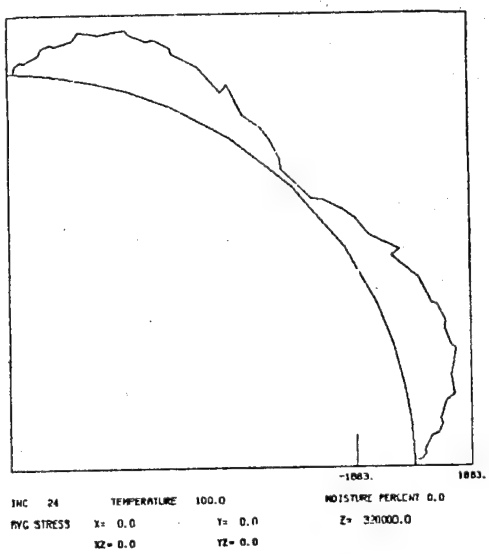


d) Interface Shear Stress (psi)

Figure 89. AS4/2220-1 Graphite/Epoxy Unidirectional Composite, 100°C, Dry (ETD); 2.20 GPa (320 ksi) Longitudinal Tensile Applied Stress.

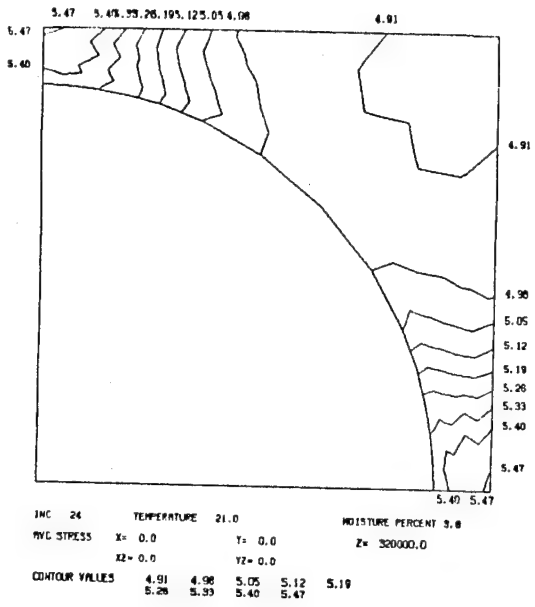


a) Octahedral Shear Stress (ksi)

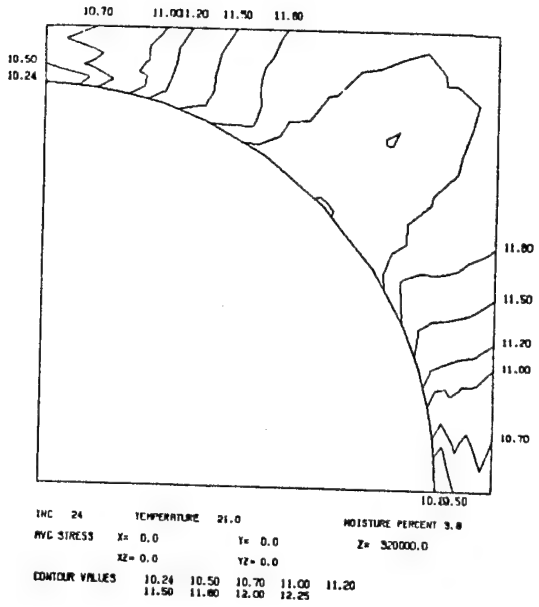


b) Maximum Principal Stress (ksi)

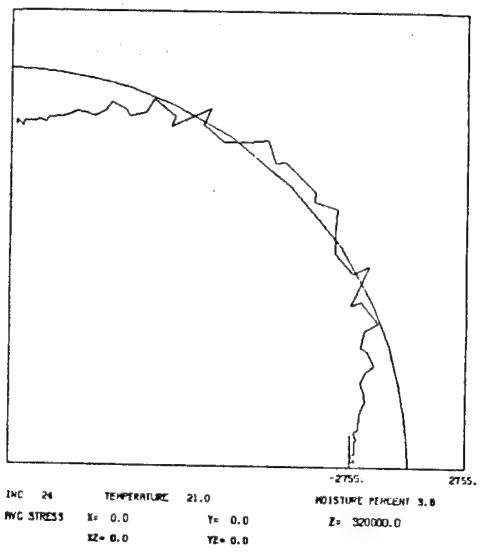


c) Interface Normal Stress (psi)

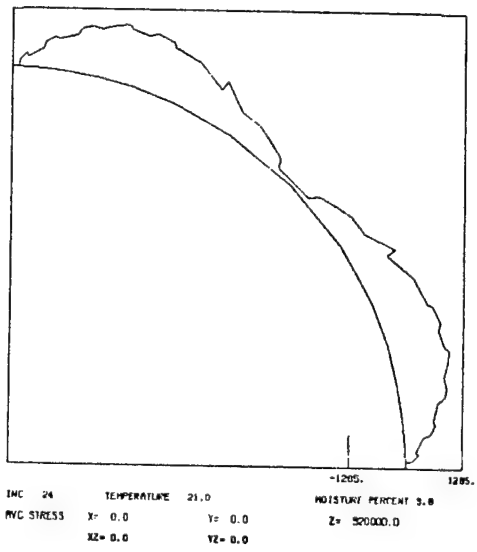


d) Interface Shear Stress (psi)

Figure 90. AS4/2220-1 Graphite/Epoxy Unidirectional Composite, Room Temperature, 3.8 Percent Moisture (RTW); 2.20 GPa (320 ksi) Longitudinal Tensile Applied Stress.

Poisson-induced contraction in the matrix being greater than that in the fiber, thus adding additional compression to that already existing at the fiber-matrix interface. If the applied loading had been compressive, the interface compressive normal stress would have decreased and, in fact, have become tensile, perhaps even sufficient to have caused interface debonding. This would lead to fiber microbuckling, a commonly observed phenomenon in compression when the individual fibers became unsupported by the surrounding matrix.

Due to the pre-existing hygrothermal stress state, the mechanical loading does not produce local stresses in direct proportion to the magnitude of the applied loading. This is demonstrated in Figures 91 and 92. These figures represent axial tensile loading at the ETW condition. Figure 91 indicates the local stress state in the matrix at approximately one-fourth the ultimate axial stress (e.g., 0.55 GPa or 80 ksi), while Figure 92 indicates the stress state at the full 2.20 GPa (320 ksi). It will be noted (Figure 91 compared to Figure 92a) that the normalized octahedral shear stress has increased by only a factor of 3.2, even though the applied loading was increased by a factor of 4. This stress actually decreased slightly during the first 0.55 GPa of axial tensile loading (compare Figure 92a to Figure 86a). Correspondingly, the maximum principal stress increased by a factor of 4.8. The interface stresses actually decreased as the applied loading increased, again due to Poisson effects.

The conclusion is that, even though the fiber may tend to govern the unidirectional composite axial strength somewhat independently of the environmental conditioning, the local stresses in the matrix are strongly influenced. Thus, under certain conditions, a matrix failure

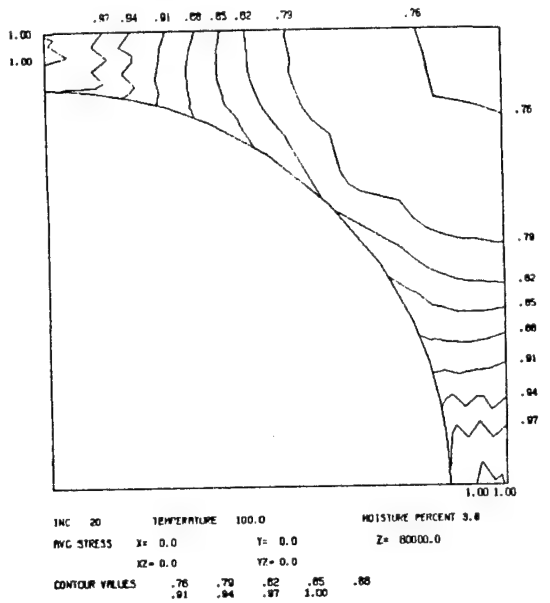


a) Octahedral Shear Stress (ksi)

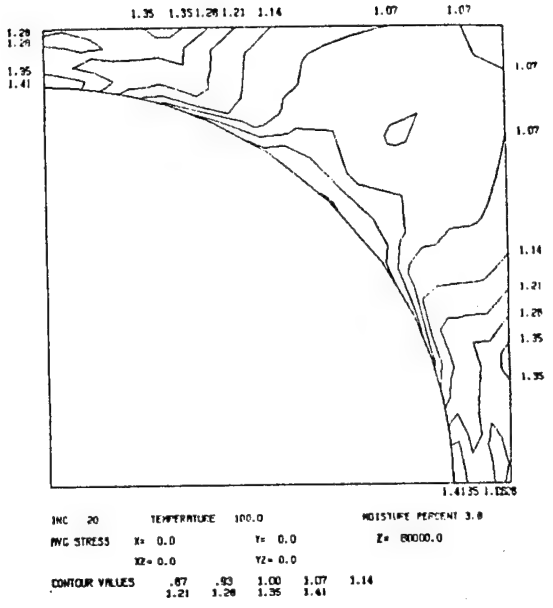


b) Maximum Principal Stress (ksi)

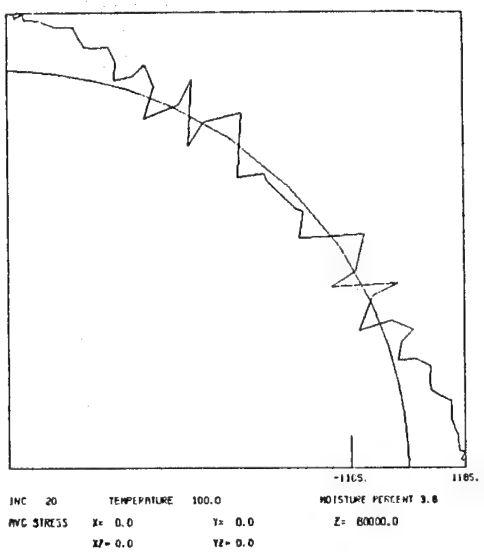


c) Interface Normal Stress (psi)

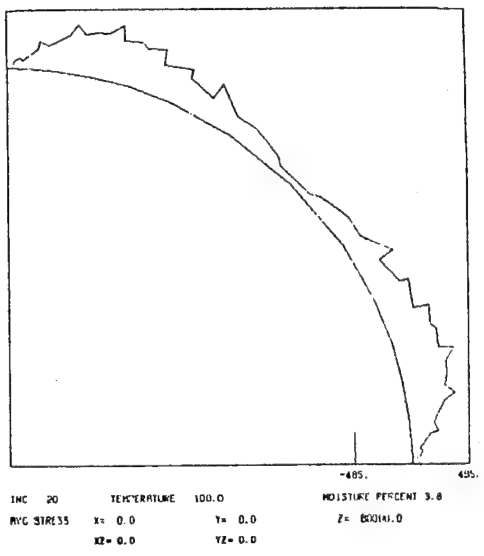


d) Interface Shear Stress (psi)

Figure 91. AS4/2220-1 Graphite/Epoxy Unidirectional Composite, 100°C, 3.8 Percent Moisture (ETW); 0.55 GPa (80 ksi) Longitudinal Tensile Applied Stress.

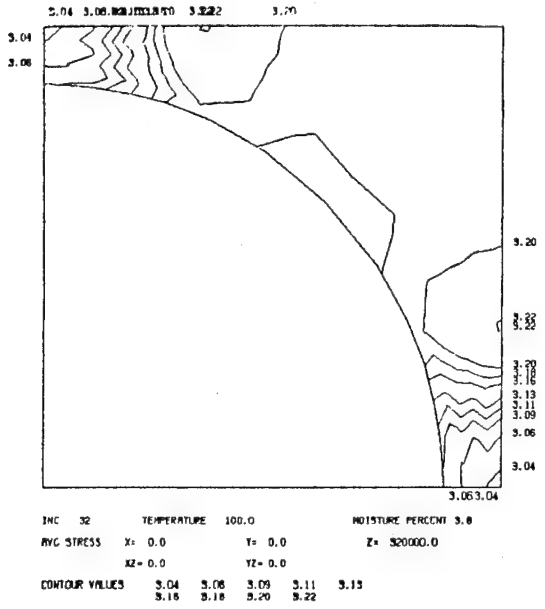


a) Octahedral Shear Stress (ksi)

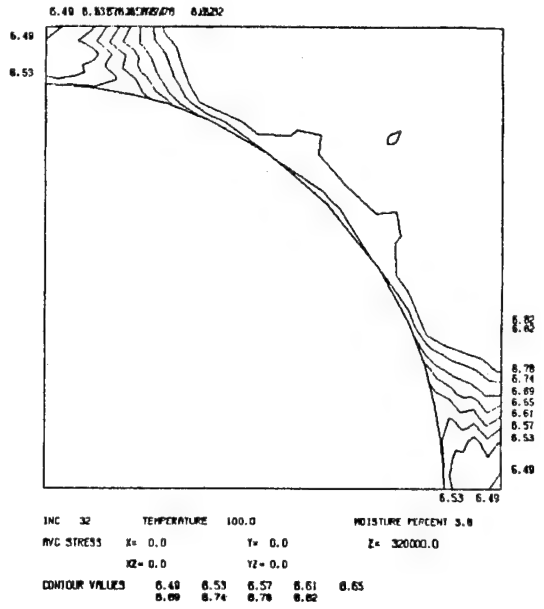


b) Maximum Principal Stress (ksi)

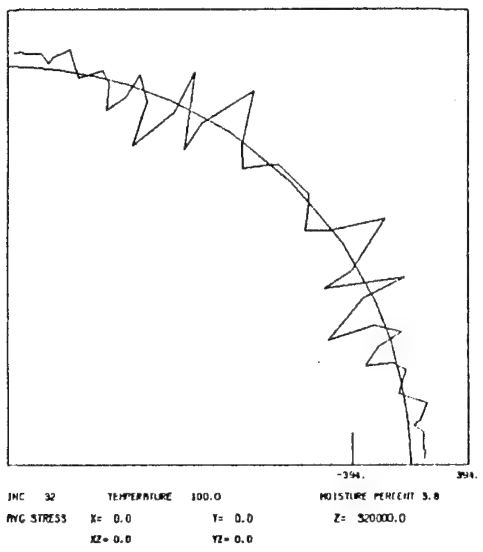


c) Interface Normal Stress (psi)

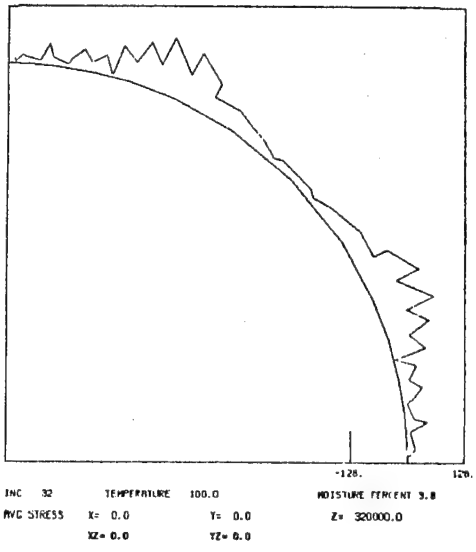


d) Interface Shear Stress (psi)

Figure 92. AS4/2220-1 Graphite/Epoxy Unidirectional Composite, 100°C, 3.8 Percent Moisture (ETW); 2.20 GPa (320 ksi) Longitudinal Tensile Applied Stress.

could initiate composite failure prior to fiber failure.

5.4.1.2.2 Transverse Tension

The predicted transverse tensile stress-strain response of the unidirectional AS4/2220-1 composite is indicated in Figure 93, for each of the four environmental conditions assumed. As previously discussed, no attempt was made to predict ultimate strength, since a specific failure criterion is generally not available within the composite materials community at this time and few experimental data for these composites are available for correlation purposes. Crack propagation at the micro level was not included here. Nevertheless, the results typified by Figure 93 indicate the influence of environmental conditions on stiffness properties and indicate the degree of nonlinear response induced by the nonlinear behavior of the matrix material.

The decrease in composite transverse stiffness with increasingly severe environmental conditions is evident by comparing the slopes of the stress-strain plots in Figure 93. Very little composite nonlinearity is exhibited, (although there is some, particularly at the more severe environmental conditions, e.g., Figure 93d), even though the matrix response is clearly in the nonlinear range in local regions of the composite. This can be seen by studying the internal stress state in the matrix material. Since no crack propagation or failure criterion was utilized, it was possible to increase the applied transverse loading to any level desired. An unrealistically high applied transverse tensile stress of 97 MPa (14 ksi) was selected, realizing that this is probably higher than the actual composite will be capable of sustaining. In this way, the stress-strain curves (Figure 93) are sure to cover the full range of actual material response. However, by applying such high

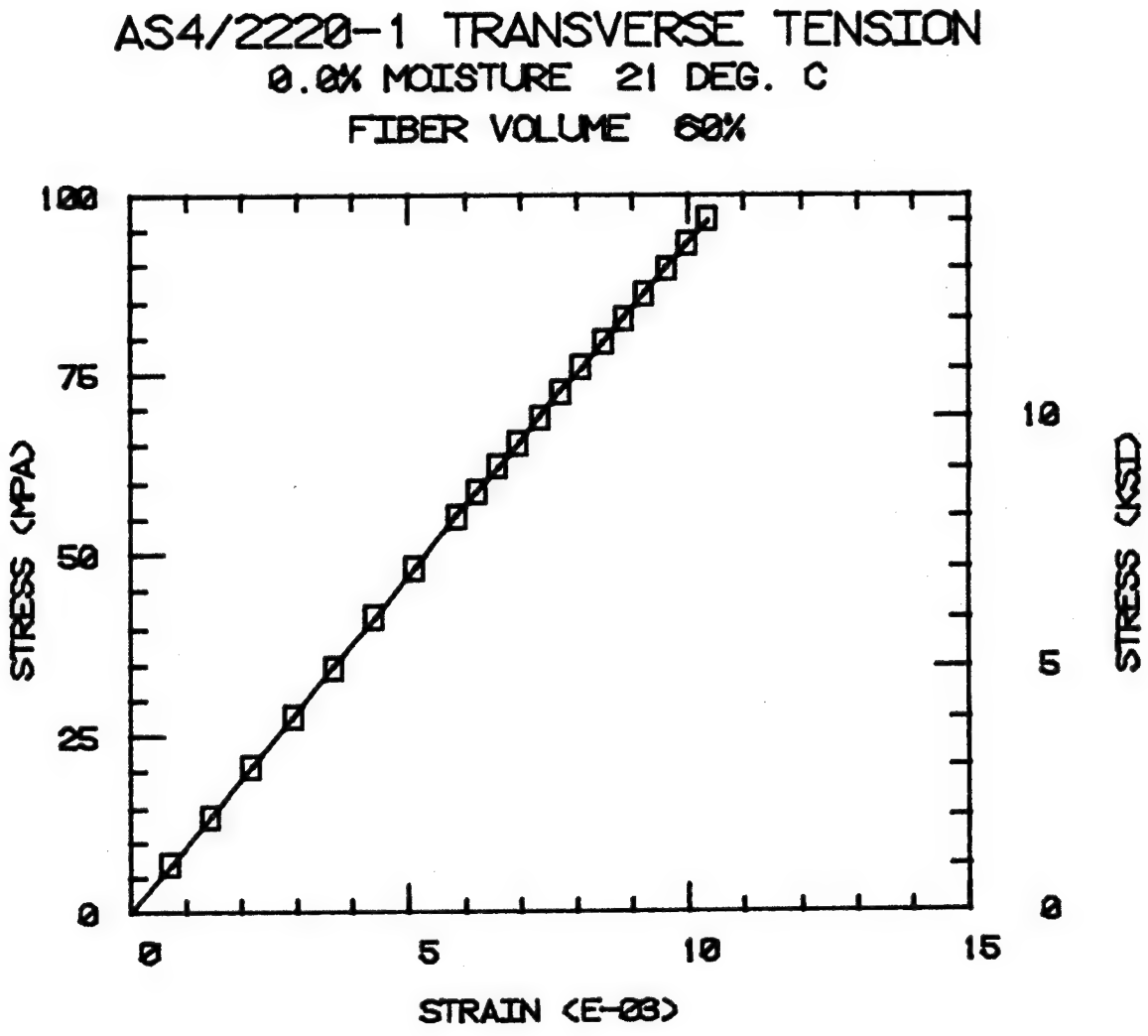


a) Room Temperature, Dry (RTD)

Figure 93. AS4/2220-1 Graphite/Epoxy Unidirectional Composite, Transverse Tensile Stress-Strain Response.

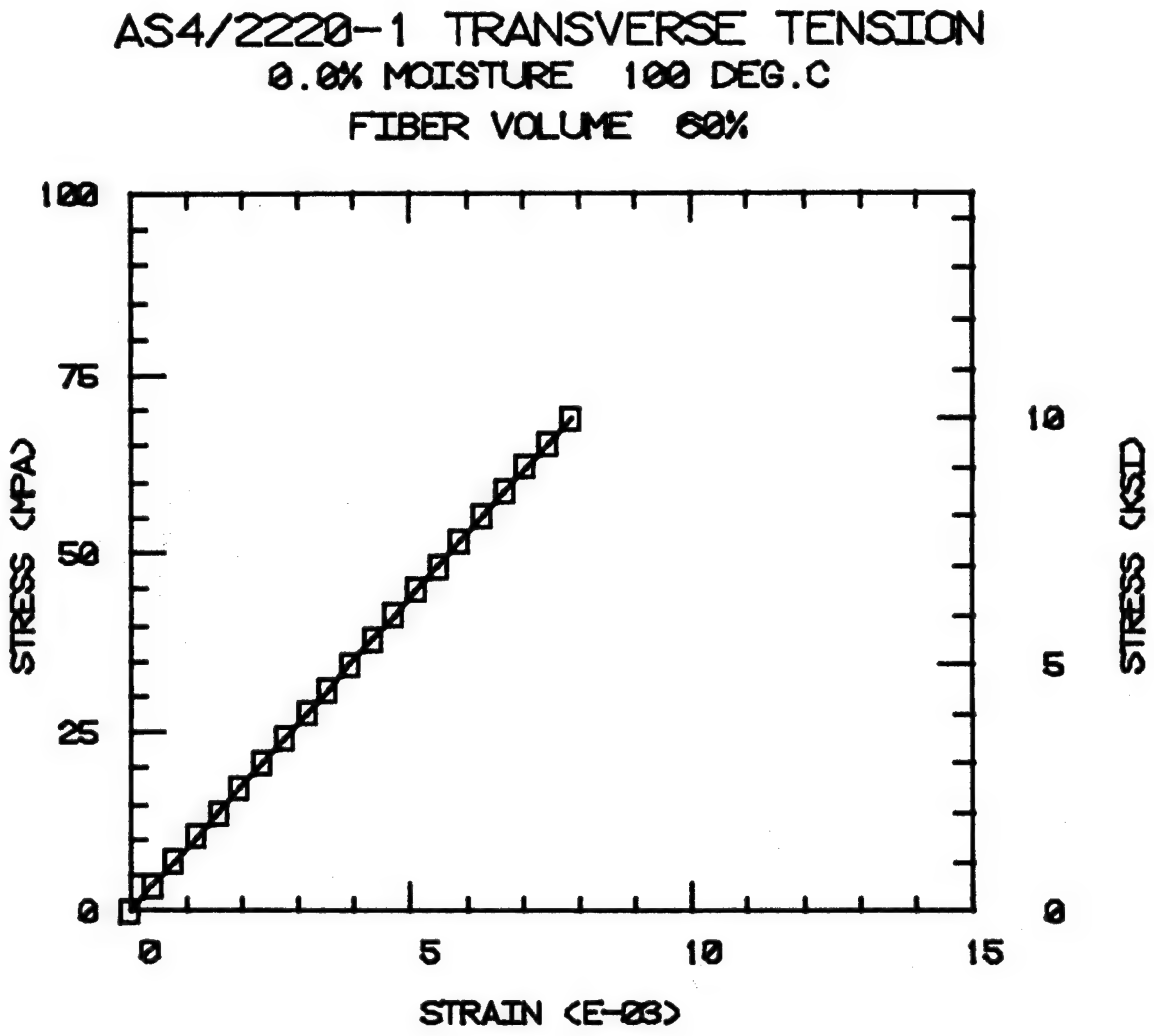


b) Elevated Temperature (100°C), Dry (ETD)

Figure 93 (continued). AS4/2220-1 Graphite/Epoxy Unidirectional Composite, Transverse Tensile Stress-Strain Response.

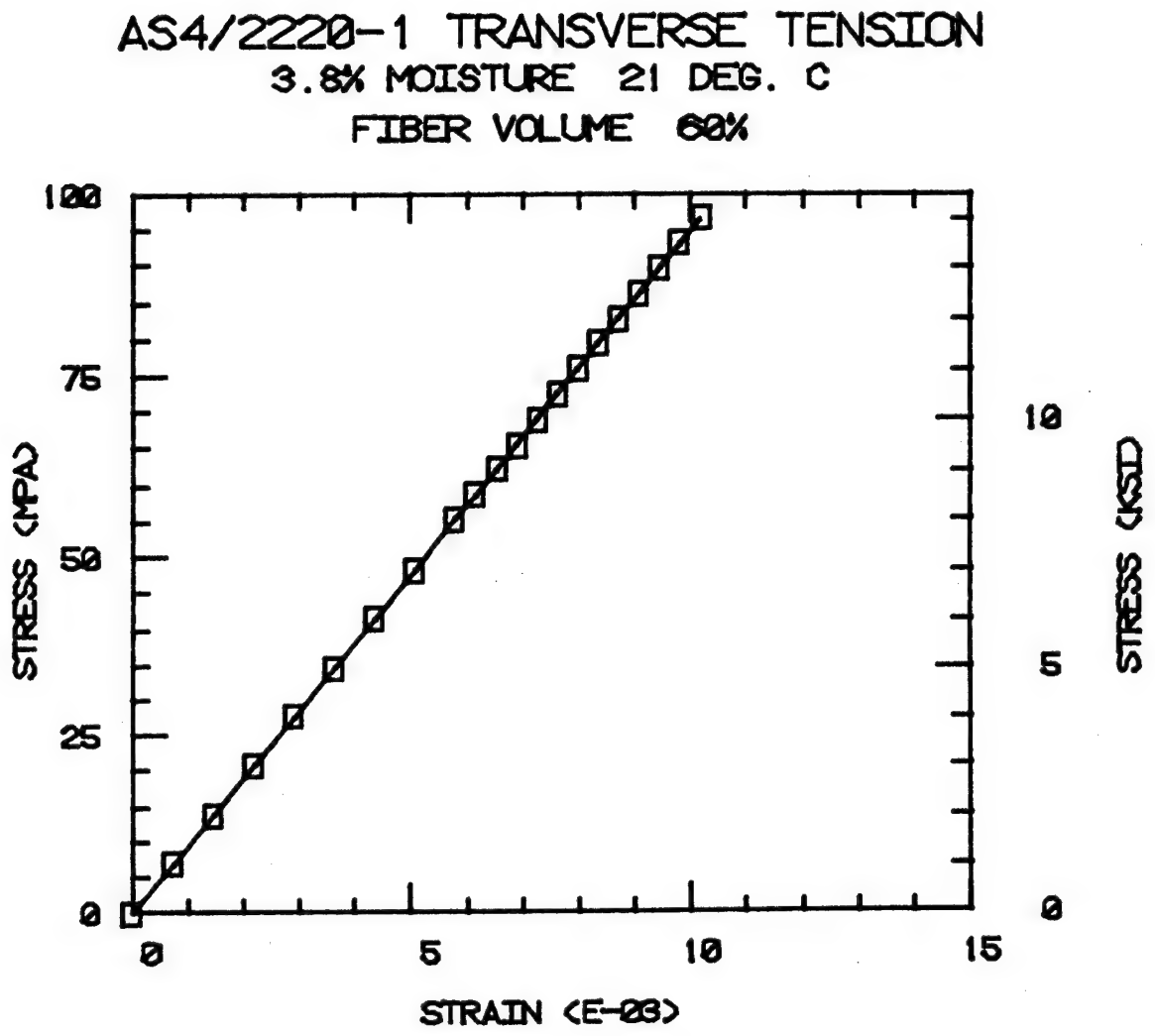


c) Room Temperature, 3.8 Percent Moisture (RTW)

Figure 93 (continued). AS4/2220-1 Graphite/Epoxy Unidirectional Composite, Transverse Tensile Stress-Strain Response.

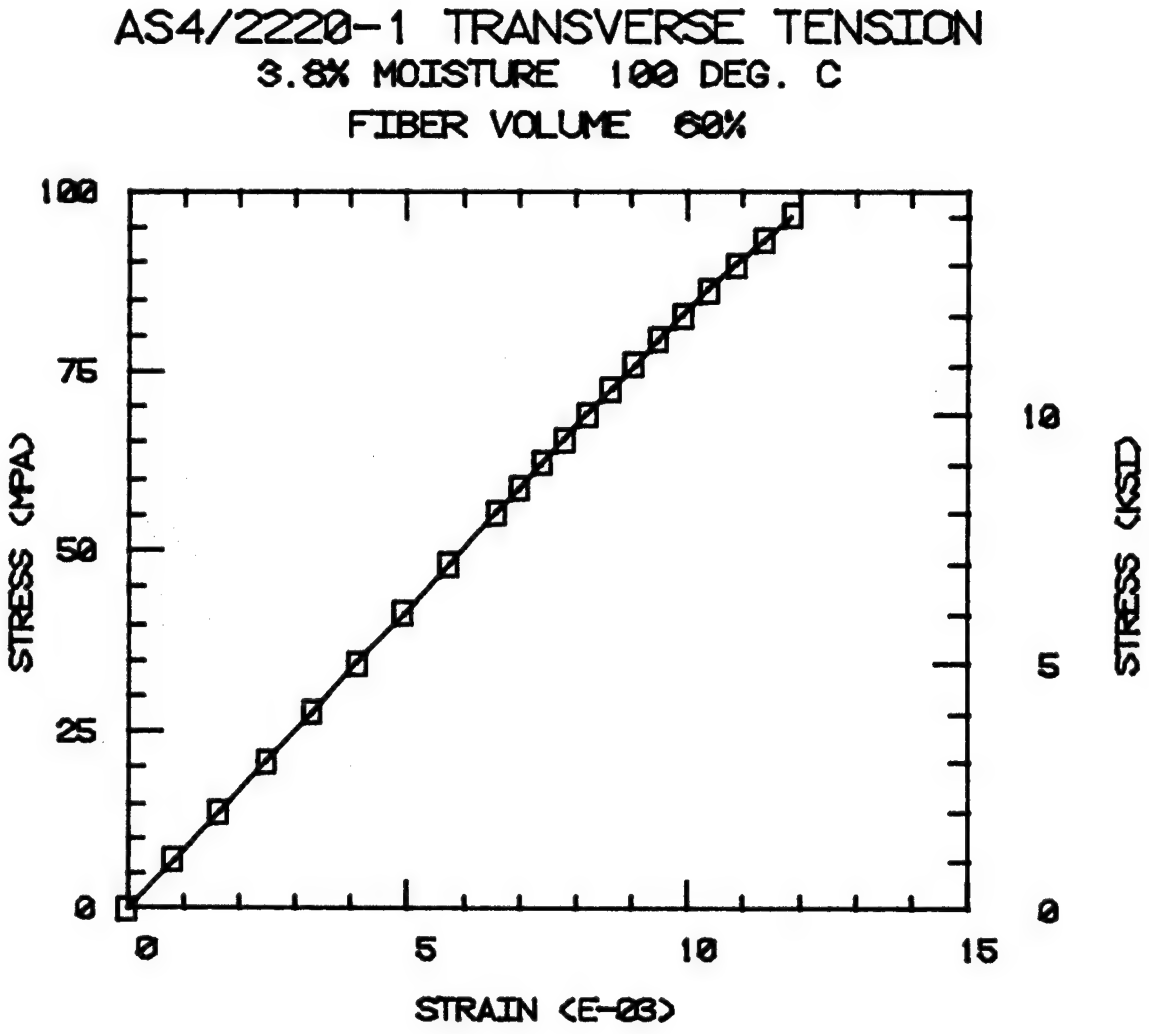


d) Elevated Temperature (100°C), 3.8 Percent Moisture (ETW)

Figure 93 (continued). AS4/2220-1 Graphite/Epoxy Unidirectional Composite, Transverse Tensile Stress-Strain Response.

loadings, it must be realized that the magnitudes of the predicted internal stresses will be unrealistically high. In this presentation, it is the general trends which are important.

Figure 94 indicates the internal stress state for the RTD condition, at an applied transverse stress of only 27.6 MPa (4 ksi). A low applied stress was deliberately selected so that all matrix systems, at all environmental conditions, could be compared at the same applied loading, without having some systems fail prematurely. This loading is applied in the horizontal or x-direction in Figure 94 and subsequent figures. The local stress distribution is thus unsymmetrical. The highest octahedral shear stress occurs along the y-axis, even though two of the three principal stresses are the highest at the interface, well away from either axis. The high maximum shear stress (Figure 94f) controls the octahedral shear stress in this case. The interface normal stress is also very high. Considering that the experimentally measured ultimate tensile stress for this 2220-1 matrix was less than 41 MPa (6 ksi) as given in Figure 65a), the matrix is probably beyond actual first failure (microcracking) even at this low applied stress. The composite would not be expected to sustain the high stresses indicated in Figure 94a before microcracking and failing.

Figure 95 includes the transverse tensile loading plots for the ETD condition. The response is similar to that for the RTD condition indicated in Figure 94.

The 21°C, 3.8 weight percent moisture content (RTW) condition is indicated in Figure 96. The highest octahedral shear stress is only about 36 percent as high as for the RTD case (Figure 96a versus Figure 94a) and it occurs at a slightly different location, viz, at the

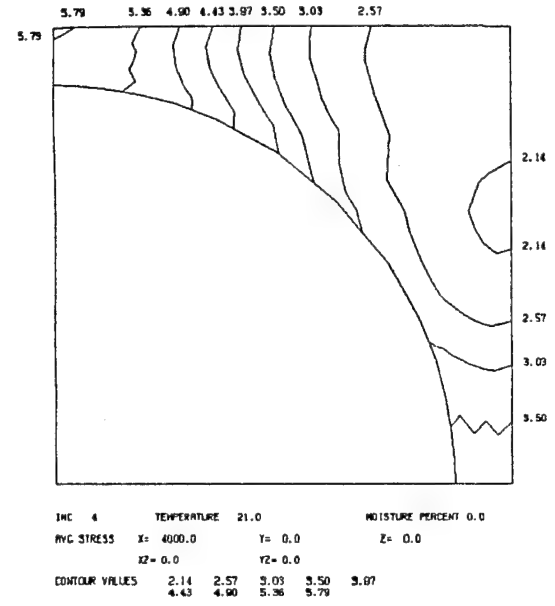


a) Octehedral Shear Stress (ksi)

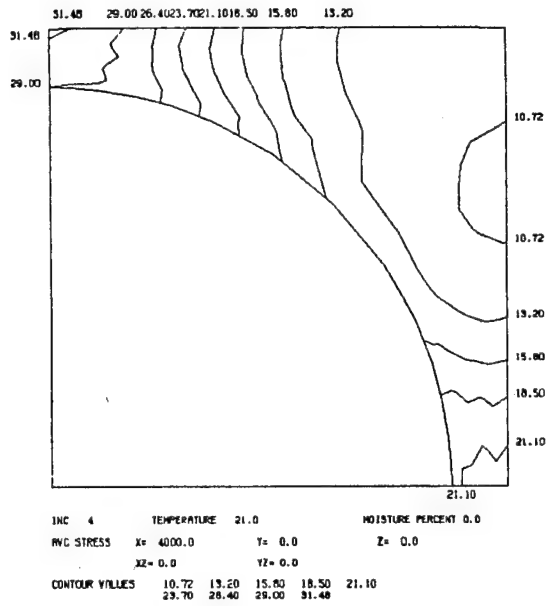


b) Maximum Principal Stress (ksi)

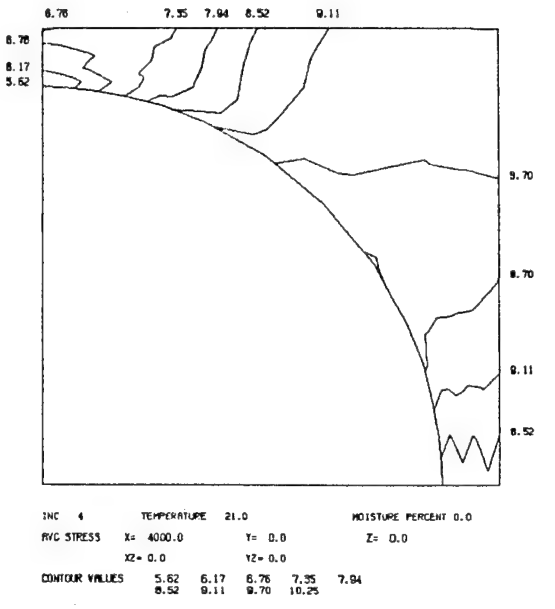


c) Minimum Principal Stress (ksi)

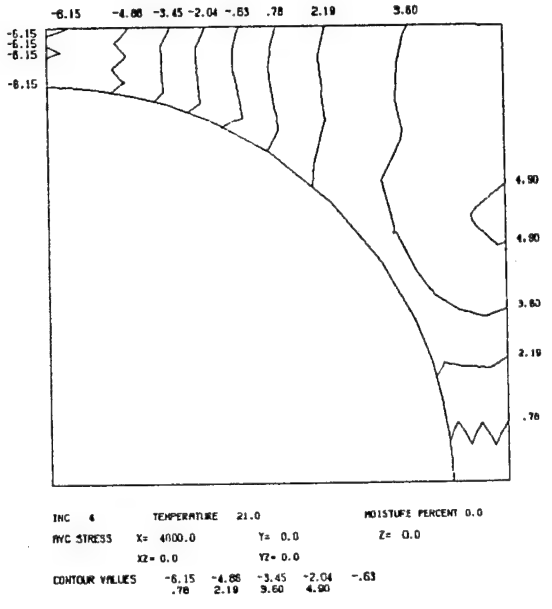


d) Intermediate Principal Stress (ksi)

Figure 94. AS4/2220-1 Graphite/Epoxy Unidirectional Composite, Room Temperature, Dry (RTD); 27.6 MPa (4 ksi) Transverse Tensile Applied Stress.

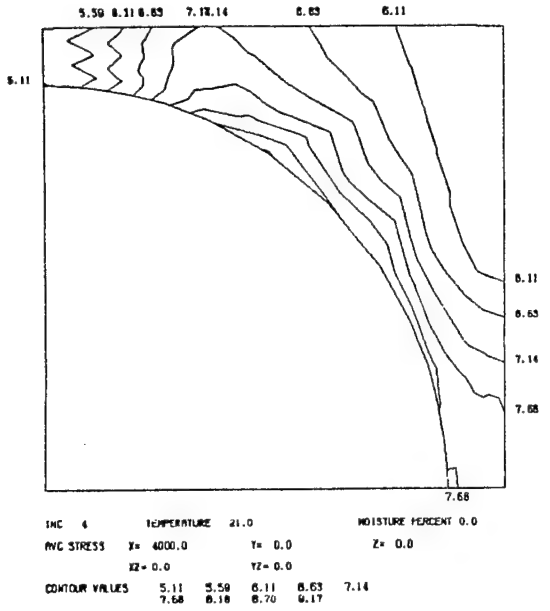


e) Intermediate Principal Stress (ksi)

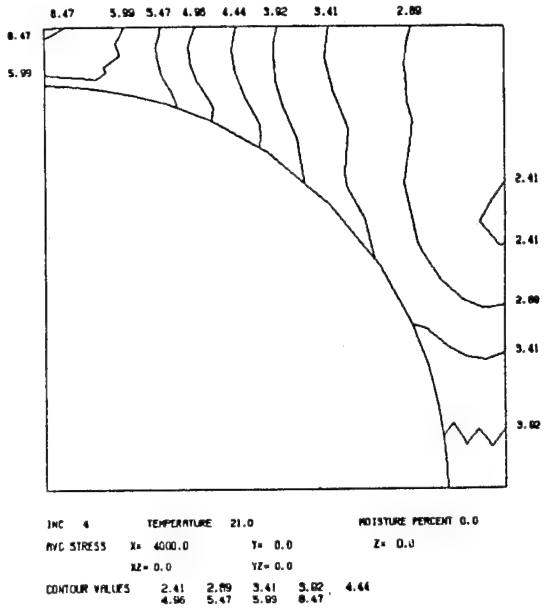


f) Maximum Shear Stress (ksi)

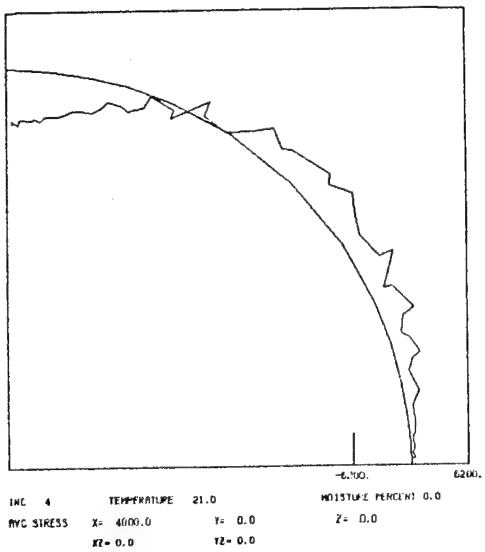


g) Interface Normal Stress (psi)

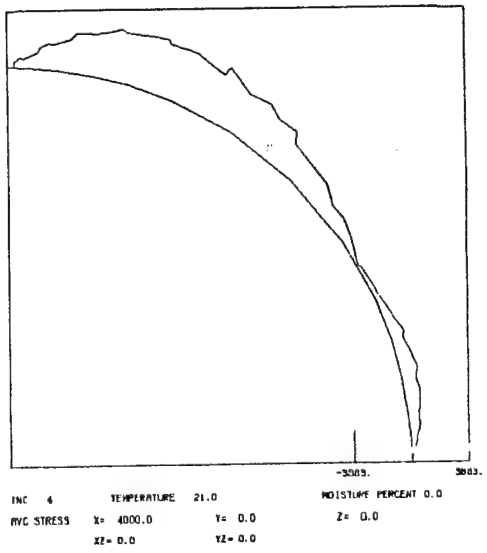


h) Interface Shear Stress (psi)

Figure 94 (continued). AS4/2220-1 Graphite/Epoxy Unidirectional Composite, Room Temperature, Dry (RTD); 27.6 MPa (4 ksi) Transverse Tensile Applied Stress.

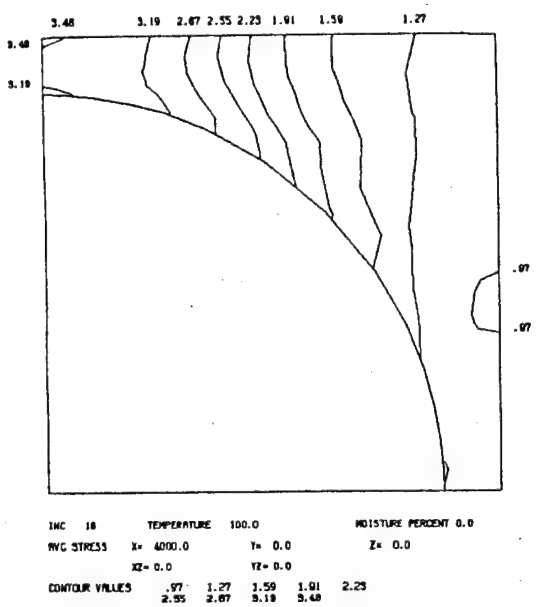


a) Octahedral Shear Stress (ksi)

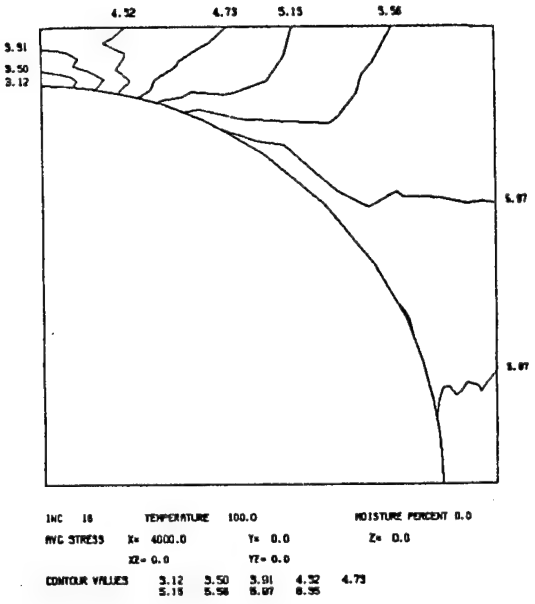


b) Maximum Principal Stress (ksi)

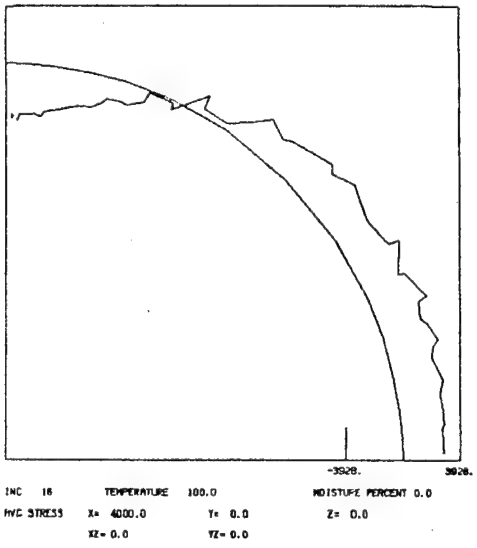


c) Interface Normal Stress (ksi)

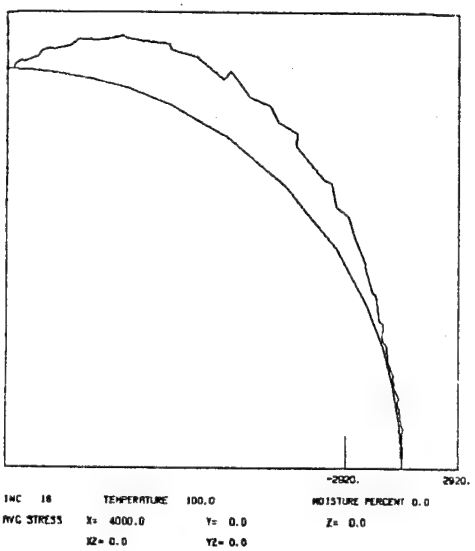


d) Interface Shear Stress (psi)

Figure 95. AS4/2220-1 Graphite/Epoxy Unidirectional Composite, 100°C, Dry (ETD); 27.6 MPa (4 ksi) Transverse Tensile Applied Stress.

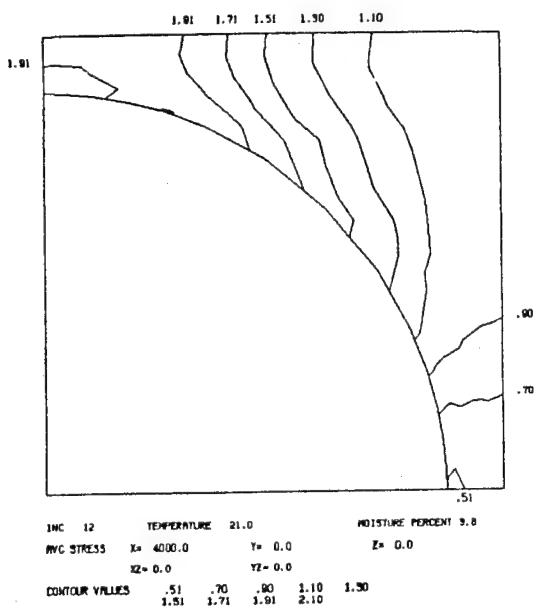


a) Octahedral Shear Stress (ksi)

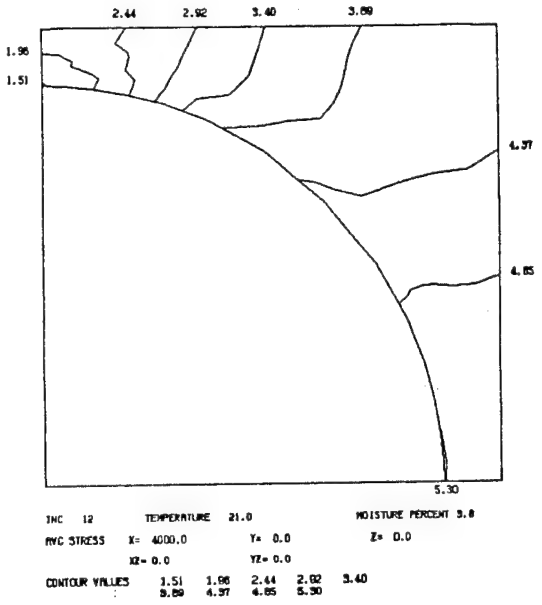


b) Maximum Principal Stress (ksi)

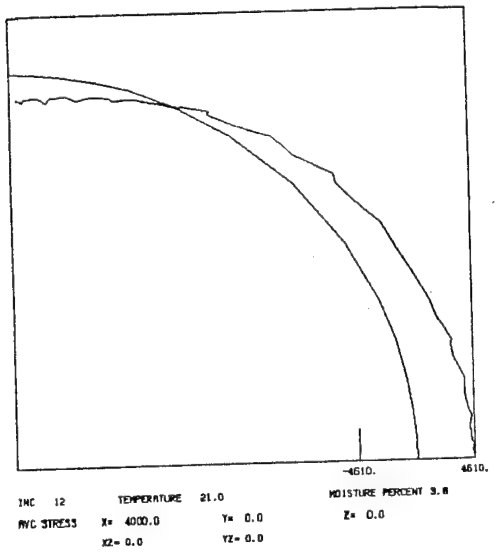


c) Interface Normal Stress (ksi)

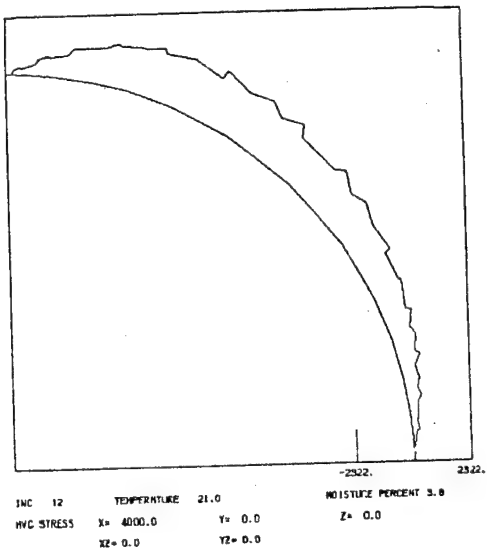


d) Interface Shear Stress (psi)

Figure 96. AS4/2220-1 Graphite/Epoxy Unidirectional Composite, Room Temperature, 3.8 Percent Moisture (RTW); 27.6 MPa (4 ksi) Transverse Tensile Applied Stress.

fiber-matrix interface as compared to in the matrix along the y-axis. This difference is reflected in the distribution of interface stresses also.

To indicate the influence of the level of loading, results for a low and high applied stress level are given in Figures 97 and 98, respectively, for the ETW condition. At the low applied stress level (27.6 MPa or 4 ksi), the hygrothermal stresses (Figure 85) still are significant. However, at 97 MPa (14 ksi) the mechanical loading dominates. Because of this, it will be noted that the local stresses do not increase in direct proportion to the level of transverse loading. For example, even though the applied stress has been increased by a factor of 3.5 between Figures 97 and 98, the octahedral shear stress is only about 2.2 times higher. This is due to the radical differences in the changes of the principal stresses. The highest maximum principal stress increases by a factor of only 3.1, but the other two principal stresses increase more dramatically in this same region. This causes a higher hydrostatic stress component to be developed, which does not contribute to the octahedral shear stress (distortional energy) level.

The special significance of this is in terms of failure criteria. For example, in the present case, a maximum normal stress criterion would predict first failure of the composite at much lower transverse normal tensile loadings than a distortional energy criterion. The present micromechanics results should be very useful in the future in establishing suitable failure criteria for composites.

5.4.1.2.3 Longitudinal Shear

Longitudinal shear is defined as the loading which induces shear stresses parallel to the fibers in the unidirectional composite. Axial

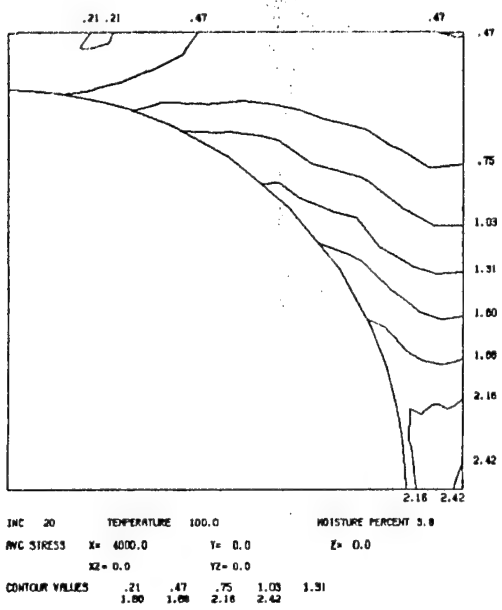


a) Octahedral Shear Stress (ksi)

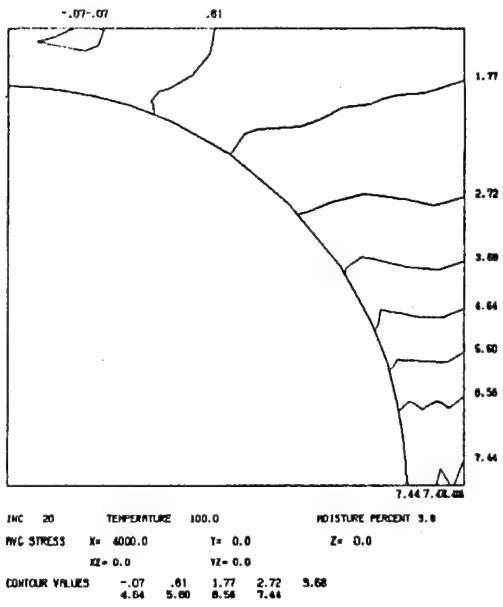


b) Maximum Principal Stress (ksi)

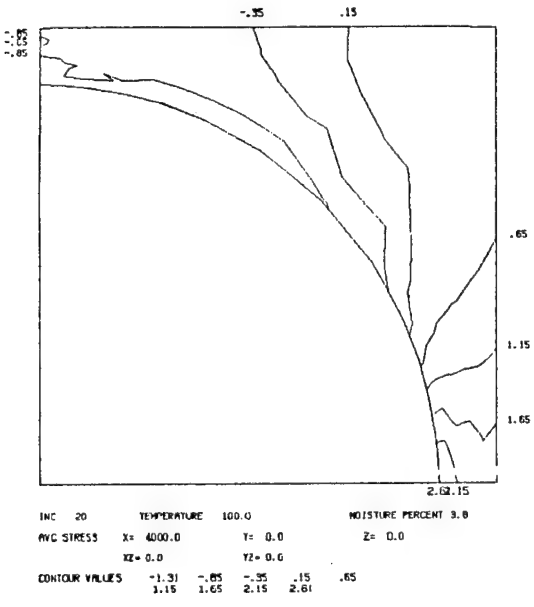


c) Minimum Principal Stress (ksi)

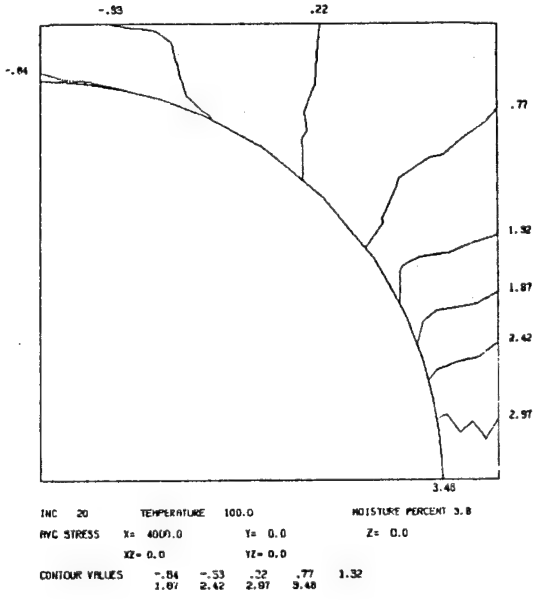


d) Intermediate Principal Stress (ksi)

Figure 97. AS4/2220-1 Graphite/Epoxy Unidirectional Composite, 100°C, 3.8 Percent Moisture (ETW); 27.6 MPa (4 ksi) Transverse Tensile Applied Stress.

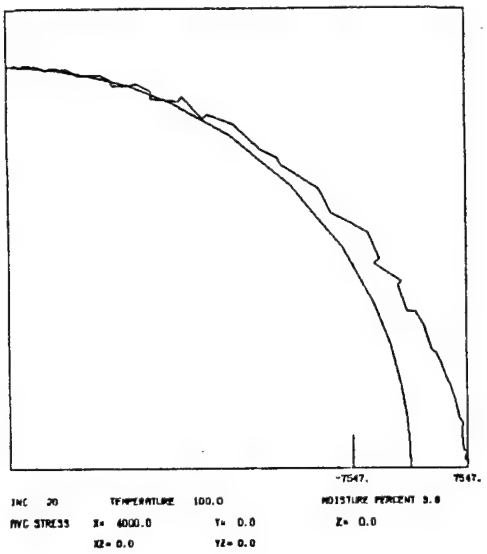


e) Interface Normal Stress (psi)

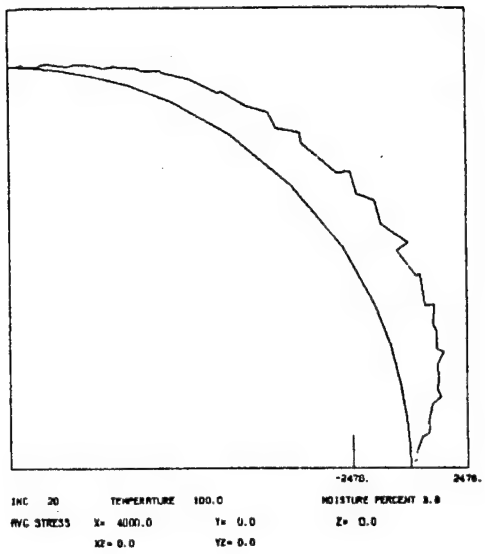


f) Interface Shear Stress (psi)

Figure 97 (continued). AS4/2220-1 Graphite/Epoxy Unidirectional Composite, 100°C, 3.8 Percent Moisture (ETW); 27.6 MPa (4 ksi) Transverse Tensile Applied Stress.

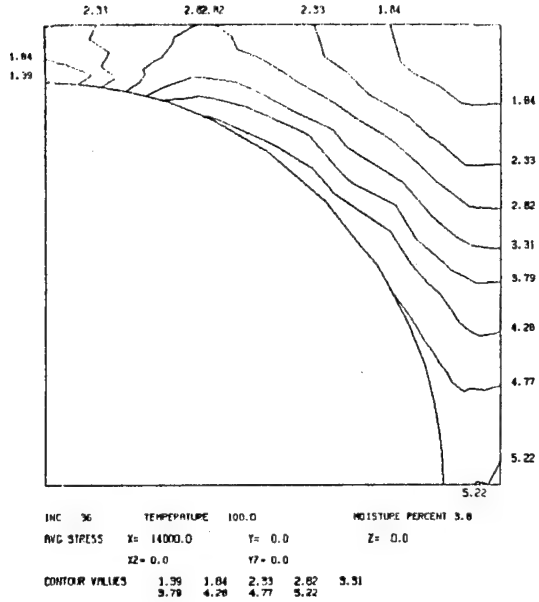


a) Octahedral Shear Stress (ksi)

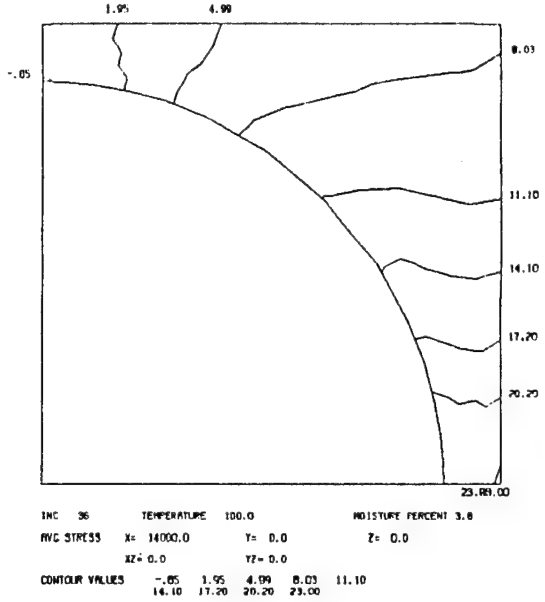


b) Maximum Principal Stress (ksi)

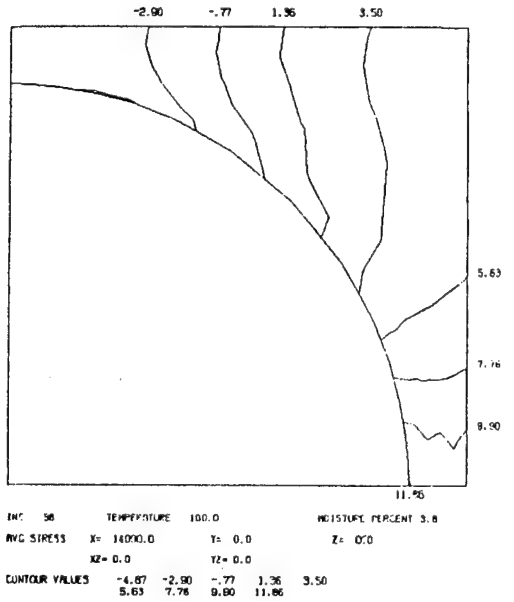


c) Minimum Principal Stress (ksi)

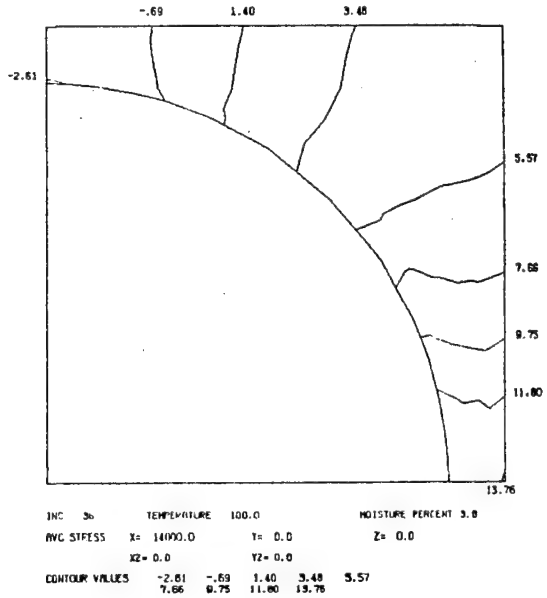


d) Intermediate Principal Stress (ksi)

Figure 98. AS4/2220-1 Graphite/Epoxy Unidirectional Composite, 100°C, 3.8 Percent Moisture (ETW); 97 MPa (14 ksi) Transverse Tensile Applied Stress.

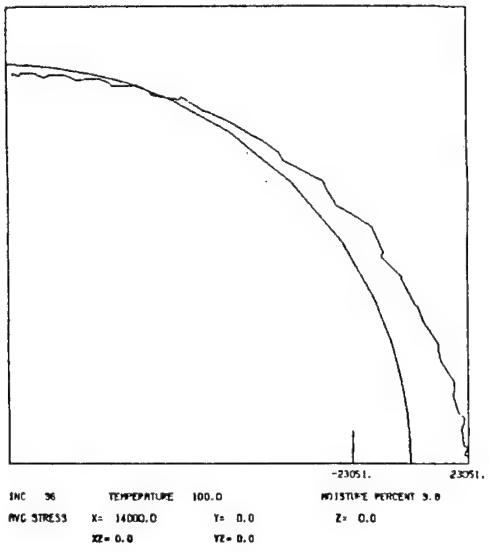


e) Interface Normal Stress (psi)

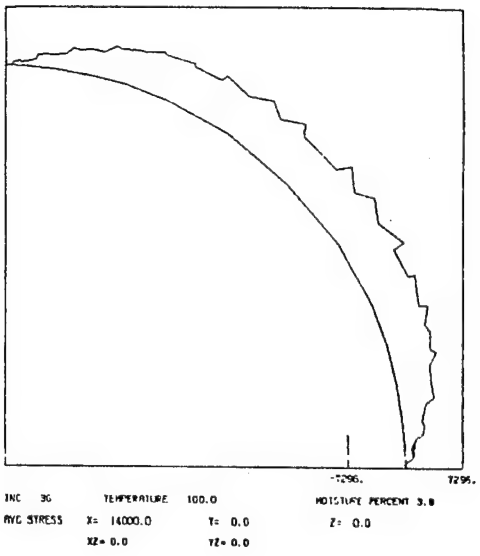


f) Interface Shear Stress (psi)

Figure 98 (continued). AS4/2220-1 Graphite/Epoxy Unidirectional Composite, 100°C, 3.8 Percent Moisture (ETW); 97 MPa (14 ksi) Transverse Tensile Applied Stress.

and transverse normal loadings induce in-plane shear stresses, i.e., shear stresses across the fibers ($\tau_{xy}$), but no shear stresses parallel to the fibers ($\tau_{xz}$ or $\tau_{yz}$). In the present examples, a $\bar{\tau}_{xz}$ shear stress only will be assumed to be applied to the composite. This is representative of the stress in a unidirectionally reinforced composite solid rod or thin-walled tube of circular cross section (with the fibers oriented along the length of the specimen) subjected to torsion, or a thin-walled, hoop-wound tube in torsion, or the in-plane shear stress induced in an individual ply of a laminate due to ply coupling effects.

Even more than transverse tensile loading, shear loading response of a unidirectional composite is very sensitive to the matrix response. This is graphically demonstrated in Figure 99, a set of four shear stress-shear strain plots representing the four environmental preconditions being considered. Figure 99a, viz, the room temperature, dry (RTD) condition, indicates only a slight degree of composite nonlinear response, and relatively low strain levels. At 100°C, dry (Figure 99b), the nonlinearity is much greater, as is the shear strain for an equal stress level. At the room temperature, wet (RTW) condition (Figure 99c), the response is somewhat comparable to the RTD condition. The combined effects of temperature and moisture (ETW), represented in Figure 99d, result in very high strains. None of this composite material shear response is particularly surprising, when the matrix shear stress-shear strain curves are considered (Figure 65b). The unidirectional composite shear response, being highly matrix-dominated, follows the unreinforced matrix shear response.

The internal stress state in the composite will be shear-dominated, of course, when a shear loading is applied. It can be expected that the

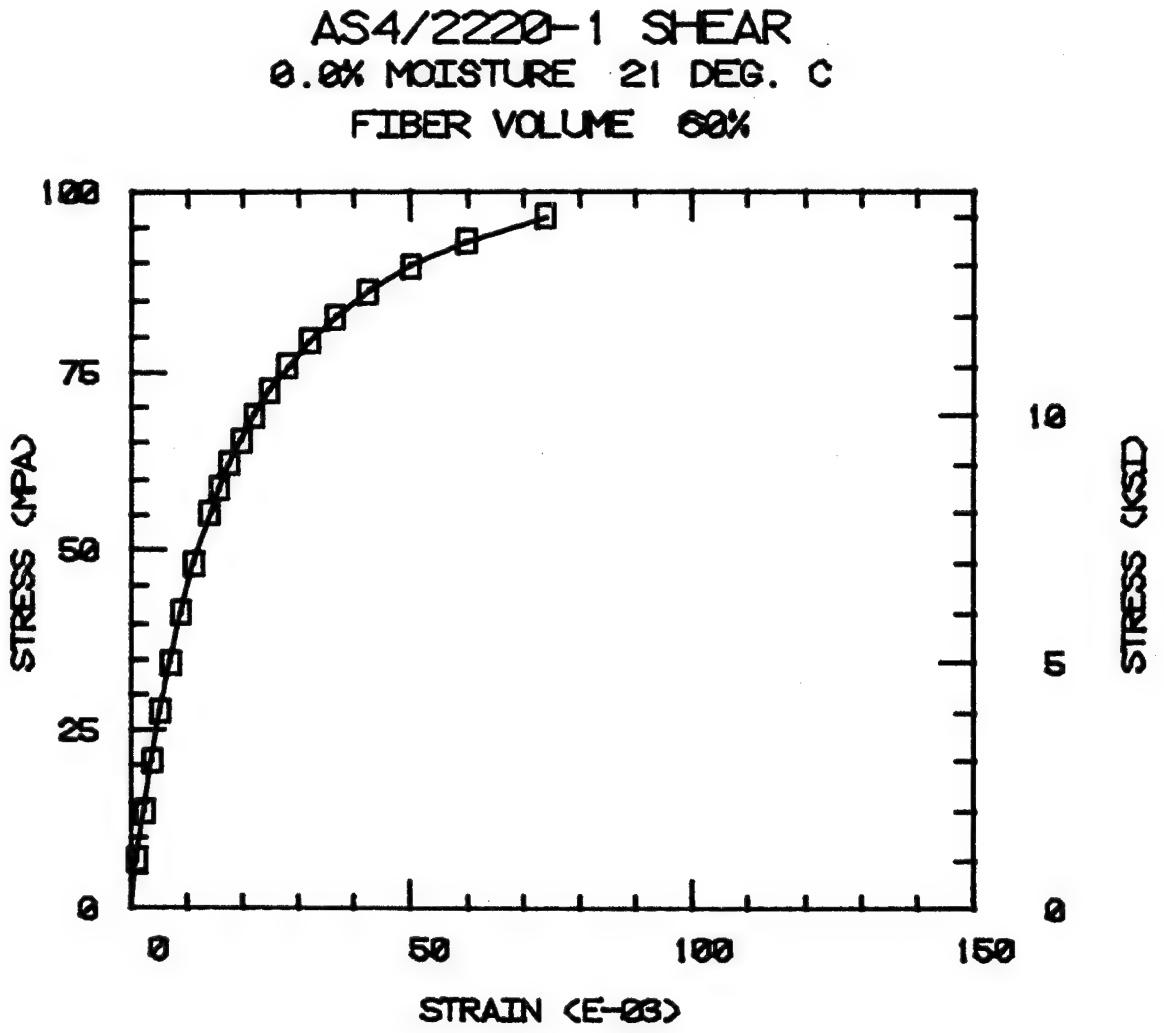


a) Room Temperature, Dry (RTD)

Figure 99. AS4/2220-1 Graphite/Epoxy Unidirectional Composite, Longitudinal Shear Stress-Strain Response.

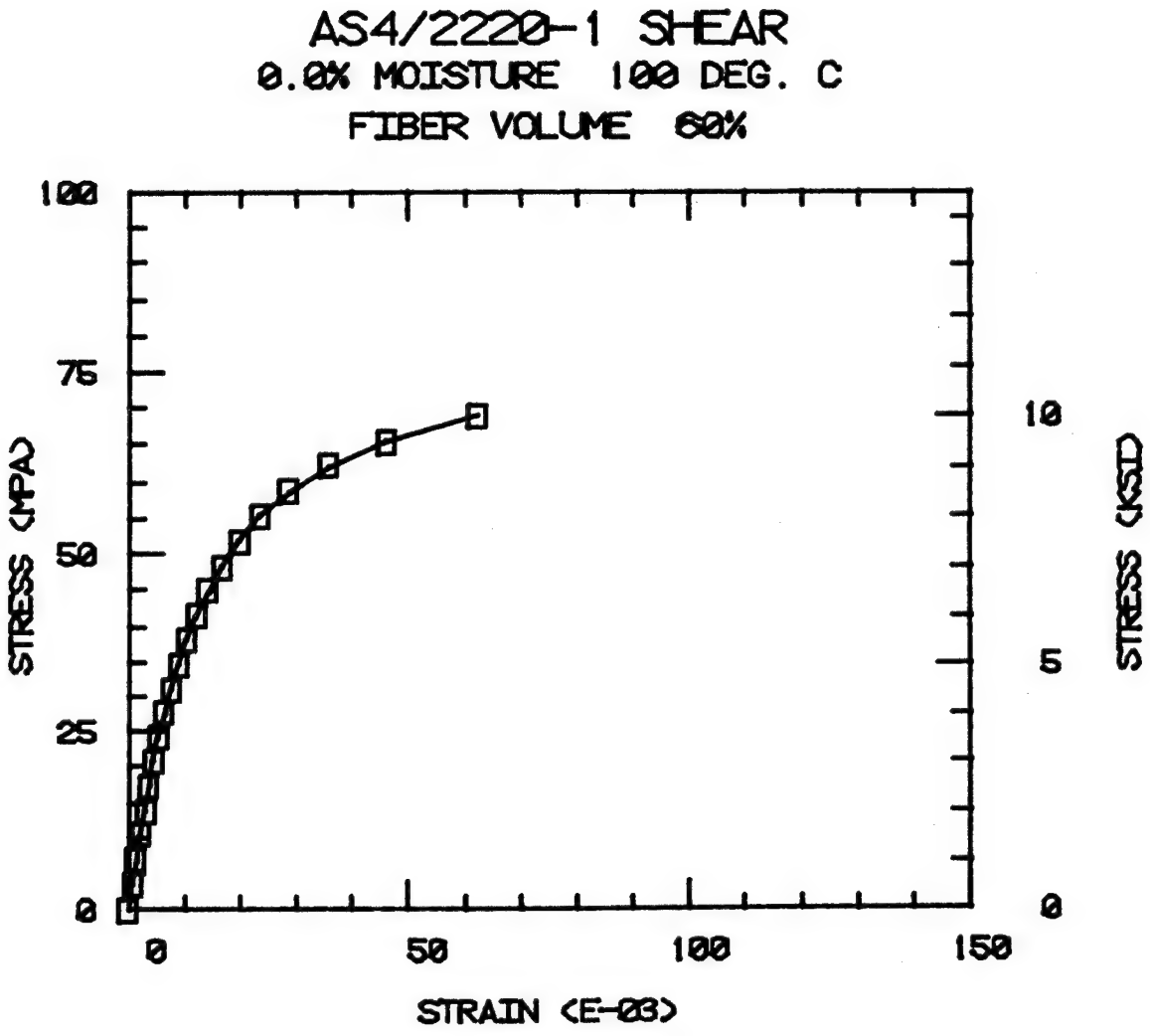


b) Elevated Temperature (100°C), Dry (ETD)

Figure 99 (continued). AS4/2220-1 Graphite/Epoxy Unidirectional Composite, Longitudinal Shear Stress-Strain Response.

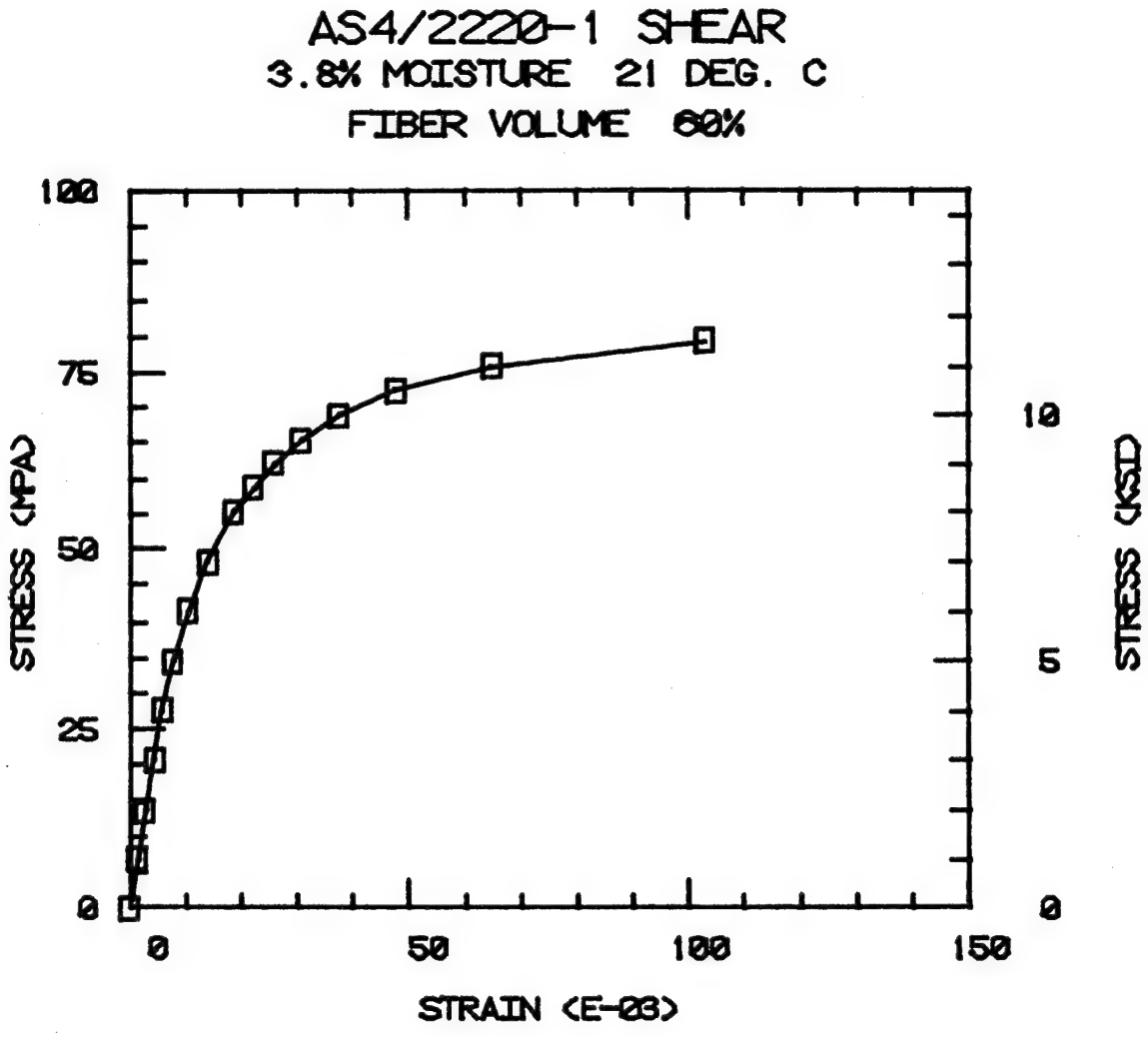


c) Room Temperature, 3.8 Percent Moisture (RTW)

Figure 99 (continued). AS4/2220-1 Graphite/Epoxy Unidirectional Composite, Longitudinal Shear Stress-Strain Response.

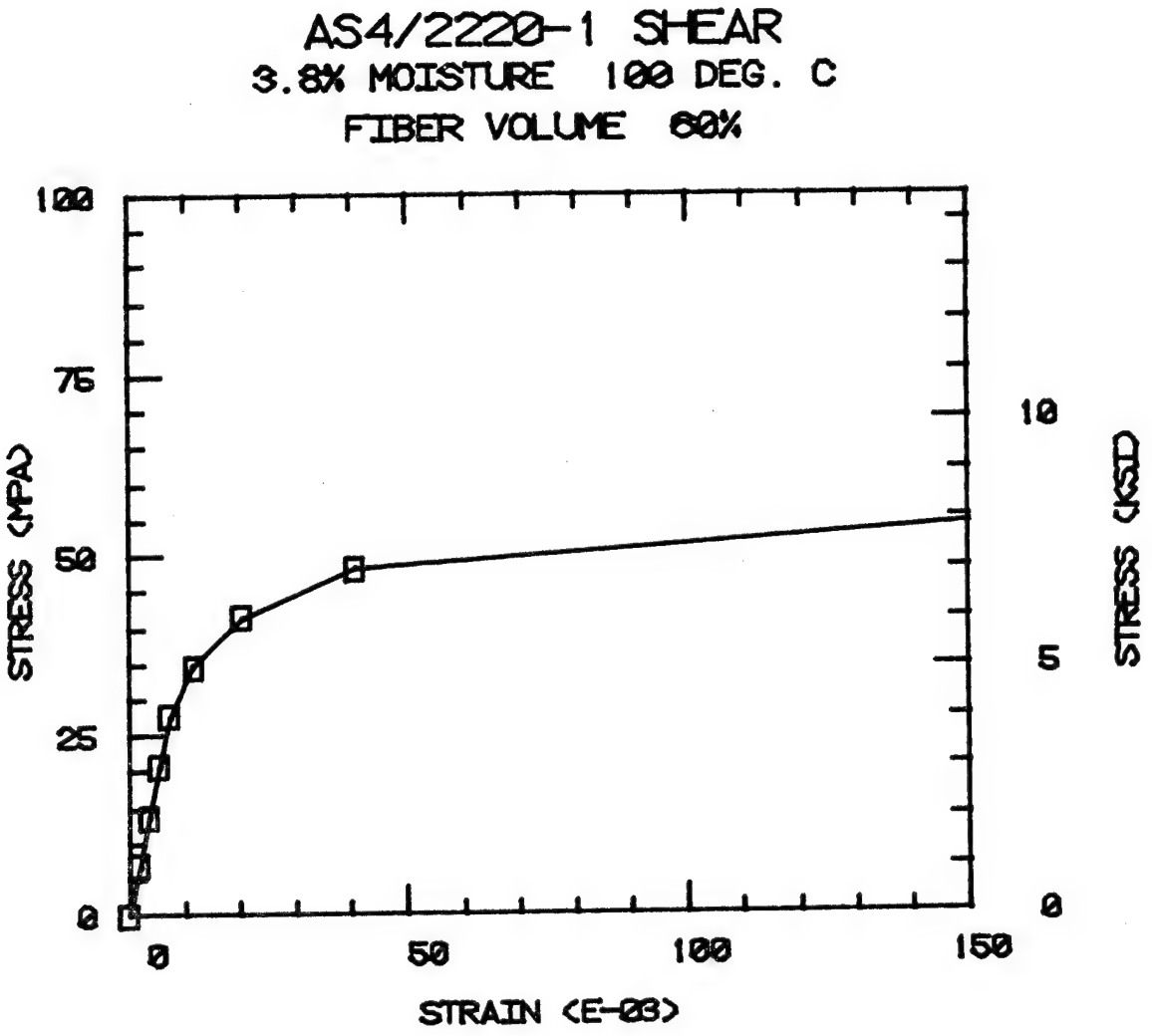


d) Elevated Temperature (100°C), 3.8 Percent Moisture (ETW)

Figure 99 (continued). AS4/2220-1 Graphite/Epoxy Unidirectional Composite, Longitudinal Shear Stress-Strain Response.

maximum and minimum principal stresses at a point will be close in magnitude and opposite in sign, and the third principal stress will be small. This is borne out by the stress contour plots. Figure 100 represents the RTD condition. By comparing Figure 100 with Figure 83 (the RTD internal stress state prior to shear loading), it will be noted that the maximum and minimum principal stresses have increased significantly, while the third principal stress has changed very little. The interface normal stress changes little, since little Poisson coupling in pure shear exists between the anisotropic fiber and the surrounding matrix. However, the shear stress at the interface changes completely, becoming very large in the region of minimum fiber spacing in the x-direction (since a $\bar{\tau}_{xz}$ shear stress is being applied).

At the ETD condition, the pre-existing stresses are low and, hence, have little influence on the subsequent shear loading response. These results are presented in Figure 101. At the RTW condition (Figure 102), the applied shear stresses also tend to dominate the pre-existing stresses.

At the ETW condition, the large residual stresses play a more significant role. For this condition, two applied shear stress levels are presented in Figures 103 and 104. At the applied shear stress of 27.6 MPa (4 ksi) represented in Figure 103, the pre-existing hygrothermal stresses are still of the same magnitude as the stresses induced by the applied shear loading. At an applied shear stress of 55.2 MPa (8 ksi), the shear loading-induced stresses clearly dominate; the distribution of the octahedral shear stress and the maximum and minimum principal stresses become much more uniform due to the extensive plastic deformation of the matrix material at the high shear stress levels. This

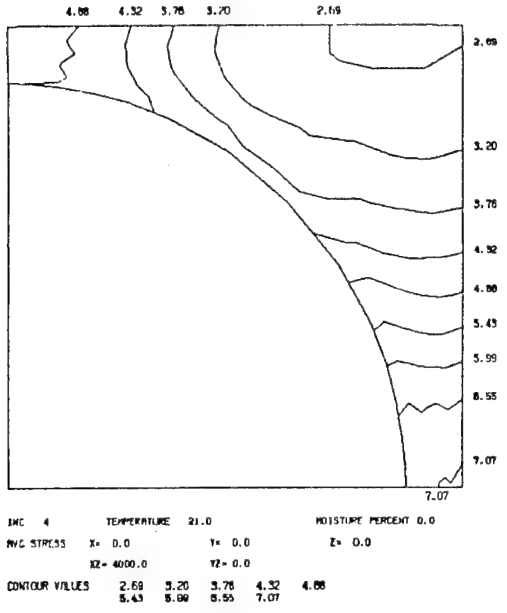


a) Octahedral Shear Stress (ksi)

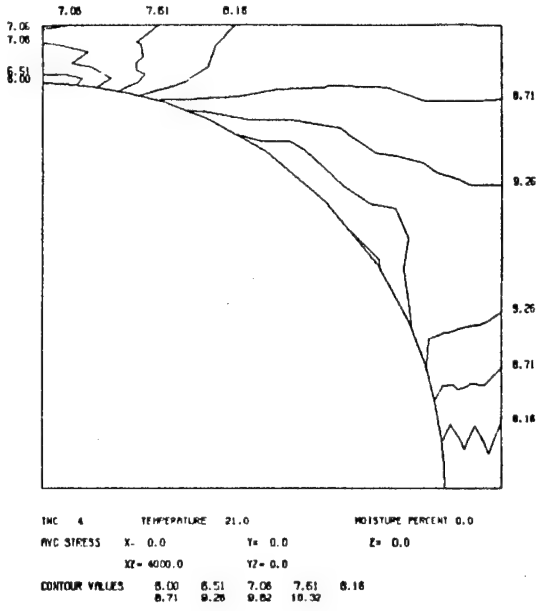


b) Maximum Principal Stress (ksi)

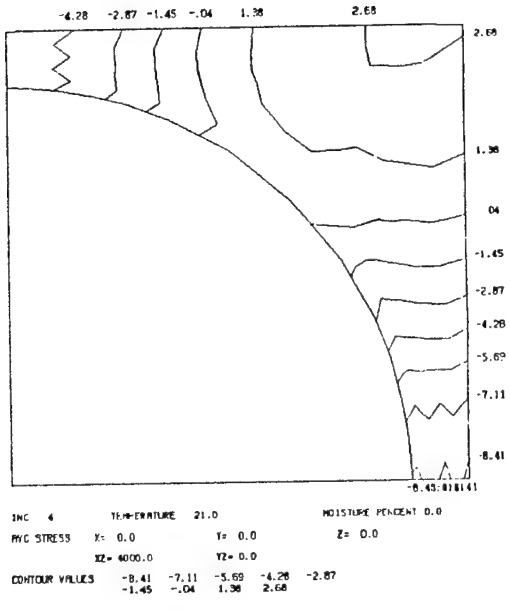


c) Minimum Principal Stress (ksi)

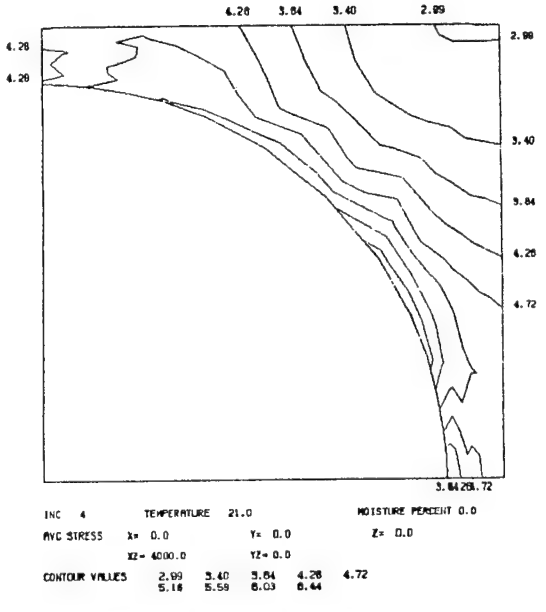


d) Intermediate Principal Stress (ksi)

Figure 100. AS4/2220-1 Graphite/Epoxy Unidirectional Composite, Room Temperature, Dry (RTD); 27.4 MPa (4 ksi) Longitudinal Shear Applied Stress.

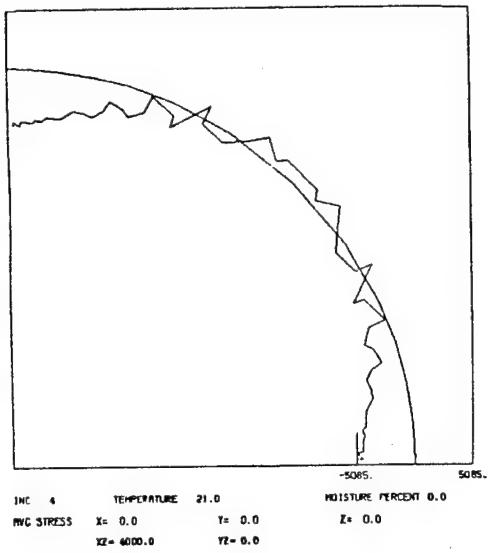


e) Interface Normal Stress (psi)

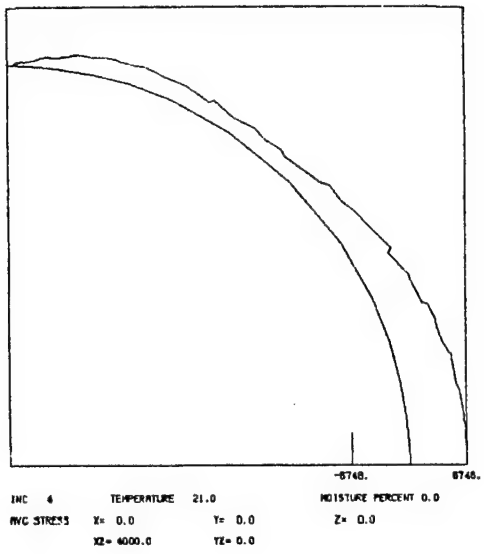


f) Interface Shear Stress (psi)

Figure 100 (continued). AS4/2220-1 Graphite/Epoxy Unidirectional Composite, Room Temperature, Dry (RTD); 27.4 MPa (4 ksi) Longitudinal Shear Applied Stress.

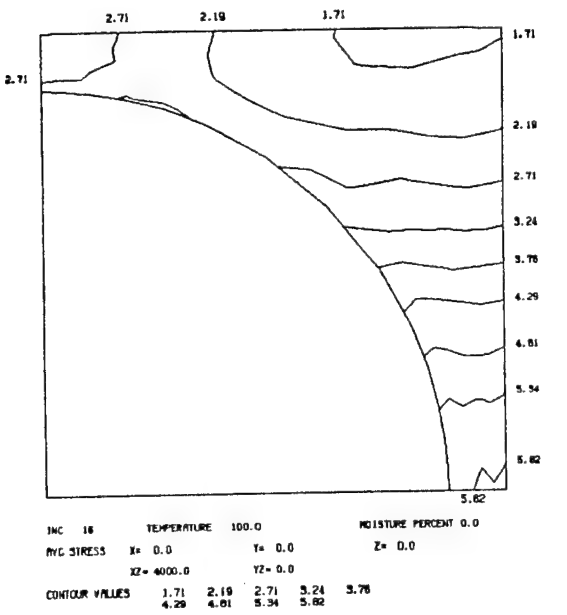


a) Octahedral Shear Stress (ksi)

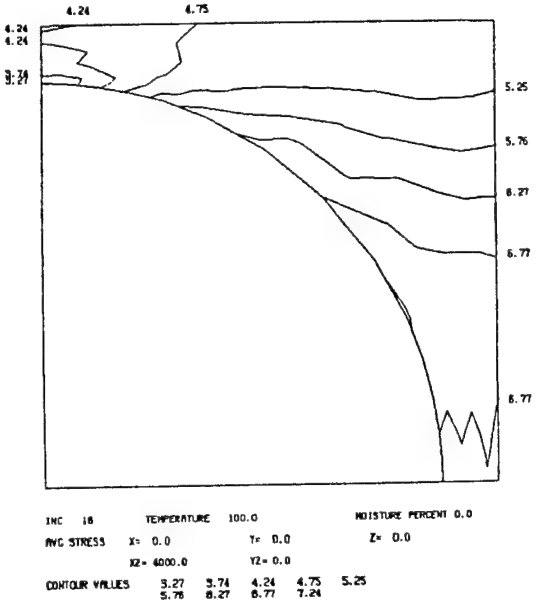


b) Maximum Principal Stress (ksi)

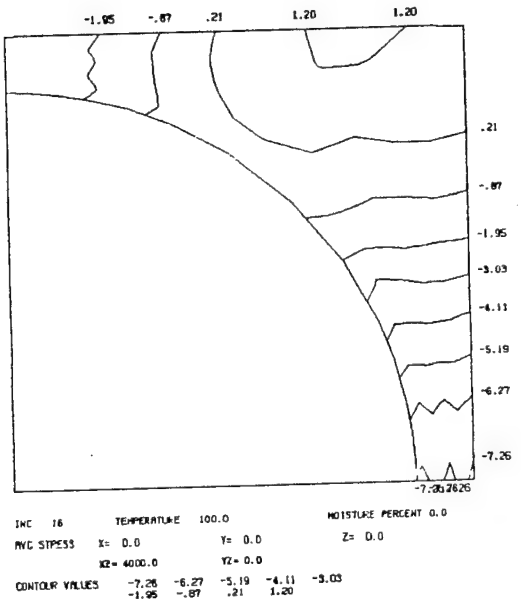


c) Minimum Principal Stress (ksi)

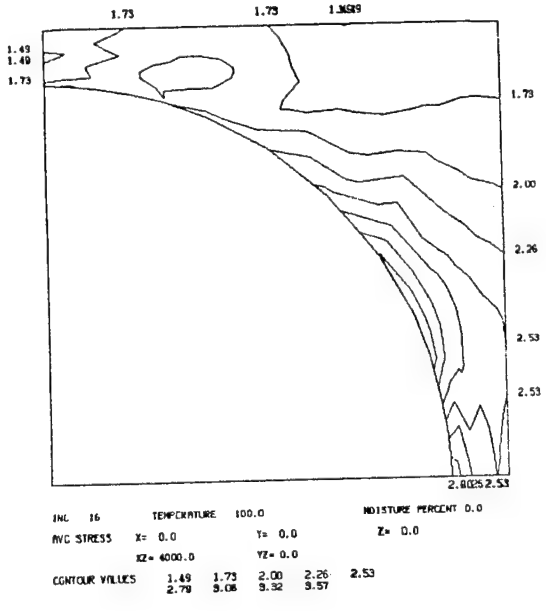


d) Intermediate Principal Stress (ksi)

Figure 101. AS4/2220-1 Graphite/Epoxy Unidirectional Composite, 100°C, Dry (ETD); 27.4 MPa (4 ksi) Longitudinal Shear Applied Stress.

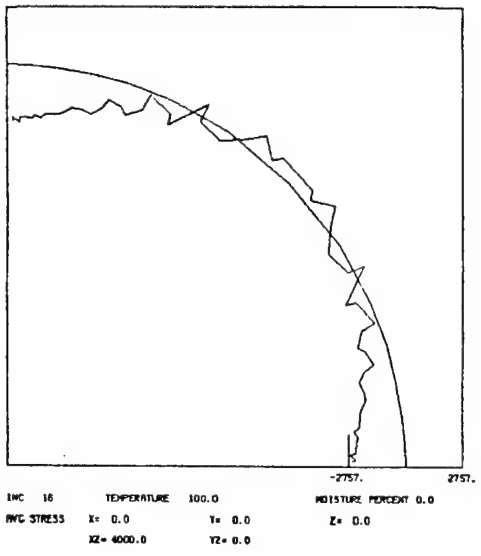


e) Interface Normal Stress (psi)

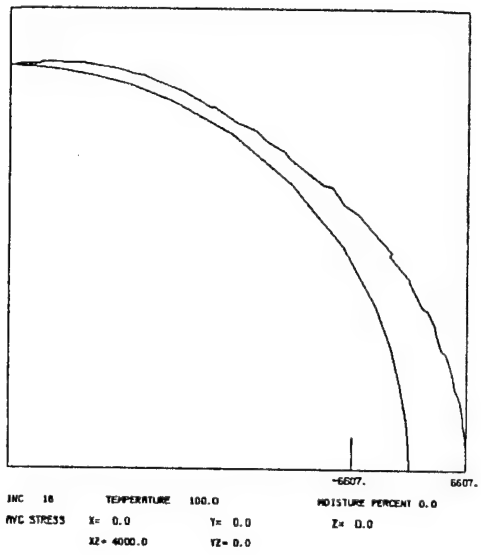


f) Interface Shear Stress (psi)

Figure 101 (continued). AS4/2220-1 Graphite Epoxy Unidirectional Composite, 100°C, Dry (ETD); 27.4 MPa (4 ksi) Longitudinal Shear Applied Stress.

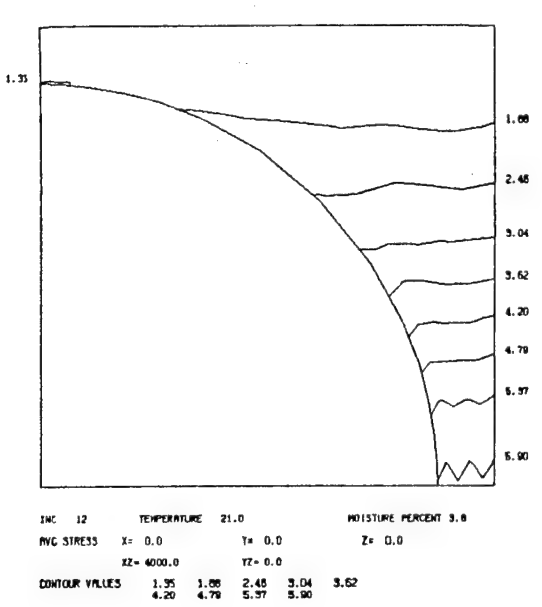


a) Octahedral Shear Stress (ksi)

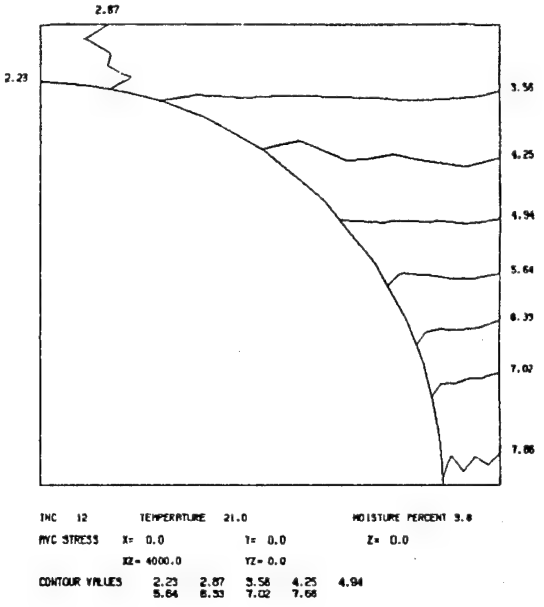


b) Maximum Principal Stress (ksi)

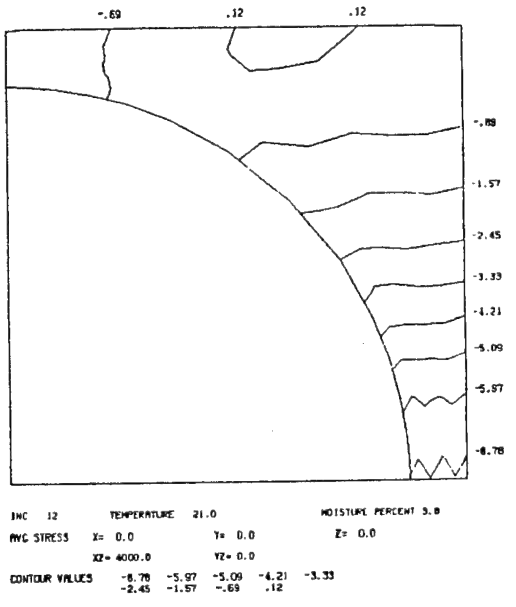


c) Minimum Principal Stress (ksi)

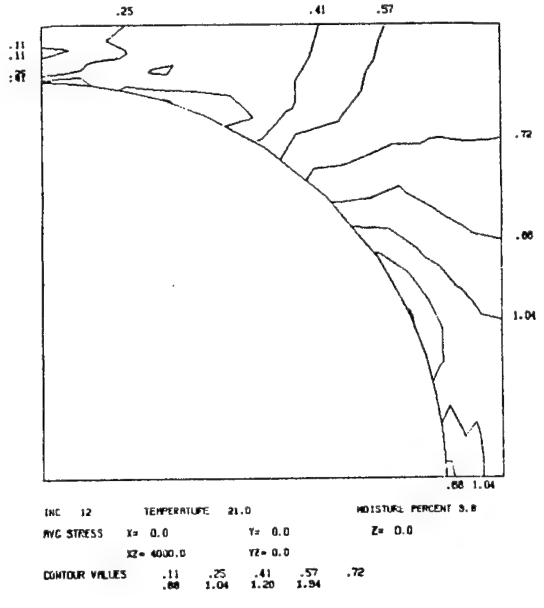


d) Intermediate Principal Stress (ksi)

Figure 102. AS4/2220-1 Graphite/Epoxy Unidirectional Composite, Room Temperature, 3.8 Percent Moisture (RTW); 27.4 MPa (4 ksi) Longitudinal Shear Applied Stress.

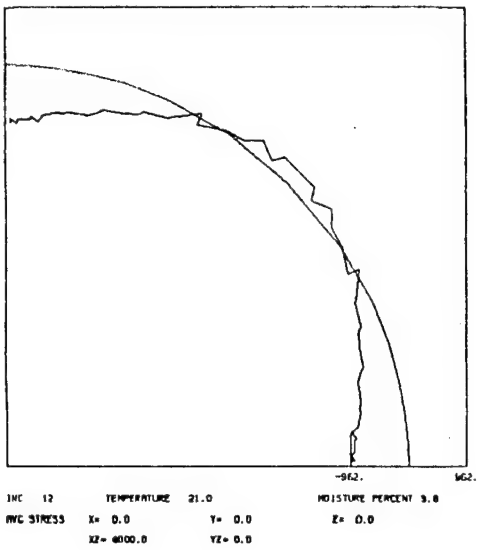


e) Interface Normal Stress (psi)

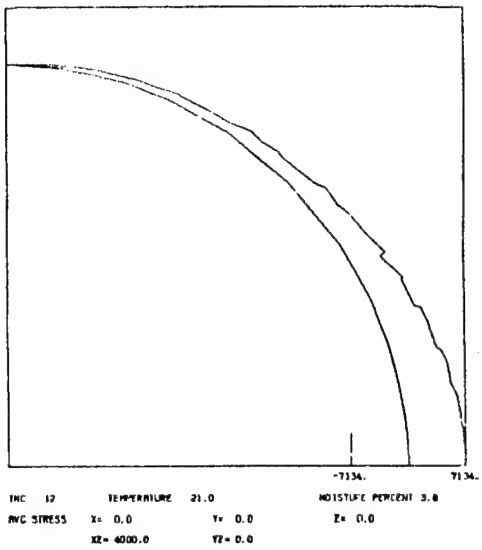


f) Interface Shear Stress (psi)

Figure 102 (continued). AS4/2220-1 Graphite/Epoxy Unidirectional Composite, Room Temperature, 3.8 Percent Moisture (RTW); 27.4 MPa (4 ksi) Longitudinal Shear Applied Stress.

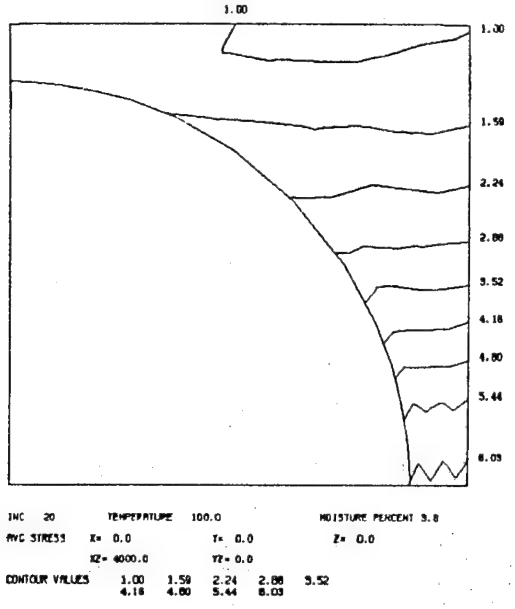


a) Octahedral Shear Stress (ksi)

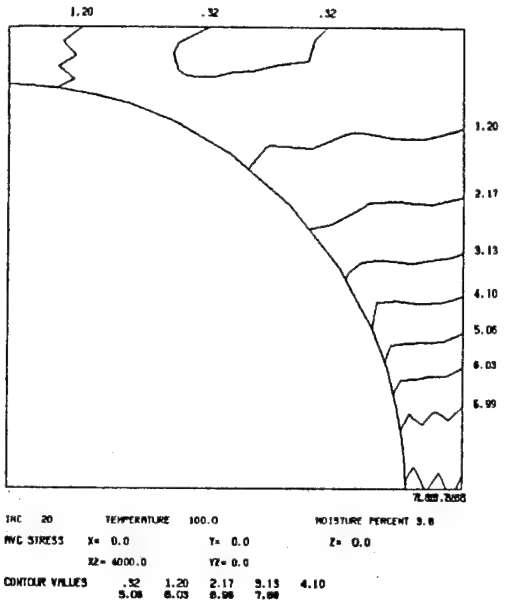


b) Maximum Principal Stress (ksi)

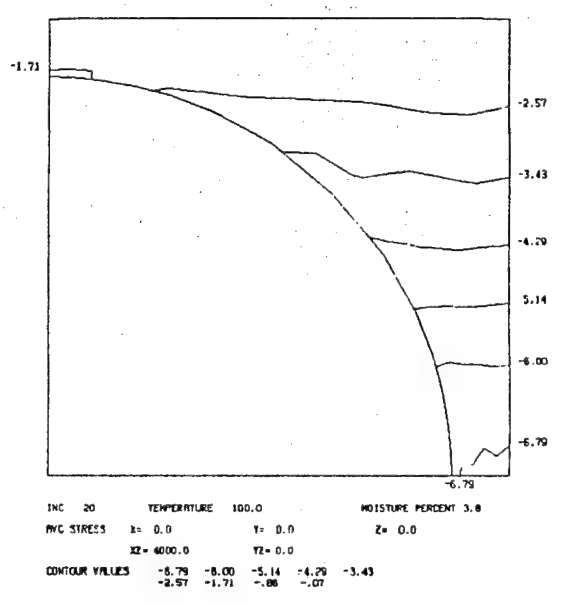


c) Minimum Principal Stress (ksi)

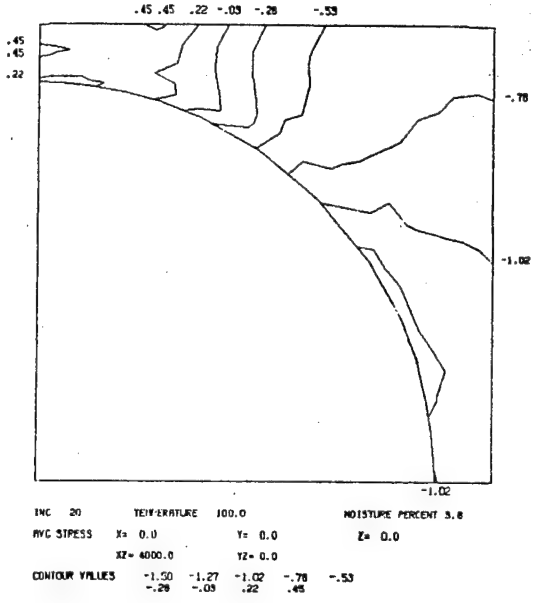


d) Intermediate Principal Stress (ksi)

Figure 103. AS4/2220-1 Graphite/Epoxy Unidirectional Composite, 100°C, 3.8 Percent Moisture (ETW); 27.4 MPa (4 ksi) Longitudinal Shear Applied Stress.

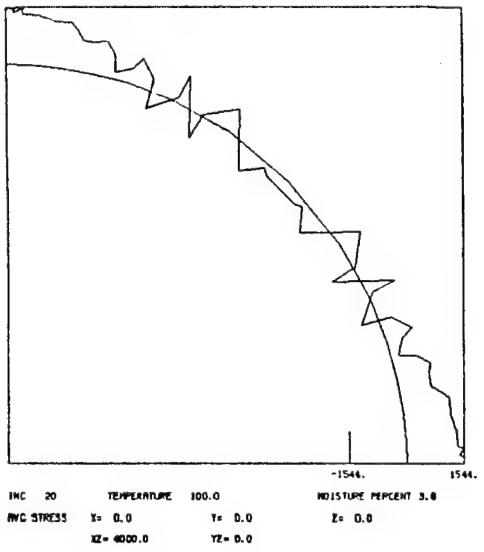


e) Interface Normal Stress (psi)

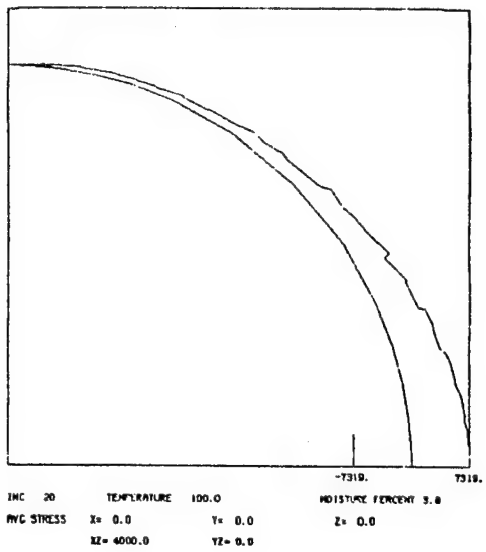


f) Interface Shear Stress (psi)

Figure 103 (continued). AS4/2220-1 Graphite/Epoxy Unidirectional Composite, 100°C, 3.8 Percent Moisture (ETW); 27.4 MPa (4 ksi) Longitudinal Shear Applied Stress.

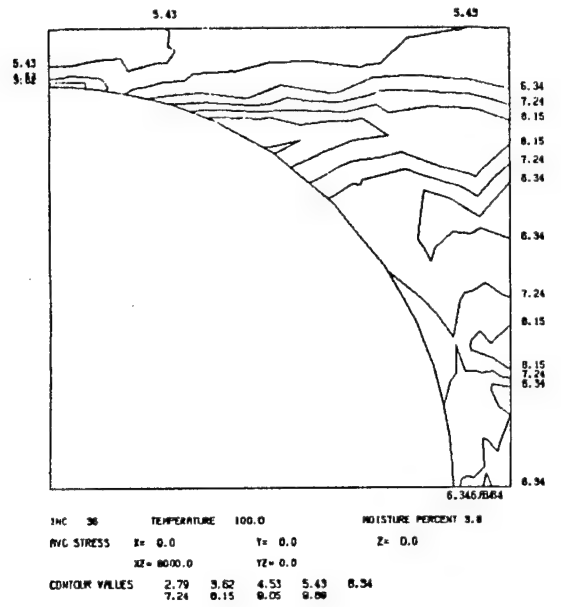


a) Octahedral Shear Stress (ksi)

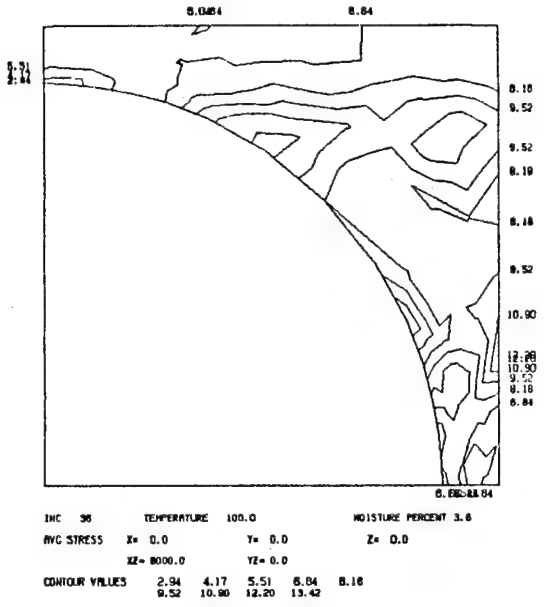


b) Maximum Principal Stress (ksi)

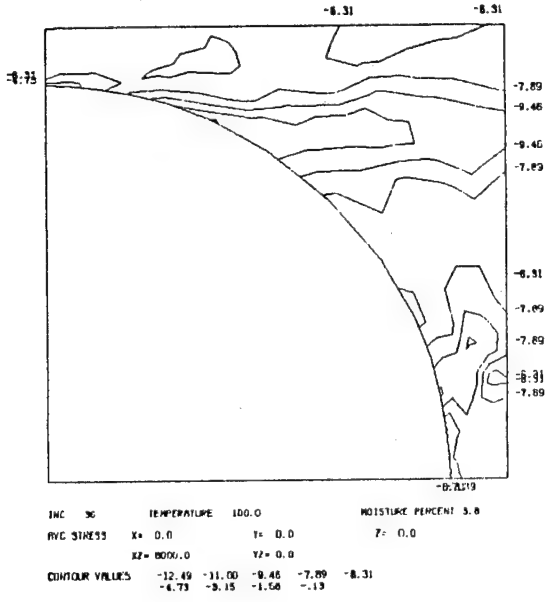


c) Minimum Principal Stress (ksi)

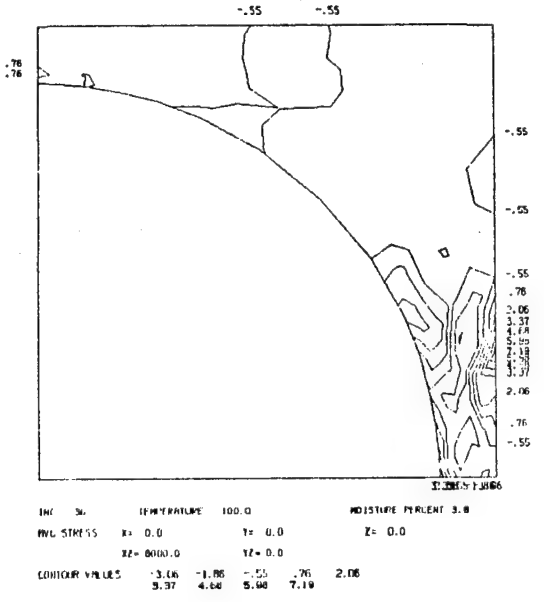


d) Intermediate Principal Stress (ksi)

Figure 104. AS4/2220-1 Graphite/Epoxy Unidirectional Composite, 100°C, 3.8 Percent Moisture (ETW); 55.2 MPa (8 ksi) Longitudinal Shear Applied Stress.

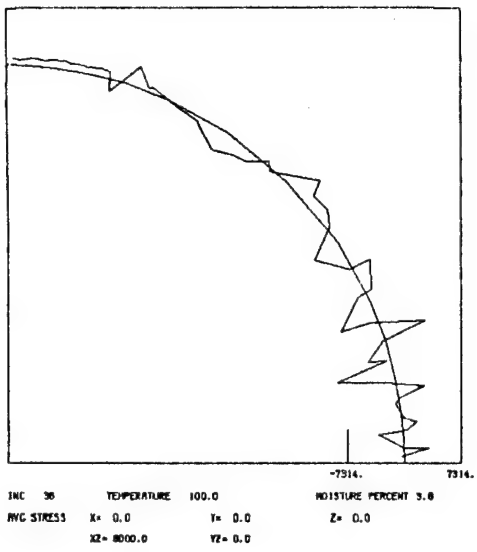


e) Interface Normal Stress (psi)

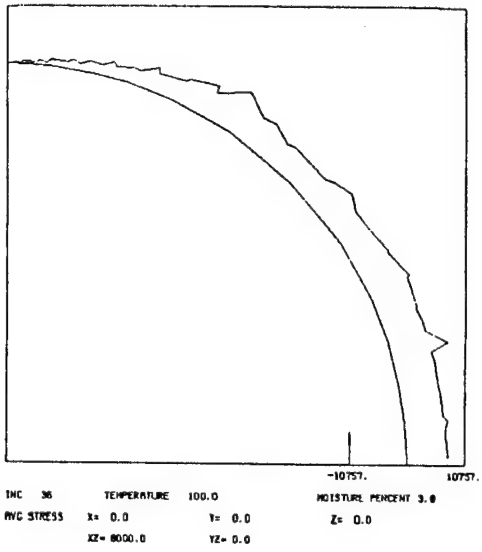


f) Interface Shear Stress (psi)

Figure 104 (continued). AS4/2220-1 Graphite/Epoxy Unidirectional Composite, 100°C, 3.8 Percent Moisture (ETW); 55.2 MPa (8 ksi) Longitudinal Shear Applied Stress.

is further indicated by the significant increase in the third principal stress (compare Figure 104d to Figure 103d).

While the somewhat extensive results and discussion presented here for the AS4/2220-1 unidirectional composite system may appear to be very detailed, much more can and should still be done studying trends. This work will best await the availability of actual unidirectional composite data to compare predictions to. These correlations will be performed in a subsequent effort.

In the following Sections 5.4.2. through 5.4.4, the same data for the 3502, 2220-3, and 914 matrix systems will be presented, but without detailed discussion. In Section 5.5, relative comparisons of the predictions for all four matrix systems in a unidirectional AS4 graphite fiber-reinforced composite will be presented and discussed.

5.4.2 AS4/3502 Unidirectional Composite

Hercules 3502 untoughened epoxy matrix was considered the baseline system in this study. The unidirectional composite stress-strain curves are presented here; plots of internal stress states are presented in Appendix E1 of Volume II.

Figure 105 presents the predicted unidirectional AS4/3502 composite axial tensile stress-strain response for each of the four environmental conditions. As previously observed for the AS/2220-1 system (see Figure 87), axial loading response is dominated by the fiber. Hence, the composite stress-strain response at all four environmental conditions is essentially the same. However, the internal stress states are not, as indicated in Figures E5 through E9 of Appendix E1 of Volume II.

The transverse tensile stress-strain plots are shown in Figure 106. There is only a slight decrease in modulus with increasinly severe

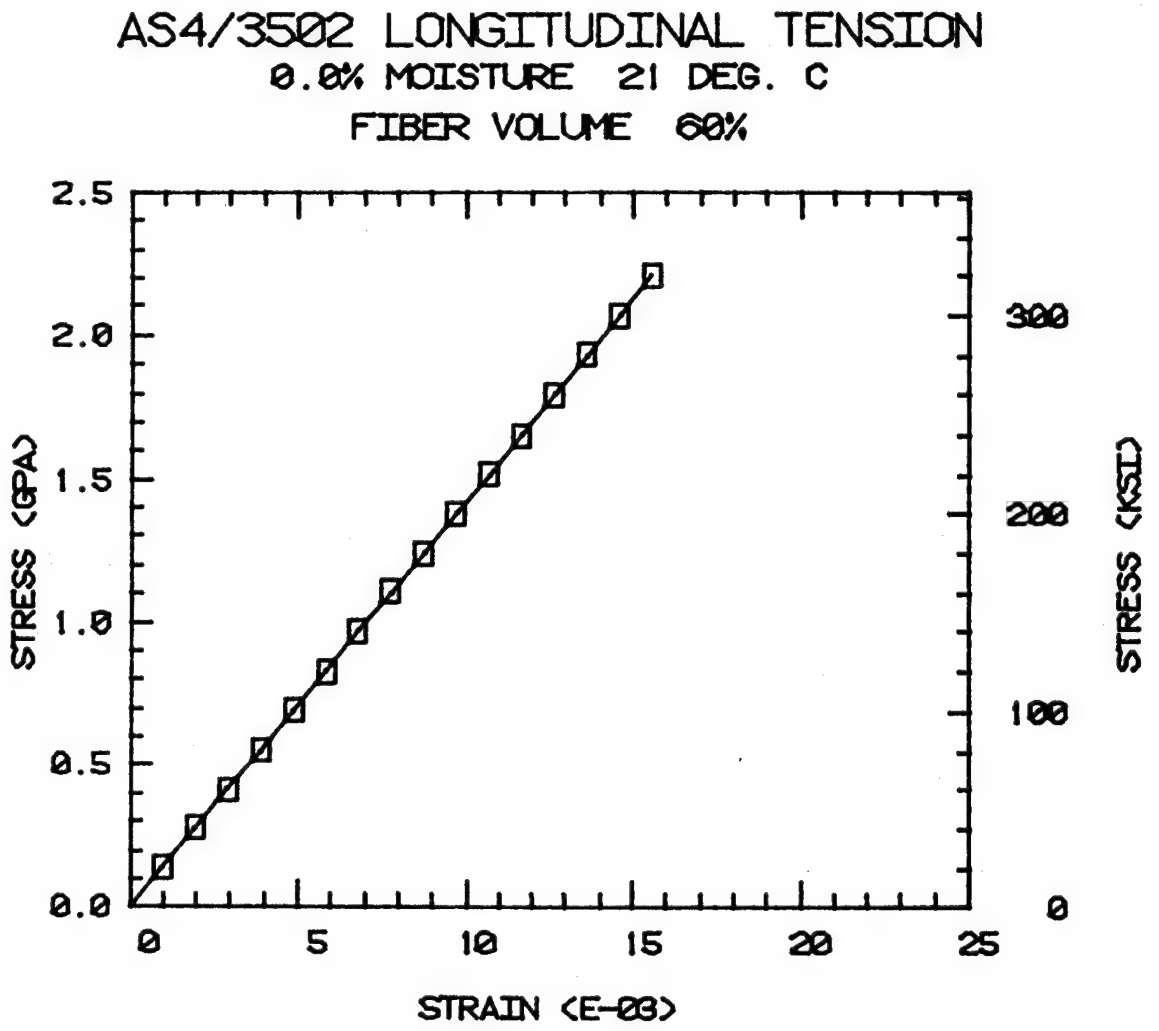


a) Room Temperature, Dry (RTD)

Figure 105. AS4/3502 Graphite/Epoxy Unidirectional Composite, Longitudinal Tensile Stress-Strain Response.

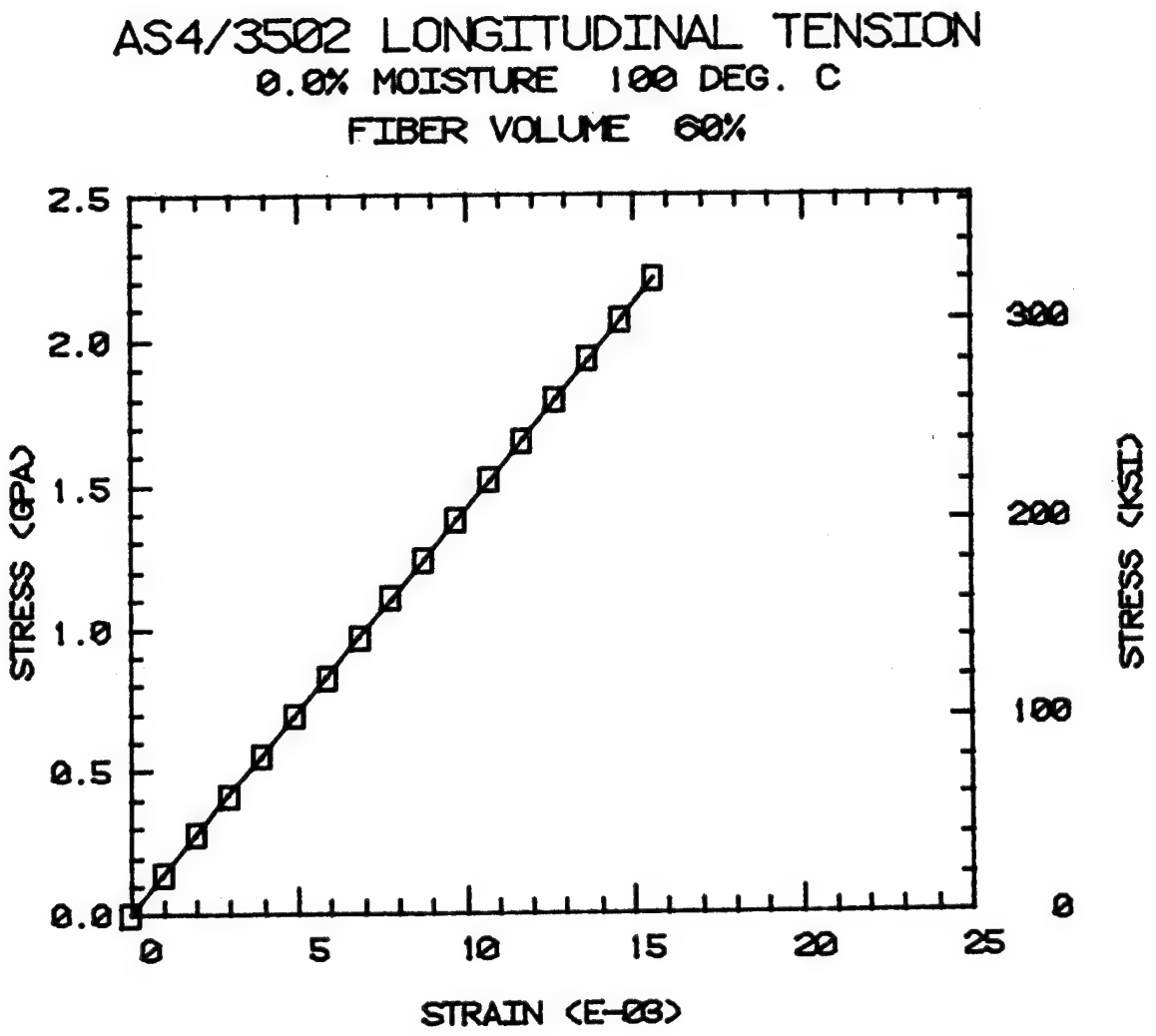


b) Elevated Temperature (100°C), Dry (ETD)

Figure 105 (continued). AS4/3502 Graphite/Epoxy Unidirectional Composite, Longitudinal Tensile Stress-Strain Response.

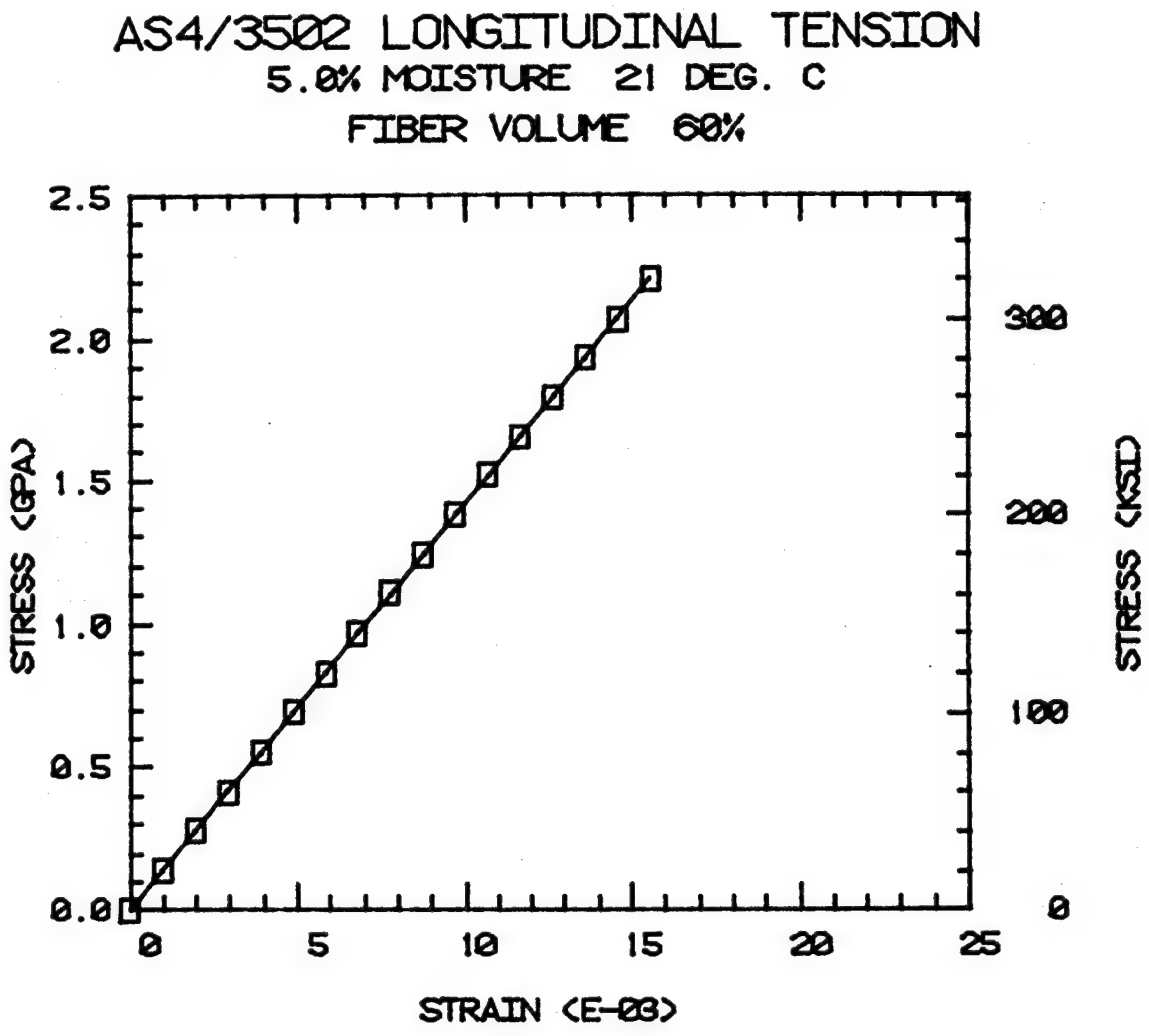


c) Room Temperature, 5.0 Percent Moisture (RTW)

Figure 105 (continued). AS4/3502 Graphite/Epoxy Unidirectional Composite, Longitudinal Tensile Stress-Strain Response.

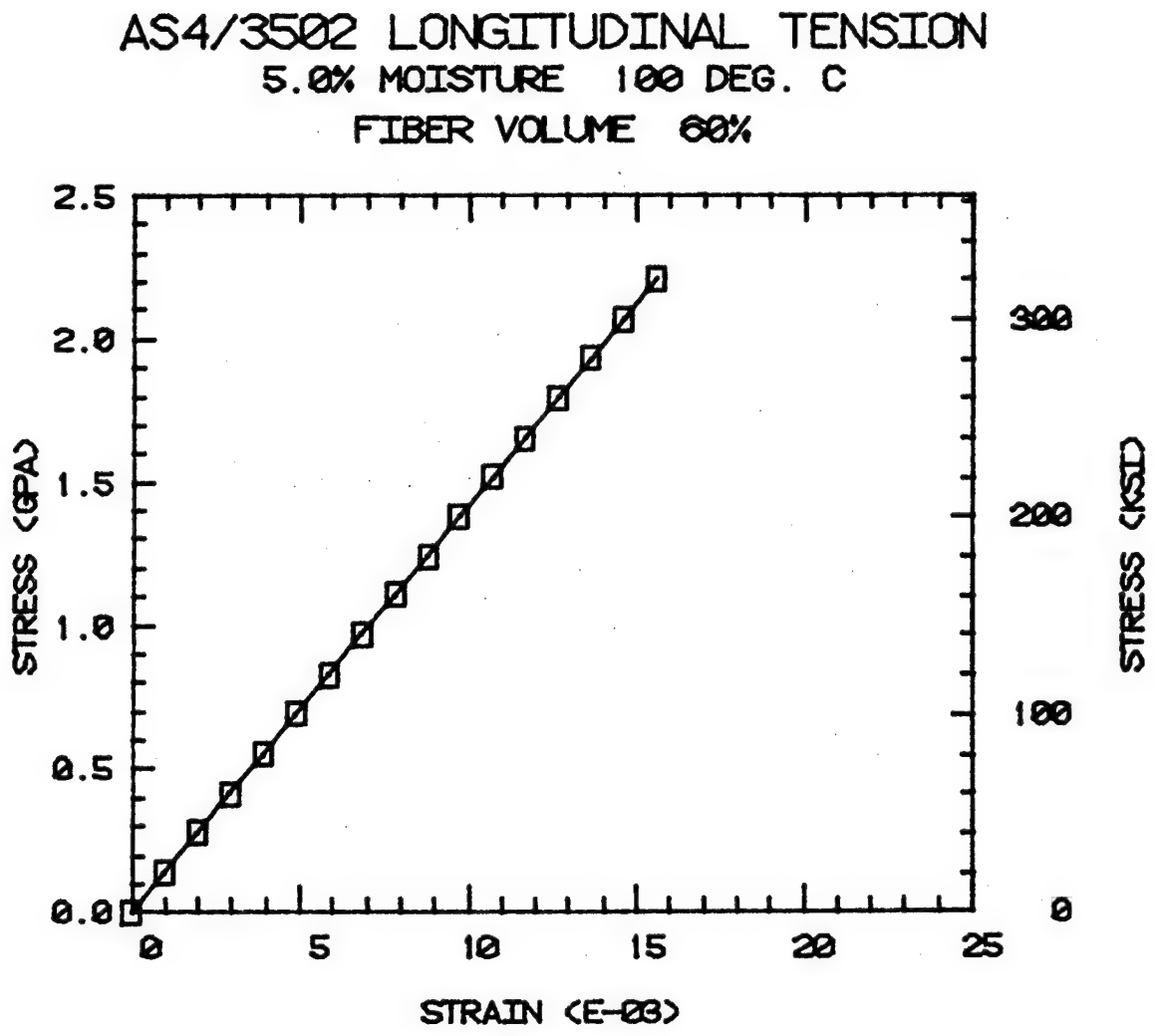


d) Elevated Temperature (100°C), 5.0 Percent Moisture (ETW)

Figure 105 (continued). AS4/3502 Graphite/Epoxy Unidirectional Composite, Longitudinal Tensile Stress-Strain Response.

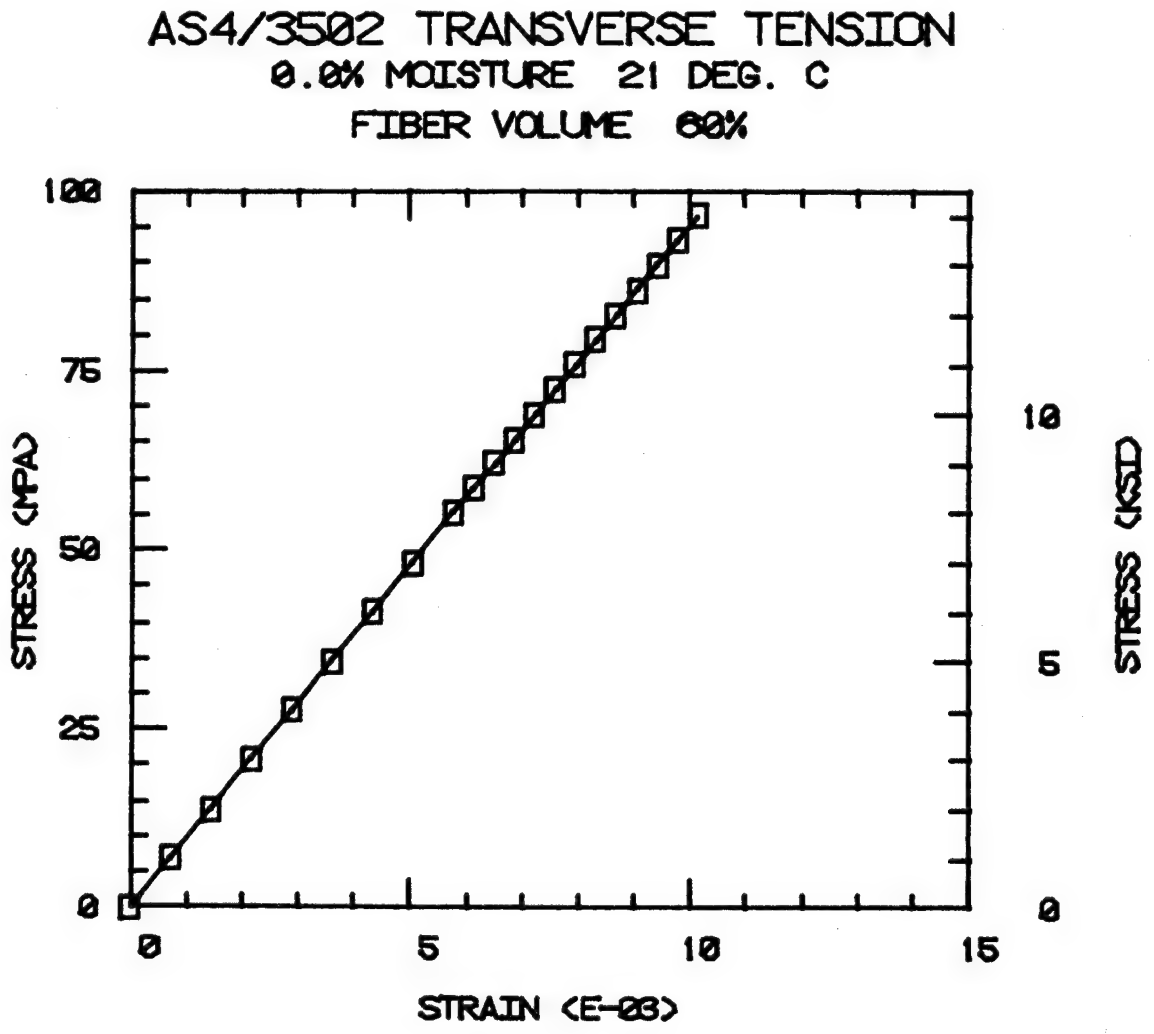


a) Room Temperature, Dry (RTD)

Figure 106. AS4/3502 Graphite/Epoxy Unidirectional Composite, Transverse Tensile Stress-Strain Response.

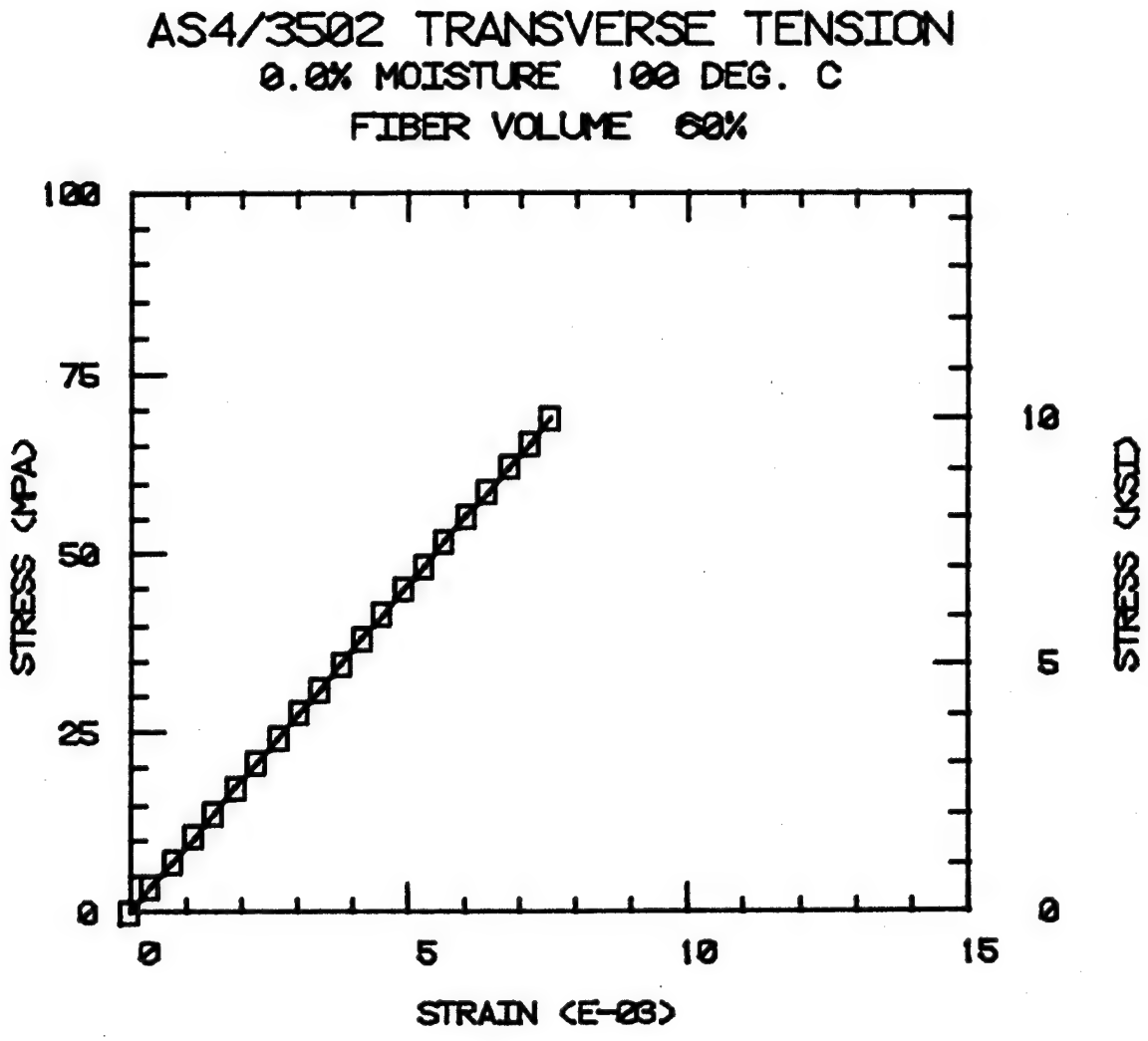


b) Elevated Temperature (100°C), Dry (ETD)

Figure 106 (continued). AS4/3502 Graphite/Epoxy Unidirectional Composite, Transverse Tensile Stress-Strain Response.

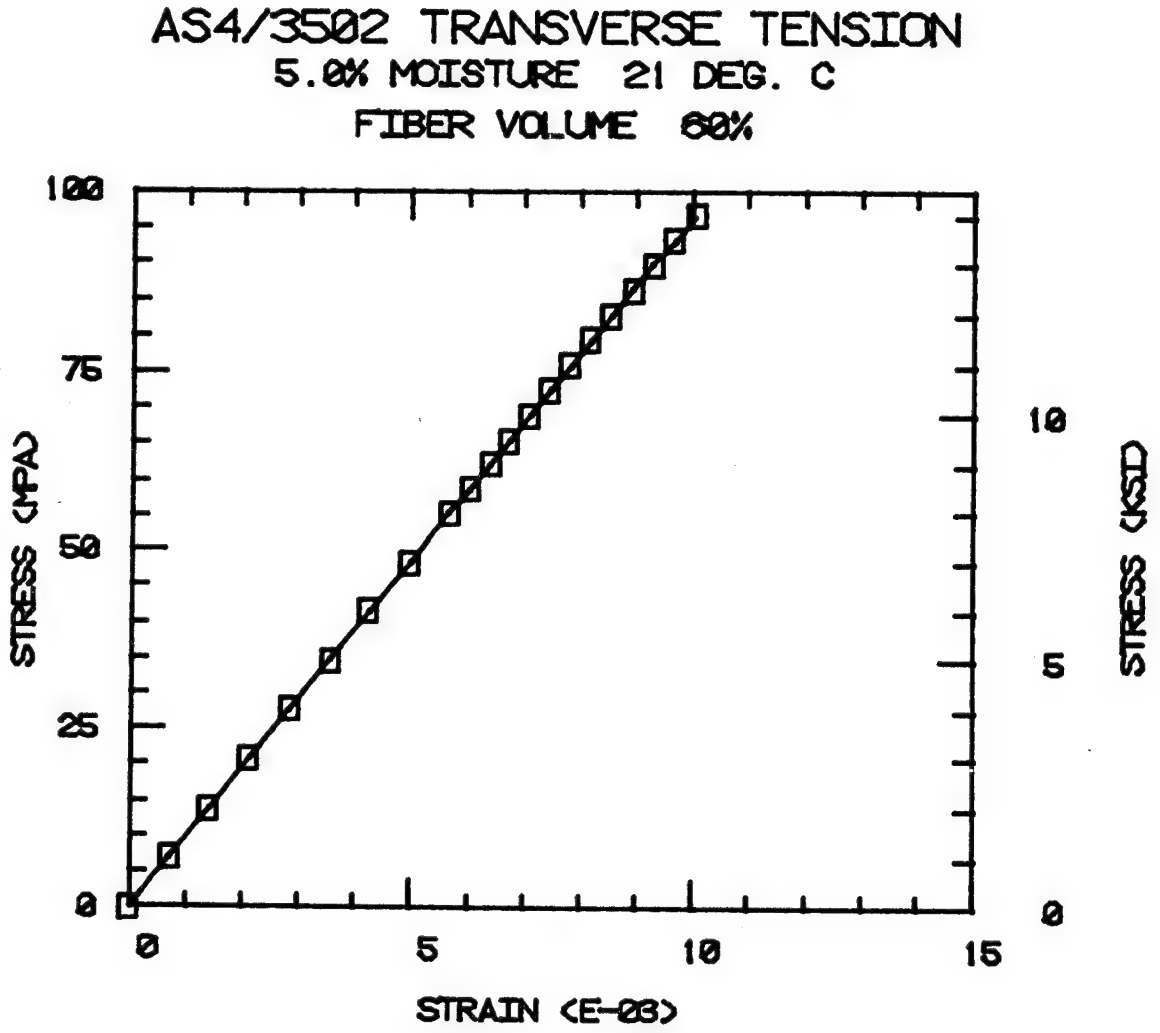


c) Room Temperature, 5.0 Percent Moisture (RTW)

Figure 106 (continued). AS4/3502 Graphite/Epoxy Unidirectional Composite, Transverse Tensile Stress-Strain Response.

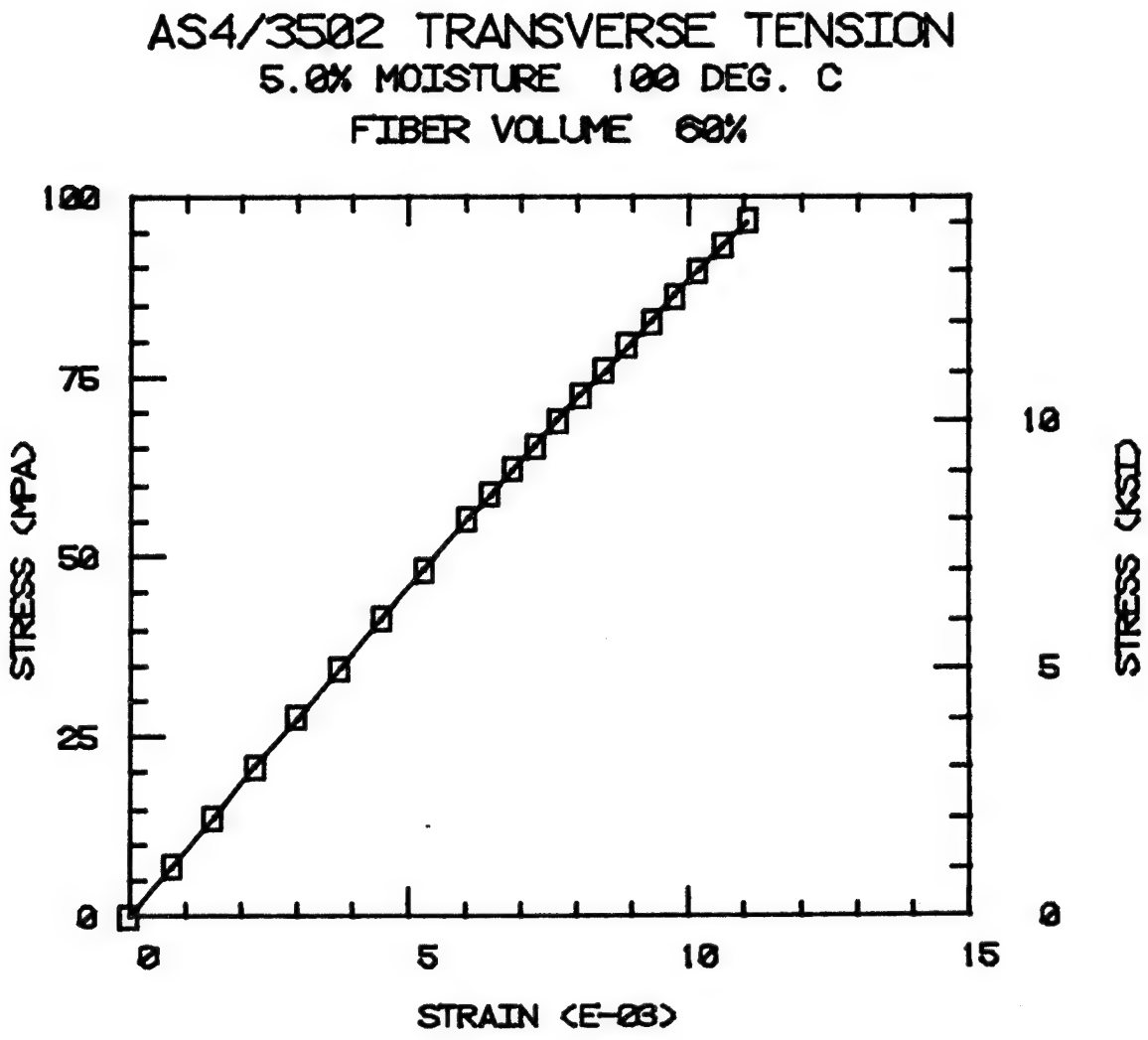


d) Elevated Temperature (100°C), 5.0 Percent Moisture (ETW)

Figure 106 (continued). AS4/3502 Graphite/Epoxy Unidirectional Composite, Transverse Tensile Stress-Strain Response.

environmental conditioning, as a comparison of the four plots of Figure 106 indicates. The degree of nonlinearity is also not pronounced, even up to the artificially high applied stress levels. The corresponding internal stress states are shown in Figures E10 through E14 of Appendix E1 of Volume II. In addition to the plots for the baseline comparison load level of 27.6 MPa (4 ksi), the stress states at the highest applied stress indicated in Figure 106d for the ETW condition are also included (Appendix Figure E14). This environmental condition maximizes the inelastic response effects, although they are very slight for the 3502 matrix material (see, for example, Figure 64b).

Longitudinal shear stress-shear strain plots for the AS4/3502 unidirectional composite system are given in Figure 107 for all four environmental conditions. Considerable nonlinearity is exhibited at all conditions, but it must be kept in mind that the failure stresses in actual composites would be somewhat lower than the levels indicated in Figure 106. For example, the 3502 matrix itself has a shear strength of only 41 to 69 MPa (6 to 10 ksi), depending on the environmental condition (see Figure 64b). Thus, the degree of nonlinearity exhibited in Figure 107 would not be exhibited in actual experimental data; the composite would be expected to fail at lower stress levels. The predicted internal stress states are included in Figures E15 through E19 of Appendix E1 of Volume II.

### 5.4.3 AS4/2220-3 Unidirectional Composite

The Hercules 2220-3 toughened epoxy exhibited properties very similar to the 2220-1 system (e.g., compare Figures 65 and 66). One significant difference, however, was the experimentally measured coefficient of moisture expansion. The 2220-1 system was measured as

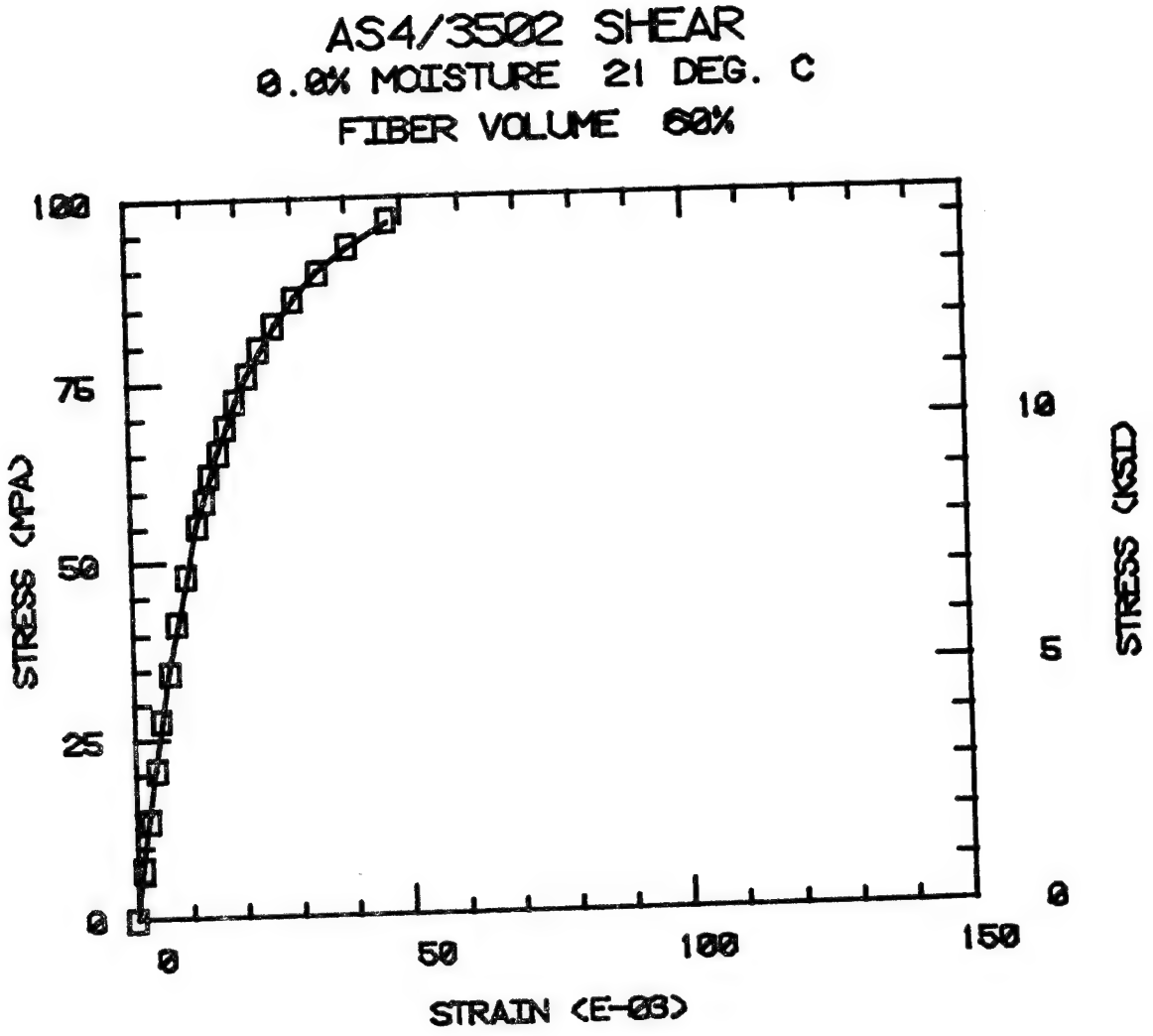


a) Room Temperature, Dry (RTD)

Figure 107. AS4/3502 Graphite/Epoxy Unidirectional Composite, Longitudinal Shear Stress-Strain Response.

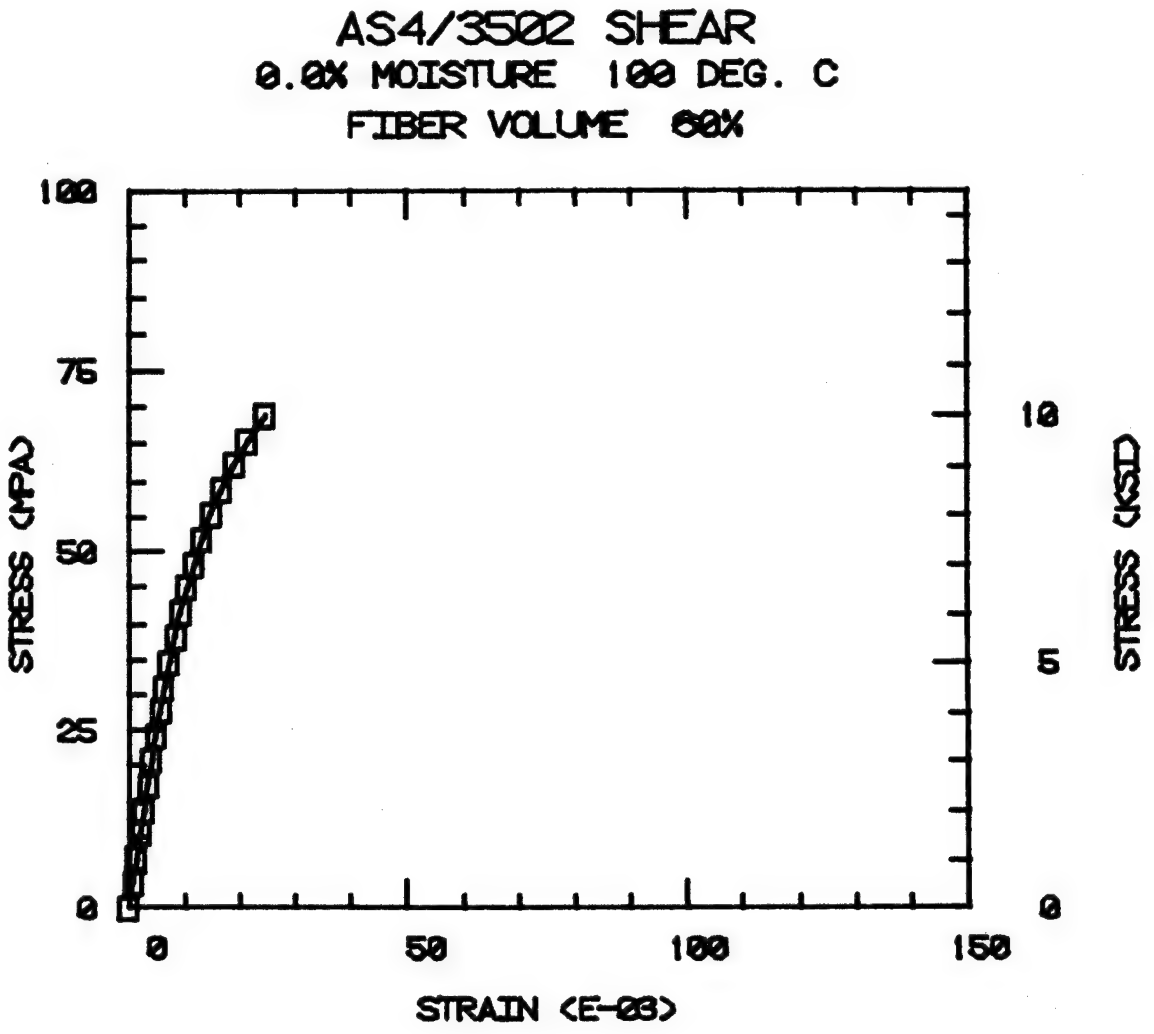


b) Elevated Temperature (100°C), Dry (ETD)

Figure 107 (continued). AS4/3502 Graphite/Epoxy Unidirectional Composite, Longitudinal Shear Stress-Strain Response.

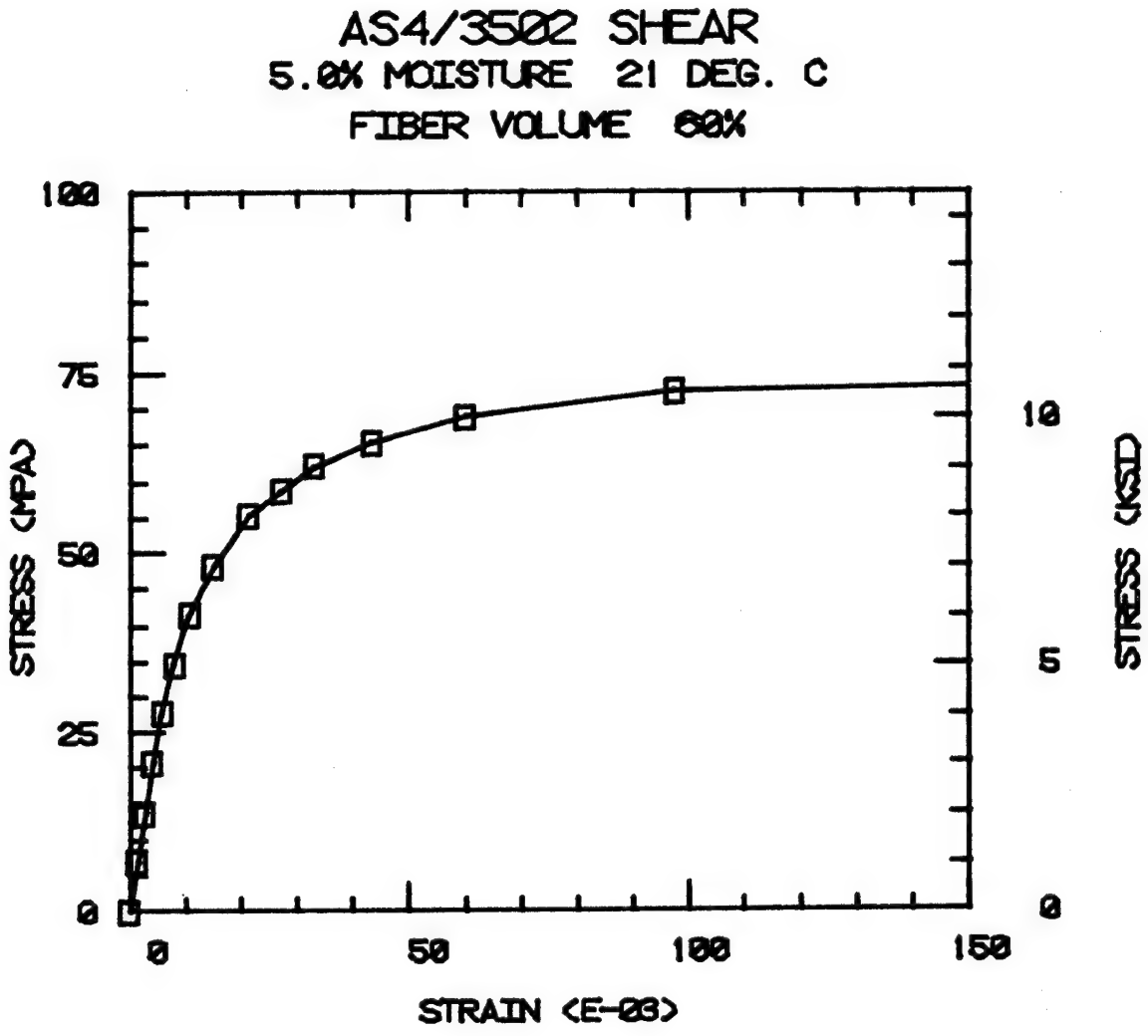


c) Room Temperature, 5.0 Percent Moisture (RTW)

Figure 107 (continued). AS4/3502 Graphite/Epoxy Unidirectional Composite, Longitudinal Shear Stress-Strain Response.

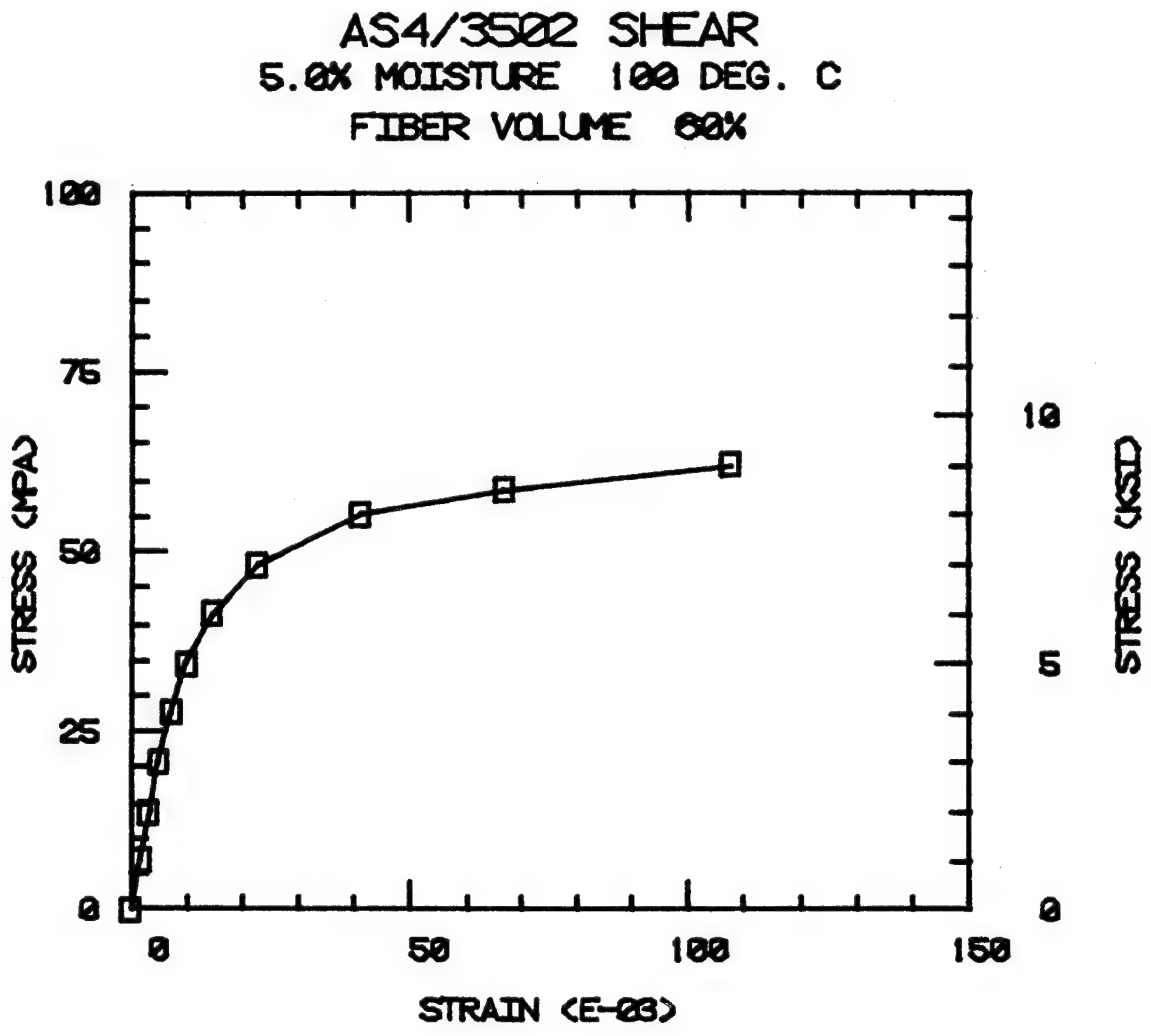


d) Elevated Temperature (100°C), 5.0 Percent Moisture (ETW)

Figure 107 (continued). AS4/3502 Graphite/Epoxy Unidirectional Composite, Longitudinal Shear Stress-Strain Response.

$1.547 \times 10^{-3}$ per weight percent moisture absorption (i.e., per %M), while the 2220-3 value was $2.499 \times 10^{-3}$/%M. These two values bounded those measured for the 3502 and 914 systems (see Table 4 of Section 3). At present it is not known with certainty that these values are correct. Further moisture expansion testing should be conducted to verify these values. Experimental data are not yet available for correlation purposes. However, the present comparisons between the predicted AS4/2220-1 and AS4/2220-3 unidirectional composite systems can be very useful in demonstrating the influence of matrix coefficient of moisture expansion, since all other parameters are very similar for these two systems.

The internal stress states due to the thermal- and moisture-induced preconditionings are indicated in Figures E20 through E23 of Appendix E2 of Volume II. By comparing these results with those of Figures 83 through 85 for the AS4/2220-1 composite, it will be noted that there are significant differences in the thermal stress states (i.e., in the RTD and ETD values). These results are not influenced by differences in the matrix moisture expansion coefficient values. While the gross response of the 2220-1 and 2220-3 systems appears to be very similar (Figure 65 versus Figure 66), there actually are definite differences (in addition to the coefficient of moisture expansion) which influence the local stress states and hence composite strength.

Longitudinal tensile stress-strain curves for the AS4/2220-3 unidirectional composite predicted by the micromechanics analysis for all four environmental conditions are given in Figure 108. Matrix or environment has little influence on this fiber-dominated response for any of the matrix systems. The corresponding internal stress states are

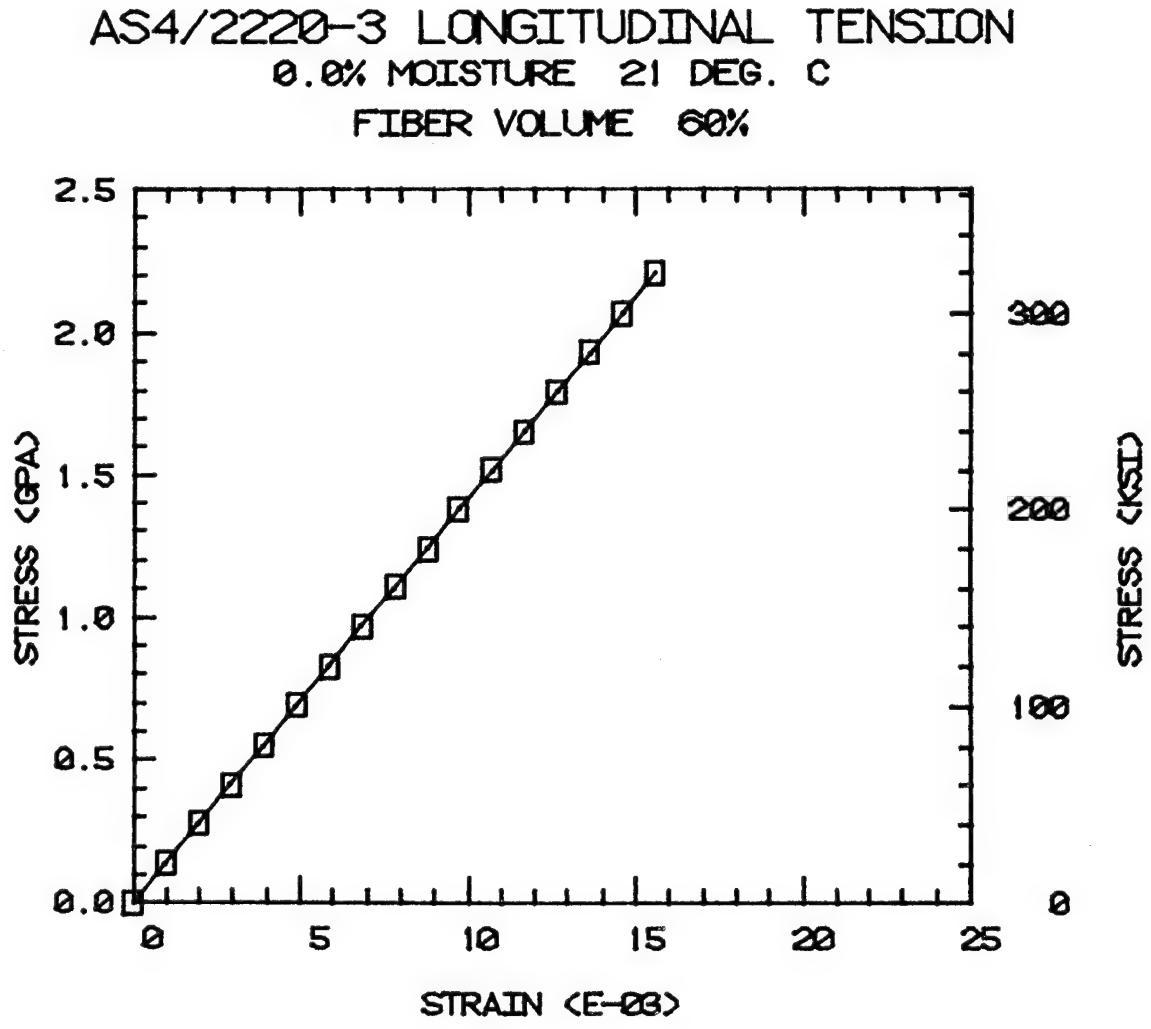


a) Room Temperature, Dry (RTD)

Figure 108. AS4/2220-3 Graphite/Epoxy Unidirectional Composite, Longitudinal Tensile Stress-Strain Response.

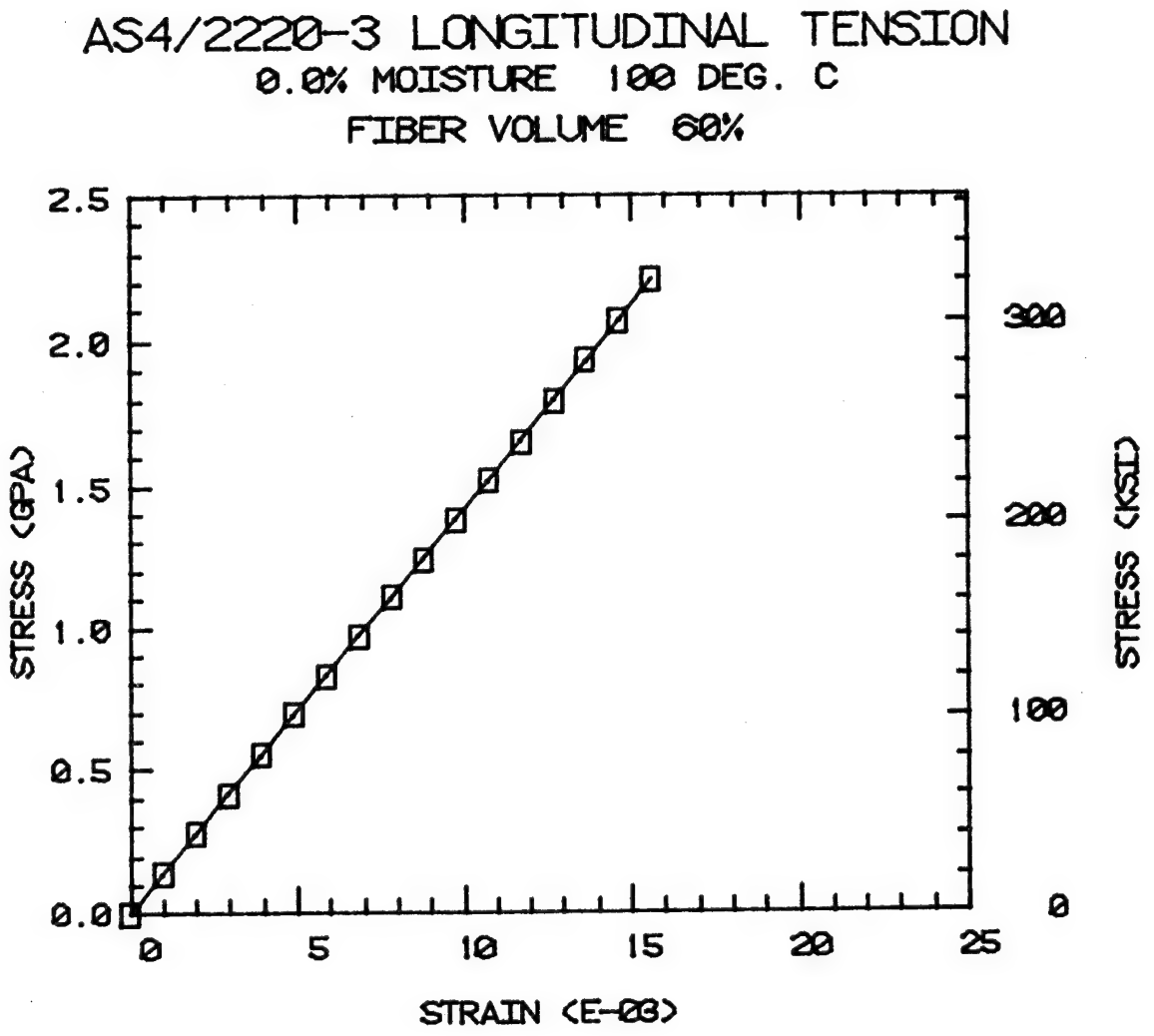


b) Elevated Temperatures (100°C), Dry (ETD)

Figure 108 (continued). AS4/2220-3 Graphite/Epoxy Unidirectional Composite, Longitudinal Tensile Stress-Strain Response.

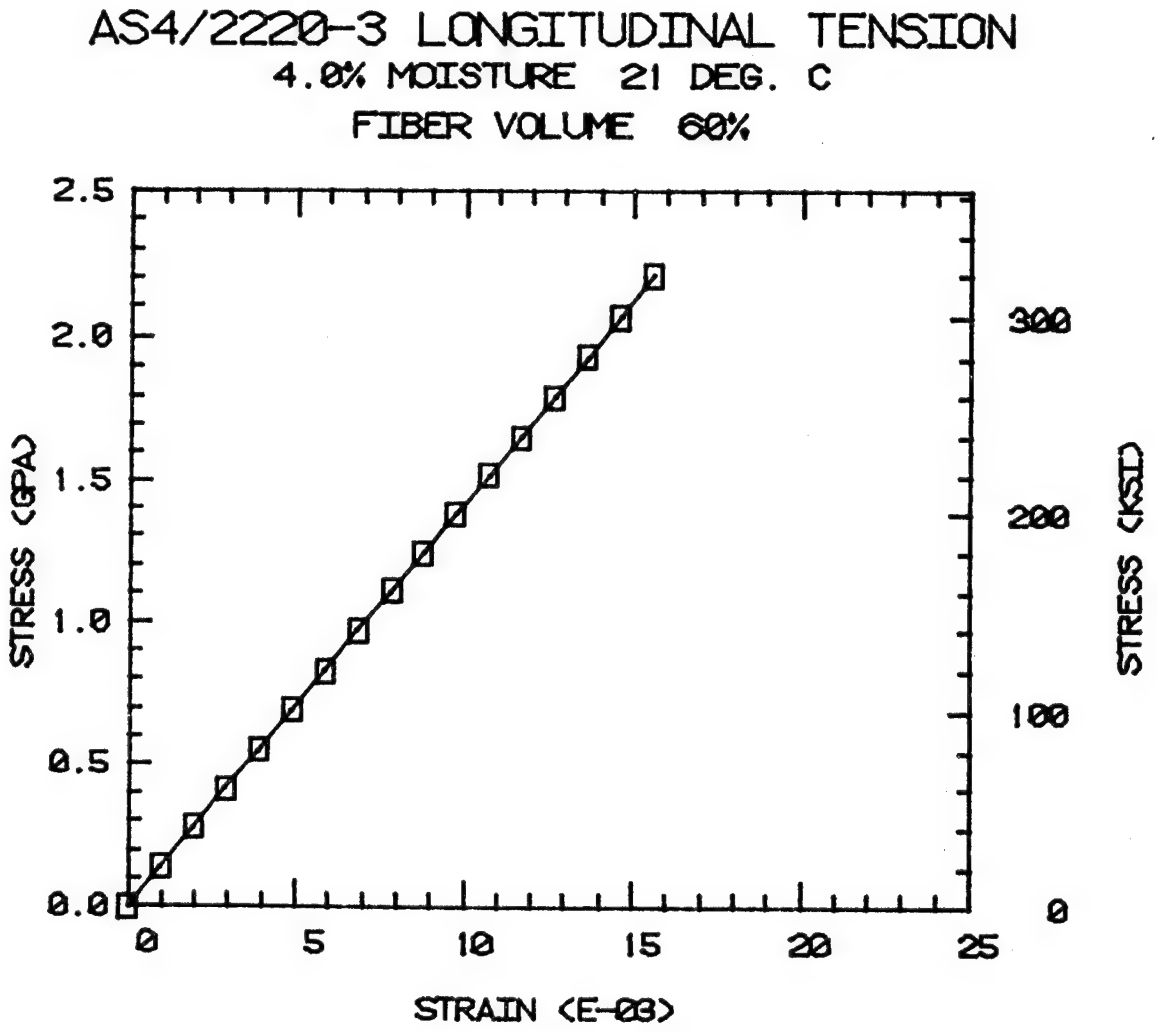


c) Room Temperature, 4.0 Percent Moisture (RTW)

Figure 108 (continued). AS4/2220-3 Graphite/Epoxy Unidirectional Composite, Longitudinal Tensile Stress-Strain Response.

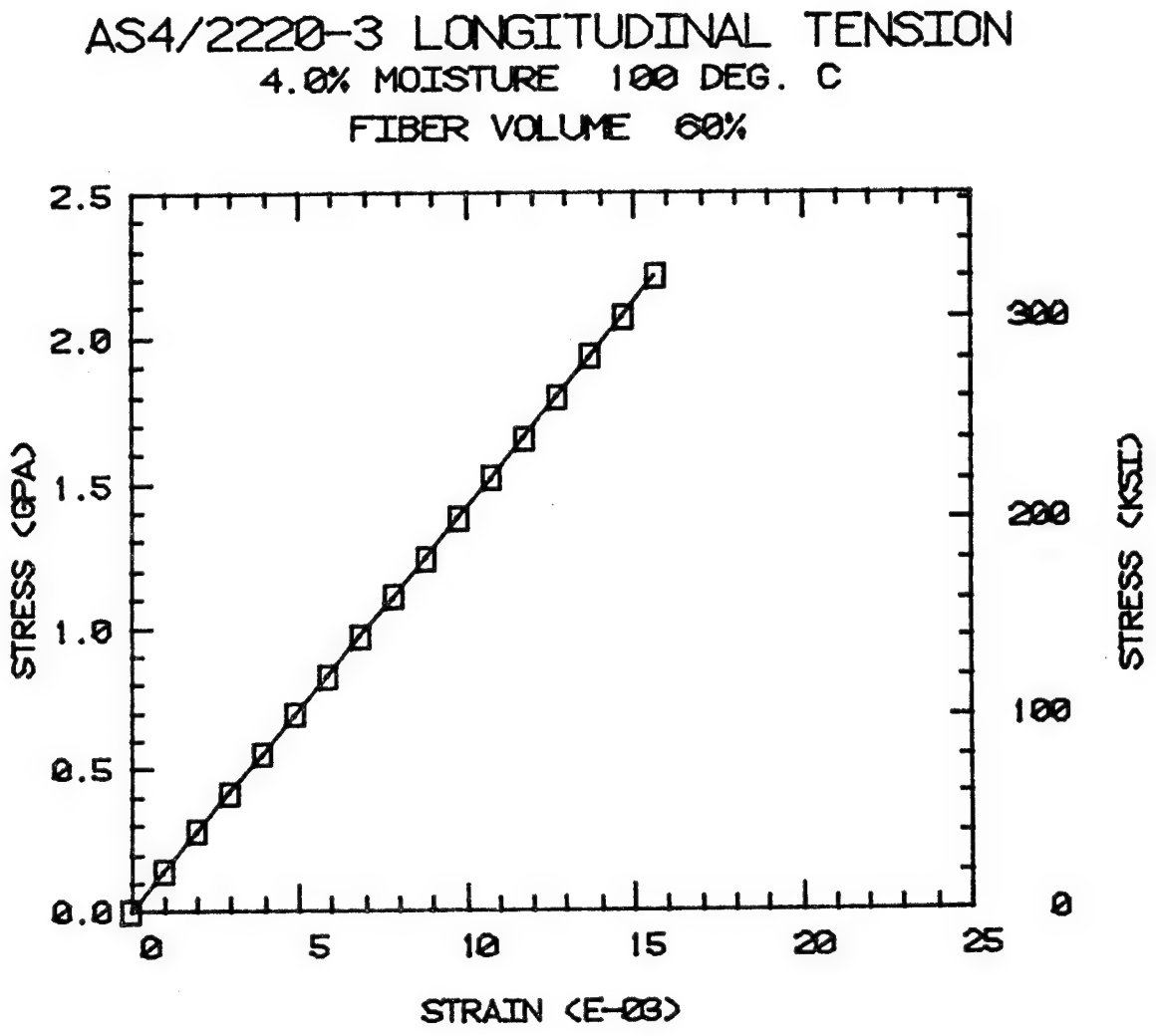


d) Elevated Temperature (100°C), 4.0 Percent Moisture (ETW)

Figure 108 (continued). AS4/2220-3 Graphite/Epoxy Unidirectional Composite, Longitudinal Tensile Stress-Strain Response.

shown in Figures E24 through E28 of Appendix E2 of Volume II. Here the differences between dry and wet conditions are significant because of the large value of matrix coefficient of moisture expansion.

The transverse tensile stress-strain responses of the AS4/2220-3 unidirectional composite is presented in Figure 109 for each of the four environmental conditions. The corresponding internal stress states are plotted in Figures E29 through E33 of Appendix E2 of Volume II. As indicated in Figure 109, the AS4/2220-3 composite exhibits only a slight degree of stress-strain nonlinearity even at the most severe environmental condition, i.e., ETW.

Longitudinal shear stress-shear strain curves are plotted in Figure 110, for all four environmental conditions. The nonlinearity is significant, even at the RTD conditions. The extent of inelastic deformation at the local level is indicated in the micromechanics plots of Figures E34 through E38 of Appendix E2 of Volume II.

5.4.4 AS4/914 Unidirectional Composite

The Fibredux 914 toughened epoxy matrix exhibited properties similar to those of the untoughened Hercules 3502 (compare Figure 67 to Figure 64). However, there was a significant difference in the measured coefficients of thermal expansion in the dry condition (see Table 3 of Section 3). The 914 system was similar in this property to the two 2220 systems. However, at the moisture-saturated condition this difference disappeared. Since a high degree of confidence in the present thermal expansion measurements exists, particularly in the dry condition, this response appears to be real, although unexpected.

This large difference in coefficient of thermal expansion between the 914 system and the 3502 system guarantees large differences in

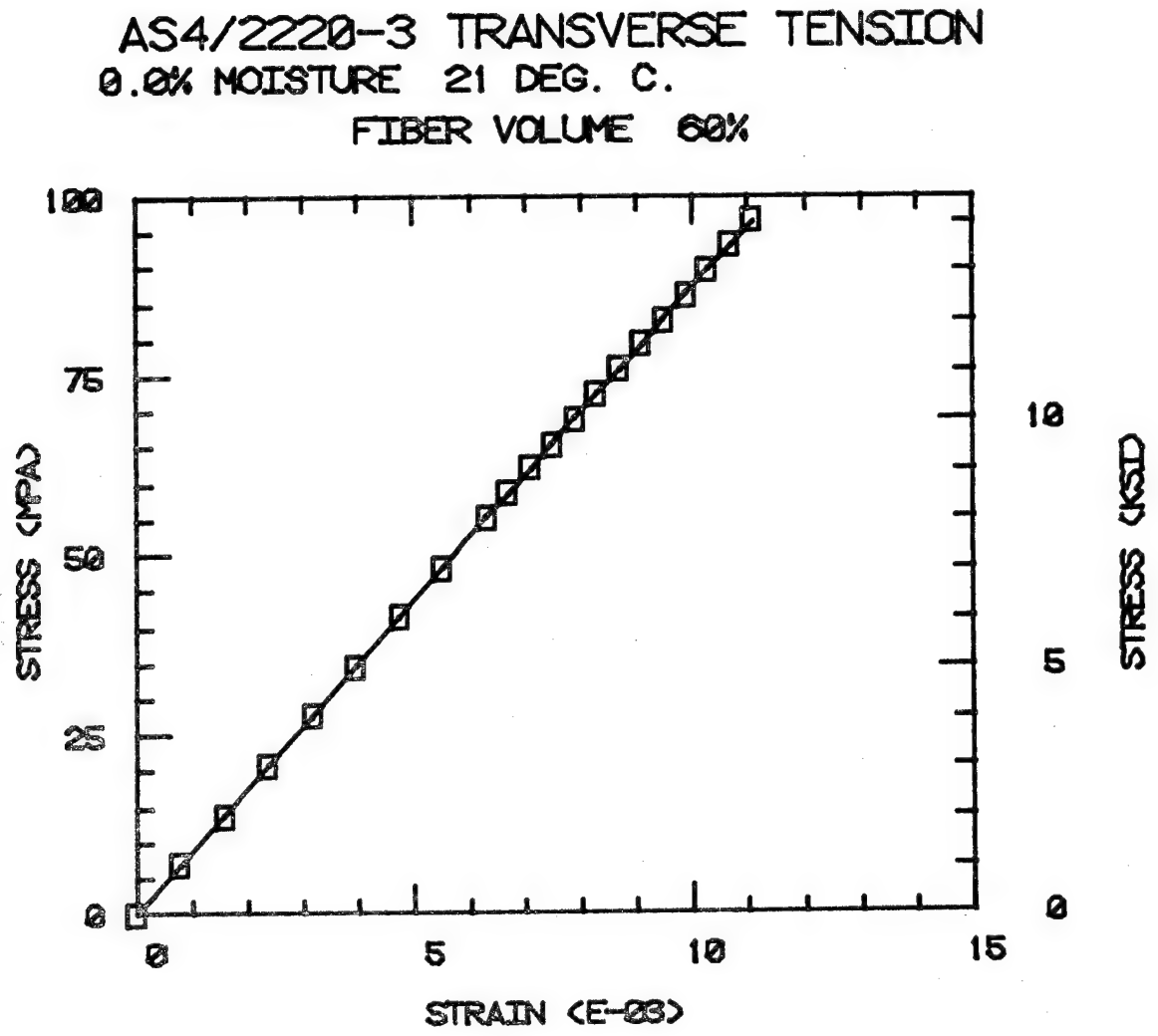


a) Room Temperature, Dry (RTD)

Figure 109. AS4/2220-3 Graphite/Epoxy Unidirectional Composite Transverse Tensile Stress-Strain Response.

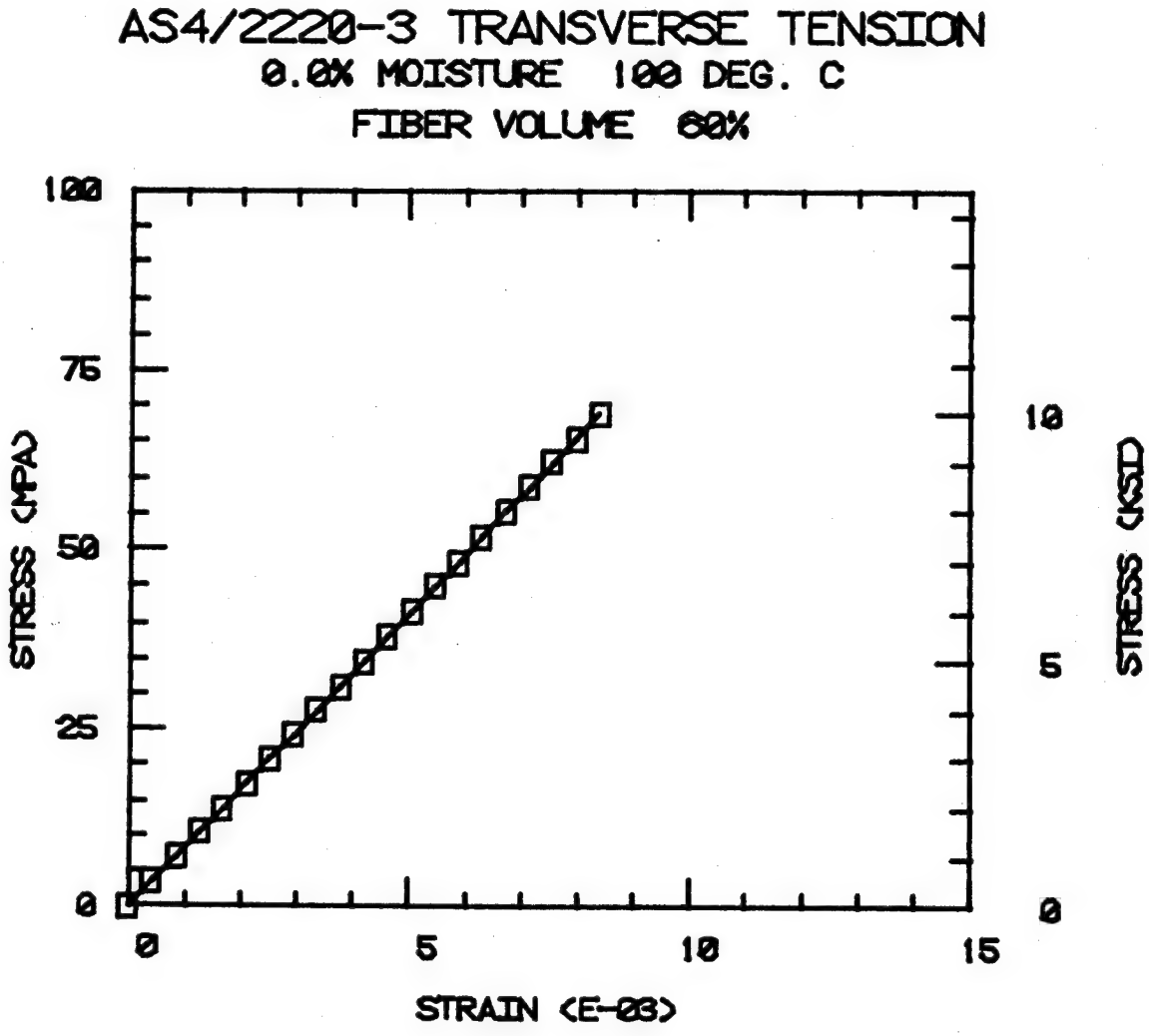


b) Elevated Temperature (100°C), Dry (ETD)

Figure 109 (continued). AS4/2220-3 Graphite/Epoxy Unidirectional Composite Transverse Tensile Stress-Strain Response.

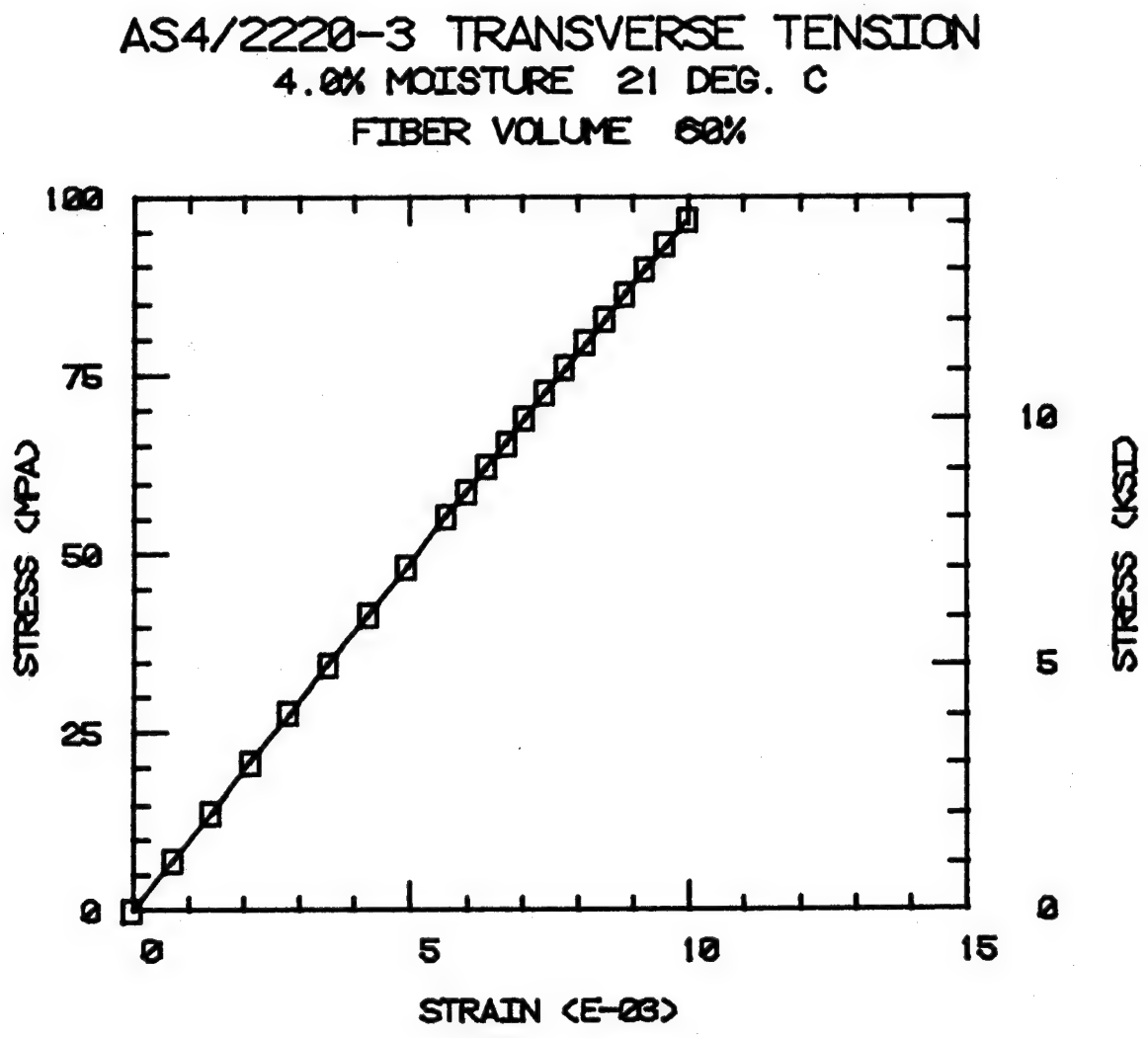


c) Room Temperature, 4.0 Percent Moisture (RTW)

Figure 109 (continued). AS4/2220-3 Graphite/Epoxy Unidirectional Composite Transverse Tensile Stress-Strain Response.

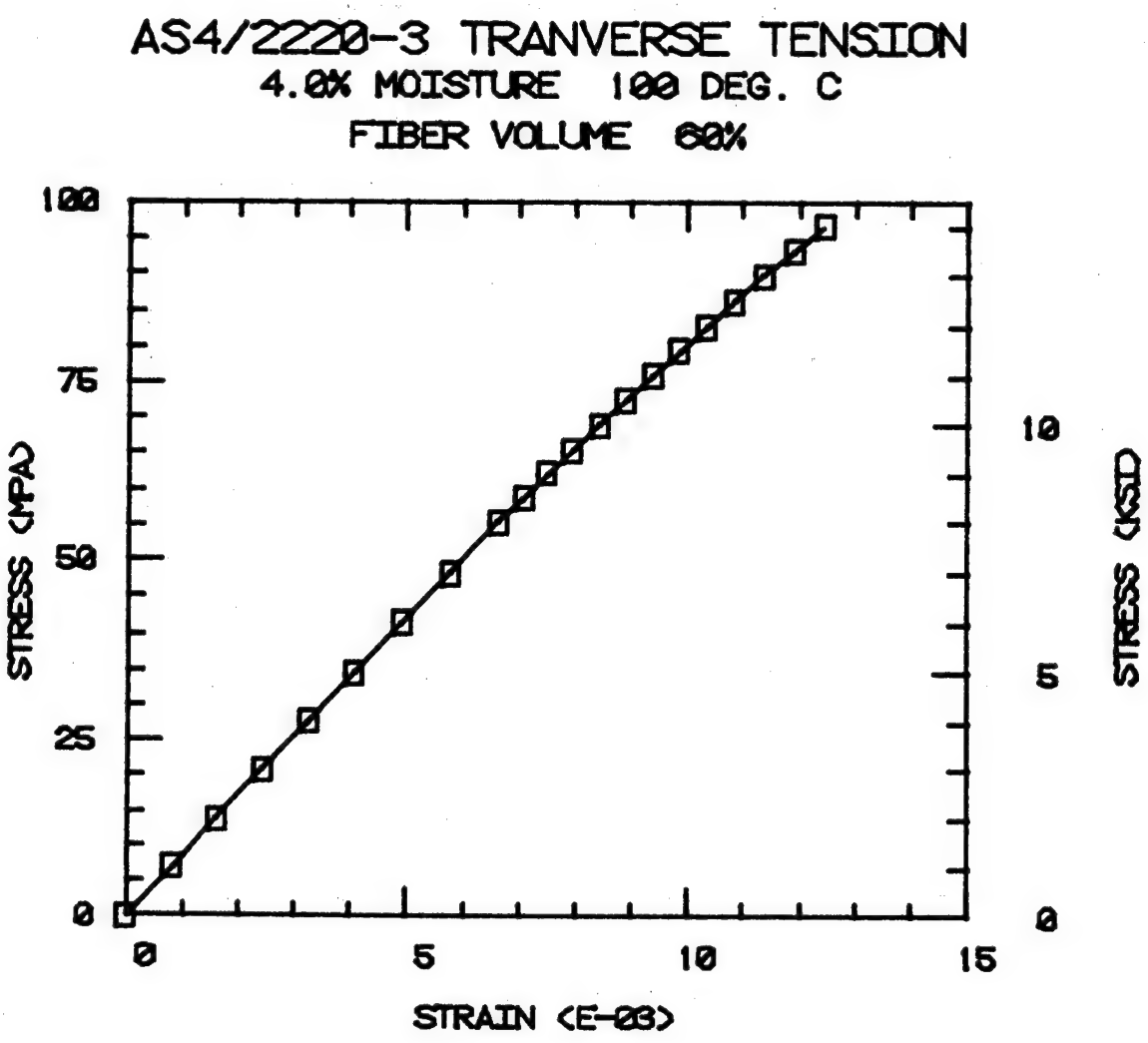


d) Elevated Temperature (100°C), 4.0 Percent Moisture (ETW)

Figure 109 (continued). AS4/2220-3 Graphite/Epoxy Unidirectional Composite Transverse Tensile Stress-Strain Response.

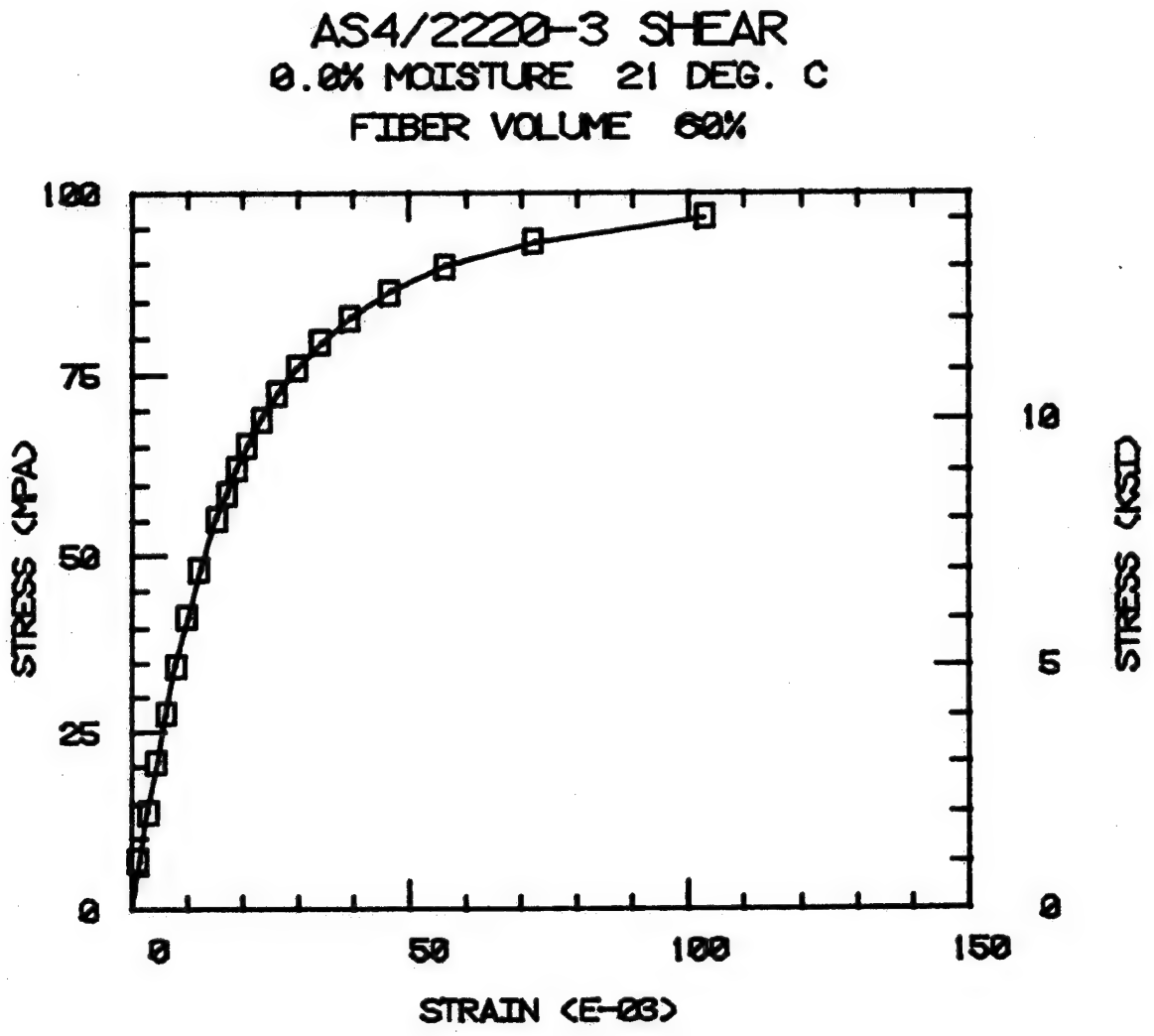


a) Room Temperature, Dry (RTD)

Figure 110. AS4/2220-3 Graphite/Epoxy Unidirectional Composite, Longitudinal Shear Stress-Strain Response.

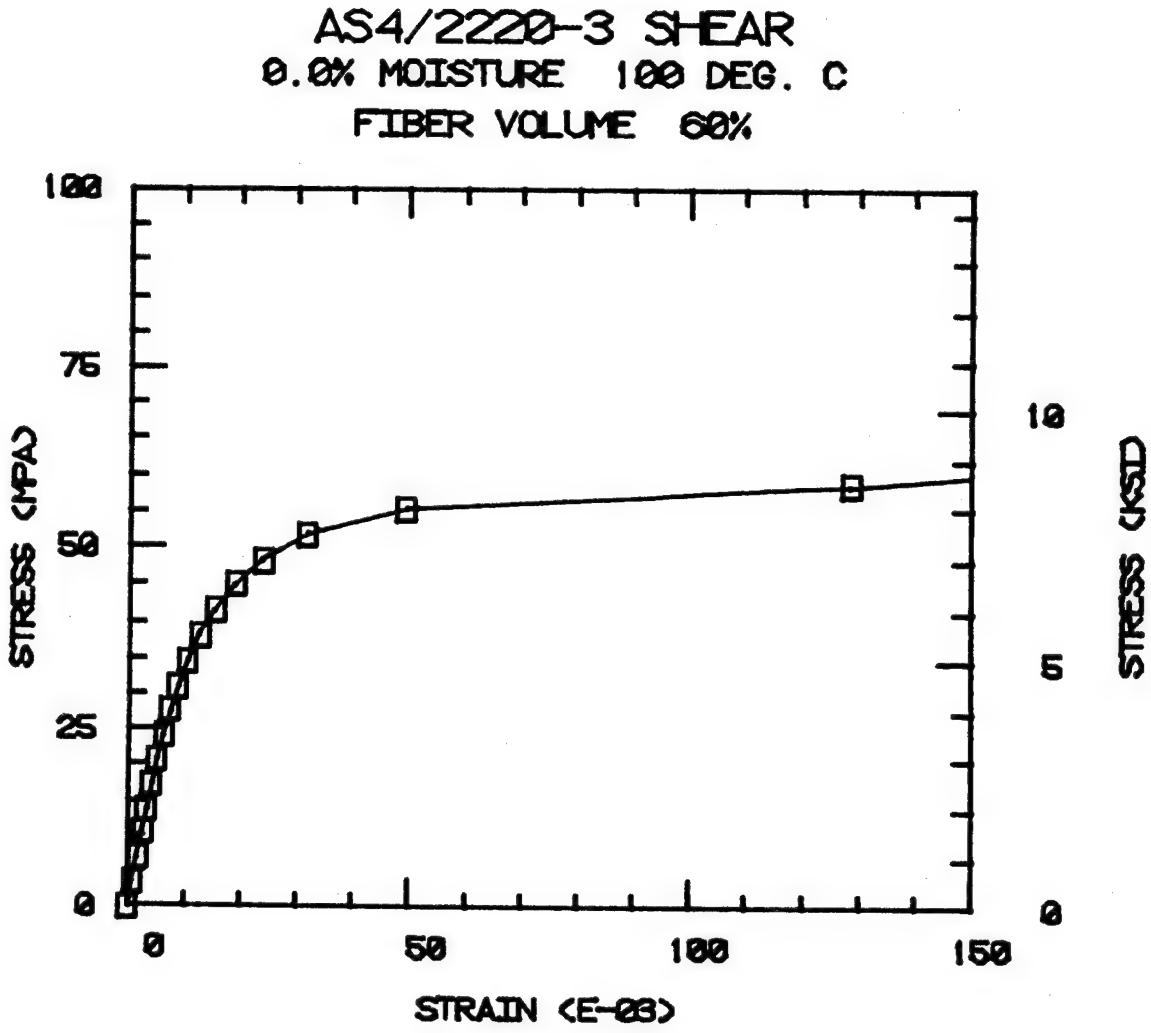


b) Elevated Temperature (100°C), Dry (ETD)

Figure 110 (continued). AS4/2220-3 Graphite/Epoxy Unidirectional Composite, Longitudinal Shear Stress-Strain Response.

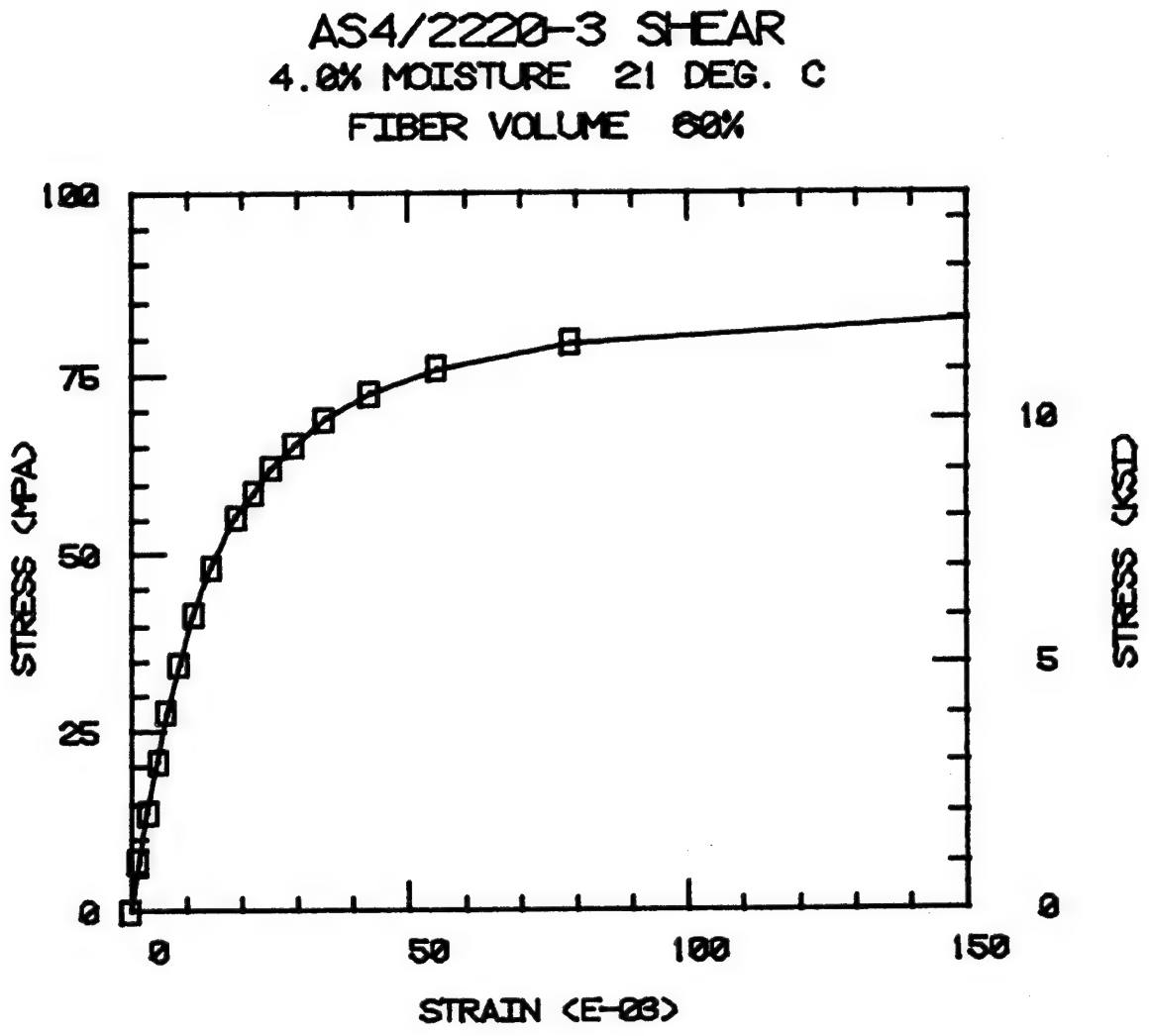


c) Room Temperature, 4.0 Percent Moisture (RTW)

Figure 110 (continued). AS4/2220-3 Graphite/Epoxy Unidirectional Composite, Longitudinal Shear Stress-Strain Response.

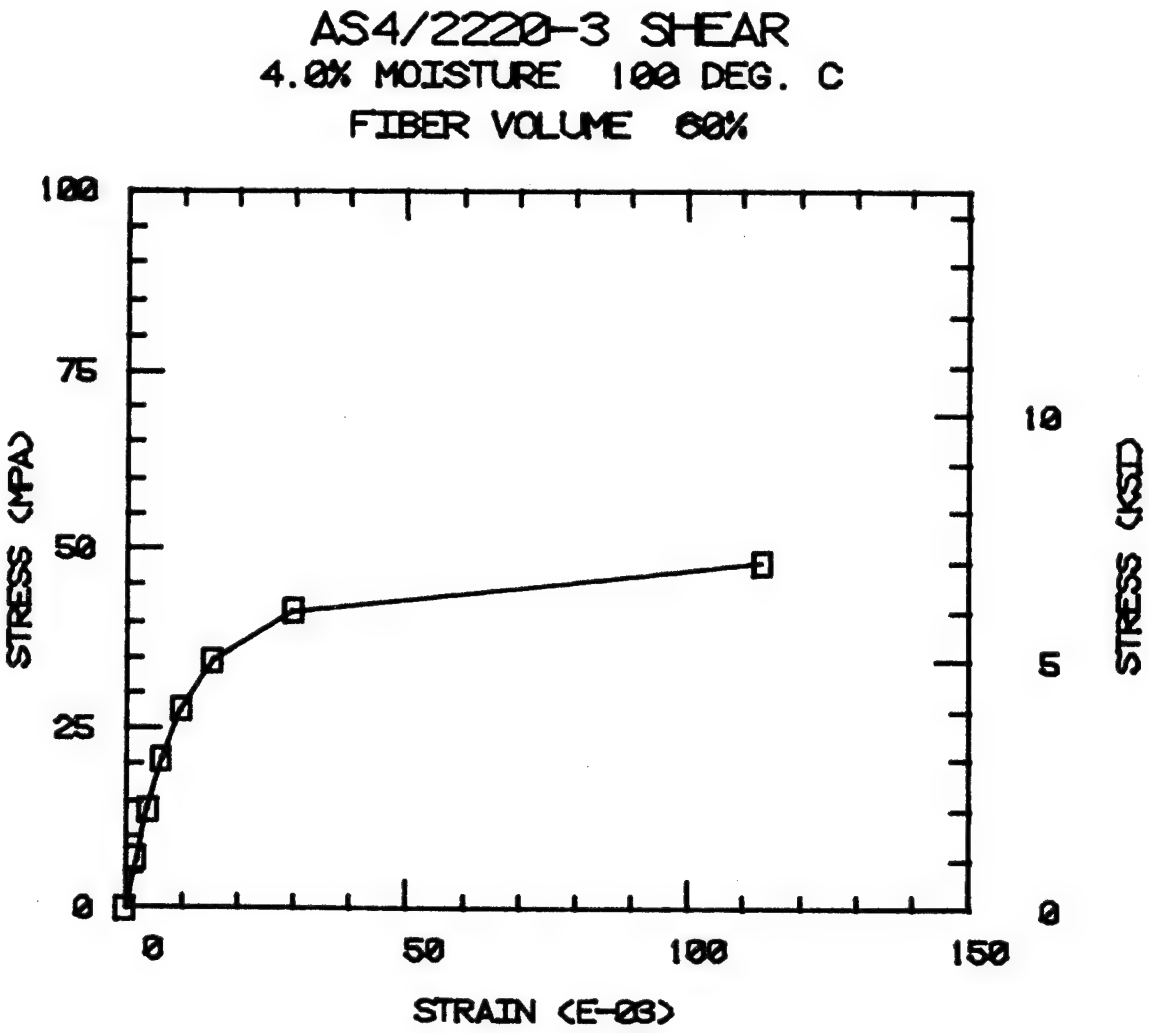


d) Elevated Temperatures (100°C), 4.0 Percent Moisture (ETW)

Figure 110 (continued). AS4/2220-3 Graphite/Epoxy Unidirectional Composite, Longitudinal Shear Stress-Strain Response.

composite response, independent of any other differences. There were other differences although not as pronounced.

The predicted internal stress states for the four different environmental conditions are indicated in Figures E39 through E42 of Appendix E3 of Volume II. The higher thermal expansion coefficient of the Fibredux 914 matrix relative to the Hercules 3502 matrix results in higher thermal stresses, as can be seen by comparing Figures E39 and E40 to Figures E1 and E2. The matrix moisture expansion coefficients were not as different (see Table 4 of Section 3). The 914 value was about 10 percent higher. However, since the maximum moisture content of the Fibredux 914 matrix was measured as 7%M and the Hercules 3502 only 5%M, the moisture-induced stresses in a Fibredux 914 matrix composite can be expected to be higher. This is demonstrated by comparing Figures E41 and E42 to Figures E3 and E4.

The longitudinal tension stress-strain curves are plotted in Figure 111. As in the other three composite systems, matrix or environment had little influence on this fiber-dominated property. The corresponding internal stress states are presented in Figures E43 through E47 of Appendix E3 of Volume II.

Transverse tension stress-strain curves for the AS4/914 unidirectional composite are plotted in Figure 112. There is a moderate influence of temperature and moisture. This is reflected more visibly in the stress contour plots of Figures E48 through E52 of Appendix E3.

AS4/914 unidirectional composite shear-stress shear strain curves are given in Figure 113 for all four environmental conditions. The composite shear strain for a given applied shear stress increases significantly with increasingly severe environmental conditions. That

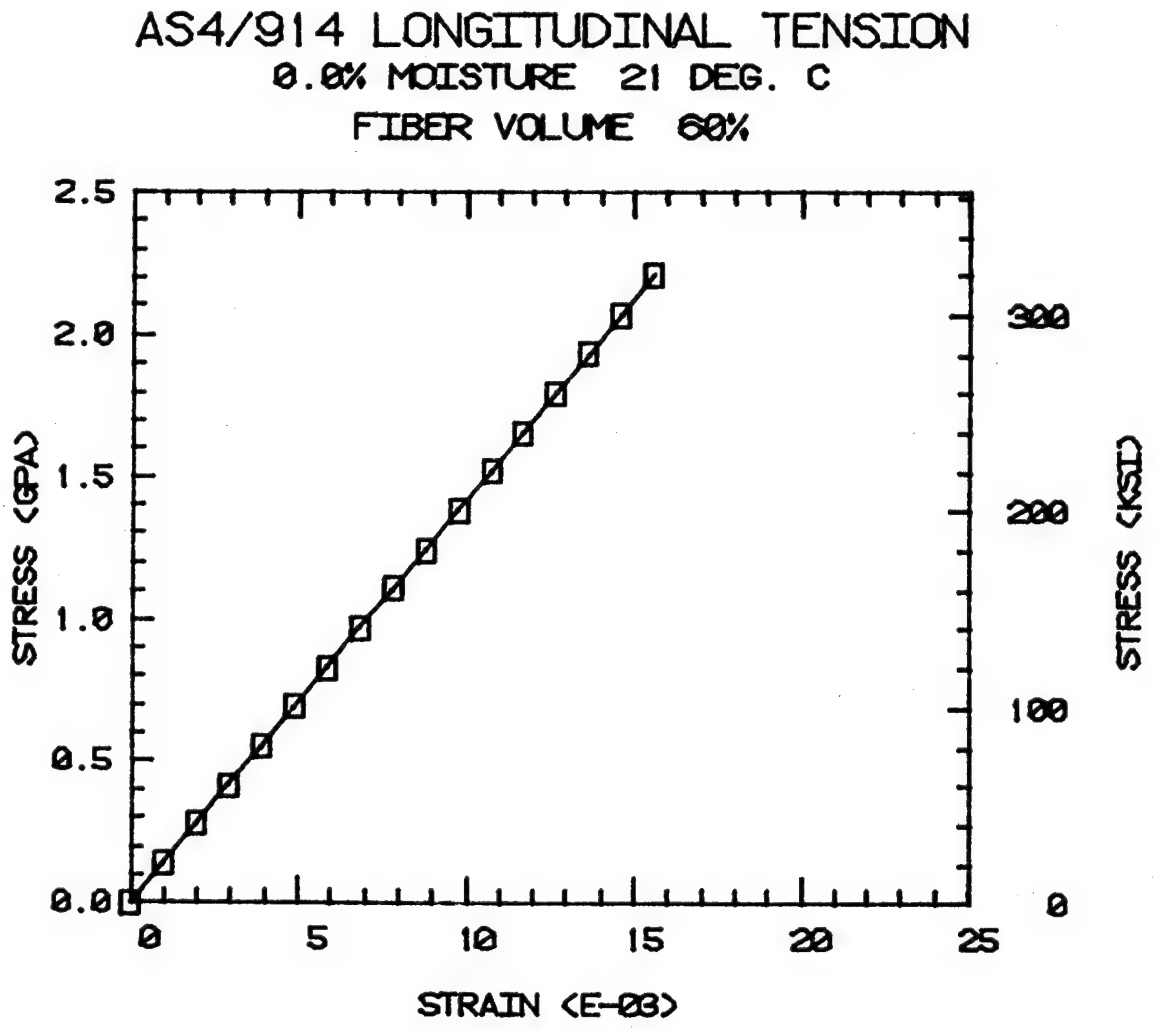


a) Room Temperature, Dry (RTD)

Figure 111. AS4/914 Graphite/Epoxy Unidirectional Composite, Longitudinal Tensile Stress-Strain Response.

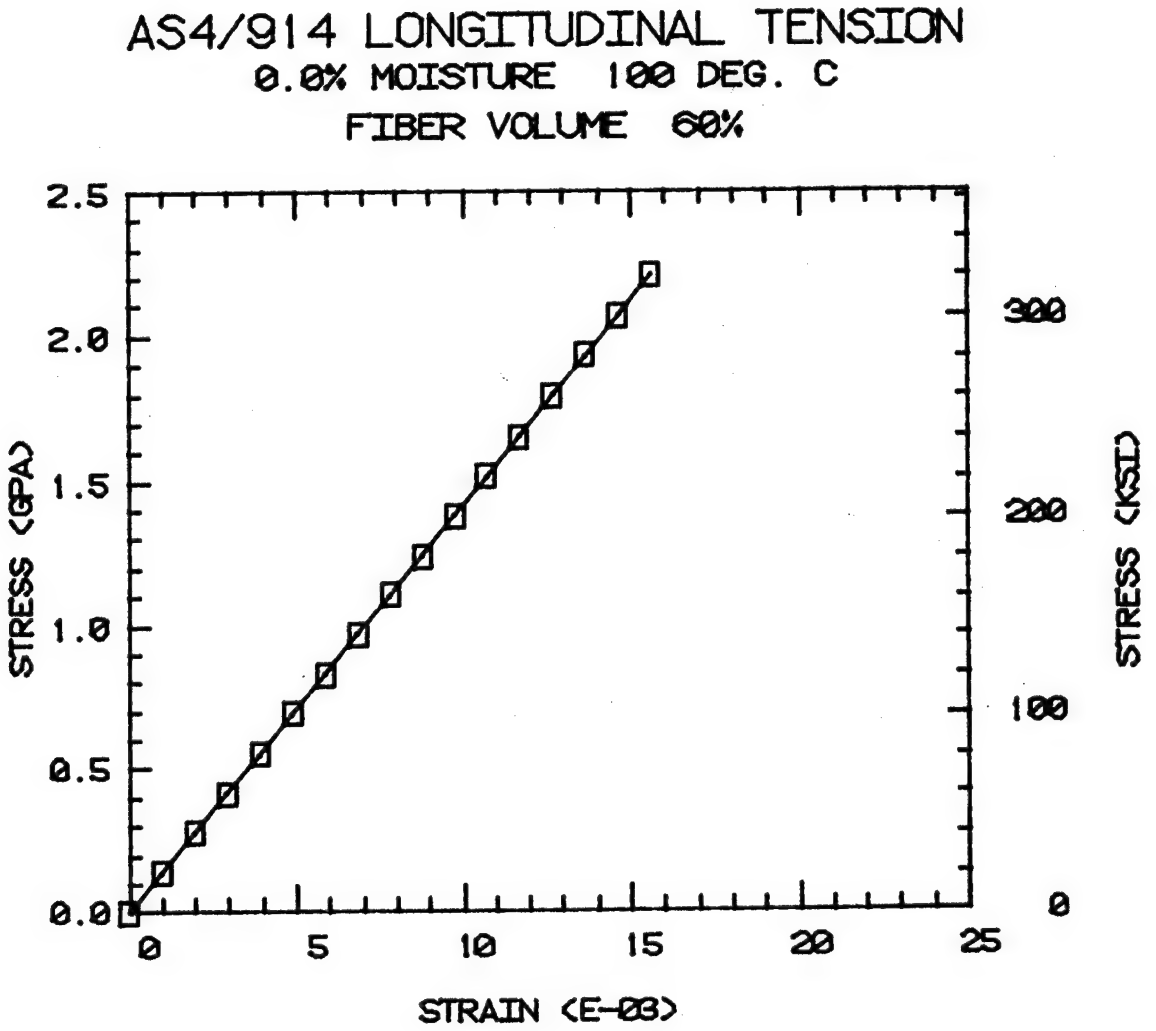


b) Elevated Temperature (100°C), Dry (ETD)

Figure 111 (continued). AS4/914 Graphite/Epoxy Unidirectional Composite, Longitudinal Tensile Stress-Strain Response.

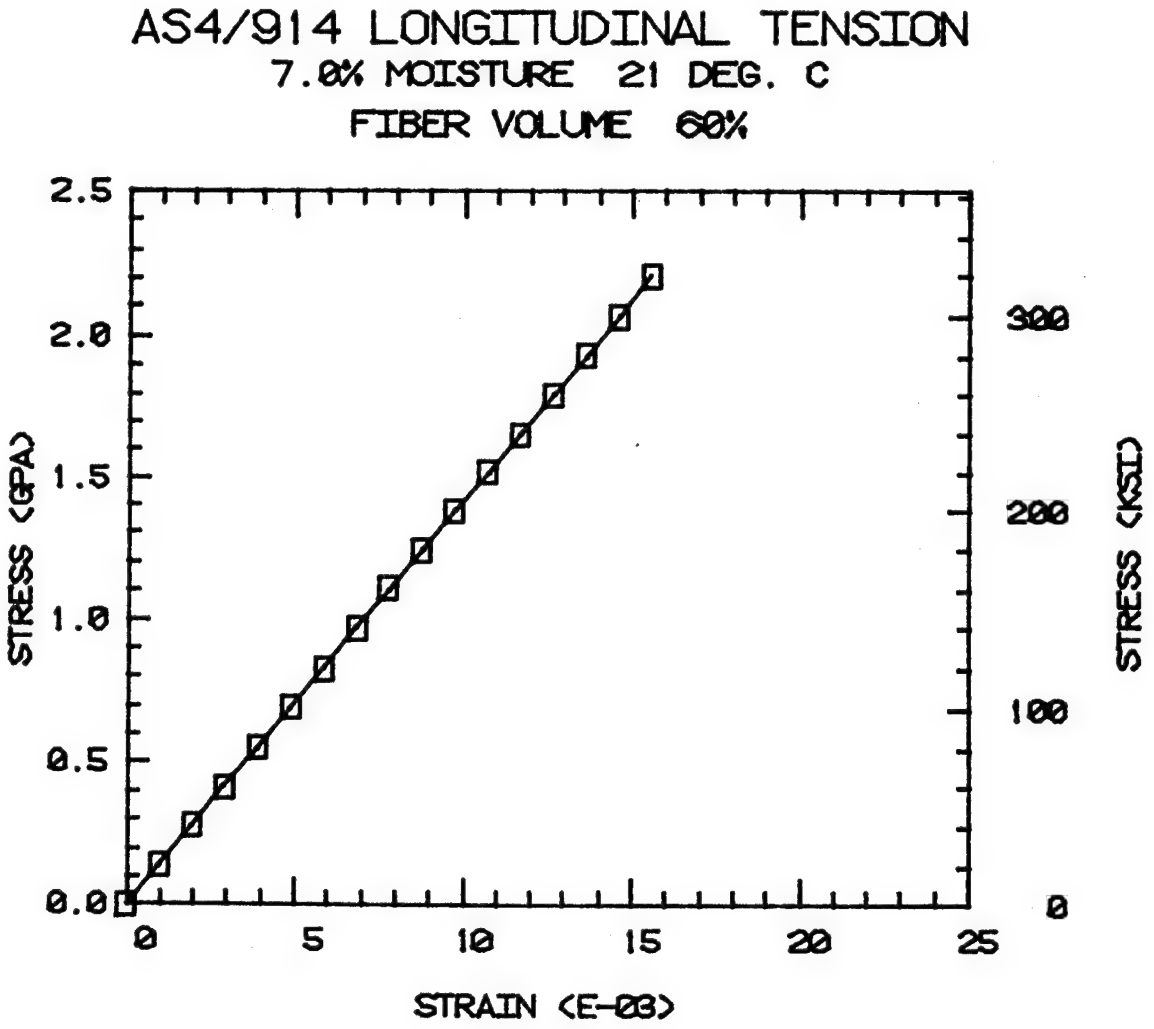


c) Room Temperature, 7.0 Percent Moisture (RTW)

Figure 111 (continued). AS4/914 Graphite/Epoxy Unidirectional Composite, Longitudinal Tensile Stress-Strain Response.

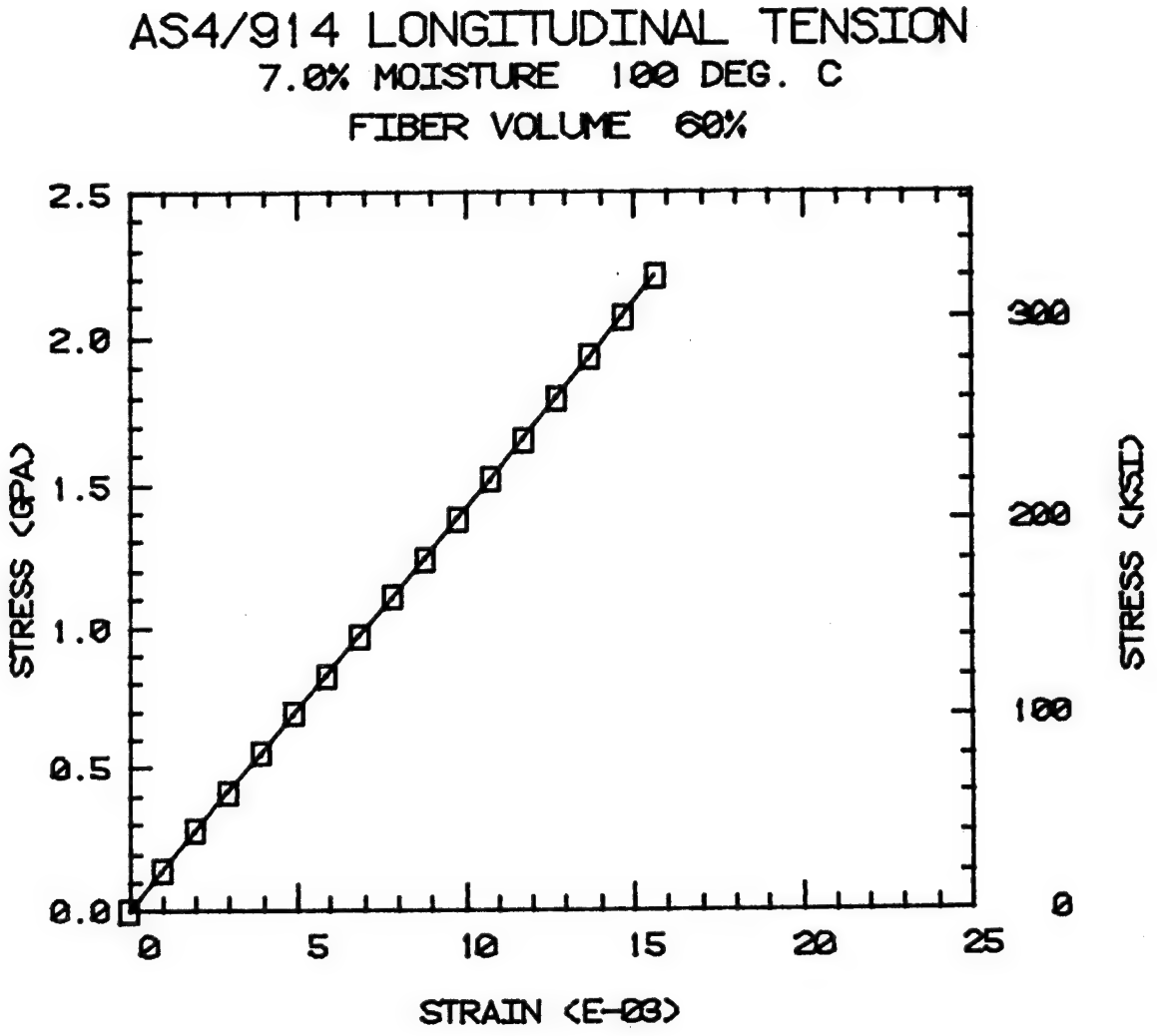


d) Elevated Temperature (100°C), 7.0 Percent Moisture (ETW)

Figure 111 (continued). AS4/914 Graphite/Epoxy Unidirectional Composite, Longitudinal Tensile Stress-Strain Response.

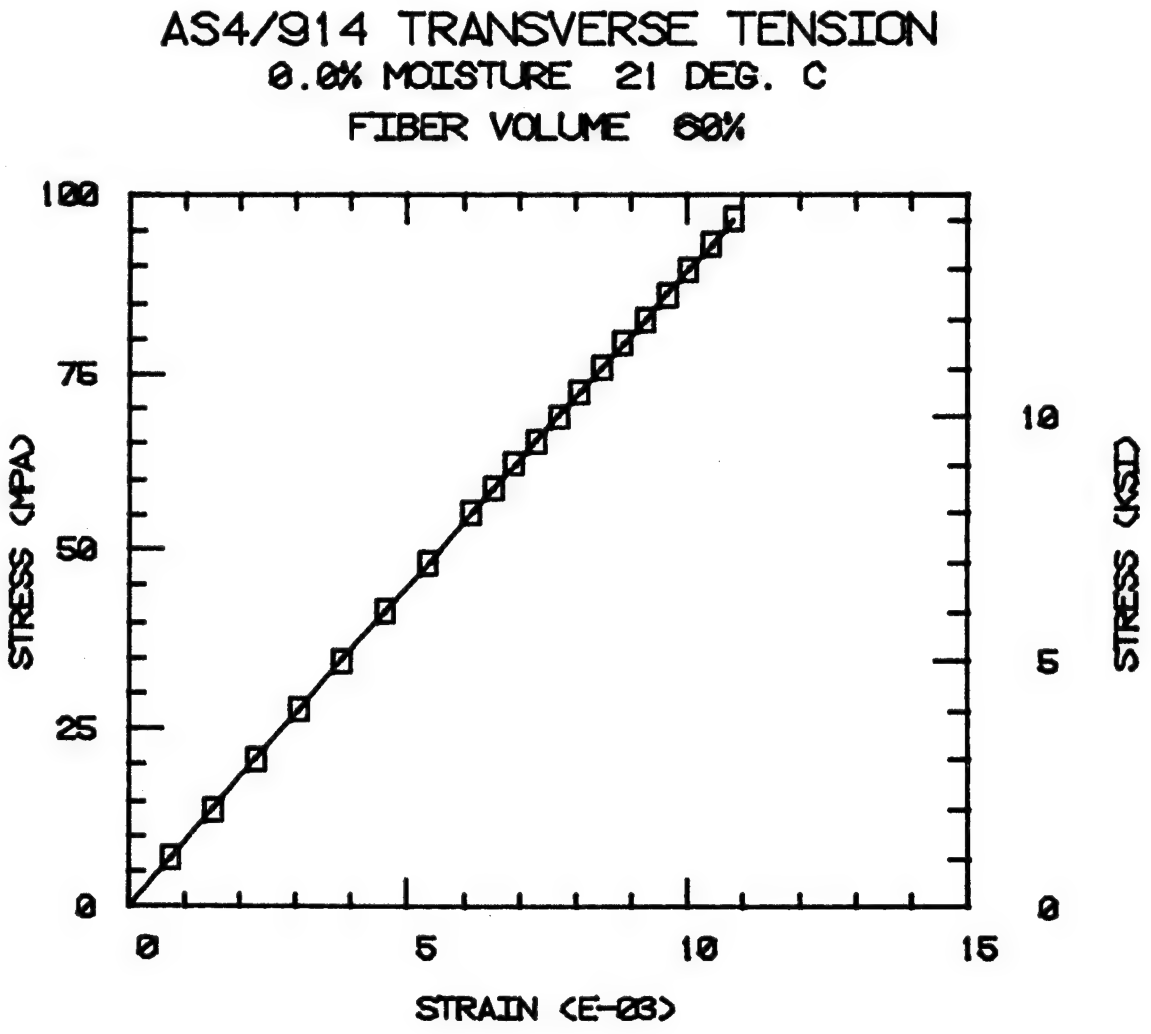


a) Room Temperature, Dry (RTD)

Figure 112. AS4/914 Graphite/Epoxy Unidirectional Composite, Transverse Tensile Stress-Strain Response.

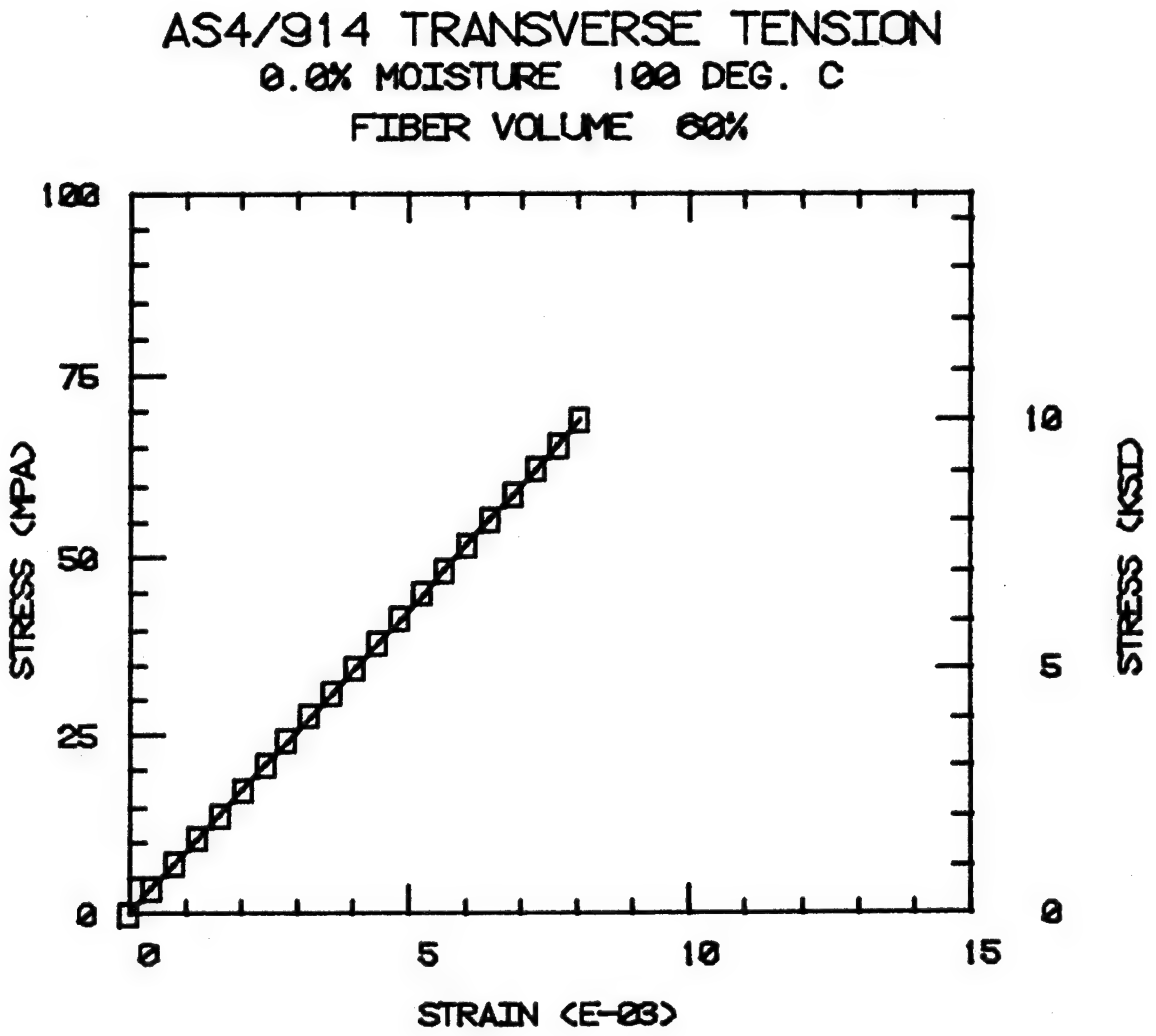


b) Elevated Temperature (100°C), Dry (ETD)

Figure 112 (continued). AS4/914 Graphite/Epoxy Unidirectional Composite, Transverse Tensile Stress-Strain Response.

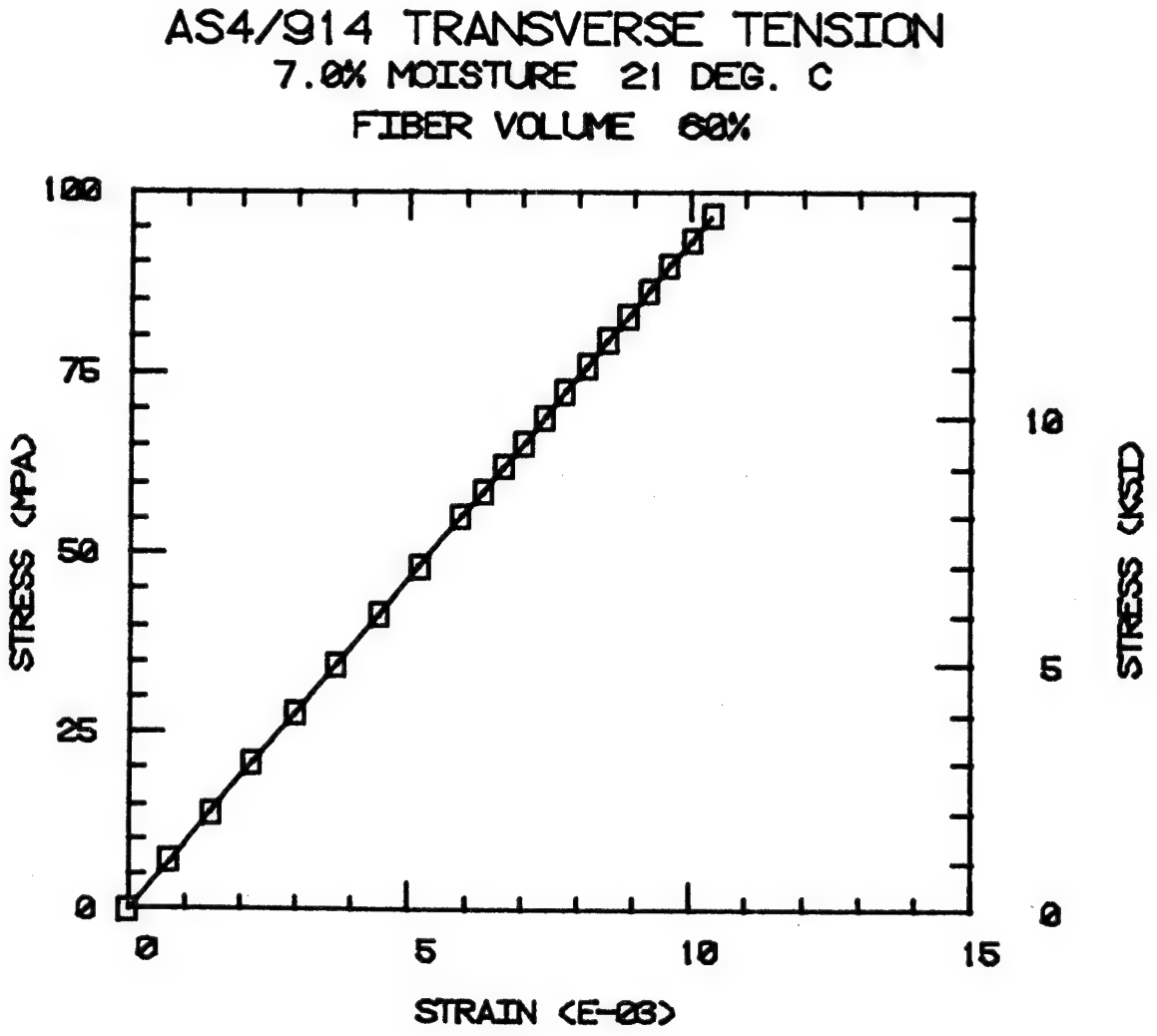


c) Room Temperature, 7.0 Percent Moisture (RTW)

Figure 112 (continued). AS4/914 Graphite/Epoxy Unidirectional Composite, Transverse Tensile Stress-Strain Response.

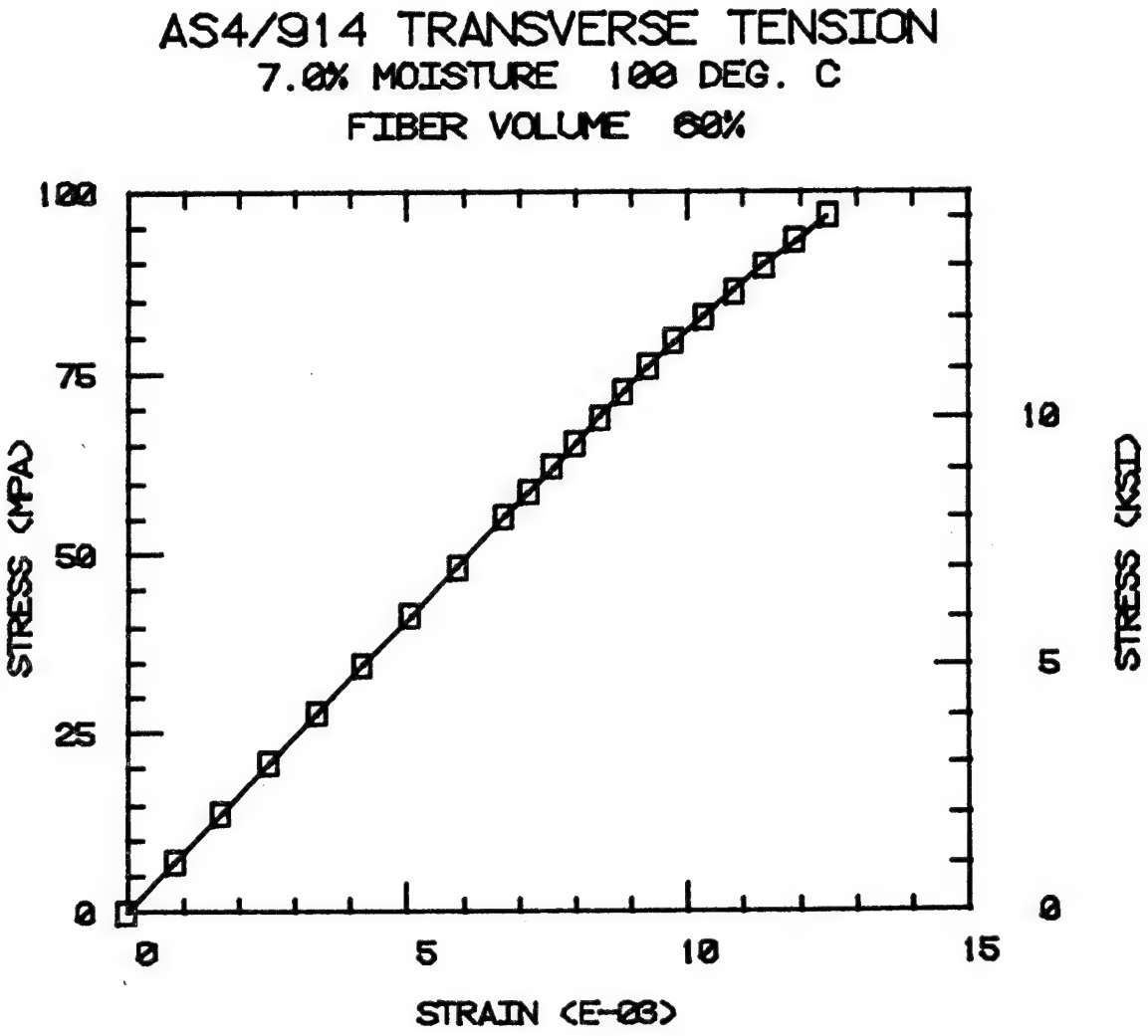


d) Elevated Temperature (100°C), 7.0 Percent Moisture (ETW)

Figure 112 (continued). AS4/914 Graphite/Epoxy Unidirectional Composite, Transverse Tensile Stress-Strain Response.

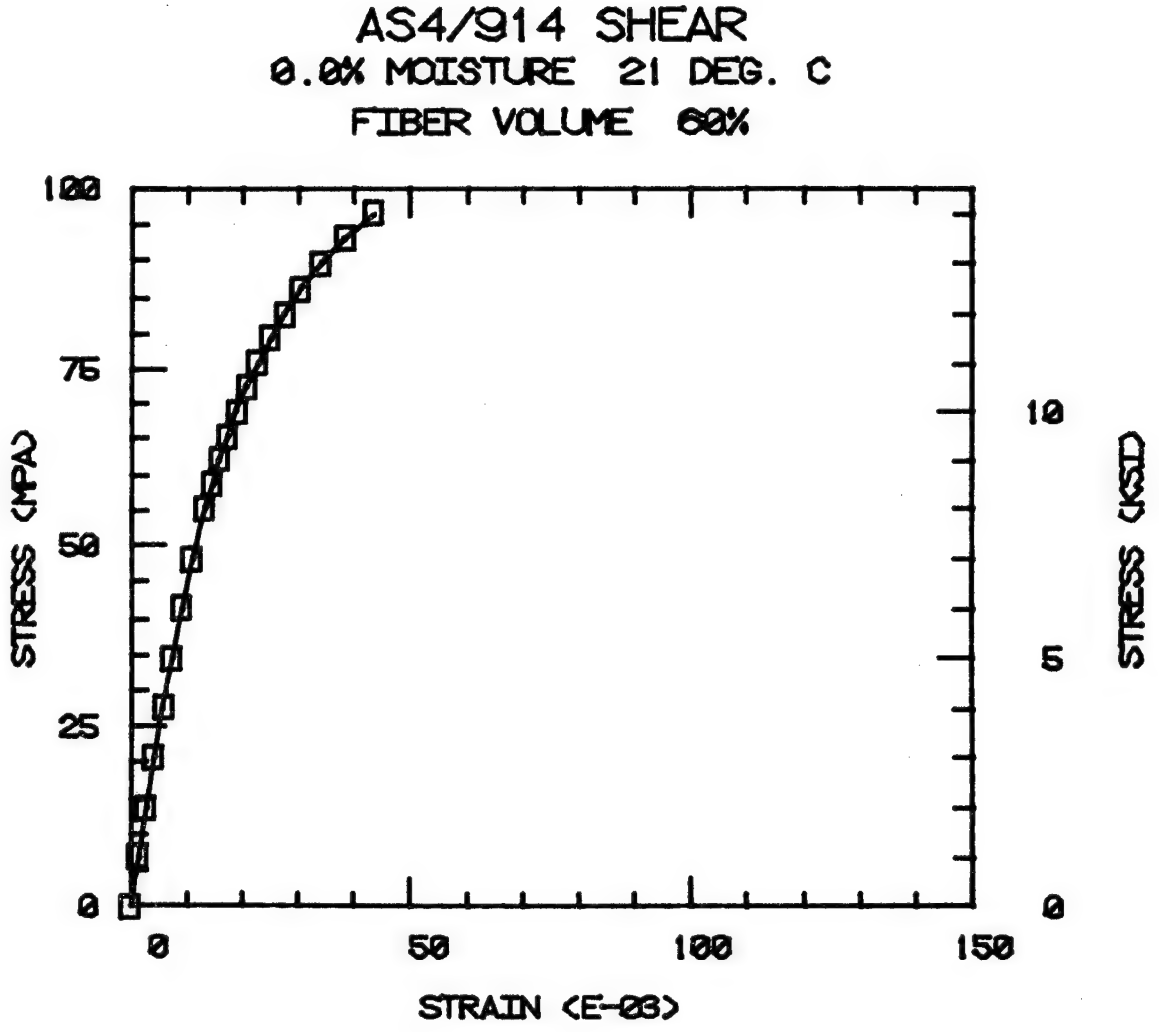


a) Room Temperature, Dry (RTD)

Figure 113. AS4/914 Graphite/Epoxy Unidirectional Composite, Longitudinal Shear Stress-Strain Response.

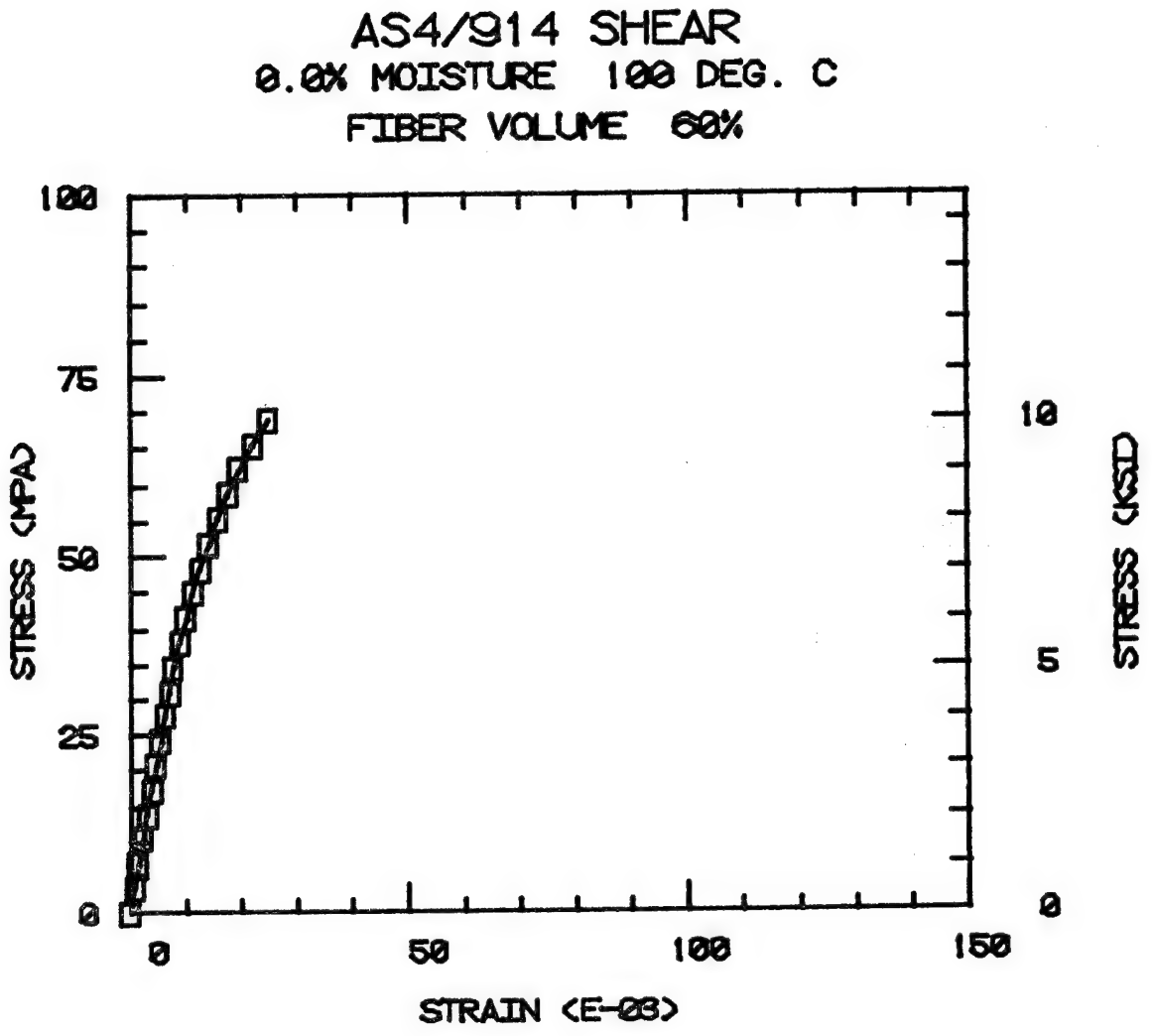


b) Elevated Temperature (100°C), Dry (ETD)

Figure 113 (continued). AS4/914 Graphite/Epoxy Unidirectional Composite, Longitudinal Shear Stress-Strain Response.

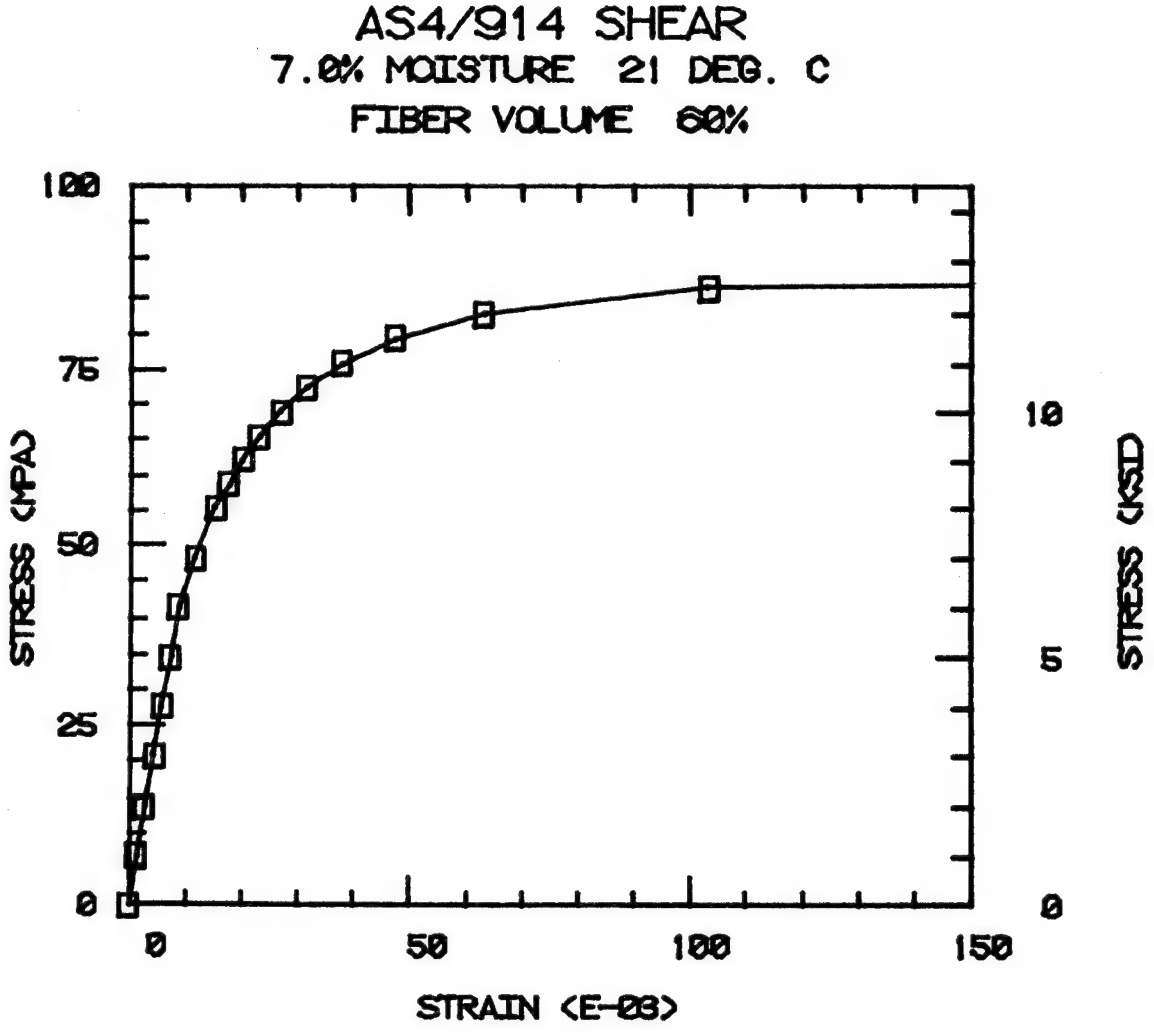


c) Room Temperature, 7.0 Percent Moisture (RTW)

Figure 113 (continued). AS4/914 Graphite/Epoxy Unidirectional Composite, Longitudinal Shear Stress-Strain Response.

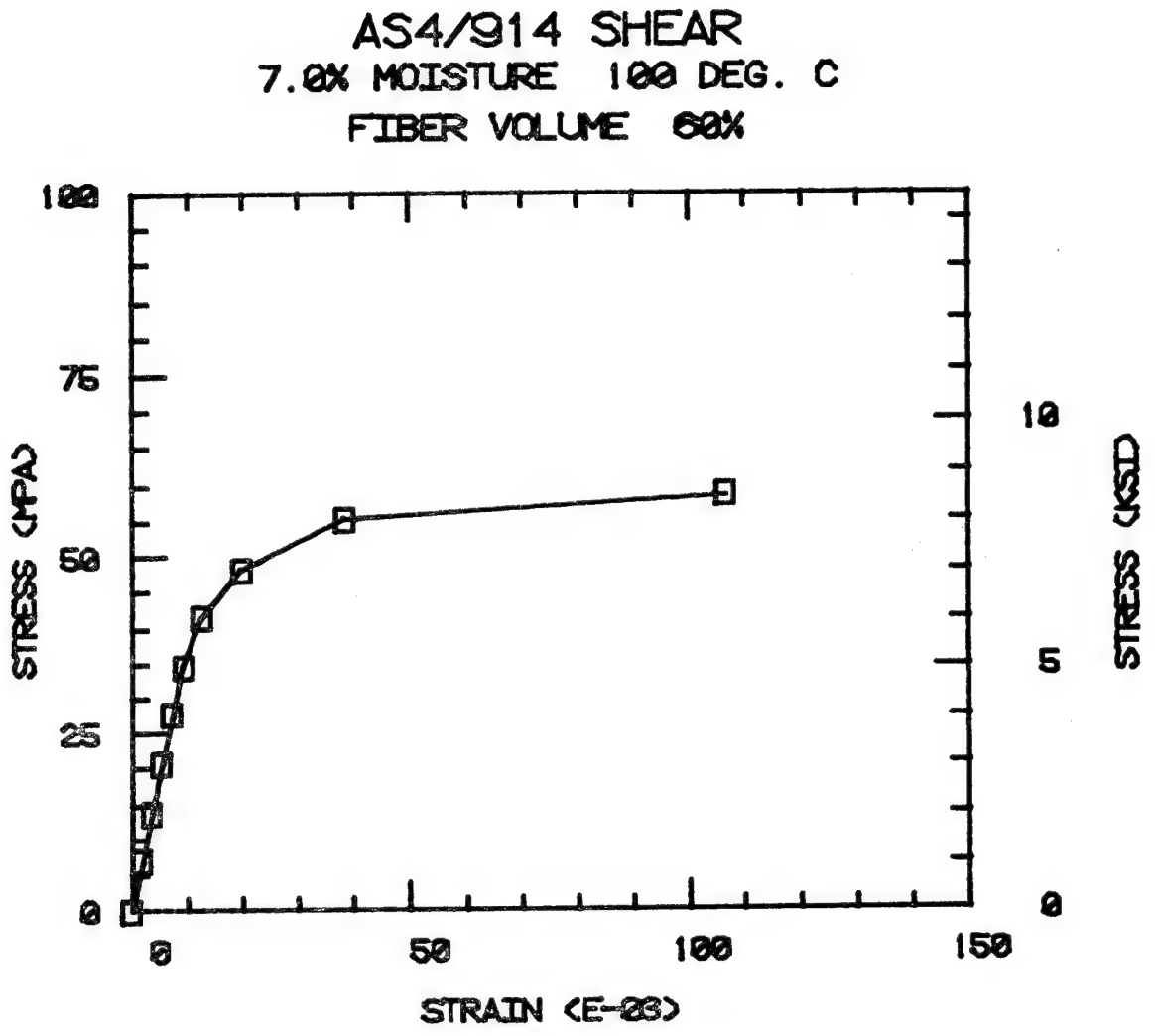


d) Elevated Temperature (100°C), 7.0 Percent Moisture (ETW)

Figure 113 (continued). AS4/914 Graphite/Epoxy Unidirectional Composite, Longitudinal Shear Stress-Strain Response.

is, the curves become increasingly nonlinear. The Fibredux 914 matrix exhibits a greater sensitivity to hygrothermal exposure than does the Hercules 3502 matrix, as a careful comparison of Figures 64 and 67 indicates. The internal stress states for the AS4/914 composite subjected to longitudinal shear are given in Figures E53 through E59 of Appendix E3 of Volume II.

## 5.5 Comparisons of Predicted Composite Response

Although the first impression may be that the Hercules 3502 and the Fibredux 914 epoxies are very similar, and that the two Hercules 2220 systems are even more so, such is not strictly the case. A closer examination of Figure 68 indicates that the Fibredux 914 exhibits a higher room temperature, dry tensile modulus than the Hercules 3502. However, it does not retain this stiffness as well with increasing temperature and, particularly, moisture. Also, the coefficient of thermal expansion of the dry Hercules 3502 is lower. The Hercules 2220-1 and 2220-3 tensile properties are very similar, but the shear stiffness of the latter system is slightly lower under all environmental conditions. This can be seen by comparing Figures 65b and 66b or Figures 70b and 70c, or 71b and 71c. Most significant, however, is the high coefficient of moisture expansion of the 2220-3 matrix. The moisture expansion coefficient of the 2220-1 system was about 25 percent lower, and that of the 2220-3 system about 25 percent higher, than the average of the other two materials.

The 2220-3 system also absorbed slightly more moisture than the 2220-1 system, 4.0 weight percent versus 3.8 weight percent. The fact that the 2220-3 system exhibited a roughly 60 percent higher moisture expansion coefficient than the 2220-1 system suggests significantly

larger influences of moisture in composite incorporating the 2220-3 system. Such a large difference in moisture expansion was not expected and it is strongly suggested that additional moisture expansion experiments be conducted before any final conclusions are drawn. Once some composites data become available, it will be possible to further establish the significance of this difference.

In view of these summary observations of the matrix material stiffness properties relative to each other, it is of interest to consider how these differences translate into predicted unidirectional composite properties. Table 6 presents a summary of the predicted composite stiffness properties for the various environmental conditions considered. These data correspond to those contained in the previously discussed Figures 87 through 113.

As can be seen in Table 6, and as expected, the axial modulus of the composite is affected very little by the differences in the four matrix materials. The predicted differences would be lost in the normal scatter of experimentally measured results. Even analytically, the influence of matrix tensile modulus alone does not dominate the prediction. For example, the Fibredux 914 matrix exhibited the highest tensile modulus at the RTD condition (see Figure 1, 10 or 68). Yet both the Hercules 3502 and 2220-1 systems resulted in slightly higher predicted composite stiffnesses. That is, other parameters such as the matrix Poisson's ratio and coefficient of thermal expansion (which influences the magnitude of the curing-induced residual stresses, also influences the composite axial stiffness.

The composite transverse modulus, being a matrix-dominated property, is more sensitive to differences between the matrix materials.

Table 6

Summary of Predicted Stiffness Properties of Various AS4 Graphite Fiber-Reinforced Unidirectional Composites (Fiber Volume = 60 Percent)

| Matrix Material and Environment | Axial Modulus $E_{11}$ (Msi) | Transverse Modulus $E_{22}$ (Msi) | Shear Modulus $G_{12}$* (Msi) | Shear Modulus $G_{12}$** (Msi) |
|---|---|---|---|---|
| 3502 | | | | |
| RT, Dry | 20.61 | 1.39 | 0.79 | 0.70 |
| 100°C, Dry | 20.58 | 1.33 | 0.72 | 0.63 |
| RT, Wet (5.0% M) | 20.59 | 1.41 | 0.70 | 0.58 |
| 100°C, Wet (5.0% M) | 20.55 | 1.34 | 0.63 | 0.50 |
| 2220-1 | | | | |
| RT, Dry | 20.61 | 1.38 | 0.78 | 0.65 |
| 100°C, Dry | 20.56 | 1.28 | 0.67 | 0.54 |
| RT, Wet (3.8% M) | 20.58 | 1.38 | 0.70 | 0.59 |
| 100°C, Wet (3.8% M) | 20.52 | 1.22 | 0.55 | 0.47 |
| 2220-3 | | | | |
| RT, Dry | 20.56 | 1.27 | 0.67 | 0.60 |
| 100°C, Dry | 20.53 | 1.19 | 0.59 | 0.49 |
| RT, Wet (4.0% M) | 20.56 | 1.42 | 0.64 | 0.59 |
| 100°C, Wet (4.0% M) | 20.50 | 1.18 | 0.52 | 0.41 |
| 914 | | | | |
| RT, Dry | 20.58 | 1.32 | 0.71 | 0.65 |
| 100°C, Dry | 20.55 | 1.24 | 0.64 | 0.60 |
| RT, Wet (7.0% M) | 20.57 | 1.35 | 0.69 | 0.65 |
| 100°C, Wet (7.0% M) | 20.51 | 1.19 | 0.54 | 0.48 |

*Initial Shear Modulus

**Secant Shear Modulus at 1.0 Percent Shear Strain

However, as indicated in Table 6, the differences in the four matrix materials considered here were not great enough to cause major differences. While the predicted differences are great enough that they could probably be detected experimentally, they are not significant in the design sense. Again, however, the predicted trends are interesting, as an indicator of what matrix properties can control. For example, even though the two Hercules 2220 systems exhibited very similar stiffness properties, the predicted composite transverse stiffness properties are almost 10 percent different in the dry condition, but little different in the wet condition. Having a detailed micromechanics analysis available, the reasons can readily be determined.

The predicted composite shear moduli varied somewhat more from matrix to matrix than the composite transverse moduli, about 20 percent. These are significant differences in themselves, and again are interesting also in the sense that the composite shear properties do not follow directly from the matrix shear properties.

Having the predicted micromechanical stress state plots for graphite fiber-reinforced composites incorporating all four matrix systems, it is possible to make many other comparisons between the systems also. These comparisons can be based on axial and transverse tensile and longitudinal shear loadings at four different environmental conditions. Since the predictive analysis technique is relatively new, it is important to make correlations with experimental data for verification purposes. This is particularly true for strength predictions, since no one failure criterion is universally accepted. Hopefully this correlation work can be performed during the next year of this study. In the meantime, many qualitative comments can be made.

The fundamental question which immediately comes to mind, of course, is "which matrix system is the best?" Unfortunately, "best" has many definitions. It depends upon the working environment and also the loading mode. Failure can take many forms, from microcracking and minor stiffness reductions to complete fracture. Some general comments can be made, however.

### 5.5.1 Hygrothermal Residual Stresses

Composite response during subsequent mechanical loading, particularly strength properties, can be strongly influenced by pre-existing internal stress states induced by excursions from the cure temperature and moisture absorption. Since a temperature decrease causes matrix contraction and moisture absorption causes matrix expansion, these two environmental influences tend to have opposing influences on the composite. The problem is greatly complicated by the fact that a graphite fiber typically expands in its axial direction during cooldown and contracts in the transverse direction (see Table 5), although at a lesser rate than the matrix material. But the fiber is not sensitive to moisture. Also, the graphite fiber is anisotropic in its stiffness properties (Table 5). Thus, the interaction between fiber and matrix is complex. Fortunately, the finite element micromechanics analysis and associated computer program is capable of modeling these many interacting influences both accurately and efficiently.

Representative results for all four unidirectional composite systems for all four environmental conditions are given in Table 7. These values were taken directly from the plots of Section 5.3 for the Hercules 2220-1 matrix and Appendix E of Volume II for the other three systems. The interested reader can go back to these many plots to obtain

Table 7

Predicted Pre-Existing Hygrothermal Stress States in Various AS4 Graphite Fiber-Reinforced Unidirectional Composites (Fiber Volume=60 Percent; Stresses in ksi)

| Stress Component (Highest Value Occurring) | Matrix Material 3502 | 2220-1 | 2220-3 | 914 |
|---|---|---|---|---|
| Room Temperature (21°C),Dry,(RTD) | | | | |
| Octahedral Shear Stress, $\tau_o$ | 5.27 | 5.13 | 3.29 | 8.24 |
| Maximum Principal Stress, $\sigma_1$ | 8.78 | 8.73 | 5.49 | 14.18 |
| Minimum Principal Stress, $\sigma_2$ | -5.14 | -5.17 | -3.31 | -8.96 |
| Intermediate Principal Stress, $\sigma_3$ | 6.84 | 6.88 | 4.10 | 11.85 |
| Interface Normal Stress, $\sigma_n$ | -5.23 | -5.24 | -3.34 | -9.14 |
| Elevated Temperature (100°C),Dry,(ETD) | | | | |
| Octahedral Shear Stress, $\tau_o$ | 3.22 | 2.69 | 1.32 | 4.64 |
| Maximum Principal Stress, $\sigma_1$ | 5.31 | 4.70 | 2.25 | 8.49 |
| Minimum Principal Stress, $\sigma_2$ | -3.23 | -2.81 | -1.34 | -5.31 |
| Intermediate Principal Stress, $\sigma_3$ | 4.29 | 3.78 | 1.63 | 7.20 |
| Interface Normal Stress, $\sigma_n$ | -3.30 | -2.85 | -1.35 | -5.45 |
| Room Temperature (21°C),Wet,(RTW) | | | | |
| Octahedral Shear Stress, $\tau_o$ | 1.54 | 1.22 | 3.03 | 1.36 |
| Maximum Principal Stress, $\sigma_1$ | 1.92 | 2.69 | 3.95 | 1.28 |
| Minimum Principal Stress, $\sigma_2$ | -2.37 | -0.97 | -4.74 | -2.01 |
| Intermediate Principal Stress, $\sigma_3$ | -1.40 | -1.40 | -4.15 | -1.20 |
| Interface Normal Stress, $\sigma_n$ | 1.96 | -0.96 | 4.11 | 1.39 |
| Elevated Temperature (100°C),Wet,(ETW) | | | | |
| Octahedral Shear Stress, $\tau_o$ | 3.14 | 1.12 | 4.44 | 4.71 |
| Maximum Principal Stress, $\sigma_1$ | 4.03 | 1.50 | 6.05 | 4.97 |
| Minimum Principal Stress, $\sigma_2$ | -4.97 | -1.55 | -7.95 | -5.91 |
| Intermediate Principal Stress, $\sigma_3$ | -4.69 | -1.09 | -7.52 | -5.54 |
| Interface Normal Stress, $\sigma_n$ | 4.13 | 1.54 | 6.48 | 5.06 |

additional information, if required. All values given in Table 7 are in units of ksi thereby permitting direct comparison since the corresponding plots are in the same units.

Considering first the room temperature, dry (RTD) condition, it can be seen that the AS4/914 composite exhibited the highest internal stresses in the matrix. The Fibredux 914 exhibited the highest stiffness (see Figure 68 and a coefficient of thermal expansion comparable to the two 2220 systems. Both 2220 systems are of lower stiffness. The 3502 system exhibited a very low coefficient of thermal expansion (see Table 3 of Section 3), although it had a stiffness comparable to the 914 system. Thus, it is not unexpected that the AS4/914 composite is predicted to have the highest internal stresses in the matrix.

The relative stress magnitudes among the composites listed in Table 7 is significant. For example, the stresses in the AS4/914 composite are from 60 to 75 percent higher than the corresponding components in the baseline AS4/3502 system. Also, the stresses in the AS4/2220-1 composite are higher than in the AS4/2220-3 composite. Although these two matrix systems are similar, the 2220-1 system has a slightly higher coefficient of thermal expansion even though its stiffness is slightly lower.

Considering the relatively low measured strengths of all four matrix materials (see Figures 72 and 74 for summary plots), these stresses are significant. In some cases, notably for the 914 matrix, the predicted principal stresses are actually higher than the measured strength. This suggests that matrix microcracking may occur in the composite during cooldown from the 177°C cure temperature. Not that microcracking would not occur at the fiber-matrix interface since the highest normal stress is compressive at this location. The fact that the

thermally induced stress is compressive is favorable to any subsequent tensile transverse loading and unfavorable to a compressive transverse loading, as subsequent discussion will emphasize.

Where the highest stresses occur is also significant. For example, at the RTD condition, the octahedral shear stress is maximum in the matrix midway between closest fiber spacings, i.e., along the x and y axes. However, the two tensile principal stresses, $\sigma_1$ and $\sigma_3$ are maximum at the fiber-matrix interface, at approximately 45° to the x and y axes. Subsequent moisture or mechanical loadings may increase the stresses in other locations more rapidly, thus shifting the location of first failure.

Referring to the ETD results, it will be noted that although the 100°C temperature is approximately halfway between the cure temperature (177°C) and room temperature (21°C), the thermally induced stresses are not half as high. Due to the combination of temperature-dependent thermal expansion and stiffness properties, the stresses in the AS4/2220-3 composite are only 40 percent as high as the room temperature values, while those in the AS4/914 composite are 60 percent as high.

The room temperature, wet (RTW) stresses reflect the strong influence of matrix moisture expansion coefficient and, to a lesser extent, the influence of moisture absorption on matrix modulus. For example, the Hercules 2220-1 matrix exhibited the lowest moisture expansion coefficient of the four materials and the 2220-3 matrix the highest value (see Table 4 of Section 3). In fact, the 2220-1 value was 60 percent lower. The moisture expansion coefficients of the other two matrix materials were almost exactly in between the values for the two 2220 systems. These matrix property differences are reflected in the

predicted composite properties for the RTW condition in Table 7. The AS4/2220-3 composite stresses, which were lower than the AS4/2220-1 composite stresses in the RTD condition, are higher in the RTW condition. This indicates the dominant influence of the high moisture expansion coefficient. While this can be seen by comparing any one of the stress components, it is particularly dramatic when comparing interface normal stresses. The interface normal stress in the AS4/2220-1 composite is reduced to almost zero, but that in the AS4/2220-3 composite is now larger than it was prior to the moisture absorption. Additionally, it has the opposite sign, i.e., it is now a tensile stress. As previously noted, this has major implications in terms of subsequent mechanical loadings being tensile or compressive and when failure will occur.

At the elevated temperature, wet (ETW) condition, the influence of the difference in moisture expansion coefficients is even more pronounced since the offsetting influence of thermally induced stresses is less. This is also indicated in Table 7. It will be noted, for example, that the AS4/2220-3 composite exhibits the highest matrix stresses in the ETW condition, while the AS4/914 composite exhibits the highest matrix stresses in the RTD condition. The AS4/2220-3 composite exhibits the lowest stresses for this condition.

The above simple comparisons make it obvious as to why there is no direct answer to the question, "which matrix is the best?" The environmental service conditions, as well as the mechanical loading, must be specified before an answer can be given. Nevertheless, the present discussion clearly indicates that the analytical tools are now available (in the form of the finite element micromechanics analysis) to

address the question.

### 5.5.2 Mechanical Loadings

Depending on the environmental conditions under which the mechanical testing is to be conducted, any of the pre-existing stress states discussed in Section 5.5.1 can be present. That is, the stresses induced by axial, transverse, or shear loadings are added to these hygrothermal stress states. But superposition does not apply since the matrix stress-strain response is not linear. Fortunately, the analysis handles these nonlinear interactions directly. The following brief discussion will address general observations and trends. Once actual experimental data for these composite systems become available, an in-depth discussion will be more meaningful.

#### 5.5.2.1 Longitudinal Tensile Loading

In the absence of composite material experimental data, longitudinal tensile loading can be dismissed rather quickly. The composite response is fiber-dominated. While the matrix plays an important role in transferring loads locally across broken fibers, its failure does not normally dictate gross failure. There are differences in predicted internal stress states, however, for different matrix materials, as shown in Table 8. It will be noted that the matrix stresses are low relative to the 2.20 GPa (320 ksi) applied stress. However, as previously discussed, the matrix strengths are also relatively low. Since the induced stresses due to axial loading are not very great, the comments made in the previous Section 5.5.1 relative to the hygrothermally induced stresses still apply.

#### 5.5.2.2 Transverse Tensile Loading

Since transverse normal loading of a unidirectional composite is

Table 8

Predicted Matrix Stresses in Various AS4 Graphite Fiber-Reinforced Unidirectional Composites Subjected to 320 ksi Longitudinal Tension (Fiber Volume = 60 Percent; Stresses in ksi)

| Stress Component (Highest Value Occurring) | Matrix Material 3502 | 2220-1 | 2220-3 | 914 |
|---|---|---|---|---|
| Room Temperature (21°C),Dry,(RTD) | | | | |
| Octahedral Shear Stress, $\tau_o$ | 8.44 | 7.62 | 6.46 | 10.21 |
| Maximum Principal Stress, $\sigma_1$ | 18.57 | 17.14 | 14.19 | 22.27 |
| Minimum Principal Stress, $\sigma_2$ | -6.17 | -6.17 | -4.32 | -9.71 |
| Intermediate Principal Stress, $\sigma_3$ | 8.01 | 7.67 | 5.42 | 12.50 |
| Interface Normal Stress, $\sigma_n$ | -6.29 | -6.29 | -4.37 | -9.95 |
| Elevated Temperature (100°C),Dry,(ETD) | | | | |
| Octahedral Shear Stress, $\tau_o$ | 6.33 | 5.66 | 4.45 | 7.80 |
| Maximum Principal Stress, $\sigma_1$ | 14.57 | 12.61 | 10.29 | 16.70 |
| Minimum Principal Stress, $\sigma_2$ | -4.39 | -4.61 | -2.27 | -6.61 |
| Intermediate Principal Stress, $\sigma_3$ | 5.63 | 4.95 | 2.90 | 8.51 |
| Interface Normal Stress, $\sigma_n$ | -4.47 | -4.00 | -2.29 | -6.76 |
| Room Temperature (21°C),Wet,(RTW) | | | | |
| Octahedral Shear Stress, $\tau_o$ | 4.40 | 5.47 | 7.17 | 4.54 |
| Maximum Principal Stress, $\sigma_1$ | 9.29 | 12.25 | 4.31 | 9.88 |
| Minimum Principal Stress, $\sigma_2$ | -0.15 | -2.69 | -2.21 | -0.73 |
| Intermediate Principal Stress, $\sigma_3$ | -0.13 | 3.39 | 1.79 | 0.81 |
| Interface Normal Stress, $\sigma_n$ | 0.39 | -2.75 | 1.85 | -0.39 |
| Elevated Temperature (100°C),Wet,(ETW) | | | | |
| Octahedral Shear Stress, $\tau_o$ | 3.38 | 3.22 | 3.43 | 3.53 |
| Maximum Principal Stress, $\sigma_1$ | 6.10 | 6.82 | 4.23 | 3.75 |
| Minimum Principal Stress, $\sigma_2$ | -2.95 | -0.24 | -5.53 | -4.50 |
| Intermediate Principal Stress, $\sigma_3$ | 2.37 | 0.13 | 3.92 | 2.67 |
| Interface Normal Stress, $\sigma_n$ | 2.42 | 0.39 | 4.52 | 3.78 |

matrix dominated, the stresses induced in the matrix are a strong function of environmental preconditioning and matrix properties. The internal stress state in the matrix for a 27.6 MPa (4 ksi) applied transverse tensile stress loading is summarized in Table 9. Because this is a relatively low applied stress, it will be noted that the thermally-induced stresses continue to dominate the RTD and ETD data. The stresses are not drastically different between Table 9 and Table 7.

This is not true of the moisture preconditioning results. Both the RTW and ETW conditions result in significant increases in the matrix internal stresses when subjected to 4 ksi transverse tension. For example, the RTW maximum principal stresses are increased by a factor of roughly two for the 2220 systems, a factor of almost four for the baseline 3502 system, and a factor of over five for the Fibredux 914 system. That is, the hygrothermal-mechanical loading interaction is not the same for all four matrix materials, primarily because of the influence of moisture on matrix stiffness. For example, the actual increase in maximum principal stress for the AS4/2220-1 composite is only 2.6 ksi due to the 4 ksi applied stress, while the increase is 5.3 ksi for the AS4/914 composite.

Similar comparisons can be made for the interface normal stress, another quantity of practical interest since composites often fail due to fiber-matrix debonding. For the RTW condition, the interface normal stress increases by about 5.5 ksi due to a 4 ksi applied stress for all but the Hercules 2220-1 system, for which it only increases by 3.7 ksi.

Quite different response will be noted at the ETW condition. The maximum principal stress increases by about 6 ksi due to a 4 ksi applied stress for all four matrix materials, and the interface normal stress

Table 9

Predicted Matrix Stresses in Various AS4 Graphite Fiber-Reinforced Unidirectional Composites Subjected to 4 ksi Transverse Tension (Fiber Volume = 60 Percent; Stresses in ksi)

| Stress Component (Highest Value Occurring) | Matrix Material 3502 | 2220-1 | 2220-3 | 914 |
|---|---|---|---|---|
| Room Temperature (21°C),Dry,(RTD) | | | | |
| Octahedral Shear Stress, $\tau_o$ | 6.02 | 5.79 | 4.04 | 8.85 |
| Maximum Principal Stress, $\sigma_1$ | 10.31 | 10.25 | 7.14 | 15.48 |
| Minimum Principal Stress, $\sigma_2$ | -6.12 | -6.15 | -4.42 | -9.99 |
| Intermediate Principal Stress, $\sigma_3$ | 9.18 | 9.17 | 6.28 | 13.95 |
| Interface Normal Stress, $\sigma_n$ | -6.19 | -6.2 | -4.42 | -10.15 |
| Elevated Temperature (100°C),Dry,(ETD) | | | | |
| Octahedral Shear Stress, $\tau_o$ | 4.03 | 3.48 | 2.07 | 5.43 |
| Maximum Principal Stress, $\sigma_1$ | 6.95 | 6.35 | 4.87 | 9.85 |
| Minimum Principal Stress, $\sigma_2$ | -4.3 | -3.92 | 4.04 | -6.44 |
| Intermediate Principal Stress, $\sigma_3$ | 6 35 | 5.94 | 4.56 | 9.04 |
| Interface Normal Stress, $\sigma_n$ | -4.33 | -3.93 | -3.00 | -6.55 |
| Room Temperature (21°C),Wet,(RTW) | | | | |
| Octahedral Shear Stress, $\tau_o$ | 2.67 | 2.10 | 3.99 | 2.63 |
| Maximum Principal Stress, $\sigma_1$ | 7.41 | 5.30 | 9.57 | 6.79 |
| Minimum Principal Stress, $\sigma_2$ | -1.45 | -2.29 | -3.25 | -1.48 |
| Intermediate Principal Stress, $\sigma_3$ | 3.50 | 4.73 | 3.15 | 2.40 |
| Interface Normal Stress, $\sigma_n$ | 7.52 | 4.61 | 9.91 | 6.78 |
| Elevated Temperature (100°C),Wet,(ETW) | | | | |
| Octahedral Shear Stress, $\tau_o$ | 4.59 | 2.42 | 4.53 | 6.07 |
| Maximum Principal Stress, $\sigma_1$ | 9.72 | 7.44 | 11.86 | 10.95 |
| Minimum Principal Stress, $\sigma_2$ | -3.71 | -1.31 | -6.46 | -5.14 |
| Intermediate Principal Stress, $\sigma_3$ | -3.51 | 3.48 | -5.91 | -4.90 |
| Interface Normal Stress, $\sigma_n$ | 9.00 | 7.55 | 12.71 | 11.00 |

also increases by about 6 ksi, except for the 3502 system which is slightly lower (an increase of only 4.9 ksi). While there was a large influence of matrix on hygrothermal stresses (Table 7), little influence of matrix on subsequent transverse tensile loading was observed.

The conclusion is that hygrothermally-induced stresses, and particular those induced by moisture, are dominant influences on transverse tensile response and cannot be neglected. At failure (assume, for example, an 8 ksi transverse tensile strength of the composite), these hygrothermal stresses are predicted to contribute approximately one-third of the stress state. That is, neglecting hygrothermal stresses would result in predicted transverse tensile failure approximately one-third too low.

Of course, in transverse compression the predicted results could be quite different, because the compressive loading induces local stresses of opposite sign. Thus, the pre-existing hygrothermal stresses could be favorable.

5.5.2.3 Longitudinal Shear Loading

A summary of the predicted internal stress states in the matrix due to an applied longitudinal shear stress of 27.6 MPa (4 ksi) is presented in Table 10. Because the applied shear stress primarily induces local shear stresses, while the hygrothermal and transverse tensile loadings primarily induce local normal stresses, the trends indicated in Table 10 are quite different than those of Table 7 or 9.

For example, because relatively little dilatation is associated with longitudinal shear loading of a composite (even when elastoplastic response occurs), the interface normal stresses are not greatly affected. The interface shear stresses are tabulated in Table 10, rather

Table 10

Predicted Matrix Stresses in Various AS4 Graphite Fiber-Reinforced Unidirectional Composites Subjected to 4 ksi Longitudinal Shear (Fiber Volume = 60 Percent; Stresses in ksi)

| Stress Component (Highest Value Occurring) | Matrix Material 3502 | 2220-1 | 2220-3 | 914 |
|---|---|---|---|---|
| Room Temperature (21°C),Dry,(RTD) | | | | |
| Octahedral Shear Stress, $\tau_o$ | 7.43 | 7.07 | 6.37 | 9.57 |
| Maximum Principal Stress, $\sigma_1$ | 10.42 | 10.32 | 7.93 | 15.30 |
| Minimum Principal Stress, $\sigma_2$ | -8.35 | -8.41 | -7.49 | -11.32 |
| Intermediate Principal Stress, $\sigma_3$ | 6.54 | 6.44 | 3.94 | 11.30 |
| Interface Shear Stress, $\tau_{nt}$ | 6.87 | 6.75 | 6.91 | 7.41 |
| Elevated Temperature (100°C),Dry,(ETD) | | | | |
| Octahedral Shear Stress, $\tau_o$ | 6.35 | 5.82 | 5.34 | 7.46 |
| Maximum Principal Stress, $\sigma_1$ | 7.72 | 7.24 | 6.51 | 10.13 |
| Minimum Principal Stress, $\sigma_2$ | -7.51 | -7.26 | -6.54 | -9.20 |
| Intermediate Principal Stress, $\sigma_3$ | 4.11 | 3.57 | 1.56 | 6.87 |
| Interface Shear Stress, $\tau_{nt}$ | 6.89 | 6.61 | 6.46 | 7.22 |
| Room Temperature (21°C),Wet,(RTW) | | | | |
| Octahedral Shear Stress, $\tau_o$ | 5.97 | 5.90 | 6.08 | 5.94 |
| Maximum Principal Stress, $\sigma_1$ | 8.02 | 7.66 | 8.57 | 7.35 |
| Minimum Principal Stress, $\sigma_2$ | -6.33 | -6.78 | -7.03 | -7.18 |
| Intermediate Principal Stress, $\sigma_3$ | -2.31 | 1.34 | -4.48 | -2.00 |
| Interface Shear Stress, $\tau_{nt}$ | 7.13 | 7.13 | 6.75 | 7.15 |
| Elevated Temperature (100°C),Wet,(ETW) | | | | |
| Octahedral Shear Stress, $\tau_o$ | 5.81 | 6.03 | 5.27 | 7.58 |
| Maximum Principal Stress, $\sigma_1$ | 8.09 | 7.88 | 10.00 | 9.01 |
| Minimum Principal Stress, $\sigma_2$ | -6.79 | -7.51 | -9.91 | -8.39 |
| Intermediate Principal Stress, $\sigma_3$ | -4.75 | -1.50 | -6.28 | -5.84 |
| Interface Shear Stress, $\tau_{nt}$ | 6.39 | 7.32 | 6.02 | 7.34 |

than interface normal stresses. As can be seen, these stresses are not strongly influenced by either matrix type or hygrothermal environment. Correspondingly, the octahedral shear stresses are higher for a 4 ksi longitudinal shear loading than for a 4 ksi transverse tensile loading.

# SECTION 6

# CONCLUSIONS AND RECOMMENDATIONS

## 6.1 Conclusions

The Hercules epoxies, viz, 3502, 2220-1, and 2220-3, were more readily processed than the Fibredux 914. The increased thermal expansion coefficient exhibited by the 914 resin and its higher shrinkage during cure required a modified processing cycle to produce acceptable castings (see Appendix A of Volume II).

The overall performance of the three toughened epoxies, i.e., Hercules 2220-1 and 2220-3 and Ciba-Geigy Fibredux 914, was better than that of the untoughened Hercules 3502 epoxy in terms of mechanical properties. The strengths and strains to failure in both tension and shear were higher in almost all cases for the Hercules 2220-1 and 2220-3. The Fibredux 914, although performing better than the Hercules 3502, exhibited much lower strengths and strain-to-failure than the Hercules 2220 epoxy systems.

The neat resin tensile and shear data were shown to be mutually inconsistent in terms of an octahedral shear (distortional energy) yield criterion. Also, the isotropic relation between the elastic costants, i.e., $G = E/2(1 + \nu)$, was shown to not be satisfied. These represent important areas for additional study.

The scanning electron microscopy (SEM) fracture study identified surface features characteristic of epoxy neat resin failures. Failure modes were identified both from the SEM photographs and from observing failures during testing. The Hercules 2220-1 and 2220-3 appeared to be less sensitive to specimen defects and environmental conditions.

Micromechanical predictions of composite properties were made

although composite experimental data needed for correlation were not available.

## 6.2 Recommendations

- Continue work to develop a high strain polymer matrix for use in graphite fiber-reinforced composites.
- Determine engineering constants and stress-strain curves for the four graphite/epoxy composites to allow correlation with micromechanics predictions.
- Perform subsequent neat resin mechanical testing at higher temperatures (eg, 121°C), to allow more accurate modeling of the behavior of these neat resins near the cure temperatures of their composites.
- Perform additional coefficient of thermal expansion (CTE) and coefficient of moisture expansion (CME) measurements for Hercules 2220-1, 2220-3, 3502 and Ciba-Geigy Fibredux 914 to confirm the current data for future use in the micromechanics analysis.
- Investigate in more detail the reasons for the differences in the tensile and shear stress-strain responses of neat polymers being used in high performance composites.
- Investigate the causes of the neat polymers not satisfying the isotropic relation between stiffness constants.
- Define composite responses desired at various environmental conditions; use the micromechanics analysis to predict fiber and matrix characteristics required to achieve these composite responses.

## REFERENCES


1. A. K. Miller and D. F. Adams, "Micromechanical Aspects of the Environmental Behavior of Composite Materials," Report UWME-DR-701-111-1, University of Wyoming, Department of Mechanical Engineering, January 1977.

2. B. G. Schaffer and D. F. Adams, "Nonlinear Viscoelastic Behavior of a Composite Material Using a Finite Element Micromechanical Analysis," Report UWME-DR-001-101-1, University of Wyoming, Department of Mechanical Engineering, June 1980.

3. D. A. Crane and D. F. Adams, "Finite Element Micromechanical Analysis of a Unidirectional Composite Including Longitudinal Shear Loading," Report UWME-DR-101-101-1, University of Wyoming, Department of Mechanical Engineering, February 1981.

4. D. S. Cairns and D. F. Adams, "Moisture and Thermal Expansion of Composite Materials," Report UWME-DR-101-104-1, University of Wyoming, Department of Mechanical Engineering, November 1981.

5. "Standard Test Method for Plane-Strain Fracture Toughness of Metallic Materials," ASTM E399, Part 7, American Society for Testing Materials, 1981.

6. D. F. Adams and B. G. Schaffer, "Analytical/Experimental Correlations of Stiffness Properties of Unidirectional Composites," Composites Technology Review, Vol. 4, No. 2, Summer 1982, pp. 45-48.

7. G. C. Grimes and D. F. Adams, "Investigation of Compression Fatigue Properties of Advanced Composites," Northrop Technical Report NOR 79-17, Naval Air Systems Command Contract N00019-77-C-0519, October 1979.

8. G. C. Grimes, D. F. Adams and E. G. Dusbalon, "The Effects of Discontinuities on Compression Fatigue Properties of Advanced Composites," Northrop Technical Report NOR 80-158, Naval Air Systems Command Contract N00019-79-C-0276, October 1980.

9. D. F. Adams and D. A. Crane, "Combined Loading Micromechanical Analysis of a Unidirectional Composite," Composites, Vol. 15, No. 3, July 1984, pp. 181-192.

10. B. G. Schaffer and D. F. Adams, "Nonlinear Viscoelastic Analysis of a Unidirectional Composite Material," Journal of Applied Mechanics, Vol. 48, No. 4, December 1981, pp. 859-865.

11. R. S. Zimmerman, D. F. Adams and B. A. Coulter, "Investigation of Moisture Effect Mechanisms in a Unidirectional E-Glass/Epoxy Composite," Report UWME-DR-201-104-1: Volume I-Summary, Volume II-Detailed Results, University of Wyoming, Department of Mechanical Engineering, July 1982.

12. D. F. Adams and D. R. Doner, "Longitudinal Shear Loading of a Unidirectional Composite," Journal of Composite Materials, Vol. 1, No. 1, January 1967, pp. 4-17.

13. D. F. Adams and D. R. Doner, "Transverse Normal Loading of a Unidirectional Composite," Journal of Composite Materials, Vol. 1, No. 2, April 1967, pp. 152-164.

14. R. L. Foye, "An Evaluation of Various Engineering Estimates of the Transverse Properties of Unidirectional Composites," Tenth National SAMPE Symposium, San Diego, California, November 1966, p. 6-31.

15. D. F. Adams and S. W. Tsai, "The Influence of Random Filament Packing on the Transverse Stiffness of Unidirectional Composites," Journal of Composite Materials, Vol. 3, July 1969, pp. 368-381.

16. D. F. Adams, "Inelastic Analysis of a Unidirectional Composite Subjected to Transverse Normal Loading," Journal of Composite Materials, Vol. 4, July 1970, pp. 310-328.

17. D. F. Adams, "Inelastic Analysis of a Unidirectional Composite Subjected to Transverse Normal Loading," Report RM-6245-PR, The Rand Corporation, May 1970.

18. R. L. Foye, "Theoretical Post-Yielding Behavior of Composite Laminates, Part I-Inelastic Micromechanics," Journal of Composite Materials, Vol. 7, No. 2, April 1973, pp. 178-193.

19. D. F. Adams and A. K. Miller, "Hygrothermal Microstresses in a Unidirectional Composite Exhibiting Inelastic Material Behavior," Journal of Composite Materials, Vol. 11, No. 3, July 1977, pp. 285-299.

20. A. K. Miller and D. F. Adams, "Inelastic Finite Element Analysis of a Heterogeneous Medium Exhibiting Temperature and Moisture Dependent Material Properties," Fibre Science and Technology, Vol. 13, No. 2, March-April 1980, pp. 135-153.

21. D. F. Adams, "High Performance Composite Materials for Vehicle Constructions; An Elastoplastic Analysis of Crack Propagation in a Unidirectional Composite," Report R-1070-PR, The Rand Corporation, March 1973.

22. D. F. Adams, "Elastoplastic Crack Propagation in a Transversely Loaded Unidirectional Composite," Journal of Composite Materials, Vol. 8, January 1974, pp. 38-54.

23. D. F. Adams, "A Micromechanical Analysis of Crack Propagation in an Elastoplastic Composite Material," Fibre Science and Technology, Vol. 7, No. 4, October 1974, pp. 237-256.

24. D. P. Murphy and D. F. Adams, "Energy Absorption Mechanisms During Crack Propagation in Meal Matrix Composites," Report UWME-DR-901-103-1, University of Wyoming, Department of Mechanical Engineering, October 1979.

25. D. F. Adams and D. P. Murphy, "Analysis of Crack Propagation as an Energy Absorption Mechanism in Metal Matrix Composites," Report UWME-DR-101-102-1, University of Wyoming, Department of Mechanical Engineering, February 1981.

26. D. F. Adams and J. M. Mahishi, "Micromechanical Predictions of Crack Propagation and Fracture Energy in a Single-Fiber Boron/Aluminum Model Composite," Report UWME-DR-201-101-1, University of Wyoming, Department of Mechanical Engineering, February 1982.

27. J. M. Mahishi and D. F. Adams, "Micromechanical Predictions of Crack Initiation, Propagation and Crack Growth Resistance in Boron/Aluminum Composites," Journal of Composite Materials, Vol. 16, November 1982, pp. 457-469.

28. J. M. Mahishi and D. F. Adams, "Fracture Behavior of a Single-Fiber Graphite/Epoxy Model Composite Containing a Broken Fibre or Cracked Matrix," Journal of Materials Science, Vol. 18 (1983), pp. 447-456.

29. J. M. Mahishi and D. F. Adams, "Three-Dimensional Elastoplastic Stress Analysis of Unidirectional Boron-Aluminum Composites Containing Broken Fibers," Report UWME-DR-201-107-1, University of Wyoming, Department of Mechanical Engineering, October 1982.

30. R. M. Richard and J. M. Blacklock, "Finite Element Analysis of Inelastic Structures," AIAA Journal, Vol. 7, No. 3, March 1969, pp. 432-438.

31. "Hercules Product Data Sheet No. 847-3: Magnamite Graphite Fiber Type AS4," Hercules, Inc., Magna, Utah, August 1981.

32. D. F. Adams and M. M. Monib, "Moisture Expansion and Thermal Expansion Coefficients of a Polymer-Matrix Composite Material," Proceedings of the Fourth Conference on Fibrous Composites in Structural Design, San Diego, California, November 1978.

| 1. Report No. | 2. Government Accession No. | 3. Recipient's Catalog No. |
|---|---|---|
| NASA CR-172303 | | |

| 4. Title and Subtitle | 5. Report Date |
|---|---|
| Investigation of the Relations Between Neat Resin and Advanced Composite Mechanical Properties Volume I - Results | November 1984 |
| | 6. Performing Organization Code |
| 7. Author(s) Richard S. Zimmerman, Donald F. Adams, David E. Walrath | 8. Performing Organization Report No. UWME-DR-301-101-1 |
| | 10. Work Unit No. |
| 9. Performing Organization Name and Address<br>Composite Materials Research Group<br>University of Wyoming<br>Laramie, WY 82071 | 11. Contract or Grant No.<br>NAG-1-277 |
| | 13. Type of Report and Period Covered<br>Technical Report<br>May 1982-May 1983 |
| 12. Sponsoring Agency Name and Address<br>National Aeronautics and Space Administration<br>Washington, D.C. 20546 | 14. Sponsoring Agency Code |

15. Supplementary Notes
Langley Technical Monitor:
Dr. Norman J. Johnston
Materials Division

Volume II under separate cover

16. Abstract

A detailed evaluation of one untoughened epoxy baseline resin and three toughened epoxy resin systems was performed. The Hercules 3502, 2220-1, and 2220-3, and Ciba-Geigy Fibredux 914 resin systems were supplied in the uncured state by NASA-Langley and cast into thin flat specimens and round dogbone specimens. Tensile and torsional shear measurements were performed at three temperatures and two moisture conditions. Coefficients of thermal expansion and moisture expansion were also measured.

Extensive scanning electron microscopic examination of fracture surfaces was performed, to permit the correlation of observed failure modes with the environmental conditions under which the various specimens were tested.

A micromechanics analysis was used to predict the unidirectional composite response under the various test conditions, using the neat resin experimental results as the required input data.

The mechanical and physical test results, the scanning electron microscope observations, and the analytical predictions were then correlated.

| 17. Key Words (Suggested by Author(s)) | 18. Distribution Statement |
|---|---|
| polymer matrices<br>toughened epoxies<br>mechanical properties<br>micromechanics predictions | Unclassified, Unlimited<br>Subject category 24 |

| 19. Security Classif. (of this report) | 20. Security Classif. (of this page) | 21. No. of Pages | 22. Price* |
|---|---|---|---|
| Unclassified | Unclassified | 263 | A12 |

* For sale by the National Technical Information Service, Springfield, Virginia 22161